TESE DE DOUTORAMENTO

# AEROGEL AND SUPERCRITICAL TECHNOLOGY FOR THE DEVELOPMENT OF SKIN AND PULMONARY DRUG DELIVERY SYSTEMS

Clara López Iglesias

**ESCOLA DE DOUTORAMENTO INTERNACIONAL**

**PROGRAMA DE DOUTORAMENTO EN INVESTIGACIÓN E DESENVOLVEMENTO DE MEDICAMENTOS**

SANTIAGO DE COMPOSTELA 2020

USC
UNIVERSIDADE
DE SANTIAGO
DE COMPOSTELA

**DECLARACIÓN DEL AUTOR/A DE LA TESIS**

D./Dña. **Clara López Iglesias**

Título da tese: **Aerogel and supercritical technology for the development of skin and pulmonary drug delivery systems**

Presento mi tesis, siguiendo el procedimiento adecuado al Reglamento y declaro que:

1) La tesis abarca los resultados de la elaboración de mi trabajo.
2) De ser el caso, en la tesis se hace referencia a las colaboraciones que tuvo este trabajo.
3) Confirmo que la tesis no incurre en ningún tipo de plagio de otros autores ni de trabajos presentados por mí para la obtención de otros títulos.

Y me comprometo a presentar el Compromiso Documental de Supervisión en el caso que el original no esté depositado en la Escuela.

En **Santiago de Compostela**, **lunes 5 de Octubre de 2020**.

Firma

USC
UNIVERSIDADE
DE SANTIAGO
DE COMPOSTELA

**AUTORIZACIÓN DEL DIRECTOR/TUTOR DE LA TESIS**

D./Dña. **Carmen I. Álvarez Lorenzo y Carlos A. García González**

En condición de: **Tutor/a y director/a**

Título de la tesis: **Aerogel and supercritical technology for the development of skin and pulmonary drug delivery systems**

INFORMA:

Que la presente tesis, se corresponde con el trabajo realizado por D/Dña **Clara López Iglesias**, bajo mi dirección/tutorización, y autorizo su presentación, considerando que reúne los requisitos exigidos en el Reglamento de Estudios de Doctorado de la USC, y que como director/tutor de esta no incurre en las causas de abstención establecidas en la Ley 40/2015.

En **Santiago de Compostela**, **lunes 5 de Octubre de 2020.**

**Firma**

USC
UNIVERSIDADE
DE SANTIAGO
DE COMPOSTELA

Se me hace raro pensar que esta etapa que ha sido mi vida durante los últimos cuatro años esté llegando a su fin. Tras la Carrera de Farmacia, donde siempre estaba claro qué había que hacer para obtener un buen resultado, entrar en el mundo de la investigación y tener que devanarme los sesos y repetir las cosas una y otra vez hasta conseguir lo propuesto supuso todo un reto para alguien impaciente como yo. Han sido unos años de desarrollo académico, pero también de un gran aprendizaje personal, con algunos momentos malos y muchísimos recuerdos bonitos. Dicen que la realización de una tesis puede ser un proceso solitario donde debemos aprender a ser independientes, pero desde luego estar acompañado de las personas adecuadas lo hace todo mucho más llevadero.

Antes de nada, me gustaría agradecer a mis directores de tesis, Carlos García y Carmen Álvarez, por su supervisión y por haber hecho posible la realización de esta tesis. A Carlos, por todas sus ideas, su continuo apoyo y dedicación; por todas las oportunidades ofrecidas que me han ayudado a crecer, como investigadora y como persona.

Al resto de profesores del grupo: Ángel Concheiro, José Luis Gómez y Mariana Landín, por todas sus aportaciones y su disposición a colaborar y echar una mano cuando hizo falta. También me gustaría mencionar al profesor Francisco Otero y a Soledad Anguiano, por su amabilidad para responder a cualquier pregunta y sus agradables conversaciones.

A mis compañeros de laboratorio. A los que me ayudaron en un principio cuando era una novata temerosa: Sonia, Alejandro, Leticia, Helena, Lorena y Luis, quien volvió como un postdoc consagrado y me aportó unas cuantas críticas constructivas. Al resto de los que me acompañaron durante todo este proceso, que hicieron el día a día en el laboratorio increíblemente llevadero, y que han hecho que termine sintiendo que tengo aquí a una gran familia. A Víctor, mi eterno compañero en el mundo de los fluidos supercríticos, por todo su apoyo, por las risas y las charlas científicas y existenciales. A Patricia, Miriam, Fernando, Ángela, María (mi gran compañera del HPLC, ¡gracias por la paciencia!), Xián y Andrea, con quienes viví tantos momentos en el laboratorio, en los descansos del café, en cenas y juergas nocturnas. A Mariana, quien estuvo con nosotros apenas unos meses pero se ha convertido en una amiga para toda la vida. A los que llegaron cuando yo ya llegaba al final, que supondrán un relevo de primera clase: Rebeca, Iago, Ana, Ana Filipa, Axel y Thoa. A los técnicos Mariano, que estaba primero, y Patricia, que vino después, por ser pilares fundamentales en el funcionamiento del laboratorio y por su infinita paciencia y disposición. Y a todo el *team Fran*, por el buen rollo y por ser unos grandes vecinos siempre dispuestos a colaborar.

También quiero hacer mención a aquellos con los que aprendí que el mundo académico no es sólo el laboratorio, que hace falta establecer relaciones para crecer y que en cualquier parte puedes encontrar gente sorprendente. Quiero agradecer la oportunidad ofrecida por la profesora Irina Smirnova de la Universidad Técnica de Hamburgo de realizar allí una estancia, así como a todos los miembros del grupo

(especialmente al profesor Pavel Gurikov y a Tamara) que me ayudaron a moverme en una planta piloto y me hicieron sentir como en casa. Y cómo no, a Sheila y David (sois los mejores compañeros de piso que podría haber pedido) y al resto de los amigos que hicieron que Hamburgo fuese un poquito menos frío.

Al profesor Diego Velasco de la Universidad Carlos III de Madrid por la oportunidad de colaborar y por acogerme tan bien en Leganés, así como a Cristina por su inestimable ayuda.

Al profesor Fernando J. Monteiro y a la Dra. Joana Barros de la Universidad de Oporto por su eterna disposición a ayudarnos con los ensayos antimicrobianos y el gran trabajo llevado a cabo.

A toda la gente de la Universidad de Santiago de Compostela que aportó su granito de arena: la Dra. Inés Ardao del grupo BioFarma del CiMUS, las profesoras Josefa Fernández y Enriqueta López de la Facultad de Física, y todo el personal de los servicios de apoyo a la investigación del CACTUS.

A quienes hace años se sentaban a mi lado en las clases de Tecnología Farmacéutica, y día de hoy siguen a mi lado, algunos en la distancia: Nati, Carmen, Mariña, Andrea, Gonzalo y Bea. Gracias a todos por seguir conmigo, ya sea aquí o en Madrid, por vuestro apoyo, por estar dispuestos a escuchar siempre y por esos reencuentros que dan la sensación de que no haya pasado el tiempo desde la última reunión. A Andrea también por compartir este proceso conmigo y ser una gran ayuda en las encrucijadas.

A Carmen y Alba. Por haber crecido conmigo. Por escucharme y compartir frustraciones, logros y proyectos. A Carmen por tu continuo interés, por el *feedback* y por tus empujones a mi fuerza de voluntad.

A todos los miembros de mi gran familia, especialmente a mis padrinos y a mi prima Sofía, que siempre han estado al pie del cañón, y a mi abuelo Ricardo, por recibirme siempre con infinita alegría. A Lela y la abuela Maricarmen, que aunque ya no me lo puedan decir sé que siempre creyeron en mí más que yo misma. A mi abuelo Vicente, quien sembró la semilla de la ciencia en la familia y sé que se alegraría de esta noticia.

A Jacobo, gracias por todos estos años compartidos. Por haber estado ahí en cada decepción y en cada logro, por haber aprendido el uno del otro y crecido y compartido proyectos. Gracias por empujarme cuando flaqueaba y por escucharme cuando tenía algún problema para ayudarme a encontrar una solución. Por los paseos para despejar la mente, las cenas y los viajes, y por enseñarme siempre a disfrutar de la vida.

A mi hermana Paula, a quien también he visto crecer y madurar durante esta etapa. Gracias por ser siempre mi gran apoyo y una genial compañera de vida.

A papá y a mamá. Por enseñarme a pensar por mí misma y a perseverar. Por habérmelo dado todo: la vida, la música, una buena educación, el cariño de una buena familia. Gracias por todos vuestros ánimos y por ayudarme a creer en mí pase lo que pase.

# INDEX

RESUMO.. i

ABBREVIATION LIST xi

1. INTRODUCTION 1
1.1. Chronic wounds 3
1.1.1. Physiological wound healing process 3
1.1.2. Factors affecting wound healing 5
1.1.2.1. Local factors 5
1.1.2.2. Systemic factors 7
1.1.3. Current approaches in wound healing treatment 8
1.1.3.1. Local drug delivery systems used in wound treatment 10
1.1.3.2. Biopolymers used as wound dressings 11
1.1.3.3. Other materials used in wound delivery 14
1.2. Obstructive pulmonary diseases 14
1.2.1. Physiopathology and treatment strategies 14
1.2.2. Drug delivery systems for pulmonary administration 16
1.2.2.1. Devices and formulations 16
1.2.2.2. Pharmaceutical requirements of the formulations 17
1.3. Supercritical fluid technology for biomedical applications 19
1.3.1. Supercritical $CO_2$: Properties and applications 19
1.3.2. Supercritical fluids in particle engineering and micronization processes 20
1.3.2.1. Rapid Expansion of Supercritical Solutions (RESS) 21
1.3.2.2. Supercritical Anti-solvent (SAS) processes 22
1.3.2.3. The Particles from Gas-Saturated Solutions (PGSS®) technique 22
1.3.3. Polysaccharide-based aerogel technology 24
1.3.3.1. Polysaccharide-based aerogels for drug delivery 26
1.3.3.2. Bio-based aerogels for tissue engineering 33
1.3.3.3. Bio-based aerogels for other biomedical applications 38
1.4. References 41

2. OBJECTIVES AND ORGANIZATION 51

SECTION I. SOLID LIPID MICROPARTICLES FROM GAS-SATURATED SOLUTIONS..55

3. MODELLING OF THE PRODUCTION OF LIPID PARTICLES USING PGSS® TECHNIQUE 57
3.1. Introduction 59
3.2. Materials and methods 61
3.2.1. Materials 61
3.2.2. Determination of the melting point of GMS in the presence of compressed $CO_2$ at different pressures 61
3.2.3. SLMPs production by the PGSS® technique 62
3.2.4. Morphological analysis and particle size distribution (PSD) 63
3.2.5. Modelling 63
3.3. Results and discussion 65
3.3.1. Melting point depression of GMS in the presence of $CO_2$ 65
3.3.2. Particle size distribution (PSD) of GMS particles 66
3.3.3. Morphological characterization and modelling of GMS particle production using neurofuzzy tool 67
3.4. Conclusions 71
3.5. References 71

4. LIDOCAINE-LOADED SOLID LIPID MICROPARTICLES (SLMPs) PRODUCED FROM GAS-SATURATED SOLUTIONS FOR WOUND APPLICATIONS 75
4.1. Introduction 77

4.2. Materials and methods ..... 79
4.2.1. Materials ..... 79
4.2.2. SLMPs production by the PGSS® technique ..... 79
4.2.3. Analysis of the morphology, size, and surface of the particles ..... 80
4.2.4. Physicochemical characterization ..... 80
4.2.5. Determination of LID encapsulation efficiency ..... 80
4.2.6. LID release tests from SLMPs ..... 81
4.2.7. Preparation of bioprinted human skin equivalents ..... 82
4.2.8. LID release tests through bioprinted human skin equivalents ..... 82
4.2.9. Antimicrobial tests ..... 83
4.2.9.1. Minimum inhibitory concentration ..... 83
4.2.9.2. Minimum bactericidal concentration ..... 84
4.2.9.3. Antimicrobial activity of LID released from GMS ..... 84
4.2.10. Statistical analysis ..... 84
4.3. Results and discussion ..... 85
4.3.1. Morphological and physicochemical properties of the SLMPs ..... 85
4.3.2. LID encapsulation efficiency ..... 87
4.3.3. LID release tests ..... 88
4.3.4. LID permeation through bioengineered skin substitutes ..... 89
4.3.5. Antimicrobial activity of the SLMPs ..... 91
4.4. Conclusions ..... 93
4.5. References ..... 94

SECTION II. CHITOSAN AEROGELS LOADED WITH VANCOMYCIN FOR WOUND APPLICATIONS ..... 99

5. VANCOMYCIN-LOADED CHITOSAN AEROGEL PARTICLES OBTAINED BY THE DRIPPING METHOD FOR CHRONIC WOUND APPLICATIONS ..... 101
5.1. Introduction ..... 103
5.2. Materials and methods ..... 105
5.2.1. Materials ..... 105
5.2.2. Preparation of chitosan aerogel beads ..... 106
5.2.2.1. Preparation of the chitosan hydrogel ..... 106
5.2.2.2. Solvent exchange ..... 106
5.2.2.3. Supercritical extraction of the gel solvent ..... 106
5.2.3. Physicochemical properties of the gel beads ..... 106
5.2.4. Water absorption assay ..... 108
5.2.5. Collagenase activity test ..... 108
5.2.6. Vancomycin encapsulation efficiency assay ..... 108
5.2.7. Vancomycin release from the aerogel particles ..... 109
5.2.8. Antimicrobial ability of the gels ..... 109
5.2.9. Cytotoxicity assay ..... 110
5.2.10. Statistical analysis ..... 110
5.3. Results and discussion ..... 110
5.3.1. Morphological and textural properties of the chitosan aerogels ..... 110
5.3.2. PBS sorption tests ..... 114
5.3.3. Collagenase activity test ..... 115
5.3.4. Vancomycin-loaded aerogels processing and properties ..... 116
5.3.5. Vancomycin release from chitosan aerogels ..... 117
5.3.6. Antimicrobial test ..... 119
5.3.7. Cytotoxicity assay ..... 121
5.4. Conclusions ..... 121
5.5. References ..... 122

6. JET CUTTING TECHNIQUE FOR THE PRODUCTION OF CHITOSAN AEROGEL MICROPARTICLES LOADED WITH VANCOMYCIN ..... 127
6.1. Introduction ..... 129
6.2. Materials and methods ..... 131
6.2.1. Materials ..... 131
6.2.2. Production of chitosan aerogel microparticles ..... 131
6.2.3. Morphology and textural properties ..... 132
6.2.4. Fluid sorption capacity test ..... 133
6.2.5. Vancomycin encapsulation efficiency and release tests ..... 133
6.2.6. Antimicrobial tests ..... 134
6.2.7. Biocompatibility tests in vitro ..... 134
6.2.7.1. Hemolytic activity test ..... 134
6.2.7.2. Cytotoxicity test ..... 135
6.3. Results and discussion ..... 135
6.3.1. Jet cutting of chitosan gels and morphology and textural properties of the resulting aerogel particles ..... 135
6.3.2. Fluid sorption capacity ..... 138
6.3.3. Drug encapsulation and release ..... 138
6.3.4. Antimicrobial tests ..... 139
6.3.5. Biocompatibility and hemocompatibility of vancomycin-loaded aerogel particles ..... 140
6.3.5.1. Hemocompatibility ..... 140
6.3.5.2. Cytocompatibility ..... 140
6.4. Conclusions ..... 141
6.5. References ..... 142

SECTION III. ALGINATE AEROGELS FOR PULMONARY DELIVERY ..... 145

7. INKJET-PRINTED AEROGEL PARTICLES FOR PULMONARY DELIVERY ..... 147
7.1. Introduction ..... 149
7.2. Materials and methods ..... 150
7.2.1. Materials ..... 150
7.2.2. Preparation of alginate aerogel beads by prilling ..... 151
7.2.3. Preparation of aerogel microspheres prepared by inkjet printing ..... 151
7.2.4. Preparation of salbutamol-loaded aerogel microspheres prepared by inkjet printing ..... 152
7.2.5. Structural and physicochemical characterization of the gels and aerogels ..... 152
7.2.6. Salbutamol sulphate loading yield and release studies ..... 153
7.2.7. Simulated lung deposition tests ..... 154
7.3. Results and discussion ..... 155
7.3.1. Gelation mechanism and processing window for alginate gel printing ..... 155
7.3.2. Optimization of the alginate gel printing and solvent exchange process ..... 156
7.3.3. Salbutamol sulphate-loaded aerogels release study ..... 159
7.3.4. *In vitro* aerodynamic drug deposition of SS-loaded aerogels ..... 162
7.4. Conclusions ..... 163
7.5. References ..... 163

8. CONCLUSIONS ..... 167

Appendix ..... 169

USC
UNIVERSIDADE
DE SANTIAGO
DE COMPOSTELA

# RESUMO

A administración local de fármacos é unha estratexia que permite alcanzar unha maior concentración no lugar de acción, requirindo menores doses cá administración sistémica e contribuíndo a unha disminución dos efectos secundarios adversos das terapias. Utilízase amplamente no tratamento das enfermidades respiratorias obstructivas que requiren unha resposta rápida. Tamén se propuxo coma alternativa noutros tratamentos tradicionalmente administrados por vía sistémica, coma a terapia antibiótica, para permitir un mellor control da dose evitando a aparición de resistencias.

As feridas crónicas, coma por exemplo as úlceras diabéticas, son aquelas cun proceso de curación alterado que permanecen semanas e incluso meses nun continuo estado de inflamación, causando dor e unha importante diminución na calidade de vida dos pacientes, podendo precisar amputacións e incluso causar a morte. Cando ocorre unha lesión na pel sa, teñen lugar unha serie de mecanismos biolóxicos de resposta destinados á rexeneración do tecido (hemostase, inflamación, proliferación e remodelación), pero unha ampla variedade de factores poden comprometer esta secuencia. Un dos máis representativos é a presenza de microorganismos, que poden interferir no entorno da ferida causando cambios metabólicos que dificultan a curación, ademais de adherirse en forma de biopelículas moi difíciles de tratar mediante terapias antibióticas convencionais. Tamén existen unha serie de factores, coma enfermidades cardiovasculares, enfermidades metabólicas e tratamentos farmacolóxicos, que favorecen a aparición destas feridas. Debido ao progresivo envellecemento da poboación, hai unha alta prevalencia destes condicionantes e xorde a necesidade de mellorar os tratamentos para as feridas para reducir os custos hospitalarios e mellorar a calidade de vida dos pacientes.

Nas últimas décadas desenvolvéronse numerosos tratamentos e cubertas para feridas que empregan dende materiais sinxelos e económicos, por exemplo gasas de algodón, ata avanzados produtos de enxeñaría tisular. Os recubrimentos de feridas deben estar adaptados aos requerimentos de cada paciente en función do tipo de ferida, sendo de gran relevancia o control do grao de humectación da ferida e a capacidade absorbente do produto no caso de feridas altamente exudativas. Entre estes produtos cabe destacar o uso de materiais basados en polímeros naturais, que destacan pola súa boa biocompatibilidade, biodegradabilidade e sostibilidade para

cesión local de axentes bioactivos que promovan a curación ou traten os factores que a evitan. Normalmente, os pacientes con feridas crónicas requiren terapia antibiótica sistémica para tratar a infección e permitir a curación. Nesta Tese proponse o uso de materiais porosos capaces de liberar localmente estes fármacos.

Por outro lado, as enfermidades pulmonares crónicas tales coma a asma e a enfermidade pulmonar obstrutiva crónica (EPOC) afectan a millóns de persoas no mundo. Ambas enfermidades presentan unha etioloxía diferente, sendo a asma unha enfermidade de orixe inmunolóxico con baixa mortalidade e a EPOC unha enfermidade frecuente en fumadores ou exfumadores e con peor pronóstico. Porén, en ambas enfermidades dáse un proceso de broncoconstrición, mediante o cal se produce un ensanche das paredes do epitelio pulmonar dando lugar a un estreitamento da vía aérea, diminuíndo o fluxo de aire circulante e dificultando o intercambio de osíxeno cos vasos sanguíneos pulmonares. Para tratar estes síntomas, pódense empregar medicamentos que atenúen a inflamación, principalmente glicocorticoides, ou fármacos que actúen coma broncodilatadores, por exemplo o sulfato de salbutamol.

No caso das enfermidades pulmonares, a terapia local mediante inhaladores adoita ser de elección, xa que evita os efectos secundarios da administración sistémica e normalmente requírese unha acción rápida, por exemplo durante unha crise. Existen unha serie de dispositivos para efectuar a inhalación, que se seleccionan en función da capacidade inspiratoria do paciente e a súa habilidade á hora de coordinar a activación do dispositivo e a inhalación. En todos os casos, inhálanse ben gotículas líquidas contendo o fármaco, ou ben partículas sólidas que poden ser o propio fármaco pulverizado ou o fármaco contido nun portador. As partículas sólidas depositanse en distintas zonas do aparello respiratorio segundo o tamaño e a densidade que presenten. Utilízase o termo diámetro aerodinámico para integrar os parámetros de tamaño e densidade. Desta forma, partículas grandes e porosas presentan o mesmo diámetro aerodinámico, e por tanto o mesmo patrón e comportamento fluidodinámico no aparello respiratorio, que partículas non porosas máis pequenas. Para alcanzar os bronquios, que son a diana da terapia local, as partículas deben presentar un diámetro aerodinámico comprendido entre 2 e 5 µm.

A tecnoloxía de fluídos supercríticos, e en concreto con $CO_2$ supercrítico, supón unha alternativa verde a procesos que requiren diversas etapas ou o emprego de disolventes orgánicos. Un fluído supercrítico é un fluído que se atopa a unhas condicións de presión e temperatura superiores ás do punto crítico da substancia (ou mestura de substancias). Nestas condicións, os fluídos supercríticos presentan propiedades intermedias entre os líquidos e os gases. Por un lado, a tensión superficial e a difusividade son similares ás dos gases, o cal facilita a transferencia de materia e a súa penetración en sólidos porosos. Por outra parte, teñen unha densidade e capacidade solvente similar á dos líquidos. O $CO_2$ é o fluído supercrítico máis empregado xa que ten alta dispoñibilidade, é seguro, non inflamable, económico e o

seu punto crítico obtense a unhas condicións baixas de presión (73,8 bar) e temperatura (31,1 °C). No sector farmacéutico propúxose o emprego de fluídos supercríticos en procesos de micronización, sistemas de liberación de fármacos, enxeñaría tisular ou de procesamento de materiais, entre outros.

Nos procesos de micronización faise uso das propiedades do $CO_2$ supercrítico coma disolvente, coma anti-solvente ou coma soluto. No caso da técnica *Particles from Gas-Saturated Solutions*® (PGSS®), emprégase $CO_2$ supercrítico coma soluto para a micronización dunha mestura fundida dun polímero ou outra substancia. O material a atomizar introdúcese nunha cámara en contacto con $CO_2$ presurizado e, despois dun tempo de contacto en condicións de presión e temperatura superiores ao punto crítico do $CO_2$, despresurízase a cámara por medio da apertura dunha válvula ata acadar presión atmosférica. A mestura atravesa un orificio, e a repentina despresurización provoca o enfriamento do material fundido (polo efecto Joule-Thomson), que precipita en forma de partículas que se recollen nun colector. A principal vantaxe desta técnica é que o $CO_2$ posúe a capacidade de interaccionar a nivel molecular coas substancias, diminuíndo o seu punto de fusión, polo que facilitaría o procesamento de materiais termolábiles e un maior rendemento enerxético do proceso. Ademais, obtense un produto seco sen necesidade de etapas de post-procesamento para eliminación de disolventes.

O $CO_2$ supercrítico é tamén a elección de preferencia para a preparación de aeroxeles. Os aeroxeles son materiais altamente porosos (80–99,8%), de baixa densidade (0,003–0,5 g/cm$^3$) e gran superficie específica (200–1200 m$^2$/g) con diámetros de poro controlados, que se obteñen ao eliminar a parte líquida dun xel danando minimamente a súa estrutura polimérica. O secado con $CO_2$ supercrítico é a opción máis habitual para o procesamento de aeroxeles, xa que evita calquera tensión superficial que conduza ao colapso estrutural do poro no proceso de evaporación do disolvente. A fase líquida do xel debe ser doluble no $CO_2$, polo que soen empregarse disolventes orgánicos (xeralmente etanol). En particular, propuxéronse os aeroxeles basados en materiais biocompatibles coma os polisacáridos para unha variedade de aplicacións biomédicas, debido á súa non toxicidade, biodegradabilidade e ampla dispoñibilidade. As potenciais aplicacións dos aeroxeles inclúen liberación de fármacos, enxeñaría de tecidos, tratamento de feridas e sistemas de diagnóstico e de imaxe, entre outros.

Neste traballo de Tese Doctoral proponse o uso de $CO_2$ supercrítico para a preparación de sistemas particulados de liberación de fármacos, primeiro mediante a técnica PGSS® e posteriormente mediante tecnoloxía de aeroxeles, para aplicación en feridas crónicas e terapia inhalatoria.

No primeiro capítulo realizouse unha modelización da técnica PGSS® para a produción de micropartículas do lípido gliceril monoestearato (GMS). Na técnica PGSS® pódense variar unha gran cantidade de parámetros de deseño e de operación para

modular a forma e tamaño das partículas a obter, principalmente a presión, temperatura e diámetro do orificio a través do cal se realiza a despresurización. A pesar de que na literatura tense discutido a influencia destes factores na produción das partículas, os intentos de modelización inclúen modelos matemáticos complexos ou que se centran noutros factores, coma por exemplo o perfil de disolución dun fármaco. Neste traballo proponse unha modelización facendo emprego de ferramentas de intelixencia artificial (redes neuronais e lóxica difusa) que axuden a simplificar os deseños experimentais e a dilucidar os efectos dos principais parámetros de procesamento nas propiedades do material obtido e no rendemento do proceso.

Primeiro realizouse un estudo do punto de fusión do lípido GMS en presenza de $CO_2$ a distintas condicións de presión, xa que é necesario determinar a rexión factible de operación co material. Para isto empregouse un autoclave de volume variable equipado cun endoscopio. Nel introduciuse un vial de vidro cunha mostra de GMS, fíxose pasar $CO_2$ a distintas temperaturas e foise variando a presión mediante a regulación do volume da cámara ata observar que o lípido fundía. Ás presións probadas (ata 200 bar) observouse unha diminución do punto de fusión de ata 9 °C (de 61 ata 52 °C). En base a estes resultados, seleccionouse o rango de valores de presión e temperatura para a modelización.

Para a modelización, previamente propúxose un deseño experimental variando as condicións de presión (120, 160 e 200 bar), temperatura (57, 62 e 67 °C) e diámetro do orificio (1 e 4 µm) para minimizar os ensaios necesarios. As partículas obtidas mediante a técnica PGSS® analizáronse mediante microscopía electrónica e óptica. As distribucións de tamaño de partícula fixéronse coas imaxes de microscopía óptica empregando análise de imaxe, obténdose os valores de diámetro medio de partícula e desviación estándar. Tamén se determinou o rendemento en base ás partículas finas obtidas. A modelización dos resultados realizouse empregando o software FormRules® v4.03, no cal se obtivo un modelo para cada un dos resultados (diámetro medio de partícula, desviación estándar e porcentaxe de partículas finas). Obtívose un modelo con excelente grao de correlación ($R^2 > 0,91$) para o tamaño medio de partícula, aínda que non foi tan preciso para os parámetros rendemento de partículas finas ($R^2 > 0,75$) e desviación estándar ($R^2 > 0,58$). O modelo aportou información sobre a influencia das condicións de procesamento en forma de regras lingüísticas SE...ENTÓN. En xeral, observouse que a temperaturas e presións altas obtíase un diámetro de partícula medio máis pequeno debido a un incremento da solubilidade de $CO_2$ no lípido fundido. No caso da desviación estándar, non se observou ningunha influencia significativa das variables. A procesabilidade foi mellor co diámetro pequeno de orificio, obténdose unha porcentaxe maior de partículas finas.

No segundo capítulo, prepararónse micropartículas lipídicas de GMS mediante a técnica PGSS® para liberación controlada de hidrocloruro de lidocaína para o tratamento combinado de dor e de prevención de infeccións en feridas. Primeiro

preparáronse partículas con contidos teóricos de lidocaína de 0, 1, 2, 4 e 10% en peso que resultaron nun pó fino, branco e en forma de gránulos soltos. A morfoloxía, tamaño de partícula, homoxeneidade e superfice das partículas evaluáronse mediante microscopía electrónica de barrido e análise de imaxe. As partículas obtidas foron non esféricas, con tamaños comprendidos entre os 20 e 120 µm e cun índice de polidispersión de 0,12. A adición de lidocaína non provocou cambios significativos na apariencia e tamaño das partículas. Posteriormente realizouse unha evaluación fisicoquímica das partículas mediante espectroscopía de infravermello, difracción de raios X e calorimetría diferencial de barrido. A presenza de lidocaína foi confirmada pola espectroscopía infravermella, e a difracción de raios X suxeriu un cambio do estado da lidocaína de cristalino a amorfo.

A eficacia de encapsulación da lidocaína nas partículas, así coma o seu perfil de cesión, evaluáronse mediante a técnica de HPLC. Para a eficacia de encapsulación, introducíronse partículas con distintas cargas de lidocaína en PBS (pH 7,4) baixo axitación e a 70 °C. Obtivéronse cargas de 69,9 ± 4,5, 59,7 ± 13,6, 79,0 ± 4,0 e 75,1 ± 0,9%, para as partículas cargadas cun 1, 2, 4 e 10% en peso de lidocaína, respectivamente. As cargas foron compatibles coas doses de fármaco recomendadas para anestesia local. Os ensaios de cesión realizáronse en células de Franz cunha membrana de nitrato de celulosa en PBS pH 7,4 e a 37 °C. A cesión das partículas foi sostida, liberándose aproximadamente un 50% do fármaco ás 4 h frente a un 85% disolto no caso da lidocaína pura. Os perfís de cesión axustáronse a distintas cinéticas de liberación, mostrando un mellor axuste a unha cinética de primeira orde ($R^2 > 0,95$) considerando un retraso no comezo da liberación.

Tamén se realizou un ensaio de permeabilidade a través dun substituto de pel obtido mediante impresión 3D. O ensaio realizouse introducindo o substituto de pel coma membrana separadora nas células de Franz cun medio de cesión de PBS pH 7,4, e comparáronse as partículas contendo lidocaína ao 4% en peso e lidocaína en pó. A administración do fármaco en forma de partículas lipídicas ralentizou o proceso de absorción a través do substituto de pel. Para simular a pel danada, retirouse a parte correspondente á derme e realizouse outro estudo de permeabilidade directamente nos insertos celulares onde se cultivaron as peles comparando pel intacta e pel danada. Neste caso, observouse unha penetración máis rápida de lidocaína a través da pel danada, xa que a derme presenta un estado maior de hidratación o cal facilita a difusión. Os substitutos de pel visualizáronse antes e despois do ensaio, comprobándose que non foran danados tras 24 h no medio de PBS.

Por último, evaluouse a actividade antimicrobiana das partículas contendo lidocaína. Primeiro determináronse as concentracións mínima inhibitoria e bactericida frente a tres cepas de bacterias frecuentemente illadas de feridas crónicas infectadas: *Escherichia coli*, *Staphylococcus aureus* e *Pseudomonas aeruginosa*. En base ás concentracións obtidas, realizouse un ensaio antimicrobiano coas partículas cun 7,5%

en peso de lidocaína. Tras 24 h de incubación dos cultivos bacterianos con lidocaína liberada polas partículas, observouse unha completa inhibición do crecemento bacteriano nos tres casos.

No terceiro capítulo preséntase o desenvolvemento de partículas de aeroxel de quitosano cargadas con hidrocloruro de vancomicina obtidas mediante xelificación e secado supercrítico para o tratamento de feridas crónicas. Primeiro preparáronse distintos hidroxeles por precipitación mediante goteo en medio básico dunha disolución acuosa de quitosano ao 2,5% en peso coa axuda dunha bomba de xeringa. As partículas deixáronse no baño de xelificación durante distintos periodos de maduración (0,5, 1, 2, 4, 10 e 24 h) para analizar a influencia deste parámetro nas propiedades texturais. Posteriormente cambiouse o disolvente dúas veces por etanol e levouse a cabo o secado con $CO_2$ supercrítico (40 °C e 120 bar, 5 g $CO_2$/min, 3,5 h). As propiedades fisicoquímicas dos aeroxeles obtidos caracterizáronse mediante análise de imaxe, picnometría de helio, técnicas de adsorción-desorción de nitróxino, microscopía electrónica de barrido, difracción de raios X e espectroscopía de infravermello. As áreas superficiais foron altas, superiores a 300 $m^2$/g na maioría dos casos, e as partículas presentaron porosidades superiores ao 96% con predominio dos macroporos (> 95%) debido aos espacios interconectados entre as fibras. O incremento no tempo de maduración deu lugar a un menor grao de encollemento do xel, con maiores tamaños de partícula, aínda que non influiu nas propiedades texturales. Realizouse un ensaio de absorción de PBS a pH 6, 7 e 8, e a elevada porosidade das partículas traduciuse nunha alta capacidade de absorción de PBS, entre un 300 e un 400% do peso das partículas. A pH 6 este valor viuse disminuído por disolución parcial do quitosano en medio ácido. Realizouse un ensaio de actividade do enzima colaxenasa en presenza dos aeroxeles de quitosano, observándose a non inhibición de dito enzima. Polo tanto, os aeroxeles non interferirían coa remodelación de coláxeno durante o proceso de curación.

A carga de vancomicina nas partículas realizouse na disolución inicial de quitosano a distintos contidos (5, 10 e 20% en peso), e as partículas de xel cargadas deixáronse no baño de xelificación durante un tempo de maduración dunha hora. A presenza de vancomicina nos aeroxeles resultantes tralo cambio de disolvente e secado supercrítico confirmouse mediante espectroscopía infravermella. A eficacia de encapsulación evaluouse disolvendo as partículas en medio ácido (HCl 0,1 M) e medindo o sobrenadante mediante espectrofotometría, e foi dun 12,1 ± 1,0, 12,9 ± 1,0 e 13,7 ± 1,4% para as partículas cunha carga teórica de 5, 10 e 20% en peso, respectivamente. A perda de vancomicina tivo lugar principalmente no cambio de disolvente, xa que se trata dun composto altamente hidrosoluble. O ensaio de cesión do antibiótico levouse a cabo suspendendo as partículas en PBS pH 7,4 nun baño termostatizado a 37 °C (60 rpm) e extraendo volumen do medio durante 48 h. O perfil de cesión axustouse a unha cinética de primeira orde, cunha liberación rápida inicial

do fármaco seguida dunha liberación máis controlada que se prolongou ata as 8 h de cesión. O perfil de vancomicina no aeroxel foi lixeiramente modificado con respecto á disolución de vancomicina pura, a cal se disolveu en máis do 90% tras cinco minutos. O perfil de cesión da vancomicina contida no aeroxel correlacionouse cunha rápida actividade antimicrobiana, cunha inhibición do crecemento dunha poboación planctónica de *S. aureus* ás 6 h de incubación cos aeroxeles, sendo por completo eliminada ás 48 h de incubación. En xeral, os aeroxeles cargados con distintas proporcións de vancomicina presentaron boa biocompatibilidade en ensaios de citotoxicidade con fibroblastos de rato.

O cuarto capítulo supuxo unha mellora da formulación estudada no terceiro capítulo, principalmente debida á redución do tamaño de partícula (o cal favorecería a súa aplicación na ferida) e ao incremento na carga de vancomicina (o cal melloraría o rendemento na fabricación de partículas). A disolución inicial de quitosano presentaba unha elevada viscosidade, o cal dificultaba o seu procesamento en forma de partículas pequenas. Para conseguir diminuír o tamaño de partícula, empregouse a técnica jet *cutting*, basada no corte mediante forzas mecánicas dun chorro de fluído e que non presenta limitacións de viscosidade. Nesta técnica, a disolución de quitosano fíxose pasar a través dun orificio a alta presión, formándose un chorro de fluído que foi cortado por un disco xiratorio con tiras de aceiro inoxidable formando gotículas esféricas. Estas pingas foron recollidas nun baño de xelificación e, tras un tempo de envellecemento, formaron partículas sólidas que foron secadas por secado supercrítico (40 °C e 120 bar, 5 g $CO_2$/min, 3,5 h).

Primeiro evaluáronse as distribucións de tamaño de partícula de aeroxeles producidos con distintas condicións da técnica *jet cutting*, principalmente a velocidade do disco xiratorio (2.000, 4.000 e 6.000 rpm) e o diámetro do orificio (400 e 500 µm). A morfoloxía e apariencia das partículas estudáronse mediante microscopía electrónica de barrido, e as distribucións de tamaño de partícula realizáronse mediante análise dinámico de imaxe, obténdose unha formulación optimizada co diámetro de orificio de 500 µm e coa velocidade de corte de 4.000 rpm en base ao diámetro medio de partícula (820 µm) e esfericidade das partículas. As partículas presentaron porosidades superiores ao 95%, densidade baixa (0,06 g/cm$^3$) e excelentes propiedades texturais (áreas superficiais de 190 m$^2$/g). As partículas foron capaces de absorber máis do 600% do seu peso en tampón fosfato, polo que presentarían unha alta capacidade de absorción de exudado.

A carga de vancomicina foi mellorada realizando a xelificación nun medio de amoníaco en etanol, obténdose unha eficacia de encapsulación do 24,6 ± 0,3%. Os ensaios de cesión realizáronse en PBS en células de Franz, obténdose un perfil de liberación controlado, cun 50% da carga liberado ás 4 h e unha liberación completa ás 24 h. En ensaios antimicrobianos frente a *S. aureus*, obtívose unha completa inhibición

das cepas bacterianas a todos os tempos de incubación (6, 24 e 48 h) en contacto cos aeroxeles cargados.

En canto á biocompatibilidade das partículas, realizouse un ensaio de hemocompatibilidade con sangue humano e outro de citocompatibilidade con fibroblastos de rato BALB/3T3. As mostras presentaron unha perfecta hemocompatibilidade, polo que non interferirían no proceso de hemostase, crucial para a curación de feridas. En canto á citocompatibilidade, os aeroxeles apenas presentaron toxicidade, obténdose valores de viabilidade celular superiores ao 80% aos tempos probados.

No quinto capítulo, desenvólvese unha formulación de micropartículas de aeroxeles de alxinato para administración pulmonar de sulfato de salbutamol mediante unha tecnoloxía de secado de xeles con fluídos supercríticos. O emprego de portadores de fármaco porosos presenta a vantaxe de que se requiren tamaños de partícula superiores aos portadores non porosos, polo que presentan mellores propiedades de fluxo con menor tendencia á aglomeración e mellor dispersión dende o dispositivo de inhalación, alcanzando a mesma zona de depósito nas vías respiratorias. Para conseguir tamaños de partícula axeitados, escolleuse a impresión por inxección de tinta térmica, que supón unha tecnoloxía reproducible, automatizada e que permite a produción de pingas de tamaño micrométrico a partir dunha disolución (tinta), que neste caso foi unha disolución de alxinato e se realizou sobre un baño de xelificación contendo cloruro cálcico 0,5 M para realizar o entrecruzamento do alxinato.

A impresión dunha disolución polimérica para a fabricación de xeles está limitada principalmente pola súa concentración. É necesaria unha determinada concentración para que a disolución poida xelificar, e á vez a concentración non pode ser moi alta xa que a disolución sería moi viscosa e dificulta a súa capacidade de impresión. Para determinar o rango de concentracións que permiten a xelificación, probouse a elaborar partículas de xel por goteo de distintas disolucións de alxinato. Determinouse que xelificaban disolucións de alxinato superiores ao 0,25% en peso. Tamén se determinou o rango de concentracións de alxinato que podían imprimirse, estando este comprendido entre o 0,25 e o 0,35% en peso. En canto ao cambio de disolvente previo ao secado supercrítico, observouse que ao facer o cambio directamente a etanol en lugar de facelo a través de dilucións seriadas de etanol/auga, mantívose mellor a esfericidade das partículas de aeroxel resultantes.

As propiedades texturais das partículas analizáronse mediante técnicas de adsorción-desorción de nitróxeno e picnometría de helio. A apariencia e morfoloxía das partículas observouse mediante microscopía electrónica de barrido SEM e FIB-SEM, e con análise de imaxe obtivéronse as distribucións de tamaño de partícula. As partículas con maior esfericidade e homoxeneidade obtivéronse a partir da disolución de alxinato ao 0,35% en peso, polo que foi a concentración elixida para realizar a carga

de fármaco. Ditas partículas presentaron unha superficie específica de 180 $m^2/g$, con diámetro medio de poro no rango do mesoporo (17,8 nm). As microsferas presentaron unha apariencia pulverulenta, cunha densidade aparente de 0,013 $g/cm^3$ e porosidade de 97,7%. O diámetro aerodinámico medio situouse en 2,4 µm, o cal entra no rango para administración pulmonar local (2–5 µm).

Para a carga do sulfato de salbutamol, empregouse un baño de xelificación contendo, ademais do cloruro cálcico, sulfato de salbutamol ao 0,35% en peso. A carga final do salbutamol nas esferas foi do 7,8% en peso, e a presenza do fármaco confirmouse mediante espectroscopía infravermella. O ensaio de cesión realizouse en células de Franz en PBS a pH 7,4 (37 °C, 100 rpm). Nos primeiros 15–30 min produciuse unha liberación rápida do fármaco (aproximadamente un 10%), seguida dunha liberación sostida durante as seguintes 10 h. Tamén se realizou a cesión en PBS pH 5,2 para simular a acidose respiratoria que se pode producir durante un episodio de asma, obténdose un perfil de cesión similar. A liberación controlada do sulfato de salbutamol observada para esta formulación pode ser especialmente interesante para manter controlados os episodios nocturnos de asma cunha única administración.

Por último, realizáronse ensaios de simulación de deposición das partículas cargadas con sulfato de salbutamol no pulmón, coa axuda dun impactador en cascada de 7 etapas e un inhalador de pó seco. As partículas retivéronse na súa maior parte nas primeiras etapas, o cal suxire que unha elevada porcentaxe do pó depositarase nos bronquios unha vez inhalado. A cantidade emitida foi próxima ao 100% da dose pretendida, o cal pon de manifiesto que o pó presenta boas propiedades de fluxo. A fracción de partículas finas foi maior ca noutros sólidos pulverulentos preparados por impresión de tinta, e incluso ca nalgúns produtos comerciais.

USC
UNIVERSIDADE
DE SANTIAGO
DE COMPOSTELA

# ABBREVIATION LIST

ANN, artificial neural networks
API, active pharmaceutical ingredient
APSD, aerodynamic particle size distribution
ASES, Aerosol Solvent Extraction System
ATR-FTIR, Attenuated total reflectance/Fourier-Transform infrared spectroscopy
BA-MDI, breath-actuated metered-dose inhaler
BCS, Biopharmaceutics Classification System
BET, Brunauer-Emmet-Teller
BJH, Barrett-Joyner-Halenda
BSA, bovine serum albumin
CCD, charge-coupled device
CFU, colony-forming units
CLSI, Clinical & Laboratory Standards Institute
COPD, chronic obstructive pulmonary disease
CRD, chronic respiratory disease
DMEM, Dulbecco's modified Eagle's medium
DPI, dry powder inhaler
DSC, differential scanning calorimetry
ECM, extracellular matrix
ED, emitted dose
EE, encapsulation efficiency
EMA, European Medicine Agency
EPOC, enfermedad pulmonar obstructiva crónica
FBS, fetal bovine serum
FDA, US Food & Drug Administration
FGF, fibroblast growth factor
FIB-SEM, focused ion beam-scanning electron microscopy
FL, fuzzy logic
FPF, fine particle fraction
FS, full scale
GAS, Gas Anti-solvent
GI, gastrointestinal
GMP, Good Manufacturing Practices
GMS, glyceryl monostearate
GRAS, generally recognized as safe
hFB, human primary fibroblast
hKC, human primary keratinocyte
HPLC, high performance liquid chromatography
ICH, International Council for Harmonization of Technical Requirements for Pharmaceuticals for Human Use
IL, interleukin
LABD, long-acting bronchodilator
LID, lidocaine hydrochloride
KGF, keratinocyte growth factor
MBC, minimum bactericidal concentration
MHA, Mueller-Hinton Agar
MHB, Mueller-Hinton Broth
MIC, minimum inhibitory concentration
Micro-CT, micro computed tomography

MMP, matrix metalloproteinase
MOC, micro-orifice collector
MRSA, methicillin-resistant *Staphylococcus aureus*
NCL, nanostructured lipid carriers
NGI, next generation impactor
NSAID, non-steroidal anti-inflammatory drug
MSCs, mesenchymal stem cells
PBS, phosphate buffer solution
PCL, poly(ε-caprolactone)
PDGF, platelet-derived growth factor
PDI, polydispersity index
PEG, polyethylene glycol
PET, polyethylene terephthalate
PGSS, Particles from Gas-Saturated Solutions
PLA, poly(lactic acid)
pMDI, pressurized metered-dose inhaler
PMMA, poly(methyl methacrylate)
PSD, particle size distribution
PTFE, polytetrafluoroethylene
RESOLV, Rapid Expansion of a Supercritical Solution into a Liquid Solvent
RESS, Rapid Expansion of Supercritical Solutions
SABD, short-acting bronchodilator
SAL, sterility assurance level
SAS, Supercritical Anti-solvent
SBF, simulated body fluid
sc$CO_2$, Supercritical carbon dioxide
SCF, Supercritical fluid
SD, standard deviation
SDS-PAGE, sodium dodecyl sulphate polyacrylamide gel electrophoresis
SEDS, Solution Enhanced Dispersion by Supercritical
SEM, scanning electron microscopy
SFEE, Supercritical Fluid Extraction of Emulsion
SLN, solid lipid nanoparticle
SLMP, solid lipid microparticle
SMI, soft mist inhaler
SS, salbutamol sulphate
TGF, transforming growth factor
THF, tetrahydrofuran
TIMP, tissue inhibitor of metalloproteinase
TPP, sodium tripolyphosphate
VEGF, vascular endothelial growth factor
WHO, World Health Organization
XRD, X-ray diffraction

# 1. INTRODUCTION



The content in this section was published in part in García-González, C.A., López-Iglesias, C., Concheiro, A., Alvarez-Lorenzo, C. Chapter 16. Biomedical Applications of Polysaccharide and Protein Based Aerogels. In *Biobased Aerogels: Polysaccharide and Protein-based Materials. Green Chemistry Series*; Thomas, S., Pothan, L.A., Mavelil-Sam, R; Royal Society of Chemistry: Cambridge, UK, 2018; pp. 295–323.

USC
UNIVERSIDADE
DE SANTIAGO
DE COMPOSTELA

# 1. INTRODUCTION

Conventional treatments based on systemic administration of drugs are useful when the biodistribution of the drug to the therapeutic target is favorable, which is mainly conditioned by the degree of irrigation of the organs and the permeability of the drug. However, several pathologies may alter drug biodistribution. For example, neurological diseases generally affect the functionality of the blood-brain barrier, making it more permeable to drugs. On the contrary, skin injuries compromise the integrity of the skin and reduce capillary density, so drug access from systemic circulation is hampered. Furthermore, reaching therapeutic drug concentrations in the target region via systemic administration requires higher doses than in local administration, so adverse side effects are more likely to take place. For example, glucocorticoids are frequently used long-term in the treatment of chronic pulmonary diseases, and can cause severe side effects such as osteoporosis, so local administration is often preferred. Also, a fast pharmacological activity is often required in these diseases, so local administration may be more effective than oral administration. In general, local administration allows for adjustment of the dosage and faster activity, avoiding adverse side effects.

## 1.1. Chronic wounds

Skin has a key role in the organism as one of the main barriers against external factors, such as pathogens and chemical agents. It also provides water balance and temperature control to the body. Therefore, when skin injury occurs, several cellular and extracellular pathways are activated to restore tissue integrity and reactivate skin biological functions [1]. In acute wounds, the self-healing process can be solved within several days. However, in chronic wounds the healing process is hampered and remains in the inflammatory phase for prolonged periods of time. Chronic wounds cause a poor quality of life in the patients, since they are often extremely painful and require specialized care and treatment, often causing long hospitalization periods. They also represent a high economic burden to healthcare systems, estimated at 3% of the total health expenditure in developed countries [2]. In Spain, only pressure ulcers represent an estimated cost of 435 million euros per year [3].

### 1.1.1. Physiological wound healing process

The first response of the body to an injury is usually the hemostatic process (Fig. 1.1a), which aims to prevent blood loss. This is mainly achieved by vasoconstriction of

the damaged blood vessels and activation of the clotting cascade and the platelets. Activated platelets adhere to the site of the injury and form a clot to reduce the loss of blood, which is strengthened by fibrin. Activated platelets start segregating substances that participate in the inflammation and healing process, including a high number of growth factors (TGF-α, TGF-β and VEGF among others) and cytokines (IL-1) [4].

The inflammatory phase (Fig. 1.1b,c) usually takes place simultaneously to the hemostatic process, and is mainly aimed to prevent microorganism colonization, as the wound compromises the physiological barrier function of the skin. Vasodilatation around the wound site occurs as a reflex response to tissue hypoxia, to promote the migration of inflammatory cells from systemic circulation to the extracellular space. This inflammation promotes the release of histamine, increasing capillary permeability so white blood cells and fluid (exudate) enter the wound [5]. Neutrophils migrate to the wound site by chemotaxis, and destroy debris and bacteria. Then macrophages infiltrate, phagocyte the neutrophils and segregate growth factors that regulate the inflammatory response, stimulate angiogenesis and enhance the formation of granulation tissue. Afterwards, lymphocytes migrate to the wound, regulating the proliferative stage.

The proliferative phase (Fig. 1.1d) is characterized by the formation of new tissue to replace the damage. Angiogenesis (formation of new blood vessels) takes place, and fibroblasts start the production of granulation tissue, mainly type III collagen and the glucosaminoglucanes of the extracellular matrix (ECM). The wound begins to contract approximately 7 days after the injury.

The remodeling phase (Fig. 1.1e) takes place few days later and for several months until the complete maturation of the scar tissue is achieved. Its duration is dependent on physiological factors (Section 1.1.2.) and the severity of the injury. In this stage, there is a balance between formation and degradation of the scar tissue, and a conversion of type III collagen towards type I takes place, leading to a more organized tissue. Collagenases are metalloenzymes that play a significant role in this step, actively participating in collagen remodeling and degradation. The normal condition of skin is restored after the remodeling phase, although it may not reach 100% of its original elasticity and tensile strength [6]. If there is not a correct degradation of the granulation tissue, a permanent scar may remain in the skin after the complete healing process.

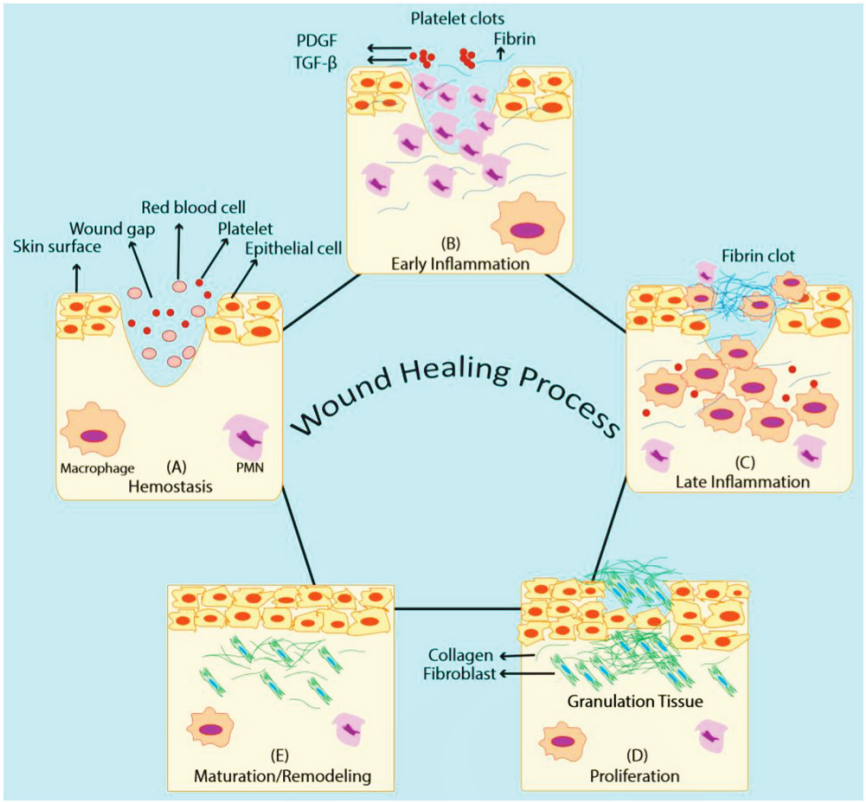


Figure 1.1. Stages of the wound healing process: (A) hemostasis, (B,C) inflammation, (C) proliferation and (D) remodeling. Each stage is regulated by a series of cells and signaling molecules, such as PDGF (platelet-derived growth factor) TGF (transforming growth factor), FGFs (fibroblast growth factors), KGFs (keratinocyte growth factors) ILs (interleukins) or VEGF (vascular endothelial growth factor) [7].
Reproduced from Ref. 7 with permission of John Wiley and Sons.

### 1.1.2. Factors affecting wound healing

The impairment of the healing process can be caused by several factors which are usually divided in two categories: those affecting the specific surroundings of the wound (local/intrinsic) and those affecting the whole body (systemic/extrinsic factors) [8,9].

#### 1.1.2.1. Local factors

The main factors affecting wound healing at a local level are oxygenation, bacterial colonization/infection and wound pH.

The transport of oxygen to the wound site is essential for the healing process [10]. All cells require oxygenation for their correct metabolism, and also leukocytes need it to produce radical oxygen species that play a critical role against microorganisms. When injury occurs, initial hypoxia causes the release of nitric oxide to promote vascularization around the wound and inflammation. Thus, hypoxia leads to impaired healing and susceptibility to infections. Vascular diseases, mainly chronic venous

insufficiency, are the main cause for this hypoxia, with the subsequent apparition of venous ulcers. They are also frequent in long-term embedded or immobilized patients.

The pH of skin is other important factor for the barrier function, since it provides protection against microorganisms and chemical agents. Healthy skin presents an acidic milieu, with a pH ranging from 4 to 6 depending on the anatomical location and age of the individual [11]. When integrity of the skin is disrupted, the blood and extracellular medium become exposed to a physiological pH level of 7.4. Most relevant pathogens need pH values of 6 and above to survive, so the wound becomes especially susceptible to bacterial colonization. Once infection is established, bacteria can secrete substances to adapt their medium towards their specific needs, usually by increasing the pH. Wound pH also plays an important role in the proteolytic activity at the wound, or in the efficacy of certain drugs like antibiotics [12].

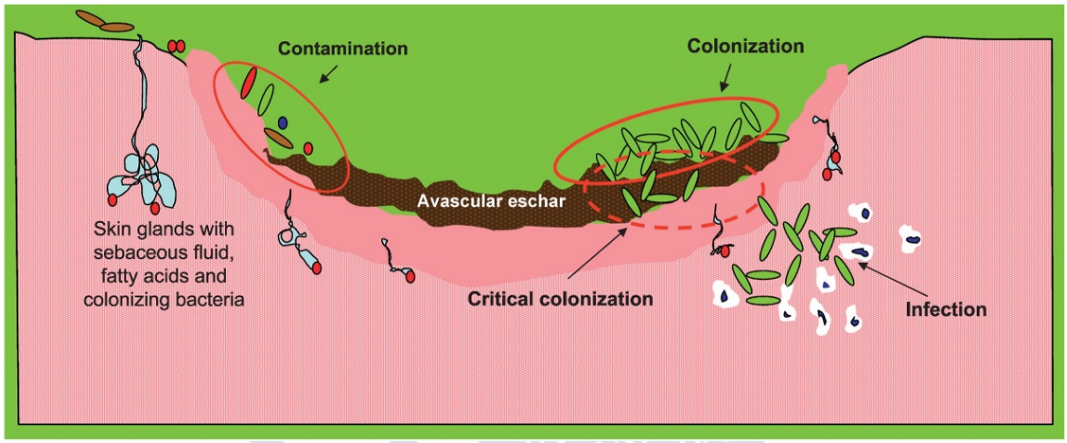


Figure 1.2. Process of formation of infection. The simple presence of bacteria in a wound is known as contamination. These bacteria may start to replicate, forming a larger population but without causing tissue damage, in a process known as colonization. When bacteria begin to invade deeper compartments, breaking through host defenses and causing tissue damage, infection occurs [13].
Reproduced from Ref. 13 with permission of Wolters Kluwer Health, Inc.

As the main barrier against microorganisms is damaged, wounds are very susceptible to bacterial colonization (Fig. 1.2). Infection occurs when these microorganisms start causing tissue damage, and the body increases the inflammatory response. Usually, an excessive amount of exudate is present in infected wounds. Persistent infection causes metabolic changes at a local level, which may aggravate wound repair conditions. For example, the metalloproteinases (MMPs) that degrade collagen in the remodeling phase are overexpressed, and excessively degrade the tissue, hindering the healing process [14]. Some infections can also alter the pH of the wound. Most bacteria can adhere to the surface of the wound or to materials used for wound treatment (e.g., gauzes, hydrocolloids) and form a layer where they can exchange signaling molecules (Quorum Sensing) and interact as a whole new community termed as biofilm [15]. Biofilms are especially difficult to treat, since bacteria coordinate their growth and develop protection against the immune response

and antibiotics. Huge research is developed to prevent biofilm formation [16,17]. This can be attained by different perspectives [18]. On one hand, several drug delivery strategies and combination of therapeutic agents can provide higher bioavailability, precise delivery to infection sites, enhanced safety and reduced risk of bacterial resistance. Moreover, biofilm can be reduced by chemical compounds that interfere with bacterial signaling. Biofilm population can also be killed or dispersed by chemical compounds and electrochemical methods. However, in clinical practice, the best treatment for biofilms in chronic wounds combine a proper debridement followed by antibiotic therapy based on bacteria susceptibility testing [19].

#### 1.1.2.2. Systemic factors

According to the World Health Organization, diabetes is a disease suffered by around 422 million people worldwide, especially in developed countries [20]. It is estimated that around 15% of diabetic patients will develop diabetic ulcers, and within these, between 14–24% will eventually need limb amputations [21]. Global prevalence of diabetic foot ulcers is 5.4–7.3% and in Europe this value is around 5.1% [22]. The incidence of this type of injuries is expected to increase along with the increase in life expectancy of diabetic patients and comorbidity, and implies huge associated costs (only in North America, the cost of diabetic foot ulcers is estimated at 900−1,300 million dollars per year). The formation of chronic leg and foot ulcers in diabetic patients involves a series of complex mechanisms including hypoxia, impaired angiogenesis, dysfunctions in fibroblasts and epidermal cells, high levels of MMPs and decreased immune response and neuropathy, among others [23].

Chronic venous disease affects millions of patients worldwide, especially in the elderly population, with higher predisposition to vascular diseases. In this disease, the endothelial vein wall presents low shear stress, which overexpresses adhesion molecules and activates the endothelium. The infiltration of inflammatory cells such as macrophages and monocytes is thus promoted, leading to the overexpression of MMPs and cytokines, structural changes in the collagen and elastin, and degradation of the ECM. This affects the skin microcirculation, varicose veins appear and the dermis is much more susceptible to suffer ulcers [24].

The metabolic changes that accompany ageing can result in a delayed wound healing in elderly patients. In this case, mechanisms participating in re-epithelialization, collagen synthesis and angiogenesis are delayed, and the inflammatory response is altered with delayed T-cell infiltration, reduced macrophage phagocytosis and altered chemokine production.

Some pharmacological treatments, especially with drugs affecting the immune response, can also alter the healing process. Glucocorticoids, for example, present anti-inflammatory activity and suppression of cellular wound responses when administered systemically. If the wound heals, granulation tissue is usually incomplete

and with lower wound contraction. Apart from inhibiting crucial pathways in the inflammation and proliferation phases, the suppression of the inflammation also renders wounds more susceptible to bacterial colonization and infection. Long-term treatments with other drugs that modulate the inflammatory response, such as non-steroidal anti-inflammatory drugs (NSAIDs), may also inhibit or reduce the healing process [25]. Chemotherapeutic drugs (such as bleomycin or fluorouracil) can also dramatically damage important cellular mechanisms as DNA, RNA or protein synthesis, impairing tissue repair [26].

Nutrition is also highly important for a correct wound healing as the tissue needs to re-synthesize all the structures that were damaged [27]. A correct glucose supply is essential to guarantee that all cells have the ATP needed for their correct metabolism. A good protein intake is also crucial to obtain essential amino acids for protein synthesis. Nutrition is also highly correlated to morbidity as many diseases are caused or worsened by bad nutrition habits (diabetes, obesity). Smoking produces a delayed wound healing and more susceptibility to infection, necrosis or wound rupture, linked to a decrease in the tensile strength of the wounds and scar tissue [28]. Besides this, smoking is also highly correlated to cardiovascular disease. Regular exercise also plays an important factor in the prevention of morbidity.

### 1.1.3. Current approaches in wound healing treatment

The high prevalence of chronic wounds has led to huge research to unveil the biological processes behind the wound healing process as well as to develop strategies for the treatment of the varied mechanisms implicated in the regeneration of the tissue.

Traditionally, the standard clinical practice involves the use of wound dressings (e.g., wound gauzes) that protect the wound from the environment and remove excessive exudate, maintaining an adequate moist environment for the healing process [29]. They are cost-effective and easy to use, but further treatments are needed to assess bacterial infections, inflammation and the removal of excessive tissue. Treatment of infection and inflammation is usually addressed by systemic administration of antibiotics and NSAIDs, respectively. The removal of dead, damaged or infected tissue is known as debridement. It requires specialized professionals and is usually one of the most painful steps for the patients [30].

Traditional dry gauzes (e.g., cotton and polyester gauzes) are inexpensive, but can cause injury when they are removed during debridement [31]. Also, they tend to excessively dry the wound, preventing the autolytic debridement that takes place in the presence of controlled amounts of exudate [32].

Thin films based on polymeric materials appear as alternatives that are comfortable for the patient, since they are flexible and low adherent, minimizing pain

during debridement. They are semipermeable, permitting the exchange of oxygen, water vapor and carbon dioxide while preventing microorganism colonization. However, their limitations in exudate sorption make them inadequate for highly exudative wounds.

Foams present similar characteristics in terms of flexibility and adaptability, and are also highly absorbent.

Hydrogels are swollen in a large amount of water, so they provide moisture to dry or poorly exudative wounds. Their main limitation is their exposure to air, which can evaporate the water causing dehydration of the hydrogel, so another covering layer is often needed.

Hydrocolloids and gel-forming agents are applied to the wound and adopt a gel state upon exudate absortion. This gel is permeable to water and oxygen, providing a moist environment and thermal insulation. The lack of mechanical stiffness of the gel makes it comfortable to remove.

In general, several aspects of the wound (i.e. injured area, moisture, presence of infection, etc.) have to be evaluated in order to select an adequate dressing that adapts to the specific requirements. The use of multilayered systems can meet the requirements of difficult-to-treat wounds as they present several layers that can deal with exudate sorption, drug delivery, etc. [33]. Enhanced diagnostic methods or combinations of materials and sensors that can monitor wound pH, temperature or infection levels are pursued to determine the stage of the wound [34]. The incorporation of these sensors to the clinical practice would be a convenient tool to select the most suitable treatment, improving wound healing and cost-efficiency.

The advent of regenerative medicine has prompted novel strategies for the treatment of chronic wounds. For example, the skin grafting from autologous sources is frequently used in surgical defects and burns. However, the area to be recovered often limits its application. Grafts from other humans (allografts) or from animals (xenografts) can also be used with the associated risks of rejection and infection [35]. Cultured epithelial autografts consist in sheets of keratinocytes from the own patient that can be applied as a permanent skin replacement.

The rise of biomedical engineering has prompted the fabrication of novel skin substitutes, usually made of a combination of biomaterials and active molecules like drugs and growth factors that can stimulate wound healing. Overall, the production and application of these bioprosthetic skin substitutes have high cost, but several studies have determined a high cost-effectiveness when comparing the total cost of wound care [36,37]. In another approach, some marketed products include mesh materials with porcine collagen or polypeptides, extracellular matrix, fibroblasts and autologous keratinocytes isolated from the patient skin biopsies (Keraheal$^{TM}$) [38]. The use of fibroblasts allows for the production of growth factors, collagen, cytokines, and

glycosaminoglycans at a local level, enhancing tissue regeneration [37]. Cell-based therapies, as those based on the use of MSC, are promising in promoting immunomodulation and tissue regeneration, but their isolation and culturing still remains challenging and standardized protocols need to be developed before adaptation to clinical use [39].

In negative pressure therapy, a vacuum is generated at the interface of the wound, removing exudate rich in cytokines and proteins and promoting blood flow to the wound. The negative pressure is usually achieved by attaching an evacuation tube to the wound dressing (usually foams) that applies vacuum. Negative pressure therapy promotes wound closure while reducing the rate of infection [40]. However, wound large areas may limit the applicability of this therapy.

#### 1.1.3.1. Local drug delivery systems used in wound treatment

Processes occurring during wound healing involve the participation of a number of growth factors and cytokines, but in some cases they are imbalanced or insufficient. In these cases, treatments with growth factors, proteins, cytokines and antibacterial agents can improve some physiological stages of the wound healing process. Despite these bioactive agents are traditionally administered systemically, local treatment is proposed to avoid systemic effects, to improve local bioavailability and to achieve a faster response [31]. In particular, local controlled delivery systems provide control of release rate and drug dose at the wound site and protect the drug from degradation by pro-inflammatory cytokines.

Topical antimicrobial agents are applied to superficially infected wounds to target bacterial burden without compromising bacterial sensitivity to the antibiotics, therefore preventing the development of bacterial resistance [41]. Silver binds to bacterial cell membrane and DNA, and interferes with bacterial electron transport, presenting a bactericidal effect. Silver is widely used as an antiseptic for the prevention and treatment of mild infections, formulated into silver-impregnated wound dressings and silver nanoparticles [42]. Low concentrations of povidone iodine or controlled-release iodine formulations are also used as antiseptic agents to provide bactericidal activity against susceptible strains, such as methicillin-resistant *Staphylococcus aureus* (MRSA). Other antimicrobial wound dressings incorporate antibiotic drugs, mostly tetracyclines and aminoglycosides. However, the use of antimicrobial agents at a local level is conditioned by the superficiality of the wound. If deep or systemic infection is suspected, systemic treatment with the pertinent antibiotic must be followed.

Growth factors directly participate in processes like cell migration, division and differentiation, and enzyme and protein production. Thus, they are able to stimulate angiogenesis and cell proliferation, affecting the inflammatory, proliferative and migratory phases of the wound healing process. Several growth factors have been topically applied in wound dressings: TGF-β1, PDGF, human growth hormone, EGF,

FGF, and PDGF, among others. The selection of an appropriate dressing, able to efficiently protect and release the growth factor at the wound site, plays an important role in the efficacy of growth factor therapy.

Other pharmaceutical ingredients clinically used for wound healing promotion include prostacyclin analogues, calcium antagonists, systemic corticosteroids, antioxidants and retinoids. Prostacyclin analogues (iloprost) and calcium antagonists (diltiazem, nifedipine) are useful for the healing of ulcers secondary to connective tissue diseases (rheumatoid arthritis and scleroderma) since they prevent limb necrosis [43]. Systemic corticosteroids promote healing by attenuating the excessive inflammatory response in the short-term use. Antioxidants (zinc) are useful in treating infection. Retinoids such as topical tretinoine improve wound healing by accelerating wound re-epithelialization, due to its effects on angiogenesis, collagen synthesis and epithelialization. Finally, local anesthetics, such as lidocaine, may have a positive effect on wound healing due to pain alleviation and reduced stress response [44].

### 1.1.3.2. Biopolymers used as wound dressings

Biomaterials used for wound healing can be classified according to their origin (natural, semi-synthetic or synthetic) or chemical nature (proteins, polysaccharides, lipids).

Biodegradable natural materials are often chosen for the development of chronic wound dressings due to their good biocompatibility, biodegradation without toxic by-products, and environmental sustainability [45]. Their structure and physicochemical properties can be tuned during the preparation (i.e. fibers, hydrogels) and can confer the ECM support, bind to cell-recognition domains and biomolecule binding sites, and present inherent properties of antimicrobial or anti-inflammatory activity.

Protein-based biopolymers

Collagen is the most abundant protein in animals [46]. It provides mechanical strength to the tissue and stimulates cell-adhesion, migration and proliferation. The use of collagen from animal sources is limited by allergic reaction and pathogen transmission, so collagen produced by heterologous expression in insect, yeast and mammalian cells or by *Escherichia coli* is preferred. Collagen is degraded by matrix metalloproteinases *in vivo*. Multiple collagen-based wound dressings (hydrogels, electrospun fibers, and scaffolds) have been developed to treat ulcers and wound burns, reducing tissue contraction and scarring, and increasing the epithelialization rate. Gelatin is obtained by denaturalization of collagen and presents similar properties, being applied as hydrogel membranes, microspheres, electrospun mats and sponges for tissue engineering.

Silk fibroin used for wound dressings is extracted by the silkworm *Bombyx mori*. Besides biocompatibility and degradability, silk fibroin presents high water and oxygen uptake, low immunogenicity, and robust mechanical properties [47], such as high toughness and elasticity. Different processing techniques have been proposed for silk fibroin scaffolds (sponges, gels, fibrils, foams, etc.), but electrospun fibers have been especially exploited.

Keratins are structural components of important skin structures (nails, hair, wool and feathers) in different animals [48]. They are insoluble proteins with roles of protection and mechanical support. The secondary structure conditions their mechanical resistance, hydration sensitivity and solubility. For wound healing applications, they present excellent biocompatibility, biodegradability and hemostatic properties, and have been formulated as films, hydrogels and sponge scaffolds.

Polysaccharides

Cellulose is the most abundant polymer found in nature. It is a linear homopolysaccharide composed by β-D-glucopyranose units linked by β-1,4 glycosidic bonds [49]. It is obtained from a series of natural sources, such as plants, seaweed, fungi and some bacteria. As most natural polymers, it is biodegradable, non-toxic and biodegradable. Bacterial cellulose is especially interesting for biomedical applications, as it is obtained at great purity levels without the by-products of vegetal cellulose (e.g., lignin, pectin and hemicellulose). Besides its good biocompatibility, it is able to retain moisture and absorb exudates.

Chitosan is a deacetylated derivative of chitin, naturally found in the exoskeleton of crustaceans, the cell wall of some fungi and yeast, and the endoskeleton of some cephalopods. Chitin is widely available, being the second most abundant polysaccharide on earth. It is a linear aminopolysaccharide consisting of units of β-(1-4)-D-glucosamine and N-acetyl-D-glucosamine [50]. Deacetylation of chitin provides chitosan with enhanced hydrosolubility in acidic medium due to protonation of the free amino groups (Fig. 1.3). Besides good cytocompatibility and biodegradability, chitosan presents intrinsic antimicrobial, hemostatic and muco-adhesive properties. The antimicrobial activity of chitosan may rely on the crosslinking between the anions of the bacteria surface and the polycations of the chitosan, which results in the alteration of membrane permeability [51]. Chitosan can be functionalized by a variety of modifications in the free amino groups produced in the deacetylation. It has been widely studied in the form of hydrogels, films, gels, powder and membranes, among others.

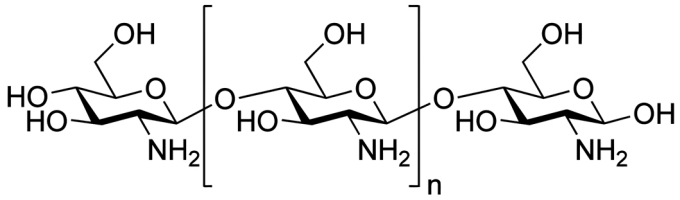


Figure 1.3. Chemical structure of chitosan. The free amino groups are responsible for the solubility of chitosan in slightly acidic solutions.
Source: own elaboration.

Alginate is a linear co-polymer made of units of β-D-mannuronic and α-L-guluronic acid (Fig. 1.4). Its anionic nature allows for its ionic crosslinking with divalent cations. It is produced by some bacteria, although the most abundant source are brown algae species. Alginate is highly hydrophilic, which provide it with high water sorption capacity. Thus, alginate-based wound dressings are able to maintain a moist environment, with reduced bacterial infection [52]. Different forms of materials can be developed from alginate, mainly hydrogels, films, wafers, foams, nanofibers, and topical formulations. Alginate dressings are generally crosslinked by ionic cross-linking with divalent cations (typically calcium). Several alginate-based wound dressings are already in the market (Algicell™, Tegagen™, SeaSorb®, Kaltostat™), but their possibilities in terms of processing methods and combination with other polymeric materials are still being extensively studied.

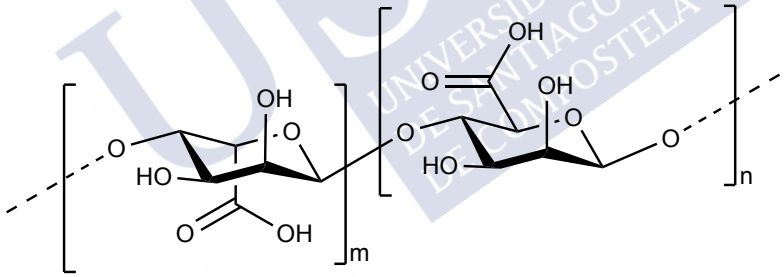


Figure 1.4. Chemical structure of alginate, composed of variable proportions of (m) α-L-guluronic and (n) β-D-mannuronic acid.
Source: own elaboration.

Hyaluronic acid is a glycosaminoglycan consisting of glucuronic acid and N-acetyl-D-glucosamine units [45]. It is highly present in the connective tissue of mammals. It is hygroscopic, so several hyaluronic acid hydrogels have been developed to help keratinocyte migration and angiogenesis, leading to better reconstruction of the damaged area and reduced scarring. This effect is highly dependent on the molecular weight of the hyaluronic acid.

#### 1.1.3.3. Other materials used in wound delivery

Lipid-based systems are widely used in drug delivery due to their affinity with cell membranes [31]. In skin, lipids are the first line of the barrier function, as they are covalently bound to the proteins that coat the layer of corneocytes. In dermatology, lipid nanoparticles received great attention due to their good adhesion to the skin, film formation capacity, and good penetration through the skin barrier. Solid lipid nanoparticles (SLN) and nanostructured lipid carriers (NLC) are able to increase the solubility and stability of active pharmaceutical ingredients, and to increase skin penetration [53]. Solid lipid microparticles (SLMPs) present similar compositions but larger particle sizes. They have been less extensively investigated, but their potential use for topical and transdermal drug delivery has been proposed [54].

## 1.2. Obstructive pulmonary diseases

Chronic respiratory diseases are diseases of the airways and other structures of the lung [55]. Chronic obstructive pulmonary disease (COPD) is an increasing global health problem. According to the World Health Organization, it is estimated that 3.28 million of people die from COPD per year, representing the fourth main cause of death worldwide and around 6% of all deaths. On the other hand, 235 million people suffer from asthma worldwide, and it is a very common chronic respiratory disease among children, especially in low-income and middle-income countries. Bronchial asthma and COPD have similar symptoms, including shortness of breath, cough and sputum, which can lead to improper diagnosis [56]. However, they differ in their pathogenesis, progression of the disease, prognosis and treatment.

### 1.2.1. Physiopathology and treatment strategies

COPD generally appears in older individuals and most patients are passive, former or active smokers [56]. Even if most symptoms are shared with asthma, cells involved in the pathophysiology are different. COPD leads to recurrent infections of the lungs, and eventually the destruction of the lung tissue, with higher mortality than asthma.

The main goals of the treatment strategies for COPD are to decrease the severity of the symptoms, to reduce the risk for exacerbation, to slow the progression of the disease and to decrease mortality [57].

The treatment of COPD is dependent on the patient symptoms and the severity of disease [58]. Nutrition indications, adapted physical exercise, treatment of comorbidities, vaccination if possible, and smoking cessation are among the general measurements that must be taken in every patient [59]. For low-risk patients presenting mild or moderate airflow obstruction and low-grade dyspnea, long-acting bronchodilators (LABDs) such as $\beta_2$-adrenergics (salmeterol, formoterol, olodaterol, vilanterol and indacaterol) and anticholinergics (tiotropium, aclidinium,

glycopyrronium and umeclidinium) are used [57]. These drugs can also provide a reduction in the number of exacerbations since they are used on a regular basis. If the disease is very mild with only a few symptomatic events, short-acting bronchodilators (SABD) such as anticholinergics (ipratropium bromide) and short-acting $\beta_2$-agonists (salbutamol and terbutaline) on demand may be indicated. These drugs are effective in the rapid control of symptoms, being able to reduce occasional symptoms and improve exercise tolerance (in fact, it is considered a doping drug [60]). High-risk patients presenting severe airflow limitation or high-grade dyspnea, need a better diagnosis of the phenotype before selecting the treatment. Dual bronchodilator therapy is a common choice, combining different long-acting beta-agonists with long-acting anticholinergics. Teophylline and derivatives are also used as they present additive effects to common bronchodilators.

A special case of COPD, known as asthma-COPD overlap phenotype, includes higher degree of bronchial eosinophilic inflammation. In this case, the use of inhaled corticosteroids in combination with the usual treatment is highly recommended.

Allergic asthma is characterized by restricted airflow secondary to airway narrowing, wall thickening and increased production of mucus by the reaction to aero-allergens [61]. The chronic inflammation in the airways is caused by plasma extravasation and influx of inflammatory cells such as neutrophils, eosinophils, macrophages, lymphocytes and mast cells. The main characteristic of asthma is its physiological nature, since there is a hypersensitivity of the airways to non-specific stimuli that would produce no effect in healthy individuals.

The treatment of asthma aims at controlling the disease, allowing patients to carry out daily activities including sports without limitations. The treatment strategy has to be individualized to the needs of every patient, taking into account the number of asthma episodes, the moment of the day they appear (nighttime asthma attacks are especially frequent) and their severity [62]. For intermitent asthma, and to prevent asthma attacks during exercise, SABD are used on demand. In mild persistent asthma, glucocorticoids (budesonide, fluticasone, beclometasone) are usually prescribed on a daily basis. An antagonist of the leukotriene receptor (montelukast or zafirlukast) can also be used, and SABD may be used as rescue medication during crisis. Moderate persistent asthma presents similar treatment and includes LABD on a daily basis. Severe types of asthma require treatments with a combination of the aforementioned drugs, sometimes supplemented with oral medication (e.g., glucocorticoids).

## 1.2.2. Drug delivery systems for pulmonary administration

### 1.2.2.1. Devices and formulations

Nowadays, there are more than 250 inhaler devices in the market for the treatment of chronic respiratory diseases [63].

The first inhalation device for the topical delivery of bronchodilators and corticosteroids dates from 1956, when Riker Laboratories invented the first pressurized metered-dose inhaler (pMDI), the Medihaler [64]. In pMDIs, the drug is suspended or dissolved in a propellant with a surfactant and a cosolvent. Propellants are volatile substances (hydrofluoroalkanes) that are gaseous at ambient temperature and pressure, but liquid when cooled or compressed, and are used to carry the drug during inhalation [65]. Surfactants stabilize the drug suspension as they reduce particle aggregation, and are also useful to lubricate the valve of the inhaler. The pMDI device is not breath-actuated, so poor hand-breath coordination may limit the efficacy of the treatment, especially in elderly or pediatric patients [66]. This problem can be overcome by the use of spacers and valve holding chambers.

Breath-actuated metered-dose inhalers (BA-MDIs) are similar to pMDIs, but the system is triggered by the flow of air generated during inhalation, so hand-breath coordination is not required [67]. They are well-tolerated and present high efficacy in the elderly population, since they can be activated even at low airflow rates. As in pMDIs, the drug is suspended in a propellant.

Dry powder inhalers (DPIs) are also activated by the inspiratory flow, but require a higher flow than BA-MDIs [64]. Thus, their efficacy may be limited by the respiratory capacity of older patients or patients suffering an asthma attack. Formulations delivered by DPIs are agglomerates of micronized drug particles, or micronized drug particles adhered to carriers (typically lactose) [68]. In both cases, the micronized drug is de-agglomerated during inhalation, reaching the target region when they present a suitable particle size.

In nebulizers, the drug can be found in an aqueous solution or suspension that is aerosolized in small droplets at high doses that cannot be achieved by DPIs or pMDIs [69]. The aerosol can be produced by different impulses such as a mechanical jet, vibration or ultrasonication. Many nebulizers are connected to face masks, and they are useful in patients with consciousness alterations or patients with difficulties using other inhalers, since they do not require any specific inhalation technique. However, they usually require an external source of energy, need daily cleaning due to risk of bacterial contamination, and require long treatment times [64].

Soft mist inhalers (SMIs) are relatively new, with only one device marketed to date (Respimat®). The drug is in an aqueous solution or suspension (without propellants), and this solution is forced through a complex nozzle that produces two fine jets of

liquid that converge generating an inhalable aerosol cloud (the soft mist). This aerosol presents lower velocity, smaller particle sizes and longer duration than pMDIs, with increased efficacy [70]. However, the volume that is released is relatively low, which limits the drugs that can be incorporated in these devices as they have to present high solubility.

#### 1.2.2.2. Pharmaceutical requirements of the formulations

Particles used for pulmonary delivery must overcome a series of defense mechanisms that the lungs have developed to avoid inhalation of hazardous materials and particles [71]. Apart from the limitation of the capability of the patient to correctly handle the inhaler devices, a correct formulation design is essential to achieve therapeutic success. The main barriers to a successful pulmonary delivery can be classified as chemical, immunological, and mechanical barriers.

If the drug is deposited in the lungs, it should dissolve in lung fluids and either be absorbed for systemic circulation (via the bronchi) or act at a local level (via the alveoli). However, there are factors that can limit drug action. For example, proteolytic enzymes can hydrolyze peptides and proteins leading to their inactivation. Surfactants can prevent the adhesion of particles to the surface of the lung, favoring phagocytation by alveolar macrophages, the main immunological barrier of the pulmonary pathway.

The mechanical barriers are mainly the mucociliary clearance, disease effects and impaction mechanisms on the upper respiratory tract. Mucociliary clearance is a natural defense of the respiratory tract aimed to deliver foreign material out of the lungs. A gel layer of mucus that can trap particles covers a layer of epithelium with cilia that move this mucus towards the oropharynx so it is swallowed or expectorated. In some pulmonary diseases, mucus can be thickened or excessively secreted, and the airways are susceptible to narrowing, which can alter drug absorption.

The respiratory tract consists of the upper (nasal and oropharyngeal), the conducting (tracheobronchial region) and the alveolated (alveoli) airways. Most inhalers deposit most of the dose in the oropharyngeal region via oral inhalation. Even with perfect physiological conditions and inhalation ability, less than 20% of the drug actually reaches the deeper lung (bronchi and alveoli), which is the target region. The place where particles are deposited in the respiratory tract, as well as their deposition mechanism, is highly dependent on their aerodynamic diameter. Aerodynamic diameter ($d_{aero}$) of a particle is defined as the diameter of a sphere of density (ρ) of 1 g/ $cm^3$ that presents the same gravitational settling velocity as the said particle [72]. This parameter is highly dependent on the geometrical diameter (d) and ρ of the particles. Thus, particles with $d_a$ higher than 5 µm will deposit in the oropharyngeal region by impaction mechanisms (Fig. 1.5). Particles lower than 1 µm are likely to suffer a process of diffusion, being suspended in the air and reaching the terminal

bronchiole so they leave the respiratory tract with exhalation. Particles with $d_{aero}$ between 2 and 5 µm will be deposited in the conducting airways, and those between 1 and 2 µm will reach the alveolar region. In both cases, particles will remain suspended in the air enough time to reach the target region, until they are deposited by a sedimentation mechanism.

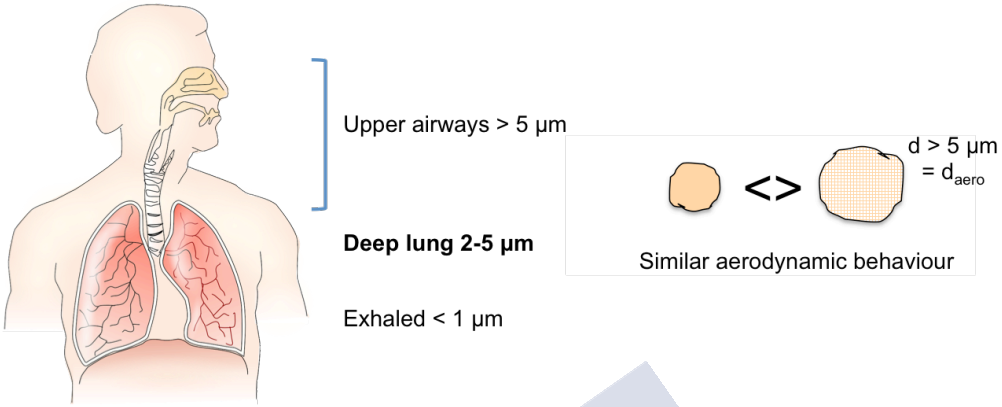


Figure 1.5. Particle deposition in the lungs according to aerodynamic diameter ($d_{aero}$). Large porous particles present similar aerodynamic diameters to non porous particles with smaller geometric diameters (d).
Source: own elaboration.

Alternatively to traditional drug carriers, large porous carriers for oral inhalation are being developed. Increasing the porosity (ε) of the particles decreases their density. This way, larger particles (with larger d) present a similar aerodynamic behavior to smaller, non-porous particles. Large particles have improved flow properties (they are easier to disperse from the inhaler), allow for higher drug loads and are less likely to be phagocyted by alveolar macrophages. High porosity of the particles can be achieved in different particle forms: hollow particles, particles with high internal porosities and agglomerates of nanoparticles (Fig. 1.6) [73].

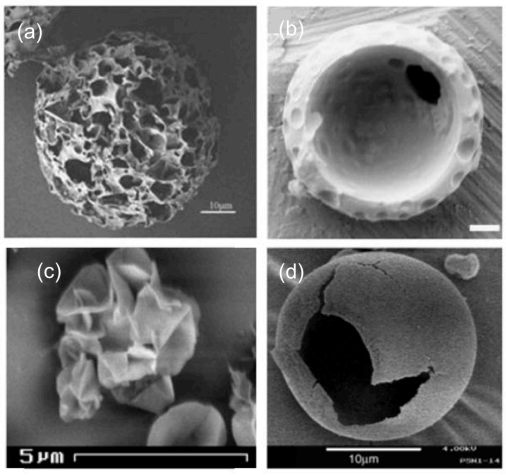


Figure 1.6. Examples of large porous particles: (a) particles with high number of pores; (b) large hollow particle; (c) crumpled-paper particles obtained by spray drying and (d) porous nanoparticle agglomerate [73].
Reproduced from Ref. 73 with permission of Eureka Science (FZC).

## 1.3. Supercritical fluid technology for biomedical applications

Supercritical fluids (SCFs) are a green alternative in many processes that involve the use of organic solvents. Therefore, they have gained importance and interest as solvents and reaction media in the chemical industry [74]. In the food, essential oils and polymer industry, they have been used as solvents in separation and extraction processes. Another major application is supercritical fluid chromatography, widely used as an analytical tool. In the pharmaceutical industry, SCFs have created expectations from the early 1980s, due to their outstanding properties, their environmentally friendly nature and their possibility to reduce the number of processing steps [75].

Moreover, SCFs open up unmet processing possibilities and new application opportunities that cannot be reached with other alternatives, especially for the production and processing of nanostructured materials.

### 1.3.1. Supercritical $CO_2$: Properties and applications

Fluids turn supercritical at conditions of pressure (P) and temperature (T) above their critical point. Under these conditions, the gas-liquid interphase no longer exists, and the fluid presents intermediate properties between the two phases. Supercritical fluids present low surface tension, gas-like diffusivity and viscosity, and liquid-like density that can be easily tuned by pressure and temperature variations.

Carbon dioxide ($CO_2$) is the most commonly used substance in SCF-related processes. It is obtained from a variety of sources, and is inexpensive, non-toxic and non-flammable. All these characteristics have given $CO_2$ the recognition as a GRAS (generally recognized as safe) substance by FDA and EMA, and its use is approved for many industrial processes. $CO_2$ is at supercritical conditions under mild conditions of pressure and temperature, with a critical point of 31.1 °C and 73.8 bar (Figure 1.7).

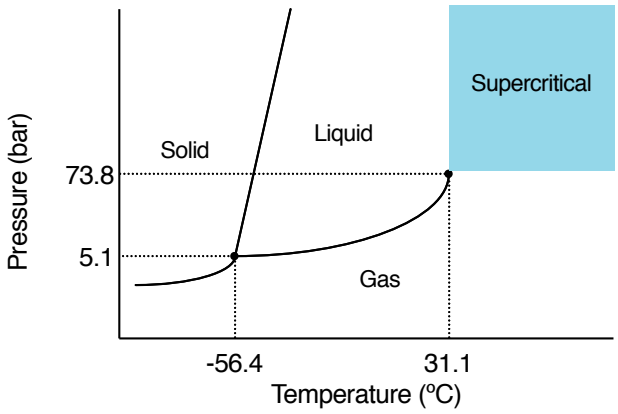


Figure 1.7. Phase diagram of carbon dioxide.
Source: own elaboration.

Supercritical $CO_2$ ($scCO_2$) is able to act as a solvent like many liquids, solubilizing other solvents and pharmaceutical active ingredients. This solvation power can be modified by changes in density. The gas-like high diffusivity can also facilitate mass transfer, with subsequent reduction in processing times. The low surface tension and viscosity (also similar to those of gases) lead to greater penetration into porous solids without causing damage to their microstructure. Furthermore, the low critical temperature allows for the processing of thermally labile materials. Usually, $scCO_2$ operating pressure ranges from 100 to 250 bar, which need high-pressure operating systems that can be safely scaled-up.

The wide possibilities and safety of $scCO_2$ have attracted the attention of several industries in the last decades, as it contributes to the United Nations Sustainable Development goals [76]. It is considered as the greener technology used in the field of food processing [77]. Its solvent capacity promoted its application in the extraction of several components, such as caffeine in decaffeination processes, removal of pesticides and metals from agricultural crops and extraction of essential oils.

SCF technology is a relatively young field and not yet widespread for the biomedical domain. Strict regulatory conditions and safety rules required in pharmaceutical manufacturing limit their application. However, SCF technology can meet the need of pharmaceutical companies to develop production processes with lower environmental impact, avoiding or reducing the use of volatile organic compounds and residues in the final product [75]. Therefore, several approaches have been made using supercritical fluids in processes that find application in several pharmaceutical fields: micronization, drug delivery, tissue engineering, bio-imaging, coating and sterilization. In general, SCF-based manufacturing technologies allow to design micro- and nanoparticles, polymeric membranes, aerogels and microporous foams [78].

### 1.3.2. Supercritical fluids in particle engineering and micronization processes

Particulate systems like micro- and nanoparticles are of increasing interest for drug delivery to the wound site. The encapsulation of bioactive agents in these carriers improves the efficacy, safety, and protection of the drug from the environment, increasing its physicochemical stability. For local delivery, microparticles are often preferred since they are unable to cross biological membranes and remain in the place of application while providing a sustained drug release.

Micronization processes involving supercritical fluids date back to 1879, when Hannay and Hogarth reported that substances dissolved in supercritical fluids under certain pressures precipitated in the form of particles when pressure was released [79]. Later in the 1980s, SCF were applied to induce crystallization of polymers, drugs and substances used in the food industry, and there have been numerous attempts to

adapt the process to the industrial scale. Processing strategies using SCF for particle micronization can be generally classified as those that use the SCF as a solvent (RESS, RESOLV), those where it acts as an anti-solvent (SAS, SEDS, ASES), and as a solute in the PGSS and similar techniques (DELOS, CPCSP) (Fig. 1.8) [75].

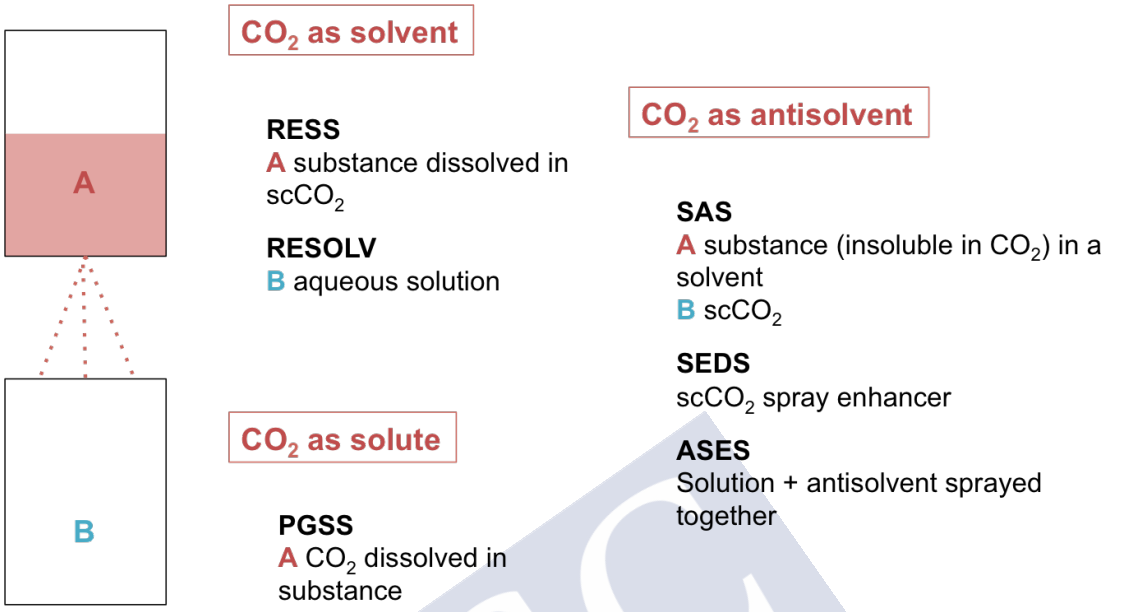


Figure 1.8. Schematic representation of the main processes for the production of micro- and nanoparticles involving supercritical $CO_2$ as a solvent, anti-solvent, or solute. Source: own elaboration.

### 1.3.2.1. Rapid Expansion of Supercritical Solutions (RESS)

In the RESS process, a substance is dissolved homogeneously in a supercritical fluid, and the mixture is rapidly expanded (usually to atmosphere pressure) through a nozzle [80]. Depressurization leads to lower $CO_2$ densities, and eventually to the insolubilization of the substance, causing its precipitation in particles with uniform size distribution. It is an environmentally friendly process, using safe substances under mild conditions and preventing solvent residues. Several substances have been processed by the RESS technique, mainly in the food and pharmaceutical industries. However, solubility of the components in $scCO_2$ is usually limited compared to traditional liquid solvents, requiring very high amounts of $CO_2$. Also, the behavior of solutes in SCFs is difficult to predict, and it would require a huge amount of experimental data in order to model the process.

A variation of this technique is the Rapid Expansion of a Supercritical Solution into a Liquid Solvent (RESOLV), where the supercritical solution is depressurized through a nozzle into an aqueous solution at room temperature [81]. This overcomes the problem of particle agglomeration during the expansion.

### 1.3.2.2. Supercritical Anti-solvent (SAS) processes

In the SAS process, the solute (or solute and carrier) is dissolved in a usual solvent miscible with $scCO_2$, typically alcohols, ketones and dimethyl sulfoxide. The solution is put in contact with the SCF, which extracts the solvent so the drug increases its concentration until it reaches supersaturation conditions and nucleates as micro- or nanoparticles. Additional washing steps are often required to remove the excess of solvent. Other techniques adapted from the SAS processes also make use of $scCO_2$ as an anti-solvent, as the Solution Enhanced Dispersion by Supercritical (SEDS) process, where $scCO_2$ acts both as anti-solvent and spray enhancer, the Aerosol Solvent Extraction System (ASES) or the Supercritical Fluid Extraction of Emulsion (SFEE) technique. In the ASES, the solution and the anti-solvent are sprayed into the precipitation vessel at the same time [75]. The SFEE allows to encapsulate poorly water-soluble drugs; the SCF interacts with the droplets of an oil-in-water emulsion, extracting the oily phase of the emulsion and leading to precipitation of microparticles [82].

### 1.3.2.3. The Particles from Gas-Saturated Solutions (PGSS®) technique

PGSS® technique uses the $scCO_2$ as a solute and high amounts (5–50 wt. %) of $CO_2$ are dissolved at moderate pressures in a molten substance, mainly a polymer, at lower melting temperatures than at ambient pressure. $scCO_2$ presents a plasticizer effect, being able to decrease the melting temperature of the substance by chemical interactions at a molecular level. After a certain contact time, the polymeric mixture is rapidly sprayed through a nozzle into a collector chamber at atmospheric pressure (Fig. 1.9). The fast depressurization causes an intense cooling effect (Joule-Thomson effect) and causes the precipitation of the substance as solid particles in the collector chamber. The morphology, size and apparent density of the particles are dependent on the operating conditions (pressure, temperature and soaking times), physicochemical properties (density and viscosity) of the melted mixture and technical details of the PGSS equipment (vessel sizes and nozzle diameter).

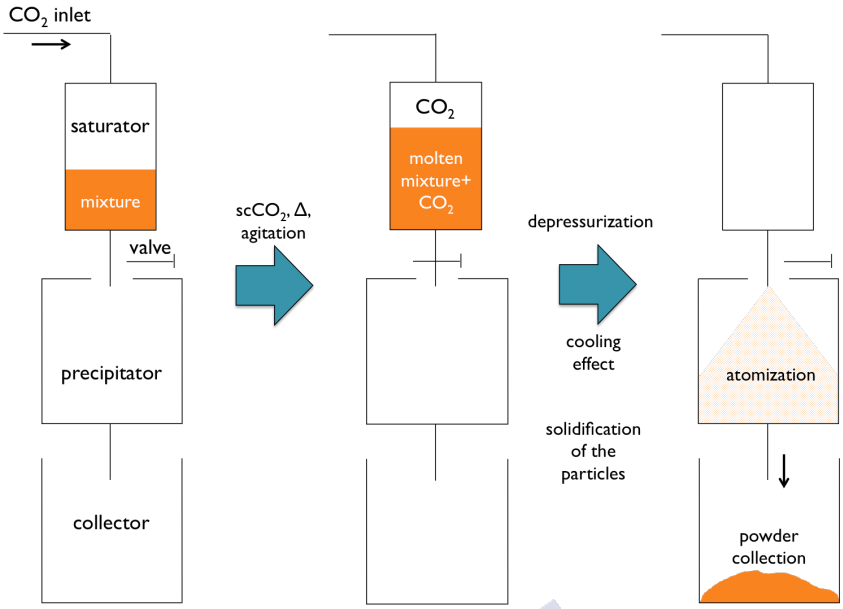


Figure 1.9. Schematic representation of the PGSS process.
Source: own elaboration.

PGSS® is an attractive choice for sensitive molecules, including peptides and proteins, since it can be operated solvent-free and requires relatively mild conditions in the initial melting step due to the plasticizing effect of melting lipid and drug under SCFs. The non-toxic nature of this technique makes it especially attractive for the food industry, and there are plenty of examples for its use in the encapsulation of food additives like antioxidants [83], vitamins [84], essential oils [85], and fatty acids [86], among others.

PGSS technique has been tested for the encapsulation of components of interest for pharmaceutical applications. Hybrid carriers of glyceryl monostearate (GMS), a waxy triglyceride, and silanized $TiO_2$ were processed using the PGSS technique and the incorporation of several bioactive agents (caffeine, glutathione and ketoprofen) was tested [87]. Loading efficiency was dependent on drug solubility, and hydrophobic drugs like ketoprofen were more efficiently loaded than hydrophilic drugs. S-(+)-ibuprofen was encapsulated in Pluronic poloxamers, Gelucire and glyceryl monostearate with high encapsulation efficiencies (> 90%) [88], with a determinant effect of glyceryl monostearate on the drug release behavior. Ibuprofen was also encapsulated in nanoparticles using a modified PGSS process [89]. Perinelli *et al.* proposed a novel technique for the preparation of bovine serum albumin (BSA) microcarriers using the PGSS technique and thus avoiding the usual organic solvent-based preparation methods [90]. An optimization study of the PGSS method based on experimental design was carried out with the purpose to improve the dissolution profile of the drug fenofibrate in Gelucire carriers [91]. The main parameters influencing drug bioavailability were the pressure and temperature of the process, and the drug load in the carriers. Similar results were obtained for the bioavailability of the low water-soluble drugs nifodipine, fenofibrate and o-vainillin in Brij S100 and

PEG4000 carriers processed by PGSS [92]. The addition of small ratios of DMSO may prevent the agglomeration of the particles as reported for the case of curcumin-loaded solid lipid particles with tristearin and soy phosphatidylcholine[93]. PGSS technique is also compatible with incorporation of inorganic nanoparticles [94]. The encapsulation efficiency of copper nanoparticles in glyceryl palmitostearate microparticles was improved to values around 60% when the initial load was augmented, even though the nanoparticles tended to form agglomerates instead of being homogeneously distributed in the lipid matrix [95].

The PGSS-drying is a variation of the PGSS technique where the initial mixture is an aqueous solution. An advantage with respect to other drying processes (such as spray-drying) is that, since the process is carried out in a closed system intertized with $CO_2$, thermal degradation and contamination of the product is reduced [96]. It has been used to encapsulate omega-3 with enhanced stability than conventionally dried powders [86], and to micronize PEG from aqueous solutions with low residual particle contents [97], among other applications.

### 1.3.3. Polysaccharide-based aerogel technology

Aerogels are solid, lightweight and open porous networks of bonded particles or nanoscale fibers that are obtained from the removal of the fluid of a gel without significant structural modifications [98]. Aerogels date back from the early 1930s, when S. S. Kistler reported the successful removal of the liquid component of gels without significant shrinkage of the structure. Aerogels were prepared by Kistler and co-workers from different materials (silica, nickel, gelatin, agar, cellulose) by replacing water with other solvents with low critical temperature [99]. To date, aerogels have attracted interest and found application in several sectors, such as thermal insulation, chemical sensors, catalysis, environmental clean-up and, during the last years, biomedical applications [100].

Aerogels are usually obtained by drying a gel with SCF. They present extremely low densities (≈ 0.003–0.5 g/cm$^3$), high surface areas (≈ 200–1200 m$^2$/g) and high porosities (≈ 80–99.8%) with controlled pore diameters [100]. According to their composition, aerogels can be prepared from a variety of materials, such as metal oxides (silica aerogels are the most studied and applied), polymers, carbon-based materials and transition metals, polysaccharides and proteins. Those prepared with biocompatible and biodegradable materials are specially interesting for biomedical applications as drug delivery systems, ultrasound contrast agents, implantable devices, biosensing and tissue engineering (Fig. 1.10). In this latter case, aerogels provided with high mesoporosities are ideal materials because they present a similar structure to the extracellular matrix.

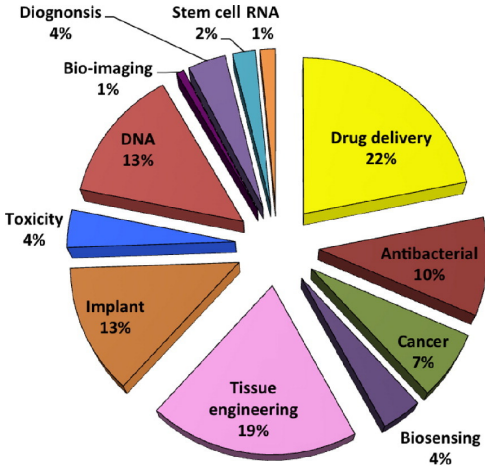


Figure 1.10. Biomedical applications of aerogels found in the literature (adapted) [100].
Reproduced from Ref. 100 with permission of Elsevier.

Usually, aerogel preparation involves four stages: sol preparation, gelation, ageing and drying [101]. In sol preparation, the precursor material is dispersed in a colloidal suspension within a solvent (Fig. 1.11). Gelation occurs when this material is crosslinked, either by chemical or physical methods [102]. Chemical crosslinking usually provides gels with enhanced strength and stability, but residual crosslinking agents in the gel may entail toxicity [103]. During the ageing period, the backbone of the gel is stabilized and mechanical strength is increased. The drying of the gel involves the elimination of the liquid phase, which can be carried out by evaporation of the solvent at ambient pressure, by freeze-drying or by supercritical drying [104].

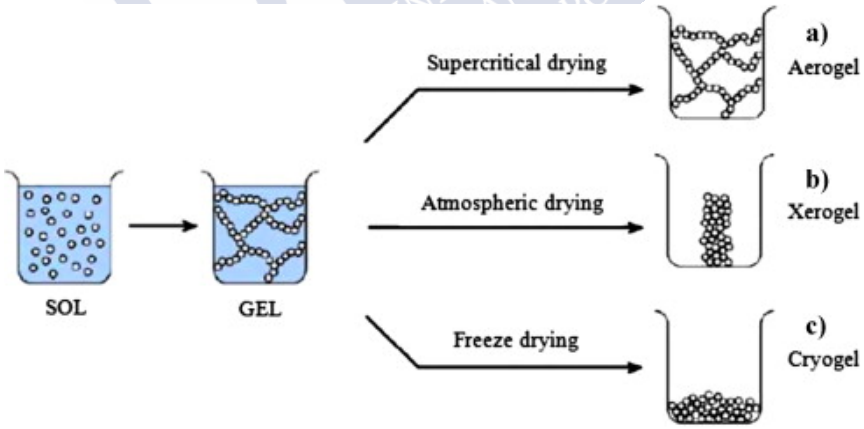


Figure 1.11. For the production of aerogels, first a polymeric dispersion is crosslinked to form a gel, and then the solvent is removed by (a) supercritical drying. This preserves better the polymeric backbone of the gel than atmospheric and freeze drying, that lead to (b) xerogels and (c) cryogels, respectively [105].
Reproduced from Ref. 105 with permission of Elsevier.

Drying at ambient pressure occurs at temperatures ranging from room temperature to 200 °C, and leads to xerogels. It is the simplest method, however, during solvent evaporation capillary pressures are applied on the surface of the aerogel, the pores collapse and the gel shrinks. In freeze-drying, solidification of the

solvent leads to the growth of crystals inside the pores, which alters and may break the porous structure of the gel. Gels obtained by freeze-drying are known as cryogels [106]. In supercritical drying, $scCO_2$ is able to solubilize the solvent and, at the same time, its high diffusivity allows its elimination without surface tension forces, leading to decreased shrinkage. Being water the most common gel solvent, it has limited solubility in $scCO_2$ and cannot be extracted, so it needs to be exchanged to another solvent. This other solvent needs to have high solubility in $scCO_2$ and is selected considering its toxicity, flammability and availability. Common solvents include ethanol, acetone and methanol because they have high solubility in $scCO_2$ or form a supercritical fluid mixture with $CO_2$ under mild supercritical conditions [104].

Polysaccharides are biodegradable natural polymers of special interest due to their high abundance, good biological performance, similar structure to the extracellular matrix and degradability by enzymes naturally present in the body or produced by the intestinal bacterial flora. They are obtained from a variety of sources including human and animal (hyaluronic acid, chondroitin sulfate, heparin, and chitin) or vegetal (alginate, pectin, starch, agar, and carrageenan) origin. Synthetic (chemical and chemoenzymatic) routes to obtain modified polysaccharides (chitosan, polysaccharide conjugates and blends) along with cost-effective production (extraction-purification) techniques to obtain biomedical grade-polysaccharides have spread the use of this family of polymers for life sciences applications. Current and future trends of polysaccharide-containing biomedical products lie in the design of the desired chemical composition to obtain the desired bioactivity, and at the proper physical structure and format (microparticles, nanoparticles, fibers, dressings, macroporous, mesoporous or dual-porous materials) to obtain an advanced physiological and biological response from the product at high performance.

#### 1.3.3.1. Polysaccharide-based aerogels for drug delivery

Bio-based aerogels offer attractive features and the high processing versatility needed for the development of emerging nanostructured drug carriers [100,107,108]. Many polysaccharides and proteins are already components of FDA- and EMA-approved medicines. Indeed, the myriad of bio-based aerogel sources allows the design of carriers with advanced features due to specific drug-carrier chemical interactions, tunable degradation rates or pH-sensitive responses. Moreover, the aerogel processing conditions can be adapted to render tailor-made internal (e.g., specific surface area, overall porosity, density and specific drug loading capacity) and external (particle size and coatings) morphological properties of interest for drug dosage form manufacturing (accurate flow properties for dosing and handling) and functioning (suitable drug release profiles and targeted release) [100,105,108–111].

Bio-based aerogel drug carriers may meet the challenges of oral administration route, notably regarding the biopharmaceutical limitations of poorly-soluble BCS-class

II and IV drugs, and the limited stability against GI tract conditions (enzymes and pH) of proteins and polypeptide drugs [112–115]. The proper formulation design for oral administration would avoid the use of more invasive routes like subcutaneous implantation or parenteral (intravenous, subcutaneous and intramuscular injections) and an enhanced drug dosing precision and longer *in vivo* biological half-life of the active agents.

There is an increasing proportion of new drug candidates that are poorly water soluble due to the advent of more complex molecular entities arising from emerging synthetic technologies and the target-based drug discovery approach [116]. According to the modified Noyes-Whitney equation, the dissolution rate of a drug can be improved by (i) increasing the contact surface area of the drug with the dissolution medium, as well as by (ii) increasing the saturation solubility of the drug in the medium. Both parameters can be properly tuned by encapsulation of BCS-class II and IV drugs in bio-based aerogels.

The outstanding specific surface area of aerogels facilitates the exposition of the loaded drugs to the GI-tract medium, thus improving the drug dissolution rate. The high inner surface area of aerogels would promote long-term stability of the small drug particles (for instance, drug nanocrystals) loaded into the carrier, as well as preventing their agglomeration. The external surface area of bio-based aerogels can also be increased by reducing the aerogel particles size by means of milling or emulsion templating. Drugs can be loaded into aerogels during any of the processing steps of the aerogel preparation, for example the gelation step, the solvent exchange step or the supercritical drying, as well as by postprocessing (e.g., supercritical and liquid $CO_2$ impregnation of aerogels) (Figure 1.12) [117–122]. The gel precursors of bio-based aerogels are usually obtained in the form of hydrogels, for example in an aqueous medium, so the loading of BCS-class II and IV drugs during the gelation step is usually discarded owing to the intrinsic low water solubility of these drugs, which in turn leads to low drug loading content. Alternatively, the direct gelation of polysaccharides in ethanol and containing BCS-class II and IV drugs has recently been reported [123,124]. The loading of the drug in the gels during the solvent exchange is regarded as an auspicious solution in the case of sufficient drug solubility in the solvent coupled to the high drug partition coefficient towards the bio-based gels. Drug encapsulation during supercritical drying is scarcely used due to the low loading yields obtained, as the drying process usually takes place in the continuous mode with a supercritical $CO_2$ flow that may solubilize and extract the drug. Finally, the supercritical impregnation of drugs in aerogels is an interesting postprocessing approach leading to a solvent-free product with high yields and no need of downstream processes. The main drawback of this approach is the need for a certain solubility of the drug in the supercritical medium to reach relevant drug loading in a reasonable timeframe. For any of the abovementioned loading strategies, the chemical groups present in the gel backbone

play a key role in the affinity of the drug for the aerogel matrix and can be tuned by the choice of polysaccharide/protein source or by derivatization.

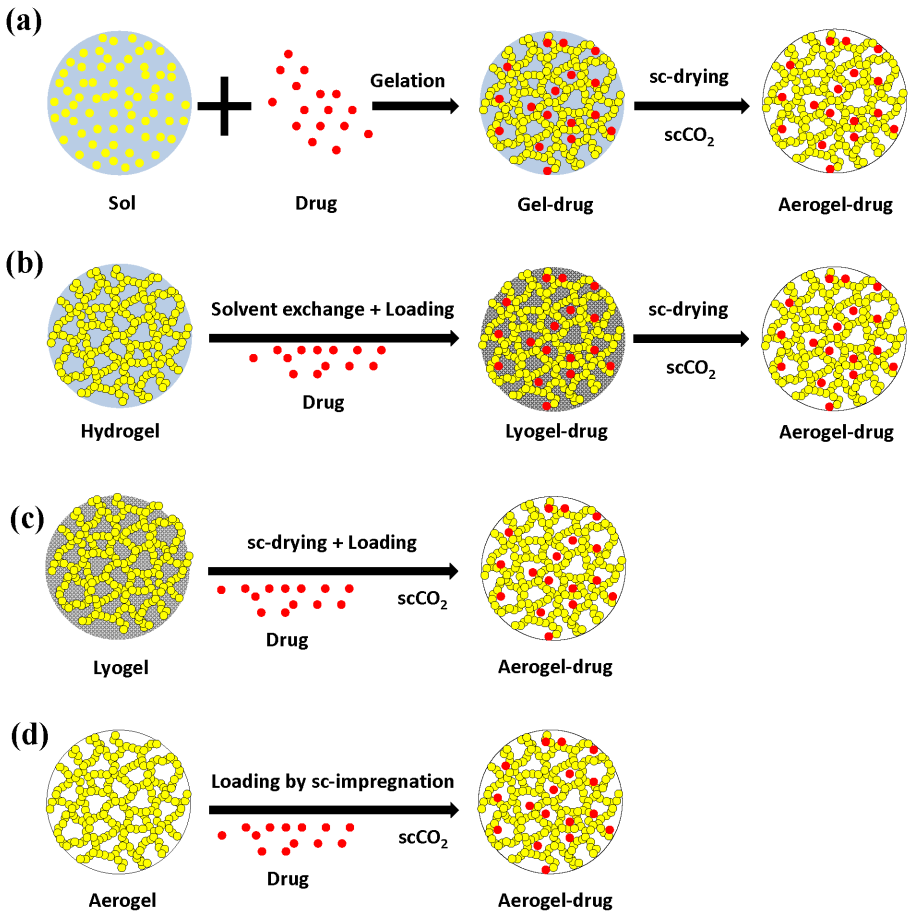


Figure 1.12. Strategies to obtain polysaccharide and protein-based aerogels loaded with drugs: (a) during the sol-gel process (co-gelation); (b) in the lyogel matrix during the solvent exchange; (c) in the lyogel matrix during the supercritical drying process; (d) in the aerogel matrix through supercritical impregnation (post-treatment method) [109].
Adapted from Ref. 109 with permission of Elsevier.

Loading during the solvent exchange step or by supercritical impregnation commonly results in the drug particles being either in the amorphous state or to be nanosized crystals. Although there is still controversy in the literature on the actual crystalline form of the drugs loaded in the aerogels, both approaches give a significant increase in the apparent drug solubility in aqueous media and subsequently drug dissolution becomes faster.

Bio-based aerogels also appear to be efficient tools for the formulation of therapeutic peptides and proteins in oral products. Several critical aspects regarding the delivery of proteins can be likely overcome using this type of nanostructured carrier. The short half-life of peptides in the GI-tract is related to the physicochemical conditions of the physiological medium, as well as the presence of proteolytic enzymes resulting in conformational changes (denaturation) or degradation [114]. The

development of a formulation targeting the lower GI-tract reduces the enzymatic degradation of proteins and peptides. Two strategies for the targeting of bio-based aerogels to the gut have so far been reported in the literature [113,125,126]. The first approach relies on certain bio-based aerogels (pectin, alginate and whey protein) that exhibit pH-dependent drug release (Fig. 1.13) [113]. Namely, pectin, a polysaccharide resistant to the degradation from proteolytic enzymes (such as protease and amylase), may be useful to prepare aerogels that release most of the drug in the colon where pectin would be digested by the local microflora [113,126]. The swelling and degradation rates of pectin aerogels are dramatically affected by the pH (1.2 and 6.5) (Fig. 1.14a) [113]. Pectin source (apple or citrus pectin) also influences both the swelling degree and the degradation rate at simulated intestinal pH conditions; apple pectin releasing the drugs (nicotinic acid and theophylline) faster with *ca.* 90% release after 1 h (Figure 1.14b).

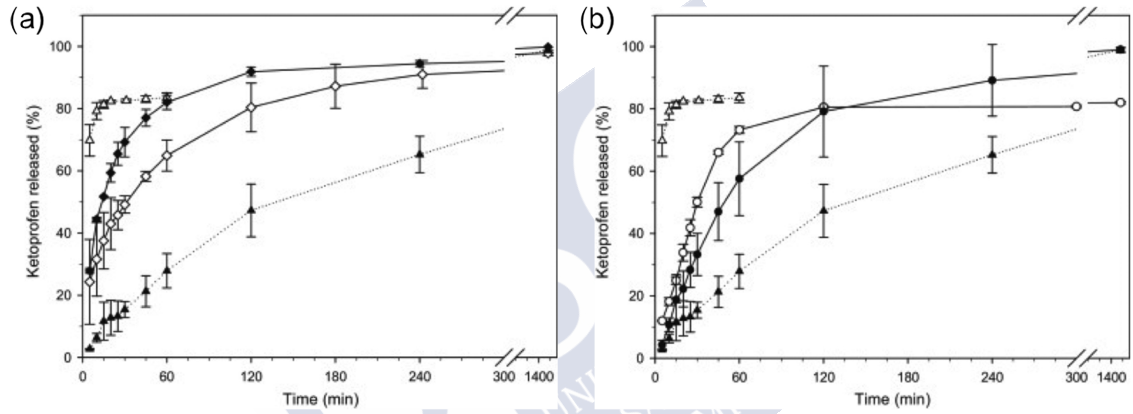


Figure 1.13. Effects of pH and polysaccharide matrix (pectin or alginate) on the release of ketoprofen from polysaccharide aerogels [112]. In vitro release profiles of ketoprofen from (a) alginate (diamonds) and (b) pectin (circles) aerogel microspheres at two different pH media (solid lines). Release studies of the aerogels were carried out at 37 °C and pH 1.2 (0.1 N HCl, dark symbols) and 6.8 (0.1 M phosphate buffer saline solution, blank symbols). Release profiles of the raw ketoprofen (dotted lines) are also plotted for the sake of comparison (dark triangles for pH 1.2 and blank triangles for pH 6.8).
Reproduced from Ref. 112 with permission of Elsevier.

Pectin aerogels in the form of microspheres have been further decorated with magnetic (maghemite) nanoparticles for targeted colonic delivery, with slight modification of the textural properties of the aerogels [126]. The incorporation of magnetic nanoparticles opens up the possibility of *in vivo* directing of the drug carrier to the target tissue with real time tracking by imaging [127]. In a different approach, bio-based aerogels were endowed with protection against the gastric medium by means of a multistep gelation process to obtain multi-membrane spheres or of enteric coatings through an aerogel post-processing method [113,117,125]. The former method would entrap the active pharmaceutical ingredient (API) in the inner layers of the aerogel avoiding burst effects and allowing a more controlled release in the lower GI tract [113,117]. The latter method was tested for starch-alginate aerogel cylinders

coated with polymethacrylates and caused a change of the mechanical behavior of the material from plastic (uncoated) to viscoelastic (coated) and an improvement in stability against humidity.

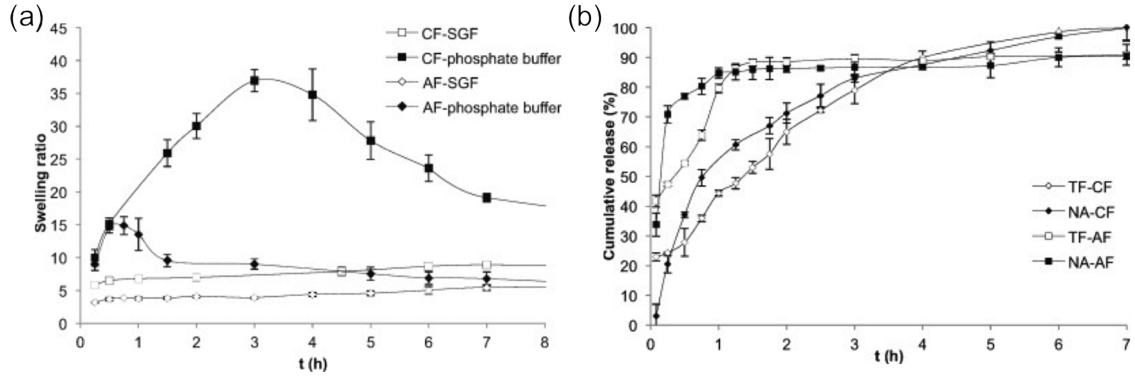


Figure 1.14. Effect of the pectin source (apple -AF- or citrus -CF- pectin) on the use of multi-membrane pectin aerogels for colonic drug delivery [113]: (a) Fluid absorption capacity at two pH conditions (pH 1.2 -SGF-, and 6.5 -phosphate buffer-); (b) Nicotinic acid (NA) and theophylline (TF) release profiles from the aerogels at simulated intestinal conditions (37 °C, pH 6.5).

Reproduced from Ref. 113 with permission of Elsevier.

Overall, bio-based aerogels are quite appealing for oral administration, although there are still some limitations that have to be overcome and challenges that need to be faced. For the targeted release of APIs a new generation of aerogels endowed with smart behavior is still to emerge. Smart aerogels may represent a step-forward from pH-dependent API release to pH-triggered or pH-responsive release. Moreover, the low apparent density of the bio-based aerogels, typically in the range of 0.06 to 0.15 g/cm$^3$, means a relatively low weight of carrier per volume unit. In the case of hard capsules, the standard capsule sizes for human medicines give a serious limitation to reaching body fill weights above 50–100 mg of aerogel carriers (in the specific favorable case where the apparent density is the same as the tapped density). The specific loading capacity of the bio-based aerogels depends on the natural polymer source, the textural properties and the drug-aerogel interactions, and usually ranges from 0.01–0.25 g drug per gram of aerogel. Therefore, the maximum dosing of capsules using aerogels as drug carriers are in the range of 0.5–25 mg of drug, which might not be sufficient for a number of treatments. In the case of tableting of aerogels, the main fact to be tested is the effect of the compression condition on the preservation of the textural properties of the bio-based aerogels. Previous studies with ordered mesoporous silica have shown that mesopores collapse [115,128]. Blending with excipients (e.g., microcrystalline cellulose) before the compression step can mitigate the loss of integrity of the mesoporous material [128]. Moreover, the flow properties of aerogel powders have been scarcely studied, even though they are of utmost importance for the tableting and capsule filling to facilitate the pneumatic transport of the aerogel, to ensure a precise control of the dosing per tablet/capsule,

as well to obtain a proper mixing of the ingredients of the formulation. The effects of the aerogel-containing tablet formulation and of the tableting process itself on the release profile of the drugs loaded in the aerogels have been only faintly studied in inorganic (silica) aerogels [129] and need to be examined. Finally, the storage stability of bio-based aerogels under different ICH climate conditions is still an uncertainty and a critical issue to be assessed for the development of aerogel drug formulations.

Drug-loaded bio-based aerogels may also find applications in orally disintegrating tablets due to the possibility of obtaining prompt drug releases from aerogels, and in floating drug dosage forms because of their low density. The inherent low density and high porosity mean aerogels exhibit high air flowability, which is especially promising for their use as carriers for the delivery of APIs in the respiratory tract, for example the pulmonary administration route by inhalation, and nasal drug delivery. Pulmonary drug delivery can be applied for the treatment of respiratory disorders, but also for systemic absorption [116]. In the former case, targeted drug delivery to the site of action is pursued in order to optimize the therapeutic effect and minimize the untoward effects. Systemic administration using the pulmonary route provides a painless and non-invasive alternative to reach blood circulation due to the high surface area and permeability of the alveolar epithelium to the flow blood supply through the pulmonary arteries, in contrast to intravenous or transdermal injections and implants, and to the low enzymatic activity if compared with the oral administration route.

For inhalation, the aerodynamic particle size plays a critical role in obtaining an optimum aerodynamic particle flow pattern, avoiding inertial impaction in the oropharyngeal region of large particles and the Brownian motion with air entrainment and exhalation of small particles. An optimum median aerodynamic diameter, for example equivalent geometric diameter of a solid sphere with the same aerodynamic diameter as the studied particles, has been proposed to be in the range of 1–5 m m for pulmonary delivery [130,131]. The median aerodynamic diameter is directly dependent on the geometric diameter and to the square root of the particles bulk density. The high porosity of aerogel particles translates into a much lower particle bulk density than that of a solid particle of the same diameter and from the same material, resulting in lower aerodynamic diameters. According to this, a geometric diameter of 2–10 µm has been proposed for aerogel particles to be administered through dry powder inhalers [132]. This larger particle size has a positive effect on the aerogel performance as less particle aggregation is likely to take place. Moreover, the wetting of aerogels when in contact with aqueous fluids in the mucous membrane or pulmonary surfactant present in the lung tissue is dramatically accelerated. Thus, the aerogels readily dissolve due to the effect of capillary forces and the high specific surface area with respect to solid particles of the same mass, resulting in a faster drug access to the blood stream [100,132].

Aerogel powders for inhalation in the 0.5–10 µm range have been prepared by jet-milling and dripping [132,133]. Aerogels were loaded with APIs (salbutamol, insulin, morphine, sildenafil citrate) during the gel solvent exchange to ethanol prior to supercritical drying, this approach being compatible with the use of heat sensitive drugs. Insulin-loaded aerogel powder from derivatized trehalose (a natural disaccharide found in several plants, bacteria, fungi and invertebrate animals) in the 0.5–10 µm particle size range was prepared by sol-gel and supercritical drying, followed by jet milling [132]. Low density (0.001–0.1 g/cm$^3$), *ca.* 95% overall porosity and specific surface areas reaching up to 1200 m$^2$/g have been reported for the trehalose aerogels. The preservation of the biological integrity and the activity of the insulin loaded into these aerogels was confirmed using the SDS-PAGE technique and with insulin receptor transfected NIH 3T3 fibroblasts cell cultures, respectively. Insulin release from the aerogels on simulated mucous membrane was very fast and uniform. Salbutamol-loaded chitosan aerogels were obtained in the form of particles of *ca.* 10 µm size and tapped densities of *ca.* 0.12 g/cm$^3$ by a dripping method of a chitosan solution into a sodium tripolyphosphate (TPP) aqueous bath followed by supercritical drying [133]. The physicochemical stability of chitosan aerogels upon storage was confirmed by a three-month test at 25 °C. Prolonged salbutamol release profiles (PBS pH 7.4) longer than 2 hours and dependent on the chitosan source (molecular weight) and TPP concentration were obtained, it was found that the aerogels are suitable for pulmonary drug delivery intended for the treatment of respiratory disorders.

Dry powder inhalation (DPI) devices seem to be the most straightforward way of administration of aerogels for inhalation [131]. Several DPI device options can be considered (unit-dose, multi-unit-dose or multidose DPI) with the administered dose being dependent on the pre-metered aerogel weight and the specific drug loading per dose. Alternatively, the delivery of the drug-loaded aerogel powder in a room where the patient is located with a total dose dependent on the aerogel concentration in the environment and the exposure duration has been proposed [132].

The nasal administration route is suitable not only for local treatment, but also for systemic delivery, drug delivery to the central nervous system through the nose-to-brain route, and vaccinations [134–136]. Nasal powder sprayers are regarded as suitable devices for the intranasal delivery of biobased aerogels. For these devices, the particle size of solid powders should be in the range of 10–50 µm, these being the lower and upper limits defined by the risk of pulmonary deposition of the powders and by the deposition in the anterior nasal cavity with poor absorption properties, respectively [137]. This aerodynamic diameter range translates into a geometric diameter range of 20–100 µm for highly porous materials such as aerogels. The processing of several bio-based aerogels with sizes in this range by means of emulsion-gelation techniques has been reported in the literature [105,107,112,138]. This approach provides not only a fine control on the particle size distribution of the

aerogel microspheres, but also a regularity in the shape and dimensions, which is important for obtaining reproducible aerodynamic flow profiles. Interestingly, the inherent gel-forming capacity of the polysaccharides and proteins used as aerogel sources is commonly aligned with mucoadhesive properties [139,140]. Mucoadhesion may prolong the residence time of the drug-loaded aerogel powder in the nasal cavity through attachment onto the nasal mucous layer and through the holding back of mucociliary drainage. The mucoadhesion of certain bio-based aerogels (alginate containing aerogels) to porcin mucin was confirmed through turbidimetric analysis [138]. The cytotoxicity of alginate-based aerogels loaded with ketoprofen, and transmucosal transport of the drug payload through the nasal epithelium have been evaluated [141]. RPMI 2650 cells were used as the best *in vitro* model alternative to excised human nasal mucosa tests (i.e. *ex vivo* model), which is the current common practice, and showed similar results regarding permeability for sodium fluorescein, as well as transepithelial electrical resistance and mucus production. Direct contact studies of ketoprofen-loaded aerogels onto the cells showed not only an absence of cytotoxicity after a one-hour incubation, but also an enhancement in the drug permeation with respect to the pure drug. Polysaccharide aerogel microspheres were loaded with a kyotorphin derivative, a neuropeptide showing analgesic behaviour of interest for nasal delivery [138,142]. An encapsulation efficiency of the kyotorphin derivative of *ca.* 80% was obtained by incorporation of the peptide into the aerogel matrix during the gelation process, although the stability and retained activity of the peptide in the aerogel were not reported [138].

#### 1.3.3.2. Bio-based aerogels for tissue engineering

Tissue engineering has been denoted as a multidisciplinary field aiming at orchestrating the trinomial combination of stem cells, resorbable scaffolds and bioactive molecules [143]. Namely, scaffolds can be used to engineer the tissue regeneration under two different strategies: (i) as an *in vitro* cell support for ulterior transplantation, and (ii) as a support to promote *in vivo* cell colonization and tissue growth. Nanostructuration of materials opens novel process windows in scaffolds architecture. On the other hand, materials from bio-based sources may favour cytocompatibility and biomimetic designs of the grafts. Thus, the use of nanostructured bio-based materials in the form of aerogels is an auspicious solution to merge the advantages from both nanostructuration and natural materials domains (Fig. 1.15) [100,144–148].

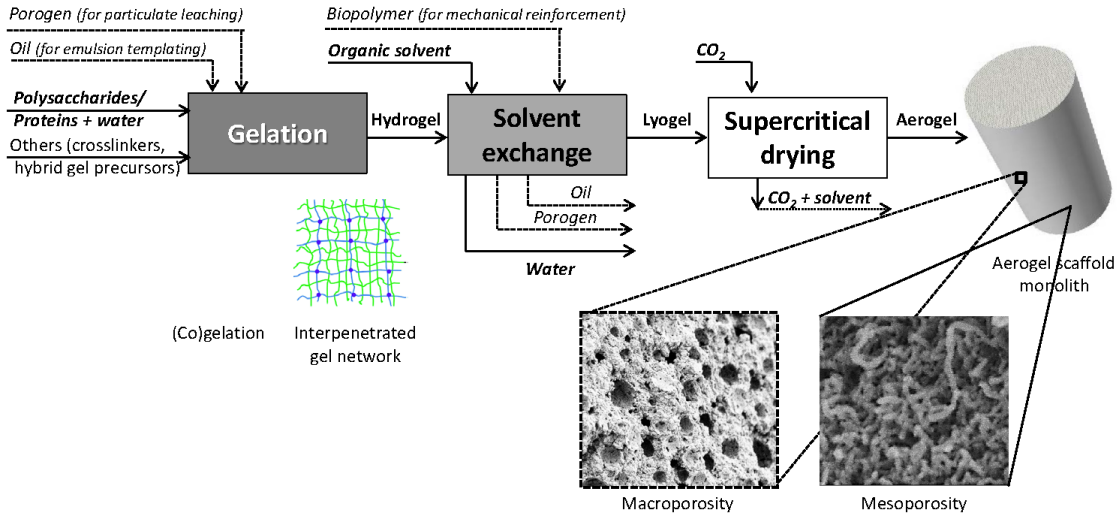


Figure 1.15. Bio-based aerogel scaffold processing steps: gelation, solvent exchange and $scCO_2$-assisted drying of gels [149]. Gelation step can occur from a single or multiple gel precursors. For multiple gel precursors, the gelation mechanism can be cogelation or interpenetrated gel network formation. The resulting aerogel scaffolds in the form of monoliths (roght) have a high porosity formed by interconnected mesopores. Alternatively, advanced properties (macroporosity, mechanical reinforcement) can be conferred to the aerogel scaffolds by combining with other techniques (dashed arrows) during the processing. Emulsion templating or particulate leaching can be used to obtain aerogel scaffolds with interconnected macroporosity (dashed square) by incorporating a hydrophobic dispersed phase and a solid porogen during the gelation step, respectively. The mechanical reinforcement of the aerogel scaffolds can be achieved by impregnation of the aerogels with a biopolymer during the solvent exchange step.
Reproduced from Ref. 149 with permission of the Royal Society of Chemistry.

High porosity, full pore interconnectivity and presence of mesopores are important features of aerogel scaffolds to promote cell attachment, angiogenesis and transport of nutrients and wastes for tissue repair. Moreover, bioactivity and cell proliferation capacity have been also claimed for certain bio-based aerogels [150–153]. Despite using potentially cytotoxic organic solvents during aerogel production, the supercritical drying process has been proven to be effective enough to reduce residual solvents to non-cytotoxic levels. Finally, aerogels processed to be used in tissue engineering need to reach the SAL-6 sterility conditions, meaning a possibility in a million of a microorganism survival, as required by regulatory agencies for terminal sterilization. The sterilization of aerogels can be quite straightforward if sterile conditions are preserved during the supercritical drying of the alcogel precursor. If sterilization is still needed, only the external outer surface of the aerogel has to be sterilized since the pore size of aerogels (i.e. 2–50 nm mesoporous range) is lower than the microorganisms size (> 0.21 µm) thus avoiding their penetration into the aerogel network.

Processing of aerogel scaffolds is a technological approach able to have a high control on the purity and the micro- and macrostructure of the material as well as to operate under milder conditions compared to other conventional methods like solvent casting, melt molding, or electrospinning. Bio-based aerogel scaffolds are obtained through methods where temperature conditions can be below 45 °C during the whole process, no additional downstream processes are necessary for purification, and the use of organic solvents can be minimized [107,145]. Moreover, $CO_2$ and organic solvents can be recycled and reused for the sake of process integration and economics. Several attempts have been carried out to optimize the supercritical drying step regarding pressure, temperature and time. From an economical point of view, these three processing parameters should be kept at a minimum value [105,151]. Nevertheless, the feasible operating region to get optimum textural properties should be accordingly established for each bio-based aerogel system. As an example, the rule-of-thumb of overestimating the processing time for supercritical drying has been reported to be detrimental for starch aerogels because of the removal of structural water from the aerogel backbone [105]. On the contrary, the underestimation of the supercritical drying time can lead to poor textural properties and aerogels with solvent contents that can be toxic for living cells. Supercritical processing time can also have an impact on the removal of the excess of cytotoxic crosslinkers in the case of bio-based aerogels obtained from chemically cross-linked hydrogels [154,155].

Bio-based aerogels can undergo intermediate processing methods to promote osteointegration. Bio-based hybrid aerogels obtained by co-gelation or interpenetration of components improve the biological properties of the resulting nanoporous material [155–157]. Chemical modifications of bio-based aerogels for bone and cartilage implants, such as derivatization with phosphate groups or oxidation, can promote the bioactivity and resorption of the material [158,159]. Nevertheless, the main biological limitations on the use of aerogels in tissue engineering are related to the intrinsic lack of macroporosity needed to promote cell colonization, proliferation and angiogenesis. Several approaches are reported in the literature to confer macroporosity to the scaffolds with certain limitations in the simultaneous control of pore particle size, overall macroporosity and pore interconnectivity [145,156,160].

Emulsion templating has been explored to obtain starch aerogel cylindrical monoliths ($L$ = 30 mm; $D$ = 6 mm) containing round and interconnected macropores of *ca.* 15 µm [145]. In this approach, oil-in-water emulsions in which the continuous aqueous phase undergoes gelation of the polysaccharide and the dispersed phase forms oil droplets are used. After solvent exchange and supercritical drying, the continuous and dispersed phases become the aerogel backbone and the macroporosity of the scaffold, respectively. This method was extended to cellulose aerogels, which showed an anisotropic distribution with interconnected macroporosity

in the 100–350 µm range and representing 62% in volume (Fig. 1.16) [161]. The resulting cellulose aerogel with macropores had a Young's modulus of 2.47 MPa and lower yield stress at 1% strain than the cellulose aerogel without macropores. The results obtained are rather promising, although further research on the effect of the processing parameters is needed. The optimization of this processing approach should lead to a better control of the macropore size distribution, as well as on the control of the overall macroporosity.

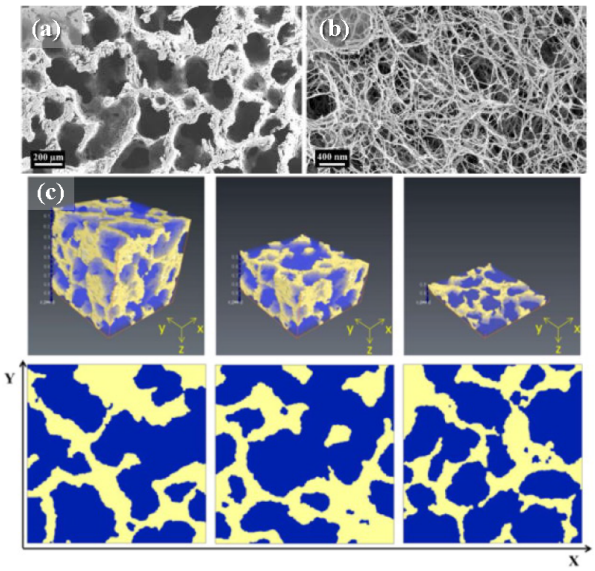


Figure 1.16. Macroporous cellulose aerogel scaffolds obtained by emulsion templating [161]: SEM pictures showed that the material (a) had interconnected macroporosity as well as (b) mesoporosity; (c) micro-CT images confirmed a uniform macroporosity all along the unit cell measured.
Reproduced from Ref. 161 with permission of Elsevier.

Incorporation of porogens during gelation followed by particulate leaching has been introduced as an alternative method to confer macroporosity to bio-based aerogels [150,162]. As an example, a bed of porogen particles (paraffin or PMMA) of selected particle sizes was formed as a negative template by thermal fusion, and then the voids of the bed filled with a solution containing the cellulose aerogel precursors. After gelation of the cellulose, the porogen was removed by leaching with an organic solvent (THF for paraffin and acetone for PMMA) and aerogels were obtained by supercritical drying. Cellulose aerogels containing interconnected macropores in the size range of the paraffin particles, with 98% porosity and Brunnauer-Emmett-Teller (BET)-specific surface areas in the 136–243 $m^2/g$ range were thus obtained (Fig. 1.18). Results showed low fibroblast viability for cellulose aerogels obtained from paraffin porogen and close to 100% for those from PMMA porogen. A certain cracking of the gel network upon the porogen leaching was noticed in the case of PMMA porogen.

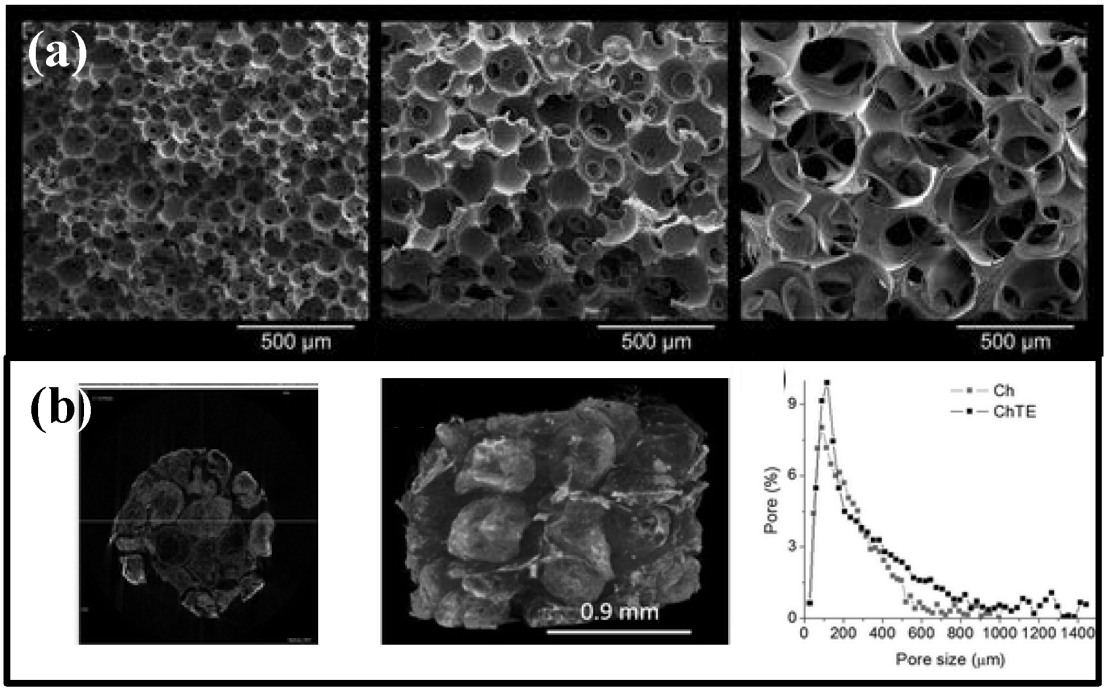


Figure 1.17. Strategies to obtain macroporous aerogel scaffolds [162,163]: (a) Leaching of porogen particles (paraffin spheres) of increasing diameter (from left to right) led to larger macropores; and (b) agglomeration of chitin gel microspheres led to aerogel scaffolds (left and centre) of the controlled macropore size (right).
Part a reproduced from Ref. 162, published under the terms of the Creative Commons BY license. Part b reproduced from Ref. 163 with permission of the Royal Society of Chemistry.

Macroporous aerogels were also attempted by means of the agglomeration of (chitin) gel microspheres followed by supercritical drying [163]. Fusion of the adjacent gel microspheres was promoted using gellan gum and the interparticular voids gave rise to the macroporosity of the resulting aerogel scaffold in the 50–200 µm range. Finally, the macroporosity was also obtained in aerogels through the foaming of $CO_2$-induced bio-based hydrogels by a controlled $CO_2$ depressurization rate followed by supercritical drying [156]. After sufficient $CO_2$ immersion time for gelation had elapsed, the $CO_2$ was depressurized at different rates. Slow depressurization rates gave rise to higher macroporosity (up to 31%) and lower macropore sizes than faster depressurization. This technique still needs further research for implementation regarding an increase in macroporosity, a further control of the macropore size and a target of full interconnectivity.

Scaffolds for hard tissue repair can notably benefit from the use of aerogels. In this case, the mechanical properties of aerogel scaffolds should match the requirements of tissue strength loads, for instance large bones [164]. A compressive modulus of pure silk fibroin aerogels increased from 19.5 to 174 kPa as the fibroin content in the original aqueous solution changed from 2 to 6 wt.% [150]. For pure aerogel scaffolds, the effect of the presence of macropores in the aerogel structure on the mechanical properties needs to be compensated. In this case, a mechanical reinforcement of

aerogel scaffolds has been proposed [146,165,166]. In the first approach, bacterial cellulose aerogels were reinforced with synthetic biopolymers (PLA, cellulose acetate, and PMMA) through impregnation during the solvent exchange, followed by anti-solvent precipitation techniques with ethanol or $scCO_2$ and supercritical drying [162,166]. Densities of the reinforced cellulose aerogels linearly increased as the synthetic polymer content increased. Reinforced cellulose aerogels showed similar mechanical compression profiles as the original aerogel, but with increased stiffness and Young's moduli with higher synthetic polymer contents. In another approach, the reinforcement of several bio-based aerogel scaffolds is claimed by a post-treatment consisting on the cross-linking of the fibers forming the aerogel backbone [165]. Unfortunately, no data on the improvement in the mechanical properties were provided.

Finally, the incorporation of growth factors in aerogel scaffolds is usually a cumbersome task, since growth factors are prone to lose activity during the solvent exchange steps and cannot be incorporated by supercritical impregnation postprocessing because of their low solubility in $scCO_2$. Supercritical foaming of synthetic polymers can surpass the abovementioned limitations to get growth factor-loaded scaffolds [167,168]. Supercritical foaming of scaffold formulations incorporating bio-based aerogel powders have thus been proposed [169]. Poly(ε-caprolactone) (PCL) scaffolds processed by supercritical foaming and containing increasing contents of starch aerogel microparticles had an impact on the increase of the scaffold porosity and a decrease in its bulk density. Notably, the presence of starch aerogel particles in the scaffolds significantly improved the size of the throat interconnection between macropores and mesenchymal stem cells (MSCs) infiltration capacity, with a minor decrease in storage and loss moduli.

#### 1.3.3.3. Bio-based aerogels for other biomedical applications

While aerogels are being currently applied in different technological fields, their use in biomedical sciences is still limited. However, interest in their use in health care sciences has been rising recently, and several applications are being studied [100]. In addition to drug delivery and tissue engineering, the excellent physicochemical properties of aerogels make them suitable for other biomedical applications. Bio-based materials such as polysaccharides and proteins are the aerogel sources that demonstrate the best characteristics for application in the human body, since they are biocompatible and stable [100,148].

*1.3.3.3.1. Wound care applications*

As it was mentioned before, wound dressings should stimulate tissue repair, facilitate the action of inflammatory cells, act as a barrier to microorganisms and provide a moist environment while removing the excess of exudate. Aerogels represent a suitable option for wound healing as they are extremely porous materials able to absorb high amounts of aqueous fluids (Fig. 1.19) such as exudates, which would prevent wounds from becoming infected. Specifically, bio-based aerogels have attracted the most interest in this field, due to their high stability, low toxicity, non-allergenic character and good biological performance [123]. During the exudate incorporation, the solid matrix of the polysaccharide or protein aerogel swells, preventing the formation of water-filled pockets that act as a culture medium to bacteria. Moreover, bio-based aerogels usually permit the incorporation of substances that facilitate the process of healing, such as antimicrobial agents.

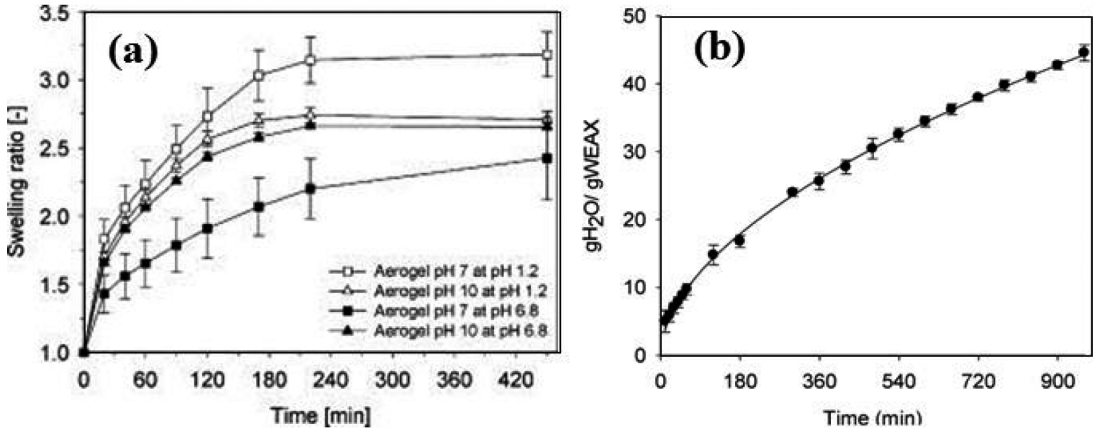


Figure 1.18. Water absorption capacity of bio-based aerogels [170,171]: (a) whey protein, and (b) arabinoxylan aerogels.
Part a reproduced from Ref. 170 with permission of Elsevier. Part b reproduced from Ref. 171, published under the terms of the Creative Common BY license.

Several aerogel materials have been studied as wound dressings. For example, core-shell polysaccharide aerogels were designed to have an amidated pectin matrix and a shell of alginate with the ability to stimulate cytokine production by monocytes [123]. The core was loaded with doxycycline, an antibiotic drug with activity against Gram-positive and Gram-negative bacteria, in order to prevent infection in the wound area. Immersion in simulated wound fluid revealed that fluid uptake was directly related to the polysaccharide content. This fluid uptake was expressed as the weight ratio of the formed hydrogel and the dry aerogel, and reached the value of 8.1 w/w. The doxycycline loaded into the matrix provided a controlled drug release in a simulated wound fluid, with an initial burst effect followed by a slow release for 48 hours.

Chitosan aerogel particles obtained by chemical crosslinking with formaldehyde showed activity against *E. coli* in agar plates and liquid medium [172]. Aerogels prepared with chitosan permit the incorporation of drugs to its matrix and meet the requirements of biocompatibility and stability, being a suitable option to be applied in wound care. On the contary, chitosan-silica hybrid aerogels were shown to be highly hemolytic [173].

Composite aerogels prepared from dialdehyde nanocellulose and collagen by freeze-drying have been evaluated as wound dressings. The aerogels presented high porosity, bulk density and wettability (with a fluid uptake of nearly 40% w/w). Composite aerogels were also tested in terms of biocompatibility and cytotoxicity using a culture of L929 cells in Dulbecco's modified Eagle's Medium for this purpose. The resulting average cell activity was 96.8%, which means the aerogels were biocompatible and suitable for wound dressing applications [174].

Other aerogel-based materials have not yet been specifically studied for wound healing applications, but some of their properties suggest that they could be useful for this purpose. This is the case of water extractable arabinoxylan, which presents a water uptake capability extended for 15 hours [171].

*1.3.3.3.2. Other applications*

In the last few decades, aerogels have gained a great deal of attention as implantable medical devices, ultra-sound contrast agents, and for biosensing, non-invasive imaging and cosmetics. However, there are few research studies that involve protein and polysaccharide-based aerogels with real application in these fields. Most research deals with their biocompatibility and biodegradability, and therefore refers only to their potential application [148].

Starch aerogels have been proposed as an intermediate material for the production of chronic invasive electrodes [175]. Aerogels are ideal materials for invasive electrodes as they present low impedance. In these devices, the starch aerogel particles act as a sacrificial template for the synthesis of an aerogel from an electrical-conducting polymer (PEDOT). PEDOT aerogels did not cause cytotoxicity when tested with fibroblasts and can be useful as a component in invasive metallic electrodes for the electrical stimulation of nerve cells due to the observed significant reduction in the electrical impedance of the electrode with its incorporation.

For other purposes, pectin-based aerogels, where the polysaccharide-based matrix is combined with magnetic nanoparticles (maghemite), may find applications as contrast agents or for magnetic resonance imaging [126].

## 1.4. References


1. Harper, D.; Young, A.; McNaught, C.-E. The physiology of wound healing. *Surgery (Oxford)* **2014**, *32*, 445–450.
2. Posnett, J.; Franks, P. The burden of chronic wounds in the UK. *Nurs. Times* **2008**, *104*, 44–45.
3. Cacicedo González, R.; *Manual de prevención y cuidados locales de heridas crónicas*; Servicio Cántabro de Salud: Santander, España, 2011; pp: 1–223.
4. Barrientos, S.; Stojadinovic, O.; Golinko, M.S.; Brem, H.; Tomic-Canic, M. Growth factors and cytokines in wound healing: Growth factors and cytokines in wound healing. *Wound Repair Regen.* **2008**, *16*, 585–601.
5. Chambers, T.; Bradley, P. Wound Exudate. *Br. J. Nurs.* **2018**, *27*, S28–S32.
6. Xue, M.; Jackson, C.J. Extracellular Matrix Reorganization During Wound Healing and Its Impact on Abnormal Scarring. *Adv. Wound Care* **2015**, *4*, 119–136.
7. Stern, D.; Cui, H. Crafting polymeric and peptidic hydrogels for improved wound healing. *Adv. Healthcare Mater.* **2019**, *8*, 1900104–1900121.
8. Guo, S.; DiPietro, L. Factors Affecting Wound Healing. *Journal of Dental Research* **2010**, *89*, 219–229.
9. Izadi, K.; Ganchi, P. Chronic Wounds. *Clin. Plast. Surg.* **2005**, *32*, 209–222.
10. Castilla, D.M.; Liu, Z.-J.; Velazquez, O.C. Oxygen: Implications for Wound Healing. *Adv. Wound Care* **2012**, *1*, 225–230.
11. Schneider, L.A.; Korber, A.; Grabbe, S.; Dissemond, J. Influence of pH on wound-healing: a new perspective for wound-therapy? *Arch. Dermatol. Res.* **2007**, *298*, 413–420.
12. Percival, S.L.; McCarty, S.; Hunt, J.A.; Woods, E.J. The effects of pH on wound healing, biofilms, and antimicrobial efficacy. *Wound Repair and Regeneration* **2014**, *22*, 174–186.
13. Landis, S.J. Chronic Wound Infection and Antimicrobial Use. *Advances in Skin & Wound Care* **2008**, *21*, 531–540.
14. Ayuk, S.M.; Abrahamse, H.; Houreld, N.N. The Role of Matrix Metalloproteinases in Diabetic Wound Healing in relation to Photobiomodulation. *J. Diabetes Res.* **2016**, *2016*, 1–9.
15. James, G.A.; Swogger, E.; Wolcott, R.; Pulcini, E. deLancey; Secor, P.; Sestrich, J.; Costerton, J.W.; Stewart, P.S. Biofilms in chronic wounds. *Wound Repair Regen.* **2008**, *16*, 37–44.
16. Das, L.; Singh, Y. Quorum Sensing Inhibition: A Target for Treating Chronic Wounds. In *Biotechnological Applications of Quorum Sensing Inhibitors*; Kalia, V.C., Ed.; Springer Singapore: Singapore, 2018; pp. 111–126.
17. Kalia, V.C. Quorum sensing inhibitors: An overview. *Biotechnology Advances* **2013**, *31*, 224–245.
18. Wolfmeier, H.; Pletzer, D.; Mansour, S.C.; Hancock, R.E.W. New perspectives in biofilm eradication. *ACS Infect. Dis.* **2018**, *4*, 93–106.
19. Omar, A.; Wright, J.; Schultz, G.; Burrell, R.; Nadworny, P. Microbial biofilms and chronic wounds. *Microorganisms* **2017**, *5*, 9–23.
20. WHO - "Diabetes." *World Health Organization* 2020.
21. Brem, H.; Tomic-Canic, M. Cellular and molecular basis of wound healing in diabetes. *J. Clin. Invest.* **2007**, *117*, 1219–1222.
22. Zhang, P.; Lu, J.; Jing, Y.; Tang, S.; Zhu, D.; Bi, Y. Global epidemiology of diabetic foot ulceration: a systematic review and meta-analysis. *Ann. Med.* **2017**, *49*, 106–116.
23. Jeffcoate, W.J.; Harding, K.G. Diabetic foot ulcers. *The Lancet* **2003**, *361*, 1545–1551.

24. Raffetto, J.D. Pathophysiology of Chronic Venous Disease and Venous Ulcers. *Surgical Clinics of North America* **2018**, *98*, 337–347.
25. Anderson, K.; Hamm, R.L. Factors That Impair Wound Healing. *J. Am. Coll. Clin. Wound Spec.* **2012**, *4*, 84–91.
26. Gordon, C.R.; Rojavin, Y.; Patel, M.; Zins, J.E.; Grana, G.; Kann, B.; Simons, R.; Atabek, U. A Review on Bevacizumab and Surgical Wound Healing: An Important Warning to All Surgeons. *Ann. Plast. Surg.* **2009**, *62*, 707–709.
27. Barchitta, M.; Maugeri, A.; Favara, G.; Magnano San Lio, R.; Evola, G.; Agodi, A.; Basile, G. Nutrition and Wound healing: An overview focusing on the beneficial effects of curcumin. *Int. J. Mol. Sci.* **2019**, *20*, 1119–1132.
28. McDaniel, J.C.; Browning, K.K. Smoking, chronic wound healing, and implications for evidence-based practice. *J. Wound Ostomy Continence Nurs.* **2014**, *41*, 415–423.
29. Dhivya, S.; Padma, V.V.; Santhini, E. Wound dressings – a review. *BioMedicine* **2015**, *5*, 24–28.
30. Baranoski, S.; Ayello, E.A. Wound dressings: An evolving art and science. *Advances in Skin & Wound Care* **2012**, *25*, 87–92.
31. Saghazadeh, S.; Rinoldi, C.; Schot, M.; Kashaf, S.S.; Sharifi, F.; Jalilian, E.; Nuutila, K.; Giatsidis, G.; Mostafalu, P.; Derakhshandeh, H.; et al. Drug delivery systems and materials for wound healing applications. *Adv. Drug Deliv. Rev.* **2018**, *127*, 138–166.
32. Jones, V.; Grey, J.E.; Harding, K.G. Wound dressings. *BMJ* **2006**, *332*, 777–780.
33. Bishop, S.M.; Griffiths, B.; Linnane, P.G.; Lydon, M.J.; Shaw, H. Multi layered wound dressing. **2010**.
34. Dreifke, M.B.; Jayasuriya, A.A.; Jayasuriya, A.C. Current wound healing procedures and potential care. *Materials Science and Engineering: C* **2015**, *48*, 651–662.
35. Augustine, R.; Kalarikkal, N.; Thomas, S. Advancement of wound care from grafts to bioengineered smart skin substitutes. *Prog. Biomater.* **2014**, *3*, 103–113.
36. Halim, A.; Khoo, T.; Shah, JumaatMohd.Y. Biologic and synthetic skin substitutes: An overview. *Indian J. Plast. Surg.* **2010**, *43*, S23–S28.
37. Han, G.; Ceilley, R. Chronic wound healing: A review of current management and treatments. *Adv. Ther.* **2017**, *34*, 599–610.
38. ter Horst, B.; Chouhan, G.; Moiemen, N.S.; Grover, L.M. Advances in keratinocyte delivery in burn wound care. *Adv. Drug Deliv. Rev.* **2018**, *123*, 18–32.
39. Nourian Dehkordi, A.; Mirahmadi Babaheydari, F.; Chehelgerdi, M.; Raeisi Dehkordi, S. Skin tissue engineering: wound healing based on stem-cell-based therapeutic strategies. *Stem Cell Res. Ther.* **2019**, *10*, 111–130.
40. Schintler, M.V. Negative pressure therapy: Theory and practice. *Diabetes Metab. Res. Rev.* **2012**, *28*, 72–77.
41. Powers, J.G.; Higham, C.; Broussard, K.; Phillips, T.J. Wound healing and treating wounds: Chronic wound care and management. *Journal of the American Academy of Dermatology* **2016**, *74*, 607–625.
42. Wilkinson, L.J.; White, R.J.; Chipman, J.K. Silver and nanoparticles of silver in wound dressings: a review of efficacy and safety. *Journal of Wound Care* **2011**, *20*, 543–549.
43. Enoch, S.; Grey, J.E.; Harding, K.G. Non-surgical and drug treatments. *BMJ* **2006**, *332*, 900–903.
44. Chvapil, M.; Hameroff, S.R.; O'Dea, K.; Peacock, E.E. Local anesthetics and wound healing. *J. Surg. Res.* **1979**, *27*, 367–371.
45. Suarato, G.; Bertorelli, R.; Athanassiou, A. Borrowing From Nature: Biopolymers and Biocomposites as Smart Wound Care Materials. *Front. Bioeng. Biotechnol.* **2018**, *6*, 137–147.
46. Chattopadhyay, S.; Raines, R.T. Collagen-based biomaterials for wound healing. *Biopolymers* **2014**, *101*, 821–833.
47. Farokhi, M.; Mottaghitalab, F.; Fatahi, Y.; Khademhosseini, A.; Kaplan, D.L. Overview of

Silk Fibroin Use in Wound Dressings. *Trends Biotechnol.* **2018**, *36*, 907–922.
48. Li, W.; Gao, F.; Kan, J.; Deng, J.; Wang, B.; Hao, S. Synthesis and fabrication of a keratin-conjugated insulin hydrogel for the enhancement of wound healing. *Colloids Surf B: Biointerfaces* **2019**, *175*, 436–444.
49. Portela, R.; Leal, C.R.; Almeida, P.L.; Sobral, R.G. Bacterial cellulose: a versatile biopolymer for wound dressing applications. *Microb. Biotechnol.* **2019**, *12*, 586–610.
50. Patrulea, V.; Ostafe, V.; Borchard, G.; Jordan, O. Chitosan as a starting material for wound healing applications. *European Journal of Pharmaceutics and Biopharmaceutics* **2015**, *97*, 417–426.
51. Younes, I.; Sellimi, S.; Rinaudo, M.; Jellouli, K.; Nasri, M. Influence of acetylation degree and molecular weight of homogeneous chitosans on antibacterial and antifungal activities. *International Journal of Food Microbiology* **2014**, *185*, 57–63.
52. Aderibigbe, B.; Buyana, B. Alginate in Wound Dressings. *Pharmaceutics* **2018**, *10*, 42–60.
53. de Souza, M.L.; dos Santos, W.M.; de Sousa, A.L.M.D.; de Albuquerque Wanderley Sales, V.; Nóbrega, F.P.; de Oliveira, M.V.G.; Neto, P.J.R. Lipid Nanoparticles As A Skin Wound Healing Drug Delivery System: Discoveries And Advances. *Curr. Pharm. Des.* **2020**, *26*, 4536–4550.
54. Gavini, E.; Albertini, B.; Rassu, G.; Di Sabatino, M.; Sanna, V.; Giunchedi, P.; Rodriguez, L.; Passerini, N. Evaluation of solid lipid microparticles produced by spray congealing for topical application of econazole nitrate. *J. Pharm. Pharmacol.* **2009**, *61*, 559–567.
55. WHO - Chronic respiratory diseases.
56. Yayan, J.; Rasche, K. Asthma and COPD: Similarities and differences in the pathophysiology, diagnosis and therapy. *Adv. Exp. Med. Biol.* **2016**, 910, 31–38.
57. Miravitlles, M.; Vogelmeier, C.; Roche, N.; Halpin, D.; Cardoso, J.; Chuchalin, A.G.; Kankaanranta, H.; Sandström, T.; Śliwiński, P.; Zatloukal, J.; et al. A review of national guidelines for management of COPD in Europe. *Eur Respir J* **2016**, *47*, 625–637.
58. Miravitlles, M.; Soler-Cataluña, J.J.; Calle, M.; Molina, J.; Almagro, P.; Quintano, J.A.; Trigueros, J.A.; Cosío, B.G.; Casanova, C.; Antonio Riesco, J.; et al. Guía española de la enfermedad pulmonar obstructiva crónica (GesEPOC) 2017. Tratamiento farmacológico en fase estable. *Arch. Bronconeumol.* **2017**, *53*, 324–335.
59. Barreiro, E.; Bustamante, V.; Cejudo, P.; Gáldiz, J.B.; Gea, J.; de Lucas, P.; Martínez-Llorens, J.; Ortega, F.; Puente-Maestu, L.; Roca, J.; et al. Guidelines for the evaluation and treatment of muscle dysfunction in patients with chronic obstructive pulmonary disease. *Arch. Bronconeumol.* **2015**, *51*, 384–395.
60. Ventura, R.; Segura, J.; Bergés, R.; Fitch, K.D.; Morton, A.R.; Berruezo, S.; Jiménez, C. Distinction of inhaled and oral salbutamol by urine analysis using conventional screening procedures for doping control. *Ther. Drug Monitor.* **2000**, *22,* 277–282.
61. Boonpiyathad, T.; Sözener, Z.C.; Satitsuksanoa, P.; Akdis, C.A. Immunologic mechanisms in asthma. *Semin. Inmunol.* **2019**, *46*, 101333–101341.
62. GEMA (Guía española del manejo del asma). *Arch. Bronconeumol.* **2009**, *45*, 2–35.
63. Usmani, O.S. Treating the small airways. *Respiration* **2012**, *84*, 441–453.
64. Rogliani, P.; Calzetta, L.; Coppola, A.; Cavalli, F.; Ora, J.; Puxeddu, E.; Matera, M.G.; Cazzola, M. Optimizing drug delivery in COPD: The role of inhaler devices. *Respir. Med.* **2017**, *124*, 6–14.
65. Smyth, H.D.C. The influence of formulation variables on the performance of alternative propellant-driven metered dose inhalers. *Adv. Drug Deliv. Rev.* **2003**, *55*, 807–828.
66. Yawn, B.; Colice, G. Practical aspects of inhaler use in the management of chronic obstructive pulmonary disease in the primary care setting. *Int. J. Chron. Obstruct. Pulmon. Dis.* **2012**, *7*, 495–502.
67. Leach, C.L.; Davidson, P.J.; Hasselquist, B.E.; Boudreau, R.J. Influence of particle size and patient dosing technique on lung deposition of HFA-beclomethasone from a

metered dose inhaler. *Journal of Aerosol Medicine* **2005**, *18*, 379–385.
68. Hoppentocht, M.; Hagedoorn, P.; Frijlink, H.W.; de Boer, A.H. Technological and practical challenges of dry powder inhalers and formulations. *Adv. Drug Deliv. Rev.* **2014**, *75*, 18–31.
69. Laube, B.L.; Janssens, H.M.; de Jongh, F.H.C.; Devadason, S.G.; Dhand, R.; Diot, P.; Everard, M.L.; Horvath, I.; Navalesi, P.; Voshaar, T.; et al. What the pulmonary specialist should know about the new inhalation therapies. *Eur. Respir. J.* **2011**, *37*, 1308–1417.
70. Anderson, P. Use of Respimat soft mist inhaler in COPD patients. *COPD* **2006**, *1*, 251–259.
71. Newman, S.P. Drug delivery to the lungs: challenges and opportunities. *Ther. Deliv.* **2017**, *8*, 647–661.
72. He, Y.; Liang, Y.; Han, R.; Lu, W.-L.; Mak, J.C.W.; Zheng, Y. Rational particle design to overcome pulmonary barriers for obstructive lung diseases therapy. *J. Control. Release* **2019**, *314*, 48–61.
73. Gharse, S.; Fiegel, J. Large porous hollow particles: Lightweight champions of pulmonary drug delivery. *CPD* **2016**, *22*, 2463–2469.
74. Kiran, E.; Debenedetti, P.G.; Peters, C.J.; *Supercritical fluids: fundamentals and applications*; Kluwer Academic Publishers: Dordrecht, Boston, 2000.
75. Pasquali, I.; Bettini, R. Are pharmaceutics really going supercritical? *Int. J. Pharm.* **2008**, *364*, 176–187.
76. Ramsey, E.; Sun, Q.; Zhang, Z.; Zhang, C.; Gou, W. Mini-Review: Green sustainable processes using supercritical fluid carbon dioxide. *J. Environ. Sci.* **2009**, *21*, 720–726.
77. Nautyal, O.H. Food processing by supercritical carbon dioxide - Review. *EC Chem.* **2016**, *21*, 111–135.
78. Chakravarty, P.; Famili, A.; Nagapudi, K.; Al-Sayah, M.A. Using supercritical fluid technology as a green alternative during the preparation of drug delivery systems. *Pharmaceutics* **2019**, *11*, 629–662.
79. VI. On the solubility of solids in gases. *Proc. R. Soc. Lond.* **1879**, *29*, 324–326.
80. Matson, D.W.; Petersen, R.C.; Smith, R.D. Production of powders and films by the rapid expansion of supercritical solutions. *J Mater Sci* **1987**, *22*, 1919–1928.
81. Kankala, R.K.; Zhang, Y.S.; Wang, S.-B.; Lee, C.-H.; Chen, A.-Z. Supercritical fluid technology: An emphasis on drug delivery and related biomedical applications. *Adv. Healthcare Mater.* **2017**, *6*, 1700433–1700463.
82. Lévai, G.; Martín, Á.; Moro, A.; Matias, A.A.; Gonçalves, V.S.S.; Bronze, M.R.; Duarte, C.M.M.; Rodríguez-Rojo, S.; Cocero, M.J. Production of encapsulated quercetin particles using supercritical fluid technologies. *Powder Technol.* **2017**, *317*, 142–153.
83. de Paz, E.; Martín, Á.; Duarte, C.M.M.; Cocero, M.J. Formulation of β-carotene with poly-(ε-caprolactones) by PGSS process. *Powder Technology* **2012**, *217*, 77–83.
84. Praveen Dhakal, S.; He, J. Microencapsulation of vitamins in food applications to prevent losses in processing and storage: A review. *Food Res. Int.* **2020**, *137*, 109326–109339.
85. Akolade, J.O.; Nasir-Naeem, K.O.; Swanepoel, A.; Yusuf, A.A.; Balogun, M.; Labuschagne, P. CO2-assisted production of polyethylene glycol / lauric acid microparticles for extended release of Citrus aurantifolia essential oil. *Journal of CO2 Utilization* **2020**, *38*, 375–384.
86. Haq, M.; Chun, B.-S. Microencapsulation of omega-3 polyunsaturated fatty acids and astaxanthin-rich salmon oil using particles from gas saturated solutions (PGSS) process. *LWT* **2018**, *92*, 523–530.
87. García-González, C.A.; Argemí, A.; Sousa, A.R.S. de; Duarte, C.M.M.; Saurina, J.; Domingo, C. Encapsulation efficiency of solid lipid hybrid particles prepared using the PGSS® technique and loaded with different polarity active agents. *J. Supercrit. Fluid.*

**2010**, *54*, 342–347.

88. Fraile, M.; Martín, ÿ.; Deodato, D.; Rodriguez-Rojo, S.; Nogueira, I.D.; Simplício, A.L.; Cocero, M.J.; Duarte, C.M.M. Production of new hybrid systems for drug delivery by PGSS (Particles from Gas Saturated Solutions) process. *J. Supercrit. Fluid.* **2013**, *81*, 226–235.
89. Chen, W.; Hu, X.; Hong, Y.; Su, Y.; Wang, H.; Li, J. Ibuprofen nanoparticles prepared by a PGSS$^{TM}$-based method. *Powder Technology* **2013**, *245*, 241–250.
90. Perinelli, D.R.; Bonacucina, G.; Cespi, M.; Naylor, A.; Whitaker, M.; Palmieri, G.F.; Giorgioni, G.; Casettari, L. Evaluation of P(L)LA-PEG-P(L)LA as processing aid for biodegradable particles from gas saturated solutions (PGSS) process. *Int. J. Pharm.* **2014**, *468*, 250–257.
91. Pestieau, A.; Krier, F.; Lebrun, P.; Brouwers, A.; Streel, B.; Evrard, B. Optimization of a PGSS (particles from gas saturated solutions) process for a fenofibrate lipid-based solid dispersion formulation. *Int. J. Pharm.* **2015**, *485*, 295–305.
92. Kravanja, G.; Knez, Ž.; Kotnik, P.; Ljubec, B.; Knez Hrnčič, M. Formulation of nimodipine, fenofibrate, and o-vanillin with Brij S100 and PEG 4000 using the PGSS$^{TM}$ process. *The Journal of Supercritical Fluids* **2018**, *135*, 245–253.
93. Pedro, A.S.; Villa, S.D.; Caliceti, P.; Melo, S.A.B.V. de; Albuquerque, E.C.; Bertucco, A.; Salmaso, S. Curcumin-loaded solid lipid particles by PGSS technology. *The Journal of Supercritical Fluids* **2016**, *107*, 534–541.
94. García-González, C.A.; Sousa, A.R.S. da; Argemí, A.; Periago, A.L.; Saurina, J.; Duarte, C.M.M.; Domingo, C. Production of hybrid lipid-based particles loaded with inorganic nanoparticles and active compounds for prolonged topical release. *Int. J. Pharm.* **2009**, *382*, 296–304.
95. Martín, V.; Gonçalves, V.; Rodríguez-Rojo, S.; Nunes, D.; Fortunato, E.; Martins, R.; Cocero, M.J.; Duarte, C. Production of copper loaded lipid microparticles by PGSS ® (particles from gas satured solutions) process. *The Journal of Supercritical Fluids* **2018**, *131*, 124–129.
96. Martín, Á.; Weidner, E. PGSS-drying: Mechanisms and modeling. *J. Supercrit. Fluid.* **2010**, *55*, 271–281.
97. Martín, Á.; Pham, H.M.; Kilzer, A.; Kareth, S.; Weidner, E. Micronization of polyethylene glycol by PGSS (Particles from Gas Saturated Solutions)-drying of aqueous solutions. *Chem. Eng. Process.* **2010**, *49*, 1259–1266.
98. García-González, C.A.; Budtova, T.; Durães, L.; Erkey, C.; Del Gaudio, P.; Gurikov, P.; Koebel, M.; Liebner, F.; Neagu, M.; Smirnova, I. An opinion paper on aerogels for biomedical and environmental applications. *Molecules* **2019**, *24*, 1815–1829.
99. Kistler, S.S. Coherent expanded aerogels and jellies. *Nature* **1931**, *127*, 741–741.
100. Maleki, H.; Durães, L.; García-González, C.A.; del Gaudio, P.; Portugal, A.; Mahmoudi, M. Synthesis and biomedical applications of aerogels: Possibilities and challenges. *Adv. Colloid Interface Sci.* **2016**, *236*, 1–27.
101. Dervin, S.; Pillai, S.C. An Introduction to Sol-Gel Processing for Aerogels. In *Sol-Gel Materials for Energy, Environment and Electronic Applications*; Pillai, S.C., Hehir, S., Eds.; Springer International Publishing: New York, USA, 2017; pp. 1–22.
102. H. Gulrez, S.K.; Al-Assaf, S.; O, G. Hydrogels: Methods of Preparation, Characterisation and Applications. In *Progress in Molecular and Environmental Bioengineering - From Analysis and Modeling to Technology Applications*; Carpi, A.; InTech: London, UK, 2011.
103. Parhi, R. Cross-linked hydrogel for pharmaceutical applications: A review. *Adv. Pharm. Bull.* **2017**, *7*, 515–530.
104. Şahin, İ.; Özbakır, Y.; İnönü, Z.; Ulker, Z.; Erkey, C. Kinetics of supercritical drying of gels. *Gels* **2018**, *4*; 3–31.
105. García-González, C.A.; Camino-Rey, M.C.; Alnaief, M.; Zetzl, C.; Smirnova, I. Supercritical drying of aerogels using CO2: Effect of extraction time on the end

material textural properties. *J. Supercrit. Fluid.* **2012**, *66*, 297–306.
106. Soleimani Dorcheh, A.; Abbasi, M.H. Silica aerogel; synthesis, properties and characterization. *J. Mat Process. Technol.* **2008**, *199*, 10–26.
107. Alnaief, M.; Alzaitoun, M.A.; García-González, C.A.; Smirnova, I. Preparation of biodegradable nanoporous microspherical aerogel based on alginate. *Carbohydr. Polym.* **2011**, *84*, 1011–1018.
108. Ulker, Z.; Erkey, C. An emerging platform for drug delivery: Aerogel based systems. *J. Control. Release* **2014**, *177*, 51–63.
109. García-González, C.A.; Alnaief, M.; Smirnova, I. Polysaccharide-based aerogels—Promising biodegradable carriers for drug delivery systems. *Carbohyd. Polym.* **2011**, *86*, 1425–1438.
110. Ubeyitogullari, A.; Ciftci, O.N. Formation of nanoporous aerogels from wheat starch. *Carbohydr. Polym.* **2016**, *147*, 125–132.
111. Paninho, A.B.; Barbosa, C.; Nogueira, I.D.; Najdanovic-Visak, V.; Nunes, A.V.M. (Ethyl lactate)-gel high pressure CO2 extraction for the processing of mesoporous gelatine particles. *J. Supercrit. Fluid.* **2013**, *83*, 35–40.
112. García-González, C.A.; Jin, M.; Gerth, J.; Alvarez-Lorenzo, C.; Smirnova, I. Polysaccharide-based aerogel microspheres for oral drug delivery. *Carbohydr. Polym.* **2015**, *117*, 797–806.
113. Veronovski, A.; Tkalec, G.; Knez, Ž.; Novak, Z. Characterisation of biodegradable pectin aerogels and their potential use as drug carriers. *Carbohydr. Polym.* **2014**, *113*, 272–278.
114. Muheem, A.; Shakeel, F.; Jahangir, M.A.; Anwar, M.; Mallick, N.; Jain, G.K.; Warsi, M.H.; Ahmad, F.J. A review on the strategies for oral delivery of proteins and peptides and their clinical perspectives. *Saudi Pharm. J.* **2016**, *24*, 413–428.
115. Singh, A.; Worku, Z.A.; Van den Mooter, G. Oral formulation strategies to improve solubility of poorly water-soluble drugs. *Expert Opin. Drug Deliv.* **2011**, *8*, 1361–1378.
116. Hillery, A.M.; Park, K. *Drug Delivery: Fundamentals & Applications*; Hillery, A.M.; CRC Press: Boca Raton, FL, USA, 2017.
117. Veronovski, A.; Knez, Ž.; Novak, Z. Comparison of ionic and non-ionic drug release from multi-membrane spherical aerogels. *Int. J. Pharm.* **2013**, *454*, 58–66.
118. García-González, C.A.; Smirnova, I. Use of supercritical fluid technology for the production of tailor-made aerogel particles for delivery systems. *J. Supercrit. Fluid.* **2013**, *79*, 152–158.
119. Mehling, T.; Smirnova, I.; Guenther, U.; Neubert, R.H.H. Polysaccharide-based aerogels as drug carriers. *J. Non-Cryst. Solids* **2009**, *355*, 2472–2479.
120. García-González, C.A.; Uy, J.J.; Alnaief, M.; Smirnova, I. Preparation of tailor-made starch-based aerogel microspheres by the emulsion-gelation method. *Carbohyd. Polym.* **2012**, *88*, 1378–1386.
121. Marin, M.A.; Mallepally, R.R.; McHugh, M.A. Silk fibroin aerogels for drug delivery applications. *J. Supercrit. Fluid.* **7**, *91*, 84–89.
122. Pantić, M.; Kotnik, P.; Knez, Ž.; Novak, Z. High pressure impregnation of vitamin D3 into polysaccharide aerogels using moderate and low temperatures. *J. Supercrit. Fluid.* **2016**, *118*, 171–177.
123. De Cicco, F.; Russo, P.; Reverchon, E.; García-González, C.A.; Aquino, R.P.; Del Gaudio, P. Prilling and supercritical drying: A successful duo to produce core-shell polysaccharide aerogel beads for wound healing. *Carbohyd. Polym.* **2016**, *147*, 482–489.
124. Tkalec, G.; Knez, Ž.; Novak, Z. Fast production of high-methoxyl pectin aerogels for enhancing the bioavailability of low-soluble drugs. *J. Supercrit. Fluid.* **2015**, *106*, 16–22.
125. Antonyuk, S.; Heinrich, S.; Gurikov, P.; Raman, S.; Smirnova, I. Influence of coating and wetting on the mechanical behaviour of highly porous cylindrical aerogel particles.

*Powder Technol.* **2015**, *285*, 34–43.
126. García-González, C.A.; Carenza, E.; Zeng, M.; Smirnova, I.; Roig, A. Design of biocompatible magnetic pectin aerogel monoliths and microspheres. *RSC Adv.* **2012**, *2*, 9816–9823.
127. Veiseh, O.; Gunn, J.W.; Zhang, M. Design and fabrication of magnetic nanoparticles for targeted drug delivery and imaging. *Adv. Drug Deliv. Rev.* **2010**, *62*, 284–304.
128. Vialpando, M.; Aerts, A.; Persoons, J.; Martens, J.; Van Den Mooter, G. Evaluation of ordered mesoporous silica as a carrier for poorly soluble drugs: Influence of pressure on the structure and drug release. *J. Pharm. Sci.* **2011**, *100*, 3411–3420.
129. Hentzschel, C.M.; Alnaief, M.; Smirnova, I.; Sakmann, A.; Leopold, C.S. Enhancement of griseofulvin release from liquisolid compacts. *Eur. J. Pharm. Biopharm.* **2012**, *80*, 130–135.
130. Fernández Tena, A.; Casan Clarà, P. Deposition of inhaled particles in the lungs. *Arch. Bronconeumol.* **2012**, *48*, 240–246.
131. Dal Negro, R.W. Dry powder inhalers and the right things to remember: a concept review. *Multidiscip Respir. Med.* **2015**, *10*, 13–16.
132. Lee, K.P.; Gould, G.L. Aerogel powder therapeutic agents. *U. S. Pat.* 6994842 B2, 2006.
133. Obaidat, R.M.; Tashtoush, B.M.; Bayan, M.F.; R, T.A.B.; Alnaief, M. Drying using supercritical fluid technology as a potential method for preparation of chitosan aerogel microparticles. *AAPS PharmSciTech* **2015**, *16*, 1235–1244.
134. Mittal, D.; Ali, A.; Md, S.; Baboota, S.; Sahni, J.K.; Ali, J. Insights into direct nose to brain delivery: current status and future perspective. *Drug Deliv.* **2014**, *21*, 75–86.
135. Grassin-Delyle, S.; Buenestado, A.; Naline, E.; Faisy, C.; Blouquit-Laye, S.; Couderc, L.-J.; Le Guen, M.; Fischler, M.; Devillier, P. Intranasal drug delivery: An efficient and non-invasive route for systemic administration: Focus on opioids. *Pharmacol. Ther.* **6**, *134*, 366–379.
136. Illum, L. Nasal drug delivery — Recent developments and future prospects. *J. Control. Release* **7**, *161*, 254–263.
137. Chien, Y.W. *Nasal systemic drug delivery*; Yie W. Chien, Kenneth S. E. Su, Shyi-Feu Chang; Marcel Dekker: New York, USA, 1989.
138. Gonçalves, V.S.S.; Gurikov, P.; Poejo, J.; Matias, A.A.; Heinrich, S.; Duarte, C.M.M.; Smirnova, I. Alginate-based hybrid aerogel microparticles for mucosal drug delivery. *Eur. J. Pharm. Biopharm.* **2016**, *107*, 160–170.
139. Chaturvedi, M.; Kumar, M.; Pathak, K. A review on mucoadhesive polymer used in nasal drug delivery system. *J. Adv. Pharm. Technol. Res.* **2011**, *2*, 215–222.
140. Smart, J.D. The basics and underlying mechanisms of mucoadhesion. *Adv. Drug Deliv. Rev.* **2011**, *57*, 1556–1568.
141. Gonçalves, V.S.S.; Matias, A.A.; Poejo, J.; Serra, A.T.; Duarte, C.M.M. Application of RPMI 2650 as a cell model to evaluate solid formulations for intranasal delivery of drugs. *Int. J. Pharm.* **12**, *515*, 1–10.
142. Tengamnuay, P.; Sahamethapat, A.; Sailasuta, A.; Mitra, A.K. Chitosans as nasal absorption enhancers of peptides: comparison between free amine chitosans and soluble salts. *Int. J. Pharm.* **3**, *197*, 53–67.
143. Sándor, G.K.B. Tissue engineering of bone: Clinical observations with adipose-derived stem cells, resorbable scaffolds, and growth factors. *Ann. Maxillofac. Surg.* **2012**, *2*, 8–11.
144. Duarte, A.R.C.; Santo, V.E.; Alves, A.; Silva, S.S.; Moreira-Silva, J.; Silva, T.H.; Marques, A.P.; Sousa, R.A.; Gomes, M.E.; Mano, J.F.; et al. Unleashing the potential of supercritical fluids for polymer processing in tissue engineering and regenerative medicine. *J. Supercrit. Fluid.* **7**, *79*, 177–185.
145. García-González, C.A.; Concheiro, A.; Alvarez-Lorenzo, C. Processing of Materials for Regenerative Medicine Using Supercritical Fluid Technology. *Bioconjugate Chem.* **2015**,

*26*, 1159–1171.

146. García-González, C.A.; Díaz-Gómez, L.A.; Concheiro, A.; Alvarez-Lorenzo, C. Patent survey on current applications of supercritical fluid technology in regenerative medicine. *Recent Pat. Nanotechnol.* **2015**, *5*, 48–58.
147. Reverchon, E.; Cardea, S. Supercritical fluids in 3-D tissue engineering. *J. Supercrit. Fluid.* **2012**, *69*, 97–107.
148. Stergar, J.; Maver, U. Review of aerogel-based materials in biomedical applications. *J. Sol-Gel Sci. Technol.* **2016**, *77*, 738–752.
149. García-González, C.A.; López-Iglesias, C.; Concheiro, A.; Alvarez-Lorenzo, C. Chapter 16. Biomedical Applications of Polysaccharide and Protein Based Aerogels. In *Green Chemistry Series*; Thomas, S., Pothan, L.A., Mavelil-Sam, R., Royal Society of Chemistry: Cambridge, UK, 2018; pp. 295–323.
150. Mallepally, R.R.; Marin, M.A.; Surampudi, V.; Subia, B.; Rao, R.R.; Kundu, S.C.; McHugh, M.A. Silk fibroin aerogels: potential scaffolds for tissue engineering applications. *Biomed. Mat.* **2015**, *10*, 035002–035011.
151. Ozdemir, E.; Sendemir-Urkmez, A.; Yesil-Celiktas, O. Supercritical CO2 processing of a chitosan-based scaffold: Can implantation of osteoblastic cells be enhanced? *J. Supercrit. Fluid.* **3**, *75*, 120–127.
152. Rinki, K.; Dutta, P.K. Chitosan based scaffolds by lyophilization and sc.CO2 assisted methods for tissue engineering applications. *J. Macromol. Sci. A* **2010**, *47*, 429–434.
153. Cai, H.; Sharma, S.; Liu, W.; Mu, W.; Liu, W.; Zhang, X.; Deng, Y. Aerogel microspheres from natural cellulose nanofibrils and their application as cell culture scaffold. *Biomacromolecules* **2014**, *15*, 2540–2547.
154. Baldino, L.; Concilio, S.; Cardea, S.; De Marco, I.; Reverchon, E. Complete glutaraldehyde elimination during chitosan hydrogel drying by SC-CO2 processing. *J. Supercrit. Fluid.* **2015**, *103*, 70–76.
155. Baldino, L.; Concilio, S.; Cardea, S.; Reverchon, E. Interpenetration of natural polymer aerogels by supercritical drying. *Polymers* **2016**, *8*, 106–117.
156. Quraishi, S.; Martins, M.; Barros, A.A.; Gurikov, P.; Raman, S.P.; Smirnova, I.; Duarte, A.R.C.; Reis, R.L. Novel non-cytotoxic alginate–lignin hybrid aerogels as scaffolds for tissue engineering. *J. Supercrit. Fluid.* **10**, *105*, 1–8.
157. El Kadib, A.; Bousmina, M. Chitosan bio-based organic–inorganic hybrid aerogel microspheres. *Chem. Eur. J.* **2012**, *18*, 8264–8277.
158. Czaja, W.; Kyrylíouk, D.D. Resorbable cellulose based biomaterial and implant, *WO Pat.* 2013126635A1, 2013.
159. Liebner, F.; Potthast, A.; Kosma, P.; Wimmer, R.; Rosenau, T. Porous solid body made of cellulose phosphate and carrying covalently bound phosphate groups on its entire surface and inner surface, useful as a cell growth substrate including bone implant- or cartilage- and bone regeneration-material, *DE Pat.* 102010011808, 2011.
160. Silva, S.S.; Duarte, A.R.C.; Carvalho, A.P.; Mano, J.F.; Reis, R.L. Green processing of porous chitin structures for biomedical applications combining ionic liquids and supercritical fluid technology. *Acta Biomater.* **3**, *7*, 1166–1172.
161. Ganesan, K.; Dennstedt, A.; Barowski, A.; Ratke, L. Design of aerogels, cryogels and xerogels of cellulose with hierarchical porous structures. *Mater. Design* **2016**, *92*, 345–355.
162. Pircher, N.; Fischhuber, D.; Carbajal, L.; Strauß, C.; Nedelec, J.M.; Kasper, C.; Rosenau, T.; Liebner, F. Preparation and reinforcement of dual-porous biocompatible cellulose scaffolds for tissue engineering. *Macromol. Mat. Eng.* **2015**, *300*, 911–924.
163. Silva, S.S.; Duarte, A.R.C.; Mano, J.F.; Reis, R.L. Design and functionalization of chitin-based microsphere scaffolds. *Green Chem.* **2013**, *15*, 3252–3258.
164. Cardea, S.; Pisanti, P.; Reverchon, E. Generation of chitosan nanoporous structures for tissue engineering applications using a supercritical fluid assisted process. *J. Supercrit.*

*Fluid.* **2010**, *54*, 290–295.

165. Ding, B.; Si, Y.; Ge, J.; Tang, X.; Huang, M.; Zhu, J.; Yu, J. Three-dimensional fiber-based airgel tissue engineering scaffold and production method thereof, *CN Pat.* 103285424A 2013.
166. Pircher, N.; Veigel, S.; Aigner, N.; Nedelec, J.M.; Rosenau, T.; Liebner, F. Reinforcement of bacterial cellulose aerogels with biocompatible polymers. *Carbohydr. Polym.* **2014**, *111*, 505–513.
167. Diaz-Gomez, L.; Concheiro, A.; Alvarez-Lorenzo, C.; García-González, C.A. Growth factors delivery from hybrid PCL-starch scaffolds processed using supercritical fluid technology. *Carbohydr. Polym.* **2016**, *142*, 282–292.
168. Diaz-Gomez, L.; Yang, F.; Jansen, J.A.; Concheiro, A.; Alvarez-Lorenzo, C.; García-González, C.A. Low viscosity-PLGA scaffolds by compressed CO2 foaming for growth factor delivery. *RSC Adv.* **2016**, *6*, 70510–70519.
169. Goimil, L.; Braga, M.E.M.; Dias, A.M.A.; Gómez-Amoza, J.L.; Concheiro, A.; Alvarez-Lorenzo, C.; de Sousa, H.C.; García-González, C.A. Supercritical processing of starch aerogels and aerogel-loaded poly(ε-caprolactone) scaffolds for sustained release of ketoprofen for bone regeneration. *J. CO2 Util.* **2017**, *18*, 237–249.
170. Betz, M.; García-González, C.A.; Subrahmanyam, R.P.; Smirnova, I.; Kulozik, U. Preparation of novel whey protein-based aerogels as drug carriers for life science applications. *J. Supercrit. Fluid.* **2012**, *72*, 111–119.
171. Marquez-Escalante, J.; Carvajal-Millan, E.; Miki-Yoshida, M.; Alvarez-Contreras, L.; Toledo-Guillén, A.R.; Lizardi-Mendoza, J.; Rascón-Chu, A. Water extractable arabinoxylan aerogels prepared by supercritical CO 2 drying. *Molecules* **2013**, *18*, 5531–5542.
172. Rinki, K.; Dutta, P.K.; Hunt, A.J.; Macquarrie, D.J.; Clark, J.H. Chitosan aerogels exhibiting high surface area for biomedical application: Preparation, characterization, and antibacterial study. *Int. J. Polym. Mater. Po.* **2011**, *60*, 988–999.
173. Ayers, M.R.; Hunt, A.J. Synthesis and properties of chitosan–silica hybrid aerogels. *J. Non-Cryst. Solids* **6**, *285*, 123–127.
174. Lu, T.; Li, Q.; Chen, W.; Yu, H. Composite aerogels based on dialdehyde nanocellulose and collagen for potential applications as wound dressing and tissue engineering scaffold. *Composites Science and Technology* **2014**, *94*, 132–138.
175. Starbird, R.; García-González, C.A.; Smirnova, I.; Krautschneider, W.H.; Bauhofer, W. Synthesis of an organic conductive porous material using starch aerogels as template for chronic invasive electrodes. *Mater. Sci. Eng. C* **2014**, *37*, 177–183.

USC
UNIVERSIDADE
DE SANTIAGO
DE COMPOSTELA

# 2. OBJECTIVES AND ORGANIZATION

As discussed in the Introduction of this Thesis, supercritical fluid technology offers great advantages in the field of materials processing for pharmaceutical applications. On one hand, it allows for the processing of materials intro microparticles via micronization, reducing or avoiding the use of organic solvents and multi-step processes. On the other hand, supercritical fluids can be used for the extraction of the liquid phase of gels to obtain aerogels without significant damage in the porous structure.

The main objective of this PhD Thesis was to implement supercritical fluid technology in the preparation of different drug delivery systems through the aforementioned techniques, with a special focus on wound and pulmonary delivery where porous materials are convenient. Specifically, the work was divided into three sections and organized as follows:

The first section (Chapters 3 and 4) corresponded to the application of the Particles from Gas-Saturated Solutions technique to obtain solid lipid microparticles. The main objectives were to confirm the advantages of using supercritical $CO_2$ in an up-scale atomization process, to understand and model the process using artificial intelligence tools, and to apply the technology for the development of a drug delivery system for wound applications.

In **Chapter 3**, *Modelling of the Production of Lipid Microparticles Using the Particles from Gas-Saturated Solutions® (PGSS®) Technique*, a study of the melting point of a commercial glyceryl monostearate under pressurized $CO_2$ was carried out to determine the feasible range of pressure and temperature in the PGSS processing. This part was carried out in collaboration with the Laboratorio de Propiedades Termofísicas (Grupo NaFoMat) from the Department of Applied Physics of the Faculty of Physics of the Universidade de Santiago de Compostela. The processability of particles with the PGSS® technique was evaluated in terms of yield of production and particle size distribution of the obtained powder. Several batches were produced under different conditions according to an experimental design, and the results were modelled using artificial intelligence tools to study the influence of those conditions on the main characteristic of the particles.

**Chapter 4**, *Lidocaine-Loaded Solid Lipid Microparticles (SLMPs) Produced from Gas-Saturated Solutions for Wound Applications*, aimed to apply the aforementioned

technique to the production of solid lipid microparticles loaded with an anesthetic drug, lidocaine hydrochloride. Lidocaine incorporation in the particles was studied and a controlled release of the drug was targeted to exploit the antimicrobial capacity of lidocaine. An innovative drug permeation test was assessed using a bioengineered skin equivalent obtained by 3D-printing. Glyceryl monostearate particles with different lidocaine contents were produced, and lidocaine inside the particles was characterized using infrared spectroscopy, X-ray diffraction and differential scanning calorimetry. Release tests were carried out in Franz cells to characterize drug release profile and to confirm the controlled release. Potential drug permeation of lidocaine through 3D-printed skin equivalents and the antimicrobial capacity of lidocaine hydrochloride against relevant bacteria in chronic wound infections were also studied. Apart from full-thickness skin, skin without epidermis was studied to simulate damaged tissue in the wound. This work was carried out in collaboration with the Department of Bioengineering and Aerospace Engineering of the Universidad Carlos III de Madrid (UC3M) in the frame of a 2-week research stay, and the Instituto de Investigação e Inovação em Saúde (INEB-i3S) of the Universidade do Porto.

The second section of this Thesis focused on the preparation of chitosan aerogels for chronic wound applications. The main objective was to develop and characterize chitosan aerogels loaded with an antibiotic agent for local antimicrobial therapy of wound infection. In **Chapter 5**, *Vancomycin-Loaded Chitosan Aerogel Particles Obtained by the Dripping Method For Chronic Wound Applications*, the textural properties of chitosan aerogels were extensively studied, as well as the influence of the ageing time on these properties. PBS absorption tests were carried out at different pHs to confirm exudate sorption from the wounds. The interference of the aerogels with collagenase, a metalloenzyme responsible for collagen remodeling during the healing process, was evaluated. The presence of vancomycin was characterized using infrared spectroscopy, and encapsulation efficiency and drug release were studied by spectrophotometry. The antimicrobial activity of the aerogels was evaluated against a susceptible *Staphylococcus aureus* strain to test the ability of the aerogels to treat and prevent wound infection. Finally, biocompatibility of the aerogels was evaluated with mouse fibroblasts.

**Chapter 6**, *Jet Cutting Technique for the Production of Chitosan Aerogel Microparticles Loaded with Vancomycin*, aimed to improve some of the limitations of the chitosan aerogel particles obtained by the dripping method, namely large particle sizes difficult to apply to wounds, and the low load of vancomycin due to loss in the solvent exchange step. The jet cutting technique was applied to reduce particle size since it permits to produce small microparticles without limitation of the viscosity of the initial solution. In an attempt to improve vancomycin loading, gelation was performed directly in ethanol. Vancomycin presents low solubility in ethanolic solutions, so lower drug loss is expected. Different conditions of the jet cutting

technique were tested to check the feasibility of the jet cutting technique and the influence of the parameters on the particle size. Morphology and textural properties were determined, particle sizes were analyzed using dynamic image analysis, and particles were characterized in terms of drug content and release, fluid sorption capacity, antimicrobial activity, hemolytic activity, and biocompatibility. The production of the chitosan aerogel particles using the jet cutting technique was carried out in collaboration with the Laboratory for Development and Modeling of Novel Nanoporous Materials and the Institute of Thermal Separation Processes of the Hamburg University of Technology (TUHH) in the frame of a 3-month research stay.

Antimicrobial tests of this section were carried out in collaboration with the Instituto de Investigação e Inovação em Saúde (INEB-i3S) of the Universidade do Porto, whereas the biocompatibility studies were performed in collaboration with the BioFarma group of the Centro Singular de Investigación en Medicina Molecular y Enfermedades Crónicas (CiMUS) of the Universidade de Santiago de Compostela.

In the third section, **Chapter 7**, *Inkjet-Printed Aerogel Particles for Pulmonary Delivery*, investigates the preparation of alginate aerogel particles for pulmonary administration. The main objective was to obtain alginate aerogel particles with adequate aerodynamic diameters that could provide a sustained release of the drug salbutamol sulphate, used in the treatment of respiratory diseases. As highly porous materials, aerogels represent advantageous formulations for pulmonary delivery. Their low density allows for the preparation of particles of large geometric diameters with similar aerodynamic diameters than smaller, non-porous particles. This way, they are better dispersed from the inhaler and less likely to be phagocyted the respiratory tract. The potential of the inkjet printing technique for the production of particles with suitable diameters was studied, as it is simple, versatile, and reproducible. An alginate solution was optimized for the printing process, in terms of alginate concentration and gelation bath conditions. After supercritical drying, the gels were characterized in terms of physicochemical and textural properties, and particle size distributions and aerodynamic diameters were determined using image analysis. The drug salbutamol sulfate was incorporated to the aerogels and drug load and release were studied in Franz cell experiments. Simulated lung deposition tests were performed in a next generation impactor to predict the deposition of particles in the respiratory tract, and were carried out in collaboration of the Food and Drug Department of the University of Parma.

USC
UNIVERSIDADE
DE SANTIAGO
DE COMPOSTELA

# SECTION I. SOLID LIPID MICROPARTICLES FROM GAS-SATURATED SOLUTIONS

USC
UNIVERSIDADE
DE SANTIAGO
DE COMPOSTELA

# 3. MODELLING OF THE PRODUCTION OF LIPID PARTICLES USING PGSS® TECHNIQUE

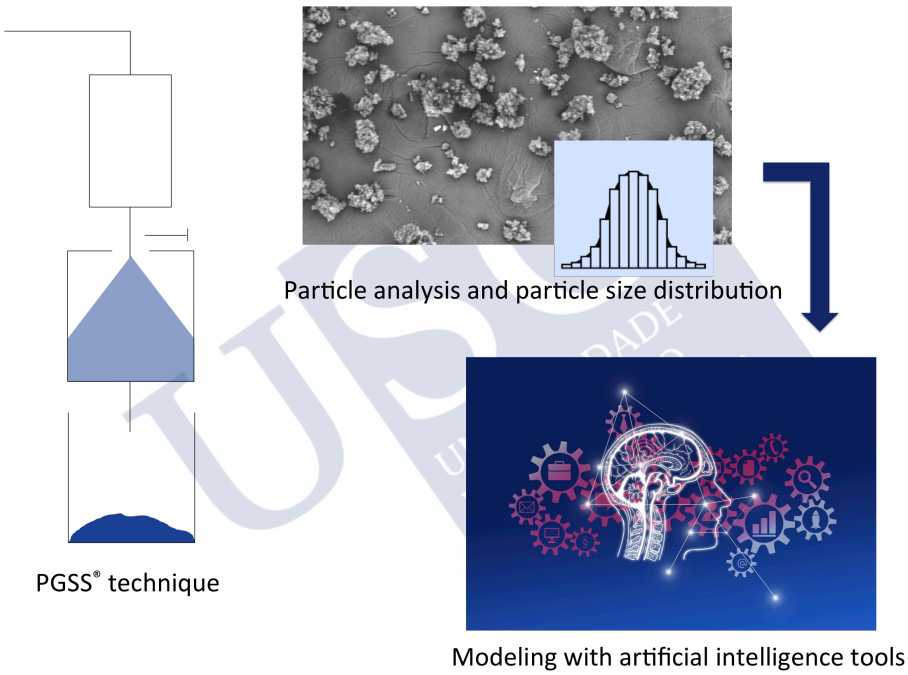


The work described in this chapter was published in López-Iglesias C. *et al* Modelling of the production of lipid microparticles using PGSS® technique. *Molecules* **2020**, 25, 927-940.

Work carried out in collaboration with the Grupo NaFoMat of the Applied Physics Department of the Universidade de Santiago de Compostela.

USC
UNIVERSIDADE
DE SANTIAGO
DE COMPOSTELA

# 3. MODELLING OF THE PRODUCTION OF LIPID PARTICLES USING PGSS® TECHNIQUE

## 3.1. Introduction

Particulate systems like microparticles have attracted interest in several biomedical, food and environmental applications [1–5]. Namely, the encapsulation of bioactive agents in these carriers improves its efficacy and safety, since better control of the dosage and release are provided [6,7]. Microparticles also enhance physicochemical stability, protecting the cargo from environmental and physiological factors [8]. The size of microparticles, between 0.1–100 μm [9], can hamper their absorption through biological membranes, increasing their permanence in the application site, thus providing local and sustained drug release and mitigating their toxic effects [10].

Lipids are advantageous matrices for particulate drug delivery systems since they are physiological compounds and therefore well tolerated by living systems [11,12]. For instance, a variety of lipids such as sorbitan esters, phosphatidylcholine, and unsaturated polyglycolized glycerides are widely used as surfactants in lipid-based formulations [13]. Among lipid systems, solid lipid microparticles (SLMPs) are easy to produce on a large scale and sterilize, exhibiting better stability properties than others, such as liposomes [14]. Several SLMP-based formulations have been developed as drug delivery systems for oral, parenteral, pulmonary, and topical applications [14,15].

Solvent-free strategies are especially attractive for the manufacturing of SLMPs from the processing, environmental and economical points of view. Namely, supercritical $CO_2$ ($scCO_2$) technology has been highlighted as a processing tool for environmentally friendly, safe and cost-efficient techniques at mild conditions ($P > 73.8$ bar and $T > 31.1$ °C) [16]. Processes based on supercritical fluid technology (foaming, sterilization) usually avoid or at least mitigate the use of organic solvents thus reducing their carbon footprint. The PGSS® (Particles from Gas-Saturated Solutions) technique is based on the use of compressed $CO_2$ or $scCO_2$ for the production of microparticles in an atomization-wise process [17–19]. PGSS® process comprises two main steps: (i) $CO_2$ sorption in the polymer, and (ii) polymer expansion and particle formation. In the first step, high amounts (5–50 wt.%) of $CO_2$ dissolve in a

molten substance at a moderate pressure in an extent depending on the soaking time and $CO_2$ affinity to the polymer [20]. Then a rapid expansion to atmospheric pressure of the melt through a nozzle causes an intense cooling effect and $CO_2$ supersaturation within the melt, resulting in the precipitation of solid particles [21]. $scCO_2$ used in the PGSS® technique differs from other compressed fluids (e.g. compressed air) used in conventional atomization processes (spray drying) in their chemical interaction with the processed polymers at a molecular level, as $scCO_2$ can decrease the melting temperature of the polymer thus contributing to costs optimization and energy consumption savings [22]. PGSS® is an adequate technique for the processing of polymeric particles incorporating termolabile compounds, although its use is limited to polymer matrices with relatively low melting temperatures and with an affinity of $CO_2$ to the polymer [23]. Compared to other processes for particle production involving the use of $scCO_2$, such as the Gas Anti-solvent (GAS), Supercritical Anti-solvent (SAS) and Supercritical Fluid Extraction of an Emulsion (SFEE) techniques, the PGSS® technique does not involve the use of any organic solvents [16,24]. Moreover, the substance to be micronized does not require to be soluble in $CO_2$, unlike in the Rapid Expansion of Supercritical Fluids (RESS) process [25,26]. Overall, PGSS® emerges as an appealing and advantageous technique for the processing of SLMPs at reduced melting temperatures and in the absence of organic solvents.

The morphology and size of the SLMPs produced by the PGSS® process are mainly influenced by the formulation (chemical composition and rheology of the compounds to be precipitated), the technical details of the equipment used (volume of the saturator, precipitator and collector, diameter of the nozzle and length of the tubing), and the operating conditions (pressure, temperature, soaking time) [27,28]. The PGSS® processing variables are numerous, making it difficult to elucidate their influence on the characteristics of the microparticles using conventional statistical methods [29–31]. Despite PGSS® being a simple and versatile method, the lack of knowledge of the effects of the variables on the results of PGSS® technology may entail an obstacle towards the robust SLMPs production and the scaling-up of the process [32]. Approaches based on DoE (design of experiments) and multiple regression have been proposed to manage the number of experiments, select the critical variables and optimize the operation conditions, but mainly regarding their influence on the dissolution profile of the drug incorporated in the particles [33]. Some mathematical models were also proposed to simulate the physicochemical processes taking place during the PGSS® processing, such as the behavior of a $CO_2$-supersaturated solution drop in low-pressure environments [34,35]. In this context, artificial intelligence technologies emerge as tools with great potential for simplifying the study of processes in which many variables are involved, even when a small number of experiments are available. Some of them, such as the neurofuzzylogic systems, allow multiple variables to be modelled and the models expressed through language, which generates in-depth knowledge about the process. Neurofuzzylogic software is a hybrid

system that combines artificial neural networks (ANNs) and fuzzy logic (FL). ANNs are computer programs that simulate how human brain processes information. They detect patterns and relationship in data, and learn from experience, leading to *black-box* mathematical models [36]. When combined with FL, the models are expressed as simple linguistic IF…THEN rules together with a membership degree, losing their black-box character and being easily understandable.

Artificial intelligence tools have been previously used in the development and optimization of microparticles [37] and polymeric and lipid nanoparticles [38,39]. To the best of our knowledge, these tools are applied in this work for the first time to model the production of SLMPs by the PGSS® technology. SLMPs consist of a matrix of commercial glyceryl monostearate (GMS), a lipid widely used as an emulsifier in pharmaceutical preparations due to its good biocompatibility and safety [40,41]. First, the melting point depression of commercial GMS in contact with $scCO_2$ was studied to establish the limits of the adequate knowledge space for the processing of PGSS®. Subsequently, an unconstrained D-optimal design for three variables (nozzle diameter, pressure and temperature) at 2, 3 and 3 levels, respectively, was used to prepare SLMPs using the PGSS® technique. The microparticles were characterized in terms of size and shape. The generated database was modelled through a neurofuzzylogic system and the design space was established with respect to the melt GMS processability (fine particle production yield) and the characteristics of the particles.

## 3.2. Materials and methods

### 3.2.1. Materials

Kolliwax® GMS II (glycerylmonostearate 40–55 type II, powder, $T_m$ = 54–64 °C) was supplied by BASF GmbH (Ludwigshafen am Rhein, Germany). $CO_2$ for the PGSS® technique (purity 99.8%) and for the melting point determination (purity 99.998%) were purchased from Praxair (Madrid, Spain) and Air Liquide (Santiago de Compostela, Spain), respectively.

### 3.2.2. Determination of the melting point of GMS in the presence of compressed $CO_2$ at different pressures

The melting point of the GMS in the presence of compressed $CO_2$ in a 0–200 bar pressure range was determined. A sample of GMS (approximately 3.5 mg) on a glass vial was placed inside a variable volume high-pressure cell, consisting of a horizontal stainless steel cylinder with an internal diameter of 2 cm and a piston to adjust the volume from 7.9 to 29.5 $cm^3$. The cell was equipped with a sapphire window (1.6 cm diameter) that allowed the detection of phase transitions through an endoscope (Olympus 5 series, Olympus, Tokyo, Japan) connected to a CCD-camera (Moticam 2000, Motic Asia, Hong Kong, China). In one sidewall of the cylinder, a second sapphire

window (6 mm in diameter) made it possible to illuminate the interior of the cell through an optical fiber. A Pt100 probe with an uncertainty of 0.02°C was used to measure the temperature in the cell wall. The pressure was measured with a Heise model DXD series digital pressure transducer, with operating range 0–500 bar and an uncertainty of 0.02% of the full scale (FS).

For the experimental trials, the cell at its maximum volume was filled with $CO_2$ at room temperature and a supply pressure of 60–65 bar. Afterwards, the system was heated to the selected temperature (from 52 to 61 °C) and the pressure was gradually increased moving the piston (i.e. reducing the volume of the chamber) until the solid was completely molten to determine the melting point value. Thus, the melting pressure of the GMS at the selected temperature was determined. Subsequently, another temperature was selected and the procedure was repeated to obtain another value of the melting curve. Temperature measurements were carried out by triplicate. Results were expressed as the mean value ± standard deviation (SD). At a fixed temperature, this device shows repeatability for the pressure lower than 11.4%. The melting point temperature of the GMS at atmospheric pressure in the same equipment was also determined.

### 3.2.3. SLMPs production by the PGSS® technique

For the particle formation protocol, 6 g of GMS powder were placed into a 250-mL high-pressure autoclave (saturator) (Eurotechnica GmbH, Bargteheide, Germany). After heating the saturator to the desired temperature (T), $CO_2$ entered the equipment at a constant flow of 7 g/min until the desired pressure (P) was reached. After 1 h of contact between the molten lipid and the compressed $CO_2$ under stirring at 400 rpm, the system was depressurized by opening the valve placed at the bottom of the saturator. When the molten lipid leaves the saturator through a nozzle, rapid depressurization causes lipid microparticles precipitation within a 2.7 L borosilicate autoclave (precipitator).

Batches of GMS particles were produced following a D-optimal experimental design for three variables: nozzle diameter (2 levels), operating temperature (3 levels) and pressure (3 levels) (Table 3.1) carried out by DataForm® v.3.1 software (Intelligensys Ltd., Stokesley, UK). GMS particles processed under different pressure and temperature conditions were denoted as GMS-*x*-*y*-*z*, where *x* is the nozzle diameter in mm, *y* the processing temperature in degrees Celsius and *z* the processing pressure in bar.

Table 3.1. Nozzle diameters and processing temperatures (T) and pressures (P) tested for the preparation of SLMPs of GMS using the PGSS® technique.

| SLMPs | Nozzle (mm) | T (°C) | P (bar) |
|---|---|---|---|
| GMS-4-57-120 | 4 | 57 | 120 |
| GMS-4-57-200 | 4 | 57 | 200 |
| GMS-4-62-120 | 4 | 62 | 120 |
| GMS-4-62-200 | 4 | 62 | 200 |
| GMS-4-67-120 | 4 | 67 | 120 |
| GMS-4-67-200 | 4 | 67 | 200 |
| GMS-1-57-120 | 1 | 57 | 120 |
| GMS-1-57-160 | 1 | 57 | 160 |
| GMS-1-57-200 | 1 | 57 | 200 |
| GMS-1-67-120 | 1 | 67 | 120 |
| GMS-1-67-160 | 1 | 67 | 160 |
| GMS-1-67-200 | 1 | 67 | 200 |

Microparticles were collected and weighed to determine the process yield according to Eq. 3.1:

$$\% \text{ fine particles} = \frac{W_f}{W_0} \cdot 100 \tag{3.1}$$

where $w_0$ is the initial weight of GMS added to the saturator and $w_f$ is the final weight of fine particles collected. Also, the amount of GMS remaining on the walls of the precipitator and the interior of the tubing was weighed to verify all the GMS had left the saturator, and what amount had not precipitated into SLMPs.

### 3.2.4. Morphological analysis and particle size distribution (PSD)

Four aliquots of each batch were characterized in terms of particle size distribution by optical microscopy using a camera (EP50, Olympus, Tokyo, Japan) provided with the software EP View (Olympus, Tokyo, Japan). The images were analyzed using the freeware ImageJ 1.49v (National Institutes of Health, USA). The particle size distributions were fitted to a normal distribution, and mean particle size and standard deviations were obtained.

Particles were also analyzed by scanning electron microscopy (SEM Zeiss EVO LS 15; Zeiss, Oberkochen, Germany) to evaluate their morphology and surface texture. Particles were previously sputtered-coated with a layer of 10 nm of iridium to improve the contrast (Q150 T S/E/ES, Quorum Technologies, Lewes, UK).

### 3.2.5. Modelling

The generated database (inputs from table 3.1 and outputs from table 3.3) was modelled using the commercial software FormRules® v4.03 (Intelligensys Ltd., Stokesley, UK) which is a hybrid system that combines Artificial Neural Networks (ANN) and fuzzy logic. Nozzle diameter, pressure and temperature were introduced as inputs, while percentage of fine particles, mean particle size and standard deviation were

introduced as outputs. A separate model was developed for each output. These models are spplited in different submodels when it is possible, to generate simple and understandable rules.

Among the statistical fitness criteria included by FormRules® (Cross Validation, Minimum Description Length, Structural Risk Minimisation, Leave One Out Cross Validation and Bayesian Information Criterion), Minimum Description Length was selected because it gives the best R-squared as well as the simplest and more intelligible rules. Modelling was carried out using the parameters shown in Table 3.2.

Table 3.2. Training parameters setting with FormRules® v4.03.

| |
|---|
| Minimization parameters |
| Ridge Regression Factor: $1e^{-6}$ |
| Model Selection Criteria |
| Minimum Description Length |
| Number of Set Densities: 2 |
| Set Densities: 2.3 |
| Adapt Nodes: TRUE |
| Max. Inputs Per SubModel: 2 |
| Max. Nodes Per Input: 10 |

Three sets of *IF ... THEN* rules were subsequently generated, one for each output. IF THEN rules are made up of two parts: the initial one, which includes the input or inputs explaining a specific output, followed by the second part describing the output characteristics, which are defined by a word and its corresponding membership degree [36].

The predictability of the models was assessed using the determination coefficient ($R^2$) defined by Eq. 3.2:

$$R^2 = \left( 1 - \frac{\sum_{i=1}^{n} \left( y_i - y_i^{'} \right)^2}{\sum_{i=1}^{n} \left( y_i - y_i^{''} \right)^2} \right) \times 100 \qquad (3.2)$$

where $y_i$ is the actual point in the data set, $y_i^{'}$ is the value calculated by the model and $y_i^{''}$ is the mean of the dependent variable. Values of $R^2$ must be lower than 99.9%, otherwise there is a risk of overtraining the neural network [42]. The larger the value of the train set $R^2$, the more the model captured the variation in the training data. Values for $R^2 > 70\%$ are indicative of reasonable model predictabilities.

The accuracy of the models was evaluated with the analysis of variance to compare predicted and experimental results, respectively. Computed *f* ratio values higher than critical *f* values for the degrees of freedom of the model, indicate no statistical significance between predicted and experimental results and hence, model accuracy.

## 3.3. Results and discussion

### 3.3.1. Melting point depression of GMS in the presence of $CO_2$

Melting pressure-temperature curve of the commercial GMS under compressed $CO_2$ was measured to determine the feasible operating range of conditions for the PGSS® technique (Fig. 3.1). This step is crucial since it is necessary to establish a set of pressure-temperature conditions (grey region in Fig. 3.1) where the lipid mixture is molten. The melting point of GMS in the presence of $CO_2$ has been previously studied [43], but these determinations are essential because it is well known that GMS can have inter-batch and inter-manufacturer variability as it is commercially provided as a mixture of components (mono- and diglycerides).

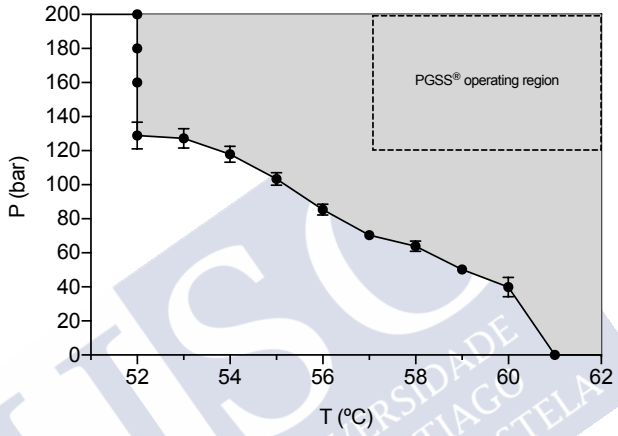


Figure 3.1. GMS melting points obtained at different pressures of $CO_2$ using a variable-volume high-pressure view cell. GMS experienced a reduction in the melting temperature as $CO_2$ pressure increased up to 120 bar. A further increase in pressure did not cause an additional melting point depletion. Grey area represents the pressure-temperature region at which GMS will be molten. The area delimited by the dashed line represents the operating region established for SLMPs production by PGSS® technique.

The melting point of the pure commercial GMS was 61 °C at ambient pressure and without $CO_2$. $CO_2$ can act as a plasticizer agent, being able to melt other substances, like lipids or polymers, below their normal melting points. Melting point depletion effect of GMS in contact with $CO_2$ was highly dependent on the working pressure and decreased proportionally up to 52 °C. This effect was related to the increase in the amount of $CO_2$ dissolved in the lipid when the pressure increases [44]. A plateau in temperature was reached at 52 °C and pressures above 120 bar were not able to melt the lipid at lower temperatures. This second effect was related to the competing mechanism of increased $CO_2$ solubility in the lipid and the hydrostatic pressure promoting the melting point depletion and increase, respectively, that are countercounted at pressures above 120 bar for GMS [43]. This reduced melting temperature in the presence of compressed $CO_2$ is advantageous for the energy

optimization of the PGSS® particle processing when transferring formulations from lab to pilot scale [45,46].

### 3.3.2. Particle size distribution (PSD) of GMS particles

Based on the melting point values obtained in Section 3.3.1, the range of values of pressure and temperature selected for the experimental study of the PGSS® processing of GMS particles were set at 120-200 bar and 57-67 °C, respectively. In this work, an increment of *ca.* 5 °C with respect to the melting temperature of GMS at a certain pressure in the presence of compressed $CO_2$ was established as a rule-of-thumb (dashed and grey rectangle in Fig. 3.1) to ensure the complete melting and to avoid clogging of the nozzle during the PGSS® expansion-spraying step. The selection of the nozzle diameter was based on the technical possibilities of the PGSS® equipment, being 4 mm and 1 mm the maximum nozzle diameter and the minimum nozzle diameter that did not cause clogging events upon depressurization using the established P-T range in the experimental design, respectively.

Table 3.3. Yield of particle production, mean diameter and standard deviation of SLMPs of GMS processed using PGSS® technique according to the conditions of the experimental design. Particles were denoted as GMS-*x*-*y*-*z*, where *x* is the nozzle diameter in mm, *y* the processing temperature in degrees Celsius and *z* the processing pressure in bar.

| SLMPs | Mean diameter (µm) | Standard deviation (µm) | % fine particles |
|---|---|---|---|
| GMS-4-57-120 | 138.7 | 47.0 | 17.4 |
| GMS-4-57-200 | 182.6 | 63.3 | 43.7 |
| GMS-4-62-120 | 128.0 | 41.8 | 12.8 |
| GMS-4-62-200 | 147.4 | 48.3 | 18.3 |
| GMS-4-67-120 | 103.5 | 33.1 | 11.0 |
| GMS-4-67-200 | 154.3 | 52.1 | 27.5 |
| GMS-1-57-120 | 171.6 | 56.8 | 39.5 |
| GMS-1-57-160 | 172.3 | 51.6 | 34.8 |
| GMS-1-57-200 | 186.2 | 57.5 | 25.7 |
| GMS-1-67-120 | 131.9 | 44.4 | 23.5 |
| GMS-1-67-160 | 130.3 | 50.0 | 27.1 |
| GMS-1-67-200 | 125.4 | 43.1 | 34.8 |

PSDs of the SLMPs showed mean diameters between 100 and 190 µm and standard deviations between 30 and 65 µm (Table 3.3). In general, the PSDs fitted well to a normal distribution (Fig. 3.2) with good correlation levels ($R^2 > 0.95$) in all cases. The yield of particle production was determined from the weight percentage of fine particles with respect to the initial GMS (Table 3.3). The loss of material during the PGSS® processing was due to GMS remaining in the tubings and the saturator of the equipment, molten material that was not solidified into particles and formed a crust in the walls of the precipitator. Some mass losses were attributed to small particles that

remained suspended in the outlet gaseous stream and were vented out during depressurization step along with the $CO_2$.

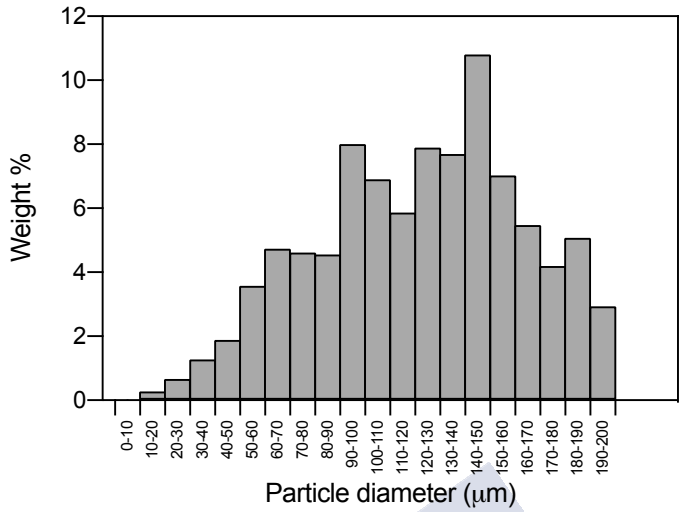


Figure 3.2. Frequency histogram of GMS-1-67-200 particles (mean particle diameter = 125.4 ± 43.1 μm). The normal distribution of this histogram is representative of all the GMS formulations tested.

### 3.3.3. Morphological characterization and modelling of GMS particle production using neurofuzzy tool

The processing of GMS using the PGSS® technique resulted in porous particles of varied shape and of lower particle diameter than the original material (Figs. 3.3 and 3.4).

Neurofuzzylogic software succeeded in modelling the influence of the parameters of pressure, temperature and nozzle diameter (inputs) on the output mean diameter (Table 3.4) with high predictability ($R^2$ > 90%) and accuracy ($p < 0.01$). The three parameters help to explain the variations in particle size, being the main effect the one of the temperature (submodel 1). An interaction between the pressure and the nozzle can be also observed (submodel 2). The predictability is also reasonable for the percentage of fine particles ($R^2$ > 75%), a parameter indicative of process yield (Table 3.4). However, adequate accuracy was not achieved with such a small number of degrees of freedom. The model shows a main effect for the interaction pressure-nozzle, but temperature also affects process yield. Variables studied do not explain sufficiently the variations in the standard deviation of particle size distribution ($R^2$ < 75%). The particle size distributions with PGSS® technique are broad and characterized by high standard deviations, probably bigger than the variations promoted by the processing parameters (temperature, pressure and nozzle diameter) used in this research. Therefore, the ANN cannot find a good model for this standard deviation.

Table 3.4. Inputs selected by FormRules® for the different outputs evaluated in this work, with their respective parameters to evaluate the quality of each model.

| Output | Submodel | Inputs selected | $R^2$ | Degrees of freedom | *f* value | Critical *f* value |
|---|---|---|---|---|---|---|
| Mean diameter | 1 | T | 91.5012 | 5 and 6 | 12.92 | 4.39 |
| | 2 | P x Nozzle | | | | |
| Standard deviation | 1 | P x Nozzle | 58.3925 | 4 and 7 | 2.46 | 4.12 |
| % fine particles | 1 | P x Nozzle | 75.1098 | 6 and 5 | 2.51 | 4.93 |
| | 2 | T | | | | |

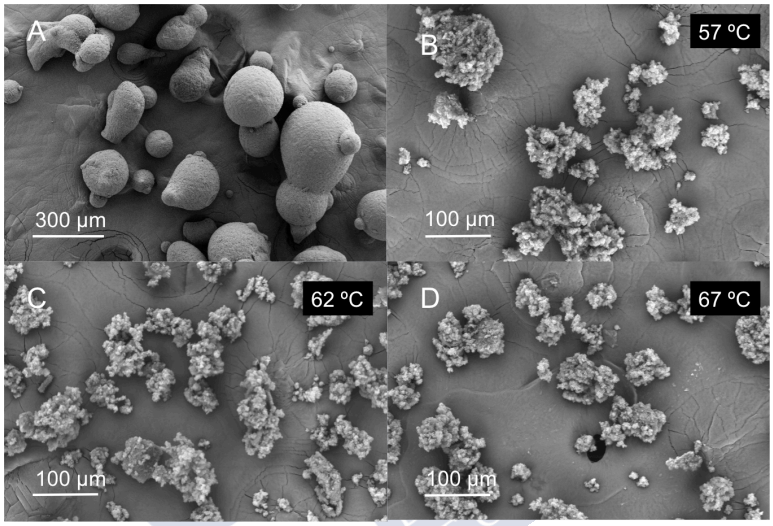


Figure 3.3. Effect of temperature in the PGSS® processing of GMS particles: (a) unprocessed GMS particles and (b) GMS-1-57-200, (c) GMS-1-62-200 and (d) GMS-1-67-200 particles. The processing with the PGSS® technique resulted in smaller particles at higher temperatures.

IF…THEN rules, generated by the neurofuzzylogic software allows acquiring knowledge in an easy way (Table 3.5). IF the temperature is low (up to 62 °C) THEN the mean particle size obtained is high (over 144.8 µm). The increase in temperature over 62 °C produces a decrease in particle size (Fig. 3.3).

On the other hand, (IF) the pressure increase (…THEN) promotes a decrease in the particle size of the microparticles (Fig. 3.4). This rule applies for both small and large nozzle diameters, being the variations in particle size wider when the large nozzle is used. Figure 3.5 represents predicted results by the model for mean particle size for the large (Fig. 3.5a) and small (Fig. 3.5b) nozzle. This effect was related to the increased solubility of $CO_2$ in molten GMS. At higher pressures, $CO_2$ solubility will increase and, upon depressurization, more nucleation bubbles will form due to $CO_2$ supersaturation, breaking the lipid into smaller particles (Fig. 3.4) [43,47].

Table 3.5. IF…THEN rules generated by FormRules® software.

| Parameter | Submodel | Rule |
|---|---|---|
| Mean diameter | 1 | IF T is low THEN mean diameter is high (1.0) |
| | | IF T is high THEN mean diameter is low (0.79) |
| | 2 | IF P is low and nozzle is large THEN mean diameter is low (1.0) |
| | | IF P is low and nozzle is small THEN mean diameter is high (0.69) |
| | | IF P is high and nozzle is large THEN mean diameter is high (0.69) |
| | | IF P is high and nozzle is small THEN mean diameter is high (0.53) |
| Standard deviation | 1 | IF P is low and nozzle is large THEN SD is low (0.63) |
| | | IF P is low and nozzle is small THEN SD is high (0.85) |
| | | IF P is high and nozzle is large THEN SD is high (0.85) |
| | | IF P is high and nozzle is small THEN SD is high (0.78) |
| % fine particles | 1 | IF nozzle is large and P is low THEN % particles is low (1.0) |
| | | IF nozzle is large and P is high THEN % particles is high (0.67) |
| | | IF nozzle is small and P is low THEN % particles is high (0.58) |
| | | IF nozzle is small and P is high THEN % particles is high (0.50) |
| | 2 | IF T is low THEN % particles is high (0.90) |
| | | IF T is medium THEN % particles is low (0.90) |
| | | IF T is high THEN % particles is low (0.56) |

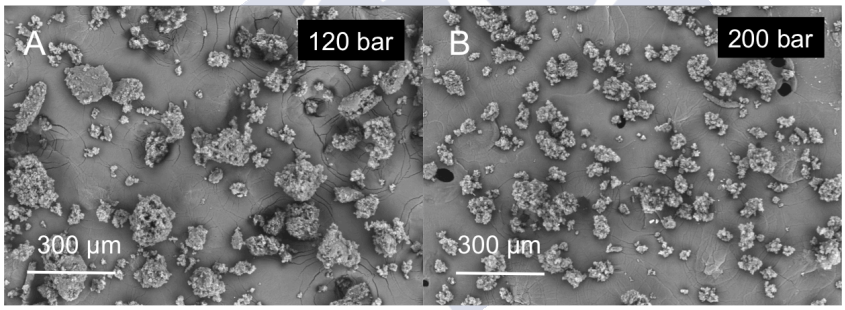


Figure 3.4. Effect of pressure in the PGSS® processing of GMS particles: (a) GMS-1-67-120 and (b) GMS-1-67-200 particles. Higher pressure led to better processed particles with smaller diameters and high porosity.

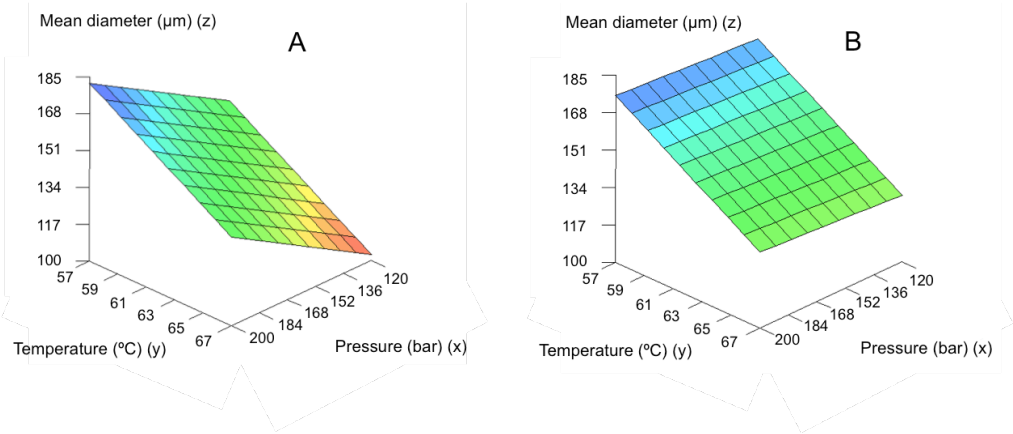


Figure 3.5. Predicted results by the model for mean particle size for the large (a) and small (b) nozzles. Using the large nozzle diameter, pressure variations produced a more pronounced effect on the mean particle diameter.

Figure 3.6 shows the predicted values for the percentage of fine particles as a function of pressure and temperature. The increase in temperature leads to a reduction in the process yield, being especially important up to 62 °C. In the temperature range of the experimental design (57–67 °C), the Joule-Thomson coefficient is very similar for the 0–200 bar pressure range [48]. At higher temperatures, the positive Joule-Thomson effect contribution may not be enough to solidify the GMS when exiting the nozzle. Under these conditions, a significant fraction of GMS is in a semi-molten state when it reaches the precipitator and forms a crust in the walls of the vessel instead of forming SLMPs that deposit on the collector.

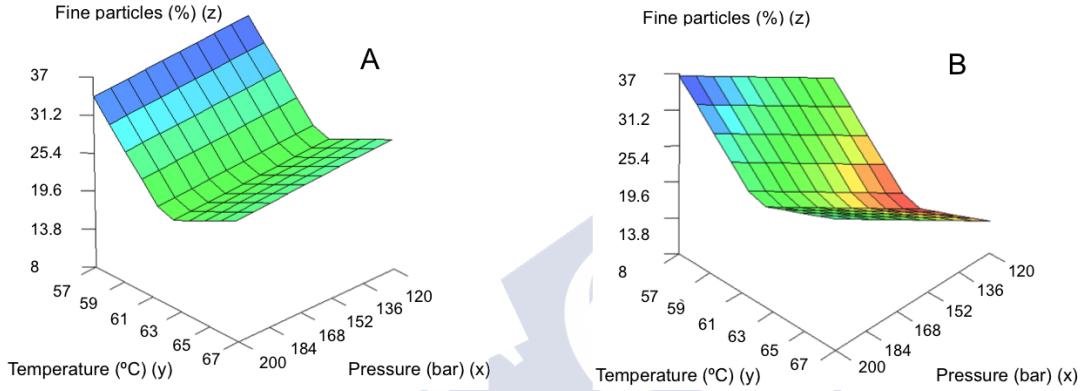


Figure 3.6. Influence of the parameters pressure and temperature on the yield of fine particle formation using (a) the large nozzle diameter and (b) the smaller nozzle diameter.

The diameter of the nozzle also influenced the fine particle yield production. In general, the process performs better when using the small size nozzle. It has been reported that lower nozzle diameters led to smaller particle sizes for other lipid-based systems [49]. Differences in the effect of pressure were also detected depending on the size of the nozzle used. When a nozzle of smaller size is used, the increase in pressure causes a slight reduction in the percentage of fines obtained. This may be related to the production of even smaller particles that remain suspended in the $CO_2$ and are therefore vented out. However, when the nozzle has a larger diameter, the effect is opposite, and the process performance is improved with increasing pressure. The pressure drop of the lipid-$CO_2$ melt through the nozzle is lower with larger nozzle diameters, leading to a decreased Joule-Thomson cooling effect. At higher pressures, this pressure drop effect is compensated by a higher $CO_2$ content in the lipid melt and particles are able to solidify and reach the collector leading to higher fine particle yield [50].

The experimental values obtained were compared with values predicted with the model, showing high accuracy of the models for mean diameter (3.7a) and fine particle fraction and (Fig. 3.7b).

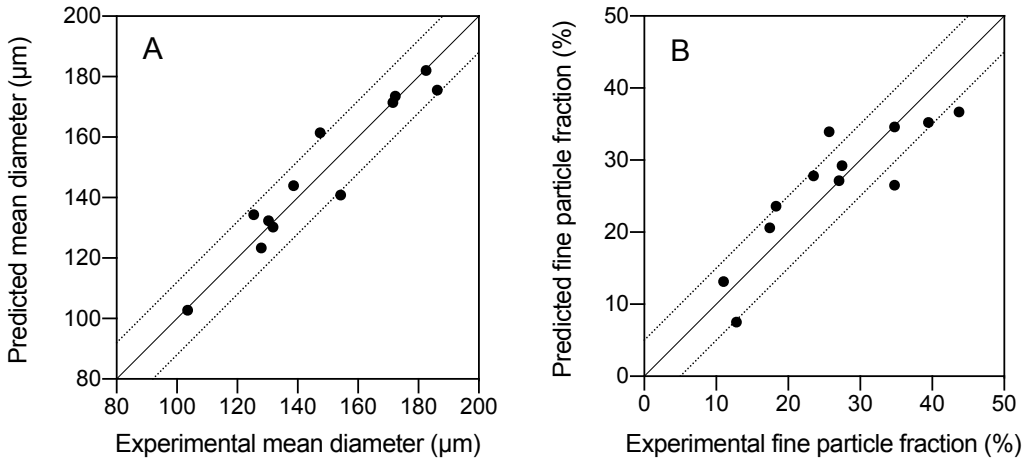


Figure 3.7. Parity plots of the predicted and experimental values of (a) mean particle size and (b) % of fine particles. Dotted lines correspond to an interval of tolerance of 10%.

## 3.4. Conclusions

PGSS® is an advantageous processing technique that allows for the manufacturing of molten substances into solid microparticles, with special interest for the processing of thermolabile compounds. Melting point measurements of GMS were essential to preliminarily determine the feasible PGSS® operating pressure and temperature conditions. The melting point depletion of GMS lipid under compressed $CO_2$ of up to 9 °C is especially relevant from the energy savings and process economics points of view. SLMPs were thus obtained at operating temperatures (57 °C) well below the normal melting point of GMS (61 °C). Artificial intelligence tools combining artificial neural networks and fuzzy logic was as a successful analytical duo to model the production of SLMPs by the PGSS® process. The obtained models served to simplify the understanding of the SLMPs processing through linguistic rules. The model unveiled that the processing pressure and temperature as well as the nozzle diameter had a certain influence on the particle size distribution of the SLMPs and yield of particle production. These operating conditions influenced remarkably the mean diameter of the particles, with smaller particles obtained at high temperatures and pressures and small nozzle diameter.

## 3.5. References

1. Nidhi; Rashid, M.; Kaur, V.; Hallan, S.S.; Sharma, S.; Mishra, N. Microparticles as controlled drug delivery carrier for the treatment of ulcerative colitis: A brief review. *Saudi Pharm. J.* **2016**, *24*, 458–472.
2. Saghazadeh, S.; Rinoldi, C.; Schot, M.; Kashaf, S.S.; Sharifi, F.; Jalilian, E.; Nuutila, K.; Giatsidis, G.; Mostafalu, P.; Derakhshandeh, H.; et al. Drug delivery systems and materials for wound healing applications. *Adv. Drug Deliv. Rev.* **2018**, *127*, 138–166.
3. Lengyel, M.; Kállai-Szabó, N.; Antal, V.; Laki, A.J.; Antal, I. Microparticles, microspheres, and microcapsules for advanced drug delivery. *Sci. Pharm.* **2019**, *87*, 20–50.
4. Galogahi, F.M.; Zhu, Y.; An, H.; Nguyen, N.-T. Core-shell microparticles: Generation approaches and applications. *JS: AMD* **2020**, S2468217920300757.

5. Sagis, L.M.C. *Microencapsulation and Microspheres for Food Applications*; Elsevier: Amsterdam, The Netherlands, 2015.
6. Kohane, D.S. Microparticles and nanoparticles for drug delivery. *Biotechnol. Bioeng.* **2007**, *96*, 203–209.
7. Perry, S.L.; McClements, D.J. Recent advances in encapsulation, protection, and oral delivery of bioactive proteins and peptides using colloidal systems. *Molecules* **2020**, *25*, 1161–1186.
8. Dalpiaz, A.; Cacciari, B.; Mezzena, M.; Strada, M.; Scalia, S. Solid lipid microparticles for the stability enhancement of a dopamine prodrug. *J. Pharm. Sci.* **2010**, *99*, 4730–4737.
9. Willerth, S. Drug delivery systems for engineering neural tissue. In *Engineering Neural Tissue from Stem Cells*; Willerth, Sl.; Elsevier, Amsterdam, The Netherlands, 2017; pp. 159–180.
10. El-Sherbiny, I.M.; El-Baz, N.M.; Yacoub, M.H. Inhaled nano- and microparticles for drug delivery. *Glob. Cardiol. Sci. Pract.* **2015**, *2015*, 2–15.
11. Li, J.; Ghatak, S.; El Masry, M.S.; Das, A.; Liu, Y.; Roy, S.; Lee, R.J.; Sen, C.K. Topical lyophilized targeted lipid nanoparticles in the restoration of skin barrier function following burn wound. *Mol. Ther.* **2018**, *26*, 2178–2188.
12. Davis, S.S. Coming of age of lipid-based drug delivery systems. *Adv. Drug Deliv. Rev.* **2004**, *56*, 1241–1242.
13. Shrestha, H.; Bala, R.; Arora, S. Lipid-based drug delivery systems. *J. Phar.* **2014**, *2014*, 1–10.
14. Jaspart, S.; Piel, G.; Delattre, L.; Evrard, B. Solid lipid microparticles: formulation, preparation, characterisation, drug release and applications. *Expert Opin. Drug Deliv.* **2005**, *2*, 75–87.
15. López-Iglesias, C.; Quílez, C.; Barros, J.; Velasco, D.; Alvarez-Lorenzo, C.; Jorcano, J.L.; Monteiro, F.J.; García-González, C.A. Lidocaine-loaded solid lipid microparticles (SLMPs) produced from gas-saturated solutions for wound applications. *Pharmaceutics* **2020**, *12*, 870–885.
16. Esfandiari, N. Production of micro and nano particles of pharmaceutical by supercritical carbon dioxide. *J. Supercrit. Fluid.* **2015**, *100*, 129–141.
17. Melgosa, R.; Benito-Román, Ó.; Sanz, M.T.; de Paz, E.; Beltrán, S. Omega–3 encapsulation by PGSS-drying and conventional drying methods. Particle characterization and oxidative stability. *Food Chem.* **2019**, *270*, 138–148.
18. Weidner, E.; Steiner, R.; Knez, Z. Powder generation from polyethyleneglycols with compressible fluids. In Process Technology Proceedings; Elsevier: Amsterdam, The Netherlands, 1996; Vol. 12, pp: 223–228.
19. Weidner, E.; Knez, Z.; Novak, Z. A process and equipment for production and fractionation of fine particles from gas saturated solutions. *World Patent WO* **1994**, 95, 21688.
20. Santos-Rosales, V.; Gallo, M.; Jaeger, P.; Alvarez-Lorenzo, C.; Gómez-Amoza, J.L.; García-González, C.A. New insights in the morphological characterization and modelling of poly(ε-caprolactone) bone scaffolds obtained by supercritical CO2 foaming. *J. Supercrit. Fluid.* **2020**, *166*, 105012–105022.
21. García-González, C.A.; Argemí, A.; Sousa, A.R.S. de; Duarte, C.M.M.; Saurina, J.; Domingo, C. Encapsulation efficiency of solid lipid hybrid particles prepared using the PGSS® technique and loaded with different polarity active agents. *J. Supercrit. Fluid.* **2010**, *54*, 342–347.
22. Fraile, M.; Martín, ÿ.; Deodato, D.; Rodriguez-Rojo, S.; Nogueira, I.D.; Simplício, A.L.; Cocero, M.J.; Duarte, C.M.M. Production of new hybrid systems for drug delivery by PGSS (Particles from Gas Saturated Solutions) process. *J. Supercrit. Fluid.* **2013**, *81*, 226–235.
23. Cifti, O.N.; Temelli, F. Formation of solid lipid microparticles from fully hydrogenated

canola oil using supercritical carbon dioxide. *J. Food Eng.* **2016**, *178*, 137–144.
24. Shekunov, B.Y.; Chattopadhyay, P.; Seitzinger, J.; Huff, R. Nanoparticles of poorly water-soluble drugs prepared by Supercritical Fluid Extraction of Emulsions. *Pharm. Res.* **2006**, *23*, 196–204.
25. Sodeifian, G.; Sajadian, S.A.; Saadati Ardestani, N.; Razmimanesh, F. Production of loratadine drug nanoparticles using ultrasonic-assisted Rapid expansion of supercritical solution into aqueous solution (US-RESSAS). *J. Supercrit. Fluid.* **2019**, *147*, 241–253.
26. Akolade, J.O.; Nasir-Naeem, K.O.; Swanepoel, A.; Yusuf, A.A.; Balogun, M.; Labuschagne, P. CO2-assisted production of polyethyleneglycol/lauric acid microparticles for extended reléase of Citrus aurantifolia essential oil. *J. CO2 Util.* **2020**, *38*, 375–384.
27. Pascual, C.D.; Subra-Paternault, P. *Supercritical Fluid Nanotechnology: Advances and Applications in Composites and Hybrid Nanomaterials*; Jenny Stanford Publishing: Singapore, 2015.
28. Tokunaga, S.; Ono, K.; Ito, S.; Sharmin, T.; Kato, T.; Irie, K.; Mishima, K.; Satho, T.; Harada, T.; Aida, T.M. *et al*; Microencapsulation of drug with enteric polymer Eudragit L100 for controlled release using the particles from gas saturated solutions (PGSS) process. *J. Supercrit. Fluid.* **2021**, *167*, 105044.
29. Haq, M.; Chun, B.-S. Microencapsulation of omega-3 polyunsaturated fatty acids and astaxanthin-rich salmon oil using particles from gas saturated solutions (PGSS) process. *Food Sci. Technol.* **2018**, *92*, 523–530.
30. Perinelli, D.R.; Bonacucina, G.; Cespi, M.; Naylor, A.; Whitaker, M.; Palmieri, G.F.; Giorgioni, G.; Casettari, L. Evaluation of P(L)LA-PEG-P(L)LA as processing aid for biodegradable particles from gas saturated solutions (PGSS) process. *Int. J. Pharm.* **2014**, *468*, 250–257.
31. Pedro, A.S.; Villa, S.D.; Caliceti, P.; Melo, S.A.B.V. de; Albuquerque, E.C.; Bertucco, A.; Salmaso, S. Curcumin-loaded solid lipid particles by PGSS technology. *The Journal of Supercritical Fluids* **2016**, *107*, 534–541.
32. Chakravarty, P.; Famili, A.; Nagapudi, K.; Al-Sayah, M.A. Using supercritical fluid technology as a green alternative during the preparation of drug delivery systems. *Pharmaceutics* **2019**, *11*, 629–662.
33. Pestieau, A.; Krier, F.; Lebrun, P.; Brouwers, A.; Streel, B.; Evrard, B. Optimization of a PGSS (particles from gas saturated solutions) process for a fenofibrate lipid-based solid dispersion formulation. *Int. J. Pharm.* **2015**, *485*, 295–305.
34. Strumendo, M.; Bertucco, A.; Elvassore, N. Modeling of particle formation processes using gas saturated solution atomization. *J. Supercrit. Fluid.* **2007**, *41*, 115–125.
35. de Azevedo, E.G.; Jun, L.; Matos, H. Modeling of particle formation from a gas-saturated solution process. *Proceedings of 6th International Symposium on Supercritical Fluids*, Versailles, France, 2003.
36. Landin, M.; Rowe, R.C. Artificial neural networks technology to model, understand, and optimize drug formulations. In *Formulation Tools for Pharmaceutical Development*; Elsevier: Amsterdam, The Netherlands, 2013; pp. 7–37.
37. Rodríguez-Dorado, R.; Landín, M.; Altai, A.; Russo, P.; Aquino, R.P.; Del Gaudio, P. A novel method for the production of core-shell microparticles by inverse gelation optimized with artificial intelligent tools. *Int. J. Pharm.* **2018**, *538*, 97–104.
38. Jara, M.O.; Catalan-Figueroa, J.; Landin, M.; Morales, J.O. Finding key nanoprecipitation variables for achieving uniform polymeric nanoparticles using neurofuzzy logic technology. *Drug Deliv. and Transl. Res.* **2018**, *8*, 1797–1806.
39. Rouco, H.; Diaz-Rodriguez, P.; Rama-Molinos, S.; Remuñán-López, C.; Landin, M. Delimiting the knowledge space and the design space of nanostructured lipid carriers through Artificial Intelligence tools. *Int. J. Pharm.* **2018**, *553*, 522–530.
40. Shah, M.; Agrawal, Y. Ciprofloxacin hydrochloride-loaded glyceryl monostearate

nanoparticle: factorial design of Lutrol F68 and Phospholipon 90G. *J. Microencapsul.* **2012**, *29*, 331–343.

41. Mu, H.; Holm, R. Solid lipid nanocarriers in drug delivery: characterization and design. *Expert Opinion on Drug Delivery* **2018**, *15*, 771–785.
42. Sampaio de Sousa, A.R.; Simplício, A.L.; de Sousa, H.C.; Duarte, C.M.M. Preparation of glyceryl monostearate-based particles by PGSS®—Application to caffeine. *J. Supercrit. Fluid.* **2007**, *43*, 120–125.
43. García-González, C.A.; Sousa, A.R.S. da; Argemí, A.; Periago, A.L.; Saurina, J.; Duarte, C.M.M.; Domingo, C. Production of hybrid lipid-based particles loaded with inorganic nanoparticles and active compounds for prolonged topical release. *Int. J. Pharm.* **2009**, *382*, 296–304.
44. Weidner, E. High pressure micronization for food applications. *J. Supercrit. Fluid.* **2009**, *47*, 556–565.
45. Van Ginneken, L.; Weyten, H. Particle Formation Using Supercritical Carbon Dioxide. In *Carbon Dioxide Recovery and Utilization*; Aresta, M.; Springer Netherlands: Dordrecht, The Netherlands, 2003; pp. 123–136.
46. Yun, J.-H.; Lee, H.-Y.; Asaduzzaman, A.K.M.; Chun, B.-S. Micronization and characterization of squid lecithin/polyethylene glycol composite using particles from gas saturated solutions (PGSS) process. *J. Ind. Eng. Chem.* **2013**, *19*, 686–691.
47. Roebuck, J.R.; Murrell, T.A.; Miller, E.E. The Joule-Thomson effect in carbon dioxide. *J. Am. Chem. Soc.* **1942**, *64*, 400–411.
48. Sampaio de Sousa, A.R. Development of Functional Particles using Supercritical Fluid Technology (Doctoral Thesis), Instituto de Tecnologia Química e Biológica, Universidade Nova de Lisboa: Oeiras, 2007.
49. Montes, A.; Litwinowicz, A.A.; Gradl, U.; Gordillo, M.D.; Pereyra, C.; Martínez de la Ossa, E.J. Exploring high operating conditions in the ibuprofen precipitation by Rapid Expansion of Supercritical Solutions process. *Ind. Eng. Chem. Res.* **2014**, *53*, 474–480.
50. Colbourn, E.; Rowe, R. Neural Computing and Pharmaceutical Formulation. In *Encyclopedia of Pharmaceutical Technology*; Marcel Dekker: New York, USA, 2005; pp. 145–157.

# 4. LIDOCAINE-LOADED SOLID LIPID MICROPARTICLES (SLMPs) PRODUCED FROM GAS-SATURATED SOLUTIONS FOR WOUND APPLICATIONS

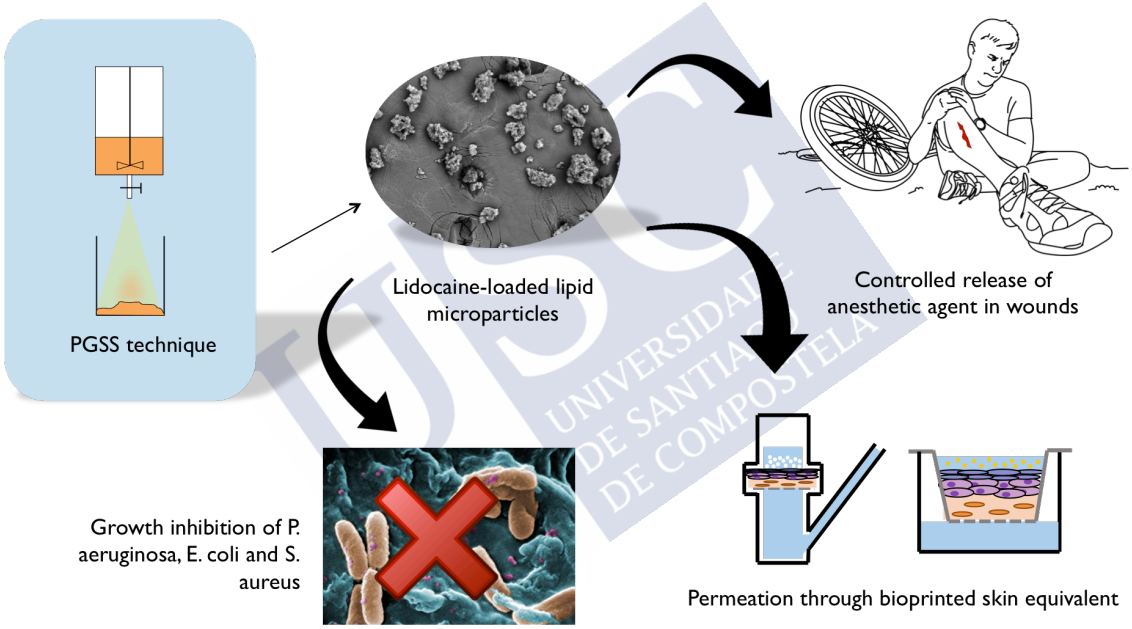


The work described in this chapter was published in López-Iglesias, C. *et al. Lidocaine-loaded solid lipid microparticles (SLMPs) produced from gas-saturated solutions for wound applications.* Pharmaceutics **2020**, 12, 870–885.

Work carried out in collaboration with the Department of Bioengineering and Aerospace Engineering of the Universidad Carlos III de Madrid (UC3M) within the frame of a 2-week research stay and the Instituto de Investigação e Inovação em Saúde of the Universidade do Porto, Portugal.

USC
UNIVERSIDADE
DE SANTIAGO
DE COMPOSTELA

# 4. LIDOCAINE-LOADED SOLID LIPID MICROPARTICLES (SLMPs) PRODUCED FROM GAS-SATURATED SOLUTIONS FOR WOUND APPLICATIONS

## 4.1. Introduction

Pain is one of the most debilitating symptoms of patients suffering from chronic and post-surgical wounds, especially during wound debridement and dressing exchange [1]. As an example, *ca.* 80% of patients suffering from venous leg ulcers report acute or chronic wound pain, which causes discomfort, stress, anxiety and, overall, poor quality of life [2–5]. Local anesthetics, and lidocaine hydrochloride (LID) in particular, have been used for decades to reduce wound pain (e.g., in post-operative analgesia) without hampering the physiological scarring process [6,7]. The mechanism of action of LID is the specific interaction and blockage of sodium channels of the sensorial neurons [8]. Through this LID–neuron interaction, when the nerve impulse arrives to the cell and the cell membrane is depolarized, sodium cations are unable to enter the neuron and the nerve impulse transmission is stopped. Furthermore, LID also has certain antimicrobial activity against common bacteria in nosocomial and surgical wound infections (e.g., *Enterococcus faecalis*, *Escherichia coli*, *Staphylococcus aureus*, and *Pseudomonas aeruginosa*), so its local infusion may also prevent bacterial colonization in post-operative wounds [9,10].

Particulate systems like micro- and nanoparticles are of increasing interest for drug delivery to the wound site [11,12]. The use of micron- and nano-sized systems based on organic and inorganic materials to deliver bioactive agents improves their efficacy and safety, and increases their physicochemical stability by protecting them from the environment (e.g., enzymatic degradation) [13–15]. Microparticles are often preferred for local drug delivery since they remain in the application site while providing a sustained drug release [15]. Lipids are regarded as advantageous components of particulate matrices for wound care, since they can mimic the natural components of skin and modulate the drug release [16–20]. Namely, solid lipid microparticles (SLMPs) usually present higher physicochemical stability and are easier

to sterilize and to scale-up than other lipid-based drug carriers like liposomes [21]. SLMPs have not been extensively studied for dermal and wound delivery, but have shown as potential candidates for topical and transdermal delivery of several drugs like econazole nitrate, testosterone, and tetracycline [22,23].

SLMPs processing usually requires the use of organic solvents and emulsifying agents, but novel processing strategies are arising to improve environmental and economic aspects. Supercritical $CO_2$ ($scCO_2$) has emerged as a processing tool for the development of new, green, and inexpensive techniques that require mild conditions and avoid/ mitigate organic solvents [14,24–26]. Namely, the PGSS® (Particles from Gas-Saturated Solutions) technique is based on the dissolution of $scCO_2$ in a molten substance, followed by a rapid expansion through a nozzle of the molten substance that causes solidification and precipitation of solid microparticles [27–30]. Unlike other compressed fluids, $scCO_2$ can interact with the processed substances at a molecular level decreasing their melting temperature, which may be advantageous for the scale-up of the process in terms of energy and cost optimization [28,31]. The processing of SLMPs using the PGSS® technique avoids the use of solvents or washing steps. High loading efficiencies of bioactive agents (insulin, recombinant human growth hormone, ibuprofen, ketoprofen) are commonly obtained using this technique [32–36]. The advantageous features of PGSS® technique can be herein exploited for the processing of SLMPs loaded with LID. These SLMPs can lead to a more prolonged release of LID and a longer duration of action than commercial LID-containing ointments, gels, and solutions. LID-loaded particles may thus adapt to the demands of the pharmacological action site (wound) where the damaged tissue accelerates drug permeation due to the absence of epidermis and the modified LID release also reduces the drug side effects of systemic absorption.

Drug permeability and toxicity in vitro test alternatives to the use of human or animal native skin are pursued to evaluate the performance of topical formulations, since these in vivo practices are constrained by economic, ethical, and practical reasons or even by regulation in the case of cosmetics [37,38]. Following the 3Rs principles and with the rise of the biomedical engineering discipline, several in vitro artificial skin models with attractive versatility and reproducibility are being commercialized or under development to reflect the three-dimensional environment of human native skin and the in vivo drug release conditions through the skin barrier [39]. 3D-bioprinting has emerged as an ideal technology to design more complex artificial skin models under automatized and standardized protocols able to mimic the native skin in a more reproducible manner [40]. The versatility of 3D-bioprinting has high translational and clinical relevance, since this technology can be exploited to produce not only full-thickness healthy skin, but also damaged skin under different pathological situations like acute and chronic wounds [41].

In this work, the PGSS® technique was implemented for the first time to produce SLMPs for specific wound delivery applications in pain and infection treatment. The SLMPs consisted on a matrix of glyceryl monostearate (GMS) loaded with LID at different contents (0, 1, 2, 4, and 10 wt.%) in an attempt to get formulations in the typical LID topical dosage range (0.5–5 wt.%) [42,43]. To the best of our knowledge, it is the first time that SLMPs loaded with LID were processed by the PGSS® technique. Obtained SLMPs were characterized in terms of physicochemical properties and drug content. Drug release behavior of LID from the SLMPs was evaluated using Franz cells and bioengineered skin substitutes with and without epidermis to evaluate the transport and release of LID through the intact skin and open wound skin tissues. Finally, the antimicrobial activity of LID released from the SLMPs against susceptible bacterial strains commonly present in infected wounds (*E. coli*, *S. aureus*, and *P. aeruginosa*) was assessed.

## 4.2. Materials and methods

### 4.2.1. Materials

Kolliwax® GMS II (glycerolmonostearate 40–55 type II, powder) was supplied by BASF (Ludwigshafen am Rhein, Germany). Lidocaine HCl monohidrate (> 99% purity) was purchased from Sigma-Aldrich (Saint Louis, MO, USA). $CO_2$ (99.8% purity) was supplied by Praxair (Madrid, Spain). Glacial acetic acid (purity > 99.0%) and acetonitrile (HPLC grade, purity > 99.9%) were purchased from Scharlau (Barcelona, Spain). NaOH (98.0% purity) was obtained from Panreac (Barcelona, Spain). Water was purified using reverse osmosis (resistivity > 18 MΩ·cm, Milli-Q, Millipore®, Madrid, Spain). Mueller-Hinton agar and broth were supplied by Merck Millipore (Darmstadt, Germany) and were used to perform the antimicrobial assays.

Human primary fibroblasts (hFBs) and human primary keratinocytes (hKCs) obtained from skin biopsies of healthy donors were obtained from the collections of biological samples of human origin, which are registered in the Registro Nacional de Biobancos para Investigación Biomédica del Instituto de Salud Carlos III with reference C.0002961. This collection is located in the Centro Comunitario de Sangre y Tejidos (CCST, Oviedo, Spain) and in the CIEMAT. Fresh frozen human plasma was provided by a local blood bank (Banco de Sangre del Centro Comunitario de Transfusión del Principado de Asturias, Oviedo, Spain), and was obtained following the standards of the American Association of Blood Banks [44].

### 4.2.2. SLMPs production by the PGSS® technique

Mixtures (6 g) of GMS manually mixed with a LID content of 0, 1, 2, 4, and 10 wt.% were loaded into a 300-mL high-pressure saturator (Eurotechnica GmbH, Bargteheide, Germany). After heating the saturator to 67 °C, $CO_2$ entered the equipment at a

constant flow of 7 g/min until a pressure of 170 bar was reached. After 1 h of contact of the compressed $CO_2$ with the molten lipid and drug under agitation at 400 rpm, the system was depressurized by the opening of a valve placed at the bottom of the saturator. The mixture was thus sprayed through a nozzle of 1 mm of diameter, and the fast depressurization caused the precipitation of the lipid-based formulation into solid microparticles inside a precipitator vessel of 2.7 L. SLMPs were then collected and kept in 50-mL Falcon tubes for further use. The SLMPs were denoted as GMS-LID*x*, *x* being the theoretical content of LID expressed as wt.%.

### 4.2.3. Analysis of the morphology, size, and surface of the particles

Images of the GMS particles processed by the PGSS® technique were obtained by scanning electron microscopy (SEM, EVO LS 15, Zeiss, Oberkochen, Germany) to evaluate the morphology, size, homogeneity, and surface of the particles. Prior to imaging, SLMPs were sputtered-coated (Q150T S/E/ES, Quorum Technologies, Lewes, UK) with a layer of 10 nm of iridium to improve the contrast. Particle sizes were measured by image analysis using ImageJ v1.49 software (National Institutes of Health, Bethesda, MD, USA).

### 4.2.4. Physicochemical characterization

Raw GMS powder, raw LID powder, GMS-LID0 and GMS-LID4 particles were analyzed by Attenuated Total Reflectance/Fourier-Transform Infrared Spectroscopy (ATR/FT-IR). A Gladi-ATR accessory equipped with a diamond crystal (Pike, Madison, WI, USA) was used. Spectra were collected in the mid-IR spectrum range (400–4000 $cm^{-1}$) using 32 scans at a resolution of 2 $cm^{-1}$. Crystallinity of the raw materials and GMS-LID0 and GMS-LID4 particles obtained by the PGSS® technique were studied by X-ray diffraction (XRD, PW-1710, Philips, Eindhoven, The Netherlands) in the 2–50° 2θ-range using a 0.02° step and Cu$K\alpha_1$ radiation. The raw materials, GMS-LID0 and GMS-LID4, were also analyzed using differential scanning calorimetry (DSC, DSC-Q100, TA Instruments; New Castle, DE, USA). Samples were weighted in an aluminum pan, cooled down from room temperature to 0 °C, and then heated up to 150 °C at a rate of 5 °C/min.

### 4.2.5. Determination of LID encapsulation efficiency

The encapsulation efficiency (EE) was evaluated by dispersing 26 mg of GMS-LID1, GMS-LID2, GMS-LID4, and GMS-LID10 particles in 10 mL of PBS pH7.4 under agitation (700 rpm). The suspensions were heated at 70 °C for 4 h until microparticles were molten and the entrapped drug was fully dissolved. Afterwards, the suspensions were centrifuged and cooled down (4000 rpm, 20 °C) and 1 mL of the supernatant was extracted and filtered with syringe filters (hydrophilic PTFE, 0.22 µm, Scharlau, Barcelona, Spain) for HPLC measurements.

LID concentration was measured by HPLC (JASCO Spain, Madrid, Spain) using a C18 column (Symmetry®, 5 µm, 3.9 × 150 mm, Waters, Milford, MA, USA) with isocratic elution [45]. The mobile phase consisted of acetonitrile:acetic acid 5% (pH 3.4 adjusted with 1 M NaOH solution) 15:85 (v/v). Flow was kept at 1 mL/min and temperature at 30 °C. LID had a retention time of 4.5 min, and the absorbance was measured at the wavelength of 262 nm. The calibration curve was carried out in the 1–100 µg/mL range ($R^2$ = 0.9995).

The encapsulation efficiency (EE) was calculated following the equation 4.1:

$$EE = \frac{w_P}{w_T} \cdot 100 \quad (4.1)$$

where $w_P$ is the amount of LID contained in the SLMPs measured by HPLC (in mg LID per mg of SLMPs) and $w_T$ is the initial amount of LID added for PGSS® processing (in mg LID per mg of GMS-LID mixture).

### 4.2.6. LID release tests from SLMPs

The release of LID from raw LID, GMS-LID1, GMS-LID2, GMS-LID4, and GMS-LID10 particles was performed in Franz diffusion cells consisting of a donor and a receptor compartment separated by a 0.45 µm cellulose nitrate membrane filter (Whatman, Little Chalfont, UK). Franz cells were kept in an orbital shaker (VWR® Incubating Mini Shaker, VWR, Chester, PA, USA) at 37 °C under agitation at 100 rpm. The volume of the receptor compartment was 6 mL and the surface available for diffusion was *ca.* 0.8 $cm^2$. The receptor compartment was filled with PBS pH 7.4 medium, and 25 mg of particles were placed in the donor compartment with 0.5 mL of PBS medium. Then, 1 mL-aliquots were taken every hour for the first 8 h and then after 24 h, and the same volume was replaced with fresh PBS solution. Samples were filtered with syringe filters (hydrophilic PTFE, 0.22 µm, Scharlau, Barcelona, Spain) and measured by HPLC (see Section 4.2.5). The release of LID from SLMPs was compared to the dissolution of 3 mg of pure LID, carried out using the same experimental set-up.

LID release profiles of the drug were fitted to the first-order (Equation 4.2) and the first-order with lag time (Equation 4.3) release kinetics models:

$$\%\ \text{LID released} = 100 \cdot (1 - e^{-k_1 \cdot t}) \quad (4.2)$$

$$\%\ \text{LID released} = 100 \cdot (1 - e^{-k_2 \cdot (t - t_{lag})}) \quad (4.3)$$

where $k_1$ and $k_2$ are the kinetic coefficients, $t$ is the elapsed release time, and $t_{lag}$ is the lag time.

### 4.2.7. Preparation of bioprinted human skin equivalents

Bioprinted human skin substitutes were generated following a previously developed method [46]. Briefly, two celular layers were printed: a dermal layer, formed by a plasma-derived fibrin matrix populated with hBFs, and an epidermal layer formed by hKCs seeded on top. Cell cultures were printed on polyethylene terephthalate (PET) cellular inserts (Falcon 353102, 4.2 $cm^2$ area, 1 µm pore diameter; Thermo Fischer Scientific, Waltham, MA, USA) in a 6-well culture plate (Corning Costar Corp., Cambridge, MA, 4.15 $cm^2$) and were allowed to differentiate at the air-liquid interface for 17 days at 37 °C in a $CO_2$ incubator in hKCs medium containing 0.5% FBS and 50 µg of ascorbic acid as differentiating medium (Fig. 4.1a). The medium was changed every three days.

### 4.2.8. LID release tests through bioprinted human skin equivalents

Firstly, the diffusion of LID dissolved in PBS from pure LID powder and the GMS-LID4 microparticles through the intact bioengineered skin equivalent, i.e. with epidermal and dermal layers, were compared. The bioengineered skin equivalents were collected (Fig. 4.1b) and cut with a scalpel in circles of 2 cm of diameter, and used as membranes in 6-mL Franz diffusion cells (Fig. 4.2a). Release tests and LID measurements by HPLC were carried out in four replicates and using the same protocols as in Section 4.2.5.

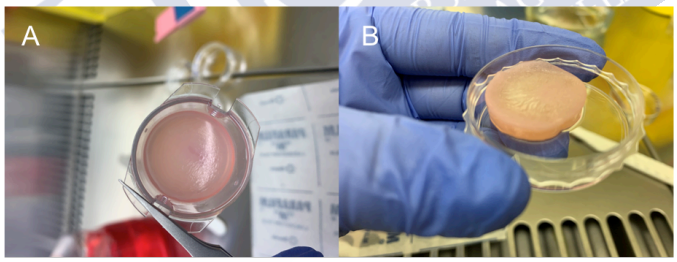


Figure 4.1. Visual appearance of (a) bioprinted human skin equivalents in cellular inserts, and (b) once removed from the inserts for certain permeation tests in Franz diffusion cells.

A second part of the LID release tests was carried out to compare the diffusion of LID from SLMPs through intact bioengineered skin equivalents (Fig. 4.2b.1) and the same skin equivalents without epidermis (only dermis, Fig. 4.2b.2) to mimic an open skin wound. Using the bioengineered skin equivalents in the cellular insert, the epidermis was removed with the help of precision forceps. The experiment was carried out in triplicate and directly in the cellular inserts adapting a protocol from the literature [47]. GMS-LID4 particles were added to each insert along with 0.5 mL of PBS to facilitate their humectation. The 6-well culture plate was filled with 10 mL of PBS pH 7.4 as the receptor medium. 1-mL aliquots were taken at the same selected times, filtered with syringe filters (hydrophilic PTFE, 0.22 µm pore diameter; Scharlau, Barcelona, Spain) and measured by HPLC (*cf.* Section 4.2.5). The extracted volume was replaced with equal volumes of fresh PBS medium.

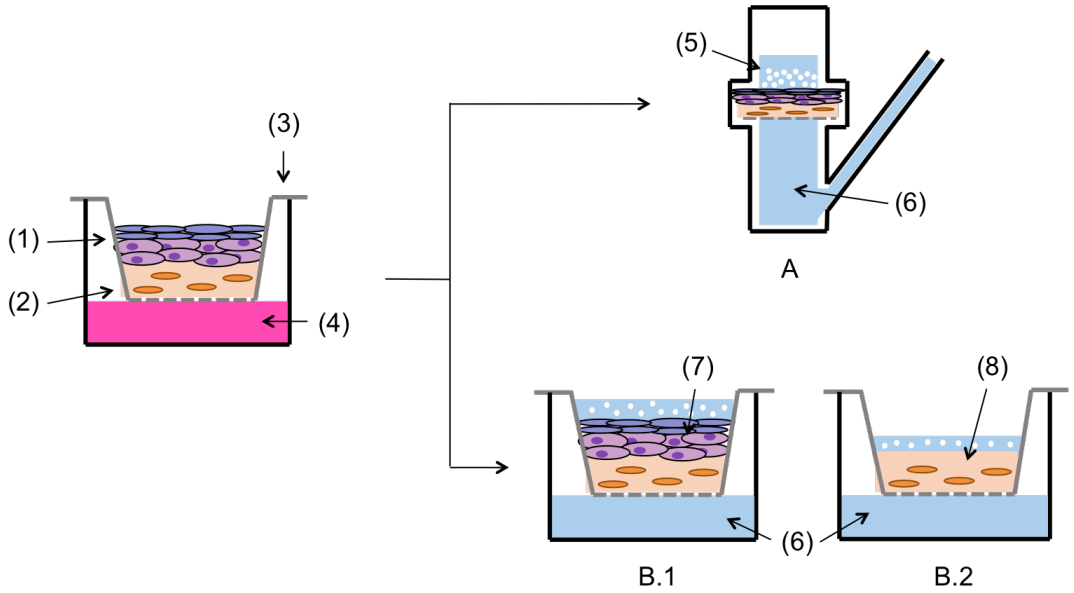


Figure 4.2. Full thickness skin substitute consisting of epidermal (1) and dermal (2) tissues was cultured on cellular inserts (3) using hKCs culture medium (4). For permeation tests, the base of the cellular insert with full thickness skin was placed as separator membrane in Franz cells (a), using raw lidocaine hydrochloride (LID) or drug-loaded GMS-LID4 particles (5) in the donor compartment. The release medium was PBS pH 7.4 (6). Another part of the experiment tested the permeation of LID from GMS-LID4 particles directly in the cellular inserts, using (b.1) either full thickness skin substitute (7) containing the keratinocyte layer, (b.2) or dermal tissue (8) without epidermis as membrane.

Histological analysis of the bioengineered skin equivalents was performed before and after (24 h) the drug release experiments to assess their integrity and whether the particles penetrated them. Skin samples were fixed in 3.7% buffered formaldehyde for 24 h and embedded in paraffin. 5-µm cross-sections were dewaxed, rehydrated and stained with hematoxylin-eosin (H&E).

### 4.2.9. Antimicrobial tests

The antimicrobial activity of LID was assessed against susceptible bacterial strains commonly present in infected wounds: *E. coli* 25922, *S. aureus* 33591 and *P. aeruginosa* PA01. Susceptibility tests to LID were performed by determination of the Minimum Inhibitory Concentration (MIC) and Minimum Bactericidal Concentration (MBC) of LID powder, according to the CLSI standards broth microdilution procedure. Furthermore, the antimicrobial activity of LID released from 40 mg of GMS-LID10 particles in 5 mL of PBS medium after 6 h was evaluated by quantifying the cultivable bacteria.

#### 4.2.9.1. Minimum inhibitory concentration

Bacteria were grown overnight at 37 °C in Mueller-Hinton Broth (MHB) at 150 rpm. After incubation, a bacterial suspension was adjusted to *ca.* $10^6$ colony forming

units (CFU/mL). Subsequently, 100 µL of bacterial suspension and 100 µL of LID at different concentrations (39400, 19700, 9850, 4925, 2463, and 1231 µg/mL) were placed in 96-well microplates and incubated for 24 h at 37 °C and 150 rpm. Bacterial growth (turbidity) was evaluated measuring absorbance at 640 nm in a microplate reader. All tests were performed in quintuplicate with two repeats. MICs were expressed in terms of µg/mL [48]. Two controls were used to perform the antimicrobial tests: a positive control representing the bacterial growth without LID (0 µg/mL) and a negative control representing the absorbance of medium without bacteria.

#### 4.2.9.2. Minimum bactericidal concentration

Bacteria were grown overnight in MHB at 37 °C and 150 rpm. After incubation, a bacterial suspension was adjusted to *ca.* $10^6$ colony forming units (CFU/mL). Then, 100 µL of bacterial suspension and 100 µL of LID (at the same concentrations as for the MIC determination) were placed in 96-well microplates and incubated for 24 h at 37 °C and 150 rpm. Subsequently, cultivable bacteria were quantified by colony counting in Mueller-Hinton Agar (MHA). All experiments were performed in quintuplicate with two repeats. MBCs were expressed in terms of µg/mL [48]. Two controls were used to perform the antimicrobial tests: a positive control representing the bacterial growth without LID (0 µg/mL) and a negative control representing the initial bacterial concentration.

#### 4.2.9.3. Antimicrobial activity of LID released from GMS

Bacteria were grown overnight in MHB at 37 °C and 150 rpm and a bacterial suspension of *ca.* $10^7$ cells/mL. GMS-LID10 particles (40 mg) were dispersed in 5 mL of PBS pH 7.4. Then, 180 µL of PBS with LID released from GMS-LID10 particles and 20 µL of bacterial suspension were placed (five for each condition) in 96 well-plates. After 24 h of incubation at 37 °C and 150 rpm, the cultivable bacteria were quantified by the colony-forming units (CFUs) method. Bacterial density (in $\log_{10}$ CFUs/mL) was plotted according to each condition. Bacterial growth without LID was used as control. All experiments were performed in quintuplicate with two repeats.

### 4.2.10. Statistical analysis

Results were reported as mean ± standard deviation. Statistical analysis of the antimicrobial tests was performed using one-way analysis of variance (ANOVA) test followed by posthoc Tukey HSD multiple comparison test (IBM® SPSS® Statistics v.22.0, Armonk, NY, USA), which was used to determine the significant difference (*p*).

## 4.3. Results and discussion

### 4.3.1. Morphological and physicochemical properties of the SLMPs

Obtained GMS particles were fine, white and free-flowing powder. The conditions of pressure and temperature for the processing of GMS particles containing LID were selected above the melting point of GMS so they would provide good processability. Thus, the SEM images showed an open and porous structure, caused by the escape of $CO_2$ from the molten lipid and sudden solidification upon depressurization (Fig. 4.3). The shape of the particles was non-spherical and particle diameter was in the 20–120 µm range with a mean of 114 µm, a standard deviation of 39 µm and a PDI of 0.12. The non-sphericity of lipid particles using the PGSS® technique is also observed using other SLMPs processing technologies like spray drying and this morphology can influence the drug release behaviour due to shorter drug diffusion pathways [49,50]. The processing of GMS together with LID did not influence the overall appearance of the particles.

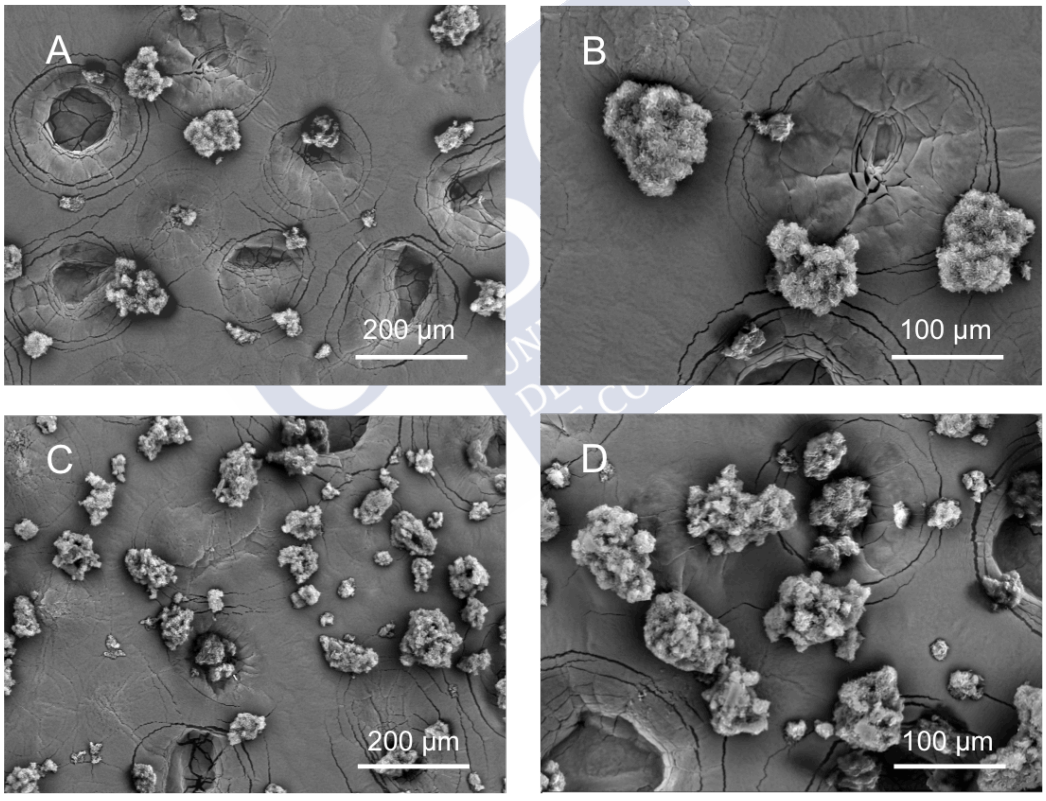


Figure 4.3. SEM images of (a,b) GMS-LID0 and (c,d) GMS-LID4 particles. The processing of GMS with LID did not influence the overall appearance and shape of the particles.

ATR/FT-IR spectroscopic studies confirmed the presence of LID in the GMS-based particles (Fig. 4.4a). The spectrum of GMS-LID4 particles showed a small band at the wavelength of 1542 $cm^{-1}$, corresponding to the characteristic band of C=O carbonyl group stretching mode of LID [51]. Spectra of pure GMS powder and GMS processed by the PGSS® technique were practically identical, proving that the processing with $scCO_2$ did not alter the chemical structure of the GMS. The XRD analysis of the GMS-

LID4 powder (Fig. 4.4b) did not show the characteristic sharp peaks of crystalline LID, suggesting the change of the drug from the crystalline to the amorphous state upon processing with the PGSS® technique. The absence of crystalline LID was also confirmed by the DSC analysis (Fig. 4.5). No peaks corresponding to crystalline LID were observed in the thermogram of the GMS-LID4 particles. The main thermal events obtained from the DSC thermograms after peak integration are summarized in Table 1.

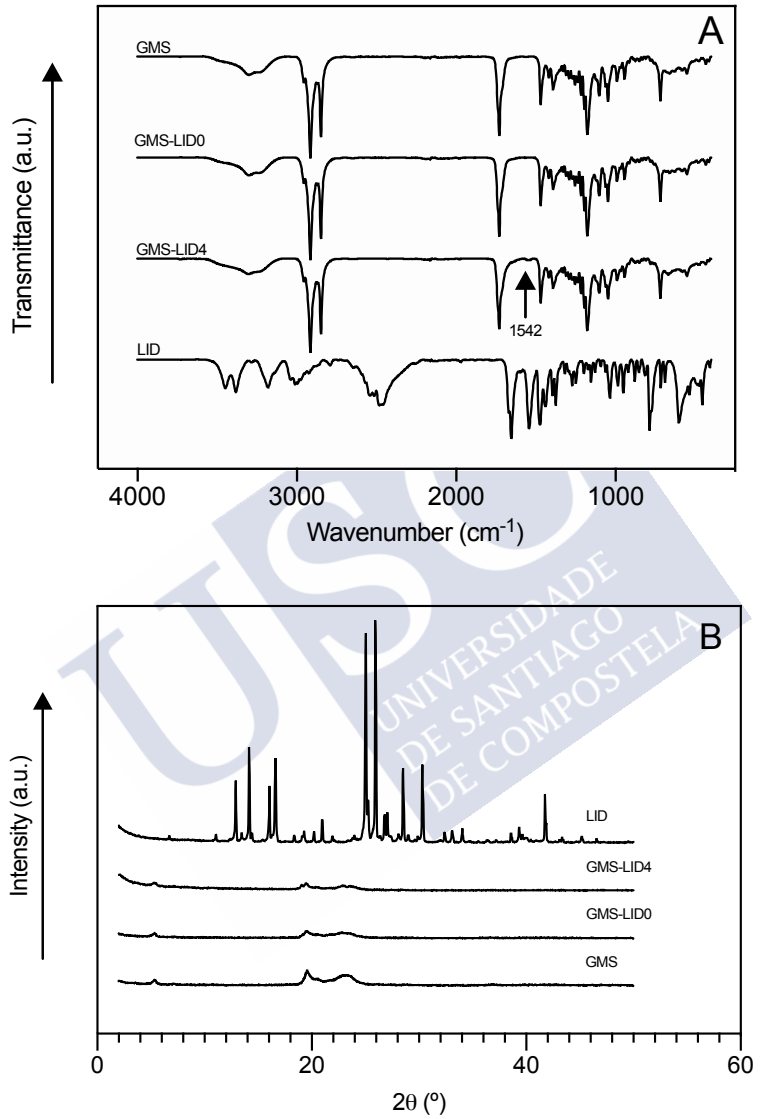


Figure 4.4. (a) ATR/FT-IR spectra and (b) XRD patterns of pure GMS, SLMPs of GMS processed by the PGSS® technique (GMS-LID0), SLMPs loaded with LID (GMS-LID4) and pure LID powder.

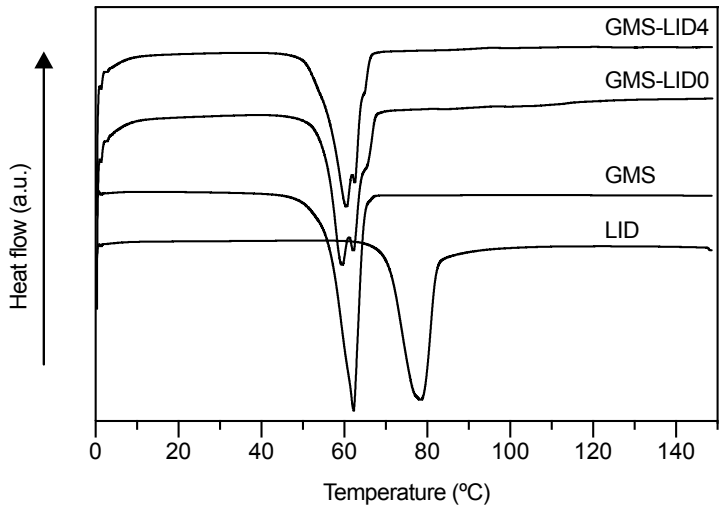


Figure 4.5. DSC thermograms of the raw materials, GMS-LID0 and GMS-LID4 particles. No peaks corresponding to crystalline LID were appreciated in the GMS-LID4 particles.

Table 4.1. Thermal properties of raw materials and GMS particles processed without (GMS-LID0) and with LID (GMS-LID4).

| Thermal event | LID | GMS | GMS-LID0 | GMS-LID4 |
|---|---|---|---|---|
| $T_m$ (°C) | 78.12 | 62.28 | 62.46 | 60.56 |
| $\Delta H_m$ (J/g) | 187.0 | 186.8 | 179.1 | 170.9 |

### 4.3.2. LID encapsulation efficiency

Initial LID contents for SLMPs processing were set in the 1–10 wt.% range taking into account the usual LID concentrations in topical LID formulations for pain treatment (0.5–5 wt.%) [42,43], and the high encapsulation efficiencies usually obtained by PGSS® technology. Accordingly, LID encapsulation efficiencies for GMS-LID1, GMS-LID2, GMS-LID4 and GMS-LID10 particles were 69.6 ± 4.5, 59.7 ± 13.6, 79.0 ± 4.0 and 75.1 ± 0.9%, respectively. These values correlated well with the encapsulation efficiency of other studies using the PGSS® technique for the loading of drugs into microparticles [27], although it is the first time LID is incorporated. $CO_2$ at supercritical conditions can act as a solvent for the drug, so drug loss could take place by the partial dissolution of the drug in $scCO_2$ and its deposition on the walls of the equipment after depressurization [52]. Unlike lidocaine, the hydrochloride salt has no measurable solubility in $scCO_2$ at temperatures up to 45 °C [53]. The solubility of LID in $scCO_2$ may increase at higher temperatures, as it occurs with other anaesthetic drugs. Nevertheless, high drug encapsulation efficiencies were herein obtained and related to the solvent-free processing of the particles and absence of downstream steps.

LID content in the different SLMPs processed by PGSS® (GMS-LID1, GMS-LID2, GMS-LID4 and GMS-LID10) was 0.7 ± 0.0, 1.2 ± 0.3, 3.2 ± 0.2 and 7.5 ± 0.2 wt.%,

respectively. The drug contents obtained in the SLMPs are thus compatible with formulations for local drug administration where recommended LID doses are 5300 mg [42,43].

### 4.3.3. LID release tests

SLMPs were suspended in PBS medium at the donor chamber of the Franz diffusion cells, forming a thin layer. A sustained release of LID from the SLMPs was obtained (Fig. 4.6), being at least 50% of the drug payload released after 4 h and the complete release attained after 24 h. The release profile was noticeably delayed with respect to the dissolution profile of pure LID in Franz cells (Figure 4.7), where more than 85% of the initial amount of LID was quantified after only 15 min, and the complete dissolution took place after 1 h. LID solutions used clinically for local infusion by subcutaneous injection present a duration of action of 0.52 h, normally keeping their effect only during a surgical procedure [54]. SLMPs providing a controlled release of the anesthetic agent could be useful to maintain local anesthesia for longer times, during the first stage of wound healing.

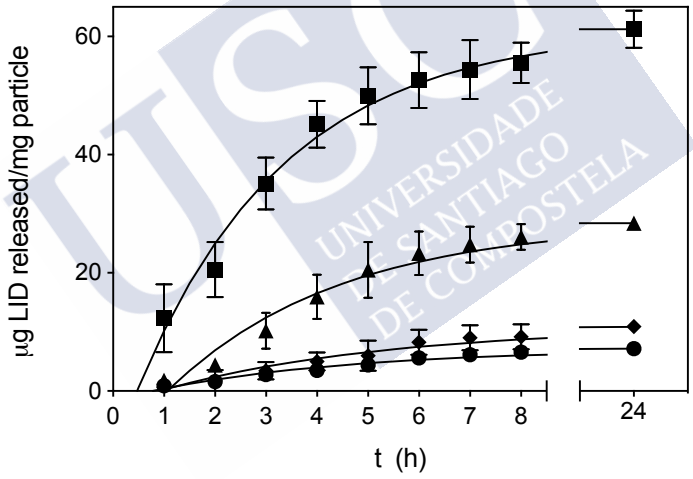


Figure 4.6. Release data of GMS-LID1 (circles), GMS-LID2 (diamonds), GMS-LID4 (triangles) and GMS-LID10 (squares) particles in PBS pH 7.4 at 37 °C and 100 rpm. Lines represent the fittings to a first-order kinetic release with lag time model (Eq. 4.3).

The LID release profile of GMS-LID1, GMS-LID2, GMS-LID4 and GMS-LID10 particles fitted well to a first-order kinetic model (Table 4.2). The first-order release occurs when the drug release rate is dependent on its concentration. The amount of drug released from the matrix is proportional to the amount remaining, so it tends to decrease with time [55]. The release profile fitted better to a first-order with lag time kinetic model. The LID dissolution in aqueous media is highly dependent on the hydration of the microparticles, since LID is a hydrophilic drug included within a lipid matrix. The hydrophobic nature of the GMS should delay this hydration and explains the lag times between 0.8 and 1.1 h. Once dissolved, LID release is conditioned by the diffusion of the drug through the lipid matrix.

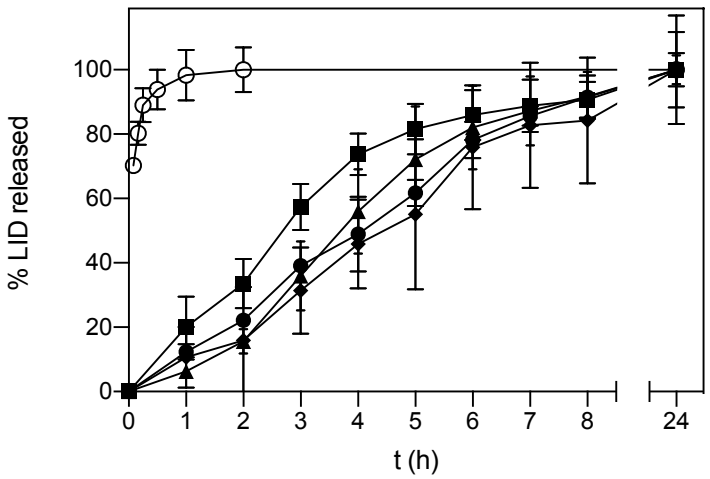


Figure 4.7. Release profile (in percentage of drug released) of raw LID (white circles), GMS-LID1 (black circles), GMS-LID2 (diamonds), GMS-LID4 (triangles) and GMS-LID10(squares) particles in PBS pH 7.4 at 37 °C and 100 rpm.

Table 4.2. Kinetic fitting parameters of LID release profiles from SLMPs in PBS pH 7.4 medium to the first-order and the first-order with lag time kinetic models according to Eqs. (2) and (3), respectively.

| SLMPs | First-order | | First-order with lag time | | |
|---|---|---|---|---|---|
| | $k_1$ ($h^{-1}$) | $R^2$ | $k_2$ ($h^{-1}$) | $t_{lag}$ (h) | $R^2$ |
| GMS-LID1 | 0.3047 | 0.938 | 0.2532 | 0.7708 | 0.966 |
| GMS-LID2 | 0.2538 | 0.941 | 0.2278 | 0.9049 | 0.959 |
| GMS-LID4 | 0.3308 | 0.963 | 0.2975 | 1.066 | 0.970 |
| GMS-LID10 | 0.3224 | 0.985 | 0.3435 | 0.4736 | 0.985 |

### 4.3.4. LID permeation through bioengineered skin substitutes

Topical anesthetics like LID block reversibly the free nerve-ending conductions in the dermis and mucosa. This process can be limited by drug diffusion through the epidermis, since in healthy skin the drug has to pass through the stratum corneum to reach dermal tissue at therapeutic concentrations [56]. The versatility of 3D-bioprinting was exploited in this work to produce different types of skin substitutes (full-thickness healthy skin and dermal layer tissue) to study the effect of epidermis barrier on LID diffusion and to mimic the open wound skin tissue.

The penetration of LID through a bioprinted skin equivalent based on two cellular layers, representing the dermis (lower layer) and the epidermis (upper layer) was thus firstly studied. The penetration of LID from GMS-LID4 particles and pure LID powder was compared using Franz cells (Fig. 4.8a). Penetration of pure LID powder dissolved in the PBS medium was faster than LID released from GMS-LID4 particles. Probably, the

release of LID from the particles acted as the limitating step, so LID firstly dissolved from the particles into the PBS medium and then passed through the membrane. Furthermore, LID powder dissolved very fast in the donor chamber and it is expected that the drug permeates faster at a higher concentration gradient between the donor and the acceptor chamber.

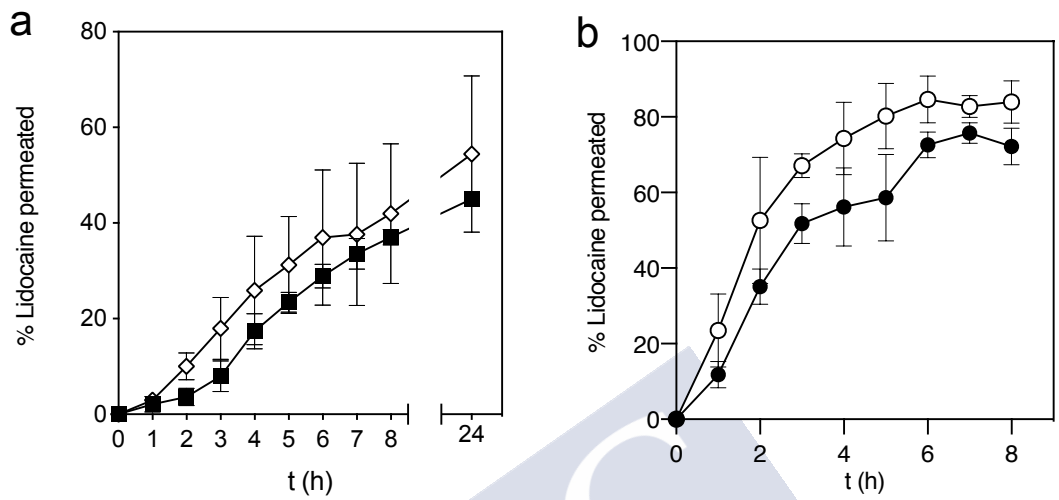


Figure 4.8. Permeability of LID through a bioengineered skin substitute comparing (a) the permeability of LID released from GMS-LID4 particles (squares) and LID powder (diamonds) in Franz cell experiments (*n* = 4), and (b) the permeability of LID released from GMS-LID4 particles through complete skin tissue (epidermal and dermal layers, black circles) and dermal layer (white circles) (*n* = 3).

The penetration of LID released from the particles through a full thickness skin substitute and through a dermal layer alone was compared (Fig. 4.8b). This study was carried out using a 3D-tissue model with skin substitutive membranes prepared in inserts and located in multi-well plates since the dermal layer was very fragile and its removal from the insert compromised the integrity of the skin equivalents. This method was also advantageous to get a more compact setup and to facilitate the run of multiple samples in parallel [47]. The dermal layer is highly hydrated, so LID dissolved in PBS diffused faster through the dermis tissue. A higher percentage of permeated LID was detected in this experiment using cellular inserts with respect to the studies in the Franz cell experiments (Fig. 4.7 and 4.8). In accordance to the Fick's second diffusion law, the faster drug permeation to the reception chamber obtained with the cellular inserts was attributed to the much larger effective diffusion area (4.2 $cm^2$) with respect to the Franz cells (0.8 $cm^2$). However, when the LID permeation values were normalized per surface area, results showed that LID contained in the GMS particles permeated faster through the full thickness skin substitute in the Franz cells (0.37 mg LID/$cm^2$ after 8 h) than in the cellular inserts (0.14 mg LID/$cm^2$ after 8 h). This difference could be attributed to a possible damage if the skin equivalent membranes during cutting and transfer to the Franz cells.

Histological analysis showed that the skin is not damaged with the presence of the GMS microparticles as all printed skin equivalents maintained their integrity in PBS medium after 24 h of topical treatment (Fig. 4.9b,d). The structures were similar to the skin equivalents initially prepared (Fig. 4.9a,c) with an intact stratum corneum, epidermis and dermis. Therefore, LID-loaded GMS microparticles have no toxic adverse effects on the skin.

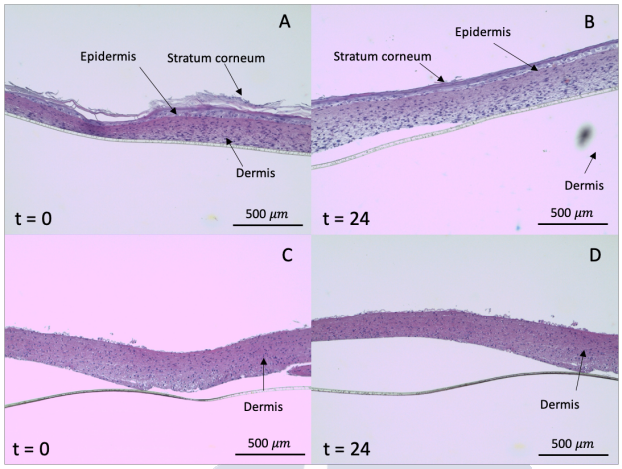


Figure 4.9. Histological analysis of fixed full thickness skin (containing epidermal and dermal layers (a and b) and skin equivalents with only dermis (c and d) before (t = 0 h) and after (t = 24 h) the LID permeation experiment from GMS-LID4 particles in the cellular inserts.

### 4.3.5. Antimicrobial activity of the SLMPs

Among the local anesthetics, LID-based formulations are the most studied medications for a supplemental antimicrobial role. The mechanism of antimicrobial action of LID is not fully elucidated but related to the dysfunction of cellular respiration, the alteration of bacterial protein synthesis and the disruption of the bacterial cell wall or cytoplasmic membrane [57–59].

The MIC and MBC values for free lidocaine were determined in this work against *E. coli*, *S. aureus* and *P. aeruginosa* bacterial strains (Figure 4.10) to define the minimum concentration of LID capable to inhibit the bacterial growth and kill bacteria, respectively. This information is of relevance in this work to define the LID content needed in the SLMP particles to obtain particles with therapeutic potential against the most common bacteria found in infected wounds. MIC is defined as the lowest concentration of antimicrobial agent that inhibits the visible bacterial growth [48]. In order to determine the MIC values, bacteria were cultured in broth containing dilutions of LID and the turbidity of the broths after 24 h of incubation was compared with the turbidity of the negative control (broth without bacteria) [60]. Three concentrations of LID (9,850, 19,700 and 39,400 µg/mL) visibly inhibited *E. coli* growth (Fig. 4.10a), whereas only the concentration of 39,400 µg/mL was able to avoid bacterial growth for *S. aureus* and *P. aeruginosa*. Accordingly, MIC for *E. coli* was 9850 µg/mL and for *S. aureus* and *P. aeruginosa* was four-fold higher (39,400 µg/mL).

Results correlate well with previous works showing that the LID at low concentrations was more active against *E. coli* strains, whereas for *S. aureus* and *P. aeruginosa* strains higher MICs of LID were needed to avoid their growth [61,62].

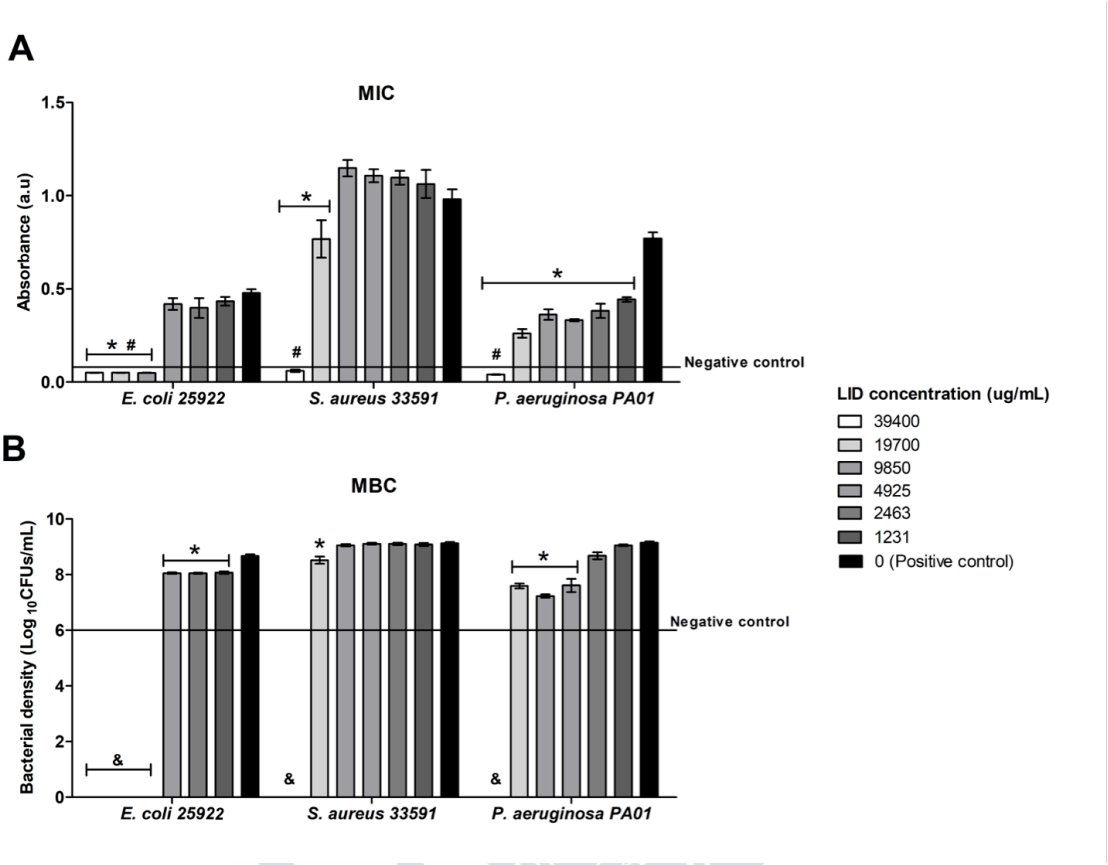


Figure 4.10 Antimicrobial activity of LID obtained by determination evaluation of MIC (a) and MBC (b) for *E. coli* 25922, *S. aureus* 33591 and *P. aeruginosa* PA01 strains. *Statistically different ($p < 0.05$) compared with bacterial growth without LID (positive control). #Absorbance of bacterial growth lower or equal to the control negative (absorbance of medium without bacteria). &statistically different ($p < 0.05$) compared with initial bacterial concentration (negative control MBC).

MBC is the lowest concentration of antimicrobial agent at which no cultivable bacteria (CFUs) are detected on a solid medium, causing bacterial death. MBC is determined as the lowest concentration of antimicrobial agent that reduces the viability of the initial bacterial inoculum by a pre-determined reduction such as ≥ 99.9%. In this work, the bactericidal activity of LID was tested against the bacterial strains used. 1 wt.% LID was enough to kill ≥ 99.9% of *E. coli* bacteria, whereas for *S. aureus* and *P. aeruginosa* a higher LID concentration (*ca.* 4 wt.%) was needed. Moreover, significant differences were found in terms of bacterial density for all strains compared to a positive control (bacteria without LID) for specific LID concentrations. For instance, for *E. coli*, the concentrations of 0.12, 0.25 and 0.5 wt.% of LID reduced 75% of bacterial density compared with positive control (Fig. 4.10b). For *P. aeruginosa*, this reduction was more pronounced with reductions higher than 95% for LID concentrations of 0.5, 1 and 2 wt.%. These results emphasized the antimicrobial

activity of LID [62–64], particularly against the most common bacteria found in infected wounds [10].

According to the MIC and MBC values of LID for *E. coli*, *S. aureus* and *P. aeruginosa* bacteria, GMS-LID10 particles were tested regarding their antimicrobial activity, since the LID concentration levels released from these particles into the medium were higher than the MIC and MBC values for the three bacterial strains. Results from GMS-LID10 particles showed an outstanding antimicrobial activity able to kill all the bacterial strains used after 24 h of incubation (Fig. 4.11). These results further emphasize the therapeutic potential of the developed local delivery approach based on dressings, in the prevention and eradication of relevant bacteria in post-operative wounds, prior to their colonization and biofilm infection establishment.

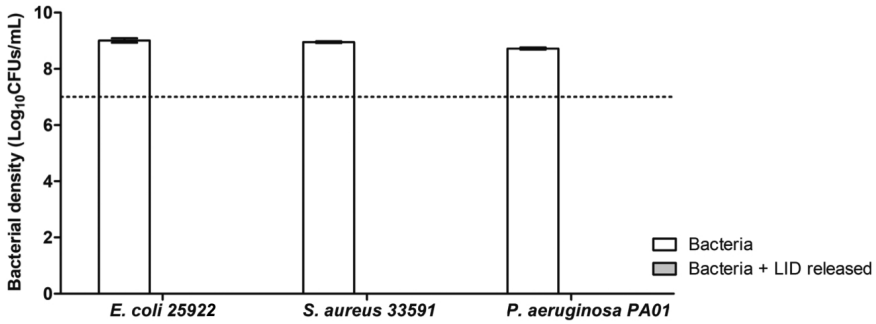


Figure 4.11. Antimicrobial activity of LID released from GMS-LID10 particles. Bacterial growth without LID after 24 h of incubation was used as control (white bars). Horizontal dashed line indicates the initial bacterial density. The LID released from GMS-LID10 particles was able to kill all bacteria after 24 h of culture.

## 4.4. Conclusions

GMS microparticles incorporating lidocaine hydrochloride for specific wound delivery applications were prepared by PGSS® technique. The obtained particles had a high encapsulation efficiency (70–79%) and a tunable lidocaine content (0.7–7.5 wt.%) that can be adapted to the required doses to get the intended anesthetic effect. The lidocaine release from the lipid particles fitted to a first-order with lag time kinetic model with 50% of the drug payload released after *ca.* 4 hours. This drug release behaviour can result in formulations with reduced doses with respect to commercial formulations with local infiltration of lidocaine. Antimicrobial tests also emphasized the therapeutic potential of the lidocaine-loaded particles in the prevention and full eradication of relevant Gram-positive and Gram-negative bacteria in post-operative wounds, prior to their colonization and biofilm infection establishment. Therefore, the lidocaine content in the formulation can be adjusted to get an attractive anesthetic-plus-antimicrobial combined effect, which is of high relevance for the management of chronic wounds. Diffusion through the skin barrier of lidocaine from the microparticles was evaluated using an innovative 3D-bioprinted skin equivalent models mimicking the

intact skin and open wound skin tissues. This *in vitro* test allowed to assess the different permeation behavior of lidocaine depending on the skin condition and failure and to confirm the non toxicity of the particles for the skin. The full potential of this *in vitro* skin model needs to be validated and the technology evaluated for the processing of other models for skin under different pathological situations.

## 4.5. References


1. Catanzano, O.; Docking, R.; Schofield, P.; Boateng, J. Advanced multi-targeted composite biomaterial dressing for pain and infection control in chronic leg ulcers. *Carbohyd. Polym.* **2017**, *172*, 40–48.
2. Briggs, M.; Nelson, E.A.; Martyn-St James, M. Topical agents or dressings for pain in venous leg ulcers. *Cochrane Database of Systematic Reviews.* **2012**, *11*, CD001177.
3. Jones, J.; Williams, H. Wound management should not be a pain. *Br. J. Community Nurs.* **2017**, *22*, S38–S46.
4. Fauziyah, H.; Gayatri, D. Pain, stress, and sleep quality in chronic wound patients. *Enferm. Clínica* **2018**, *28*, 176–179.
5. Woo, K.Y. Wound-related pain: Anxiety, stress and wound healing. *Wounds UK* **2010**, *6*, 92–98.
6. Kesici, S.; Kesici, U.; Ulusoy, H.; Erturkuner, P.; Turkmen, A.; Arda, O. Effects of local anesthetics on wound healing. *Braz. J. Anesthesiol. (English Edition)* **2018**, *68*, 375–382.
7. Steele, K. Topical treatments for acute and chronic wound pain. *J. Palliat. Med.* **2017**, *20*, 560–561.
8. Barletta, M.; Reed, R. Local nesthetics. *Vet. Clin. N. Am. Small* **2019**, *49*, 1109–1125.
9. Razavi, B.M.; Fazly Bazzaz, B.S. A review and new insights to antimicrobial action of local anesthetics. *Eur. J. Clin. Microbiol, Infect. Dis.* **2019**, *38*, 991–1002.
10. Parr, A.M.; Zoutman, D.E.; Davidson, J.S.D. Antimicrobial activity of lidocaine against bacteria associated with nosocomial wound infection. *Ann. Plast. Surg.* **1999**, *43*, 239–245.
11. Saghazadeh, S.; Rinoldi, C.; Schot, M.; Kashaf, S.S.; Sharifi, F.; Jalilian, E.; Nuutila, K.; Giatsidis, G.; Mostafalu, P.; Derakhshandeh, H.; et al. Drug delivery systems and materials for wound healing applications. *Adv. Drug Deliv. Rev.* **2018**, *127*, 138–166.
12. Johnson, N.; Wang, Y. Drug delivery systems for wound healing. *Curr. Pharm. Biotechnol.* **2015**, *16*, 621–629.
13. Gref, R.; Minamitake, Y.; Peracchia, M.; Trubetskoy, V.; Torchilin, V.; Langer, R. Biodegradable long-circulating polymeric nanospheres. *Science* **1994**, *263*, 1600–1603.
14. Chakravarty, P.; Famili, A.; Nagapudi, K.; Al-Sayah, M.A. Using supercritical fluid technology as a green alternative during the preparation of drug delivery systems. *Pharmaceutics* **2019**, *11*, 629–662.
15. Ranjan, S.; Fontana, F.; Ullah, H.; Hirvonen, J.; Santos, H.A. Microparticles to enhance delivery of drugs and growth factors into wound sites. *Ther. Deliv.* **2016**, *7*, 711–732.
16. Radtke, M.; Souto, E.B.; Müller, R.H. Nanostructured lipid carriers: A novel generation of solid lipid drug carriers. *Pharm. Technol. Eur.* **2005**, *17*, 45–50.
17. Müller, R.H.; Radtke, M.; Wissing, S.A. Solid lipid nanoparticles (SLN) and nanostructured lipid carriers (NLC) in cosmetic and dermatological preparations. *Adv. Drug Deliv. Rev.* **2002**, *54*, S131–S155.
18. Davis, S.S. Coming of age of lipid-based drug delivery systems. *Adv. Drug Deliv. Rev.* **2004**, *56*, 1241–1242.
19. Wang, W.; Lu, K.; Yu, C.; Huang, Q.; Du, Y.-Z. Nano-drug delivery systems in wound treatment and skin regeneration. *J. Nanobiotechnol.* **2019**, *17*, 82–96.
20. Li, J.; Ghatak, S.; El Masry, M.S.; Das, A.; Liu, Y.; Roy, S.; Lee, R.J.; Sen, C.K. Topical

lyophilized targeted lipid nanoparticles in the restoration of skin barrier function following burn wound. *Mol. Ther.* **2018**, *26*, 2178–2188.

21. Jaspart, S.; Piel, G.; Delattre, L.; Evrard, B. Solid lipid microparticles: formulation, preparation, characterisation, drug release and applications. *Expert Opin. Drug Deliv.* **2005**, *2*, 75–87.
22. Gavini, E.; Albertini, B.; Rassu, G.; Di Sabatino, M.; Sanna, V.; Giunchedi, P.; Rodriguez, L.; Passerini, N. Evaluation of solid lipid microparticles produced by spray congealing for topical application of econazole nitrate. *J. Pharm. Pharmacol.* **2009**, *61*, 559–567.
23. Rahimpour, Y.; Javadzadeh, Y.; Hamishehkar, H. Solid lipid microparticles for enhanced dermal delivery of tetracycline HCl. *Colloids Surf B: Biointerfaces* **2016**, *145*, 14–20.
24. García-González, C.A.; López-Iglesias, C.; Concheiro, A.; Alvarez-Lorenzo, C. Biomedical Applications of Polysaccharide and Protein Based Aerogels. In *Biobased Aerogels: Polysaccharide and Protein-based Materials*; Thomas, S., Pothan, L.A., Mavelil-Sam, R.; Royal Society of Chemistry: Cambridge, UK, 2018; Chapter 16; pp. 295-323.
25. Kankala, R.K.; Zhang, Y.S.; Wang, S.-B.; Lee, C.-H.; Chen, A.-Z. Supercritical fluid technology: An emphasis on drug delivery and related biomedical applications. *Adv. Healthcare Mater.* **2017**, *6*, 1700433–1700463.
26. García-González, C.A.; Smirnova, I. Use of supercritical fluid technology for the production of tailor-made aerogel particles for delivery systems. *J. Supercrit. Fluid.* **2013**, *79*, 152–158.
27. García-González, C.A.; Argemí, A.; Sousa, A.R.S. de; Duarte, C.M.M.; Saurina, J.; Domingo, C. Encapsulation efficiency of solid lipid hybrid particles prepared using the PGSS® technique and loaded with different polarity active agents. *J. Supercrit. Fluid.* **2010**, *54*, 342–347.
28. Sampaio de Sousa, A.R.; Simplício, A.L.; de Sousa, H.C.; Duarte, C.M.M. Preparation of glyceryl monostearate-based particles by PGSS®—Application to caffeine. *J. Supercrit. Fluid.* **2007**, *43*, 120–125.
29. Ndayishimiye, J.; Chun, B.S. Formation, characterization and release behavior of citrus oil-polymer microparticles using particles from gas saturated solutions (PGSS) process. *J. Ind. Eng. Chem.* **2018**, *25*, 201-207.
30. Martín, A.; Cocero, M.J. Micronization processes with supercritical fluids: Fundamentals and mechanisms. *Adv. Drug Deliv. Rev.* **2008**, *60*, 339–350.
31. Dohrn, R.; Bertakis, E.; Behrend, O.; Voutsas, E.; Tassios, D. Melting point depression by using supercritical CO2 for a novel melt dispersion micronization process. *J. Mol. Liq.* **2007**, *131–132*, 53–59.
32. Chen, W.; Hu, X.; Hong, Y.; Su, Y.; Wang, H.; Li, J. Ibuprofen nanoparticles prepared by a PGSS™-based method. *Powder Technology* **2013**, *245*, 241–250.
33. Fraile, M.; Martín, ÿ.; Deodato, D.; Rodriguez-Rojo, S.; Nogueira, I.D.; Simplício, A.L.; Cocero, M.J.; Duarte, C.M.M. Production of new hybrid systems for drug delivery by PGSS (Particles from Gas Saturated Solutions) process. *J. Supercrit. Fluid.* **2013**, *81*, 226–235.
34. Salmaso, S.; Elvassore, N.; Bertucco, A.; Caliceti, P. Production of solid lipid submicron particles for protein delivery using a novel supercritical gas-assisted melting atomization process. *J. Pharm. Sci.* **2009**, *98*, 640–650.
35. Salmaso, S.; Bersani, S.; Elvassore, N.; Bertucco, A.; Caliceti, P. Biopharmaceutical characterisation of insulin and recombinant human growth hormone loaded lipid submicron particles produced by supercritical gas micro-atomisation. *Int. J. Pharm.* **2009**, *379*, 51–58.
36. Argemí, A.; Domingo, C.; Sampaio de Sousa, A.R.; M. Duarte, C.M.; García-gonzález, C.A.; Saurina, J. Characterization of new topical ketoprofen formulations prepared by drug entrapment in solid lipid matrices. *J. Pharm. Sci.* **2011**, *100*, 4783–4789.
37. Abd, E.; Yousuf, S.; Pastore, M.; Telaprolu, K.; Mohammed, Y.; Namjoshi, S.; Grice, J.;

Roberts, M. Skin models for the testing of transdermal drugs. *Clin. Pharm. Adv. App.* **2016**, *Volume 8*, 163–176.

38. Neupane, R.; Boddu, S.H.S.; Renukuntla, J.; Babu, R.J.; Tiwari, A.K. Alternatives to biological skin in permeation studies: Current trends and possibilities. *Pharmaceutics* **2020**, *12*, 152–176.
39. Niehues, H.; Bouwstra, J.A.; El Ghalbzouri, A.; Brandner, J.M.; Zeeuwen, P.L.J.M.; van den Bogaard, E.H. 3D skin models for 3R research: The potential of 3D reconstructed skin models to study skin barrier function. *Exp. Dermatol.* **2018**, *27*, 501–511.
40. Velasco, D.; Quílez, C.; Garcia, M.; del Cañizo, J.F.; Jorcano, J.L. 3D human skin bioprinting: a view from the bio side. *J. 3D Print. Med.* **2018**, *2*, 141–162.
41. Kogelenberg, S. van; Yue, Z.; Dinoro, J.N.; Baker, C.S.; Wallace, G.G. Three-dimensional printing and cell therapy for wound repair. *Adv. Wound Care* **2018**, *7*, 145–156.
42. Sansone, P.; Passavanti, M.B.; Fiorelli, A.; Aurilio, C.; Colella, U.; De Nardis, L.; Donatiello, V.; Pota, V.; Pace, M.C. Efficacy of the topical 5% lidocaine medicated plaster in the treatment of chronic post-thoracotomy neuropathic pain. *Pain Manag.* **2017**, *7*, 189–196.
43. Jeong, Y.J.; Kim, H.J.; Kwon, H.; Shim, H.; Seo, B.F.; Jung, S.-N. The use of topical lidocaine gel during intermaxillary fixation procedure. *J. Craniofac. Surg.* **2016**, *27*, e475–e477.
44. American association of blood banks; Walker, R.H. *Technical manual*; American Association of blood banks: Bethesda, MD, USA, 1993.
45. Al-Salman, H.N.K.; Al-Jadaan, S.; Alnuaim, M.; Hassan, H. Estimation of lidocaine-HCl in pharmaceutical drugs by HPLC- UV system. *Am. J. PharmTech Res.* **2017**, *7*, 369-378.
46. Cubo, N.; Garcia, M.; del Cañizo, J.F.; Velasco, D.; Jorcano, J.L. 3D bioprinting of functional human skin: production and *in vivo* analysis. *Biofabrication* **2016**, *9*, 015006-015017.
47. Hsu, H.-H.; Kracht, J.-K.; Harder, L.E.; Rudnik, K.; Lindner, G.; Schimek, K.; Marx, U.; Pörtner, R. A method for determination and simulation of permeability and diffusion in a 3D tissue model in a membrane insert system for multi-well plates. *JoVE* **2018**, 56412–56423.
48. Pankey, G.A.; Sabath, L.D. Clinical relevance of bacteriostatic versus bactericidal mechanisms of action in the treatment of Gram-positive bacterial infections. *Clin. Infect. Dis.* **2004**, *38*, 864–870.
49. Khosa, A.; Reddi, S.; Saha, R.N. Nanostructured lipid carriers for site-specific drug delivery. *Biomed. Pharmacother.* **2018**, *103*, 598–613.
50. Battaglia, L.; Gallarate, M.; Panciani, P.P.; Ugazio, E.; Sapino, S.; Peira, E.; Chirio, D. Techniques for the Preparation of Solid Lipid Nano and Microparticles. In *Application of Nanotechnology in Drug Delivery*; Sezer, A.D.; InTech: London, UK, 2014.
51. Wei, Y.; Nedley, M.P.; Bhaduri, S.B.; Bredzinski, X.; Boddu, S.H.S. Masking the bitter taste of injectable lidocaine HCl formulation for dental procedures. *AAPS PharmSciTech* **2015**, *16*, 455–465.
52. García-González, C.A.; Sousa, A.R.S. da; Argemí, A.; Periago, A.L.; Saurina, J.; Duarte, C.M.M.; Domingo, C. Production of hybrid lipid-based particles loaded with inorganic nanoparticles and active compounds for prolonged topical release. *Int. J. Pharm.* **2009**, *382*, 296–304.
53. Weinstein, R.D.; Muske, K.R.; Moriarty, J.; Schmidt, E.K. The solubility of benzocaine, lidocaine, and procaine in liquid and supercritical carbon dioxide. *J. Chem. Eng. Data* **2004**, *49*, 547–552.
54. Sweet, P.T.; Magee, D.A.; Holland, A.J.C. Duration of intradermal anaesthesia with mixtures of bupivacaine and lidocaine. *Canad. Anaesth. Soc. J.* **1982**, *29*, 481–483.
55. Mathematical models of drug release. In *Strategies to Modify the Drug Release from Pharmaceutical Systems*; Elsevier, 2015; pp. 63–86.

56. Manjunatha, R.G.; Sharma, S.; Narayan, R.P.; Koul, V. Effective permeation of 2.5 and 5% lidocaine hydrochloride in human skin using iontophoresis technique. *Int. J. Dermatol.* **2018**, *57*, 1335–1343.
57. Fazly Bazaz, B.S.; Salt, W.G. Local anaesthetics as antibacterial agents: effects on cellular respiration and the leakage of cytoplasmic constituents. *Microbios* **1983**, *37*, 139–149.
58. Schmidt, R.M.; Rosenkranz, H.S. Antimicrobial activity of local anesthetics: lidocaine and procaine. *J. Infect. Dis.* **1970**, *121*, 597–607.
59. Ohsuka, S.; Ohta, M.; Masuda, K.; Arakawa, Y.; Kaneda, T.; Kato, N. Lidocaine hydrochloride and acetylsalicylate kill bacteria by disrupting the bacterial membrane potential in different ways. *Microbiol. Immunol.* **1994**, *38*, 429–434.
60. Hasselmann, C. Determination of minimum inhibitory concentrations (MICs) of antibacterial agents by broth dilution. *Clin. Microbiol. Infect.* **2003**, *9*, 4–15.
61. Pelz, K.; Wiedmann-Al-Ahmad, M.; Bogdan, C.; Otten, J.-E. Analysis of the antimicrobial activity of local anaesthetics used for dental analgesia. *J. Med. Microbiol.* **2008**, *57*, 88–94.
62. Gajraj, R.J.; Hodson, M.J.; Gillespie, J.A.; Kenny, G.N.; Scott, N.B. Antibacterial activity of lidocaine in mixtures with Diprivan. *Br. J. Anaesth.* **1998**, *81*, 444–448.
63. Driver, R.P.; Granus, V.A.; Yassa, Y.J. Growth inhibition of Staphylococcus aureus by propofol/lidocaine admixture. *Anesth. Analg.* **1998**, *86*, 166S.
64. Johnson, S.M.; Saint John, B.E.; Dine, A.P. Local anesthetics as antimicrobial agents: A review. *Surg. Infect.* **2008**, *9*, 205–213.

USC
UNIVERSIDADE
DE SANTIAGO
DE COMPOSTELA

# Section II. Chitosan Aerogels Loaded with Vancomycin for Wound Applications

USC
UNIVERSIDADE
DE SANTIAGO
DE COMPOSTELA

# 5. VANCOMYCIN-LOADED CHITOSAN AEROGEL PARTICLES OBTAINED BY THE DRIPPING METHOD FOR CHRONIC WOUND APPLICATIONS

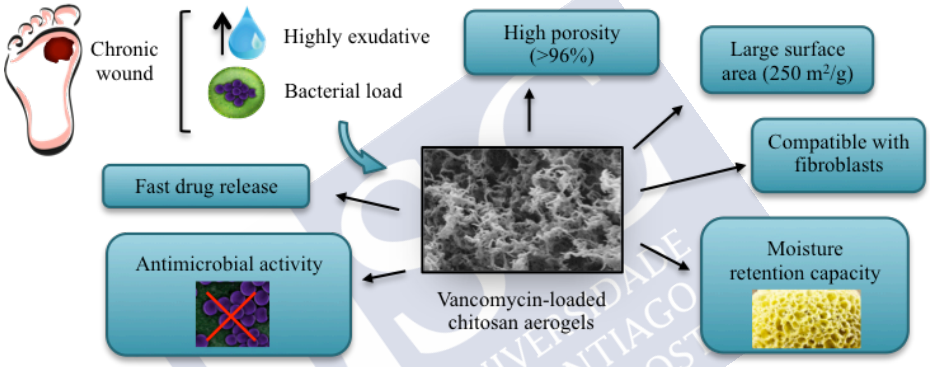


The work described in this chapter was published in López-Iglesias, C. *et al.* Vancomycin-loaded chitosan aerogel particles for chronic wound applications. *Carbohydrate Polymers* **2018**, 204, 223–231.

Work carried out in collaboration with the Instituto de Investigação e Inovação em Saúde of the Universidade do Porto, Portugal and the BioFarma group of the Centro Singular de Investigación en Medicina Molecular y Enfermedades Crónicas of the Universidade de Santiago de Compostela.

USC
UNIVERSIDADE
DE SANTIAGO
DE COMPOSTELA

# 5. VANCOMYCIN-LOADED CHITOSAN AEROGEL PARTICLES OBTAINED BY THE DRIPPING METHOD FOR CHRONIC WOUND APPLICATIONS

## 5.1. Introduction

The healing process under normal physiological conditions in response to an injury comprises a series of steps (hemostasis, inflammation, proliferation and resolution) that lead to the complete replacement of the damaged tissue [1,2]. However, the healing process is hampered in chronic wounds such as diabetic foot ulcers, venous leg ulcers and pressure ulcers and remains in the inflammatory phase for prolonged periods of time [3]. Prospective studies indicate that the incidence of chronic wounds will increase because of poor health habits and the progressive ageing of the population [4].

Hypoxia, changes in pH and microbial burden are among the factors hindering the normal healing process resulting in a chronic wound [5]. Thus, materials for wound management should possess good oxygen permeability to avoid hypoxia and permit a normal cell metabolism. They should also have a high aqueous fluid recruitment to favor a correct exudate management [6]. On the other hand, the use of materials for the local treatment and prevention of infections in the wound site is an auspicious solution for the treatment of chronic wounds [7,8].

Products in the form of gauzes, foams, hydrocolloids and other types of dressings are already commercially available for the treatment of chronic wounds [9]. The world market for wound management is increasing with expected sales of $21.85 billion by year 2021 [10]. Particularly, it can be forecasted that the market share of new technologies and materials for wound management, e.g., endowed with antimicrobial properties, will have outstanding growth prospects with respect to traditional dressings.

Aerogels are nanostructured dry materials with high porosity (> 95%) and large surface area (> 300 $m^2/g$) that can provide advanced performances for wound healing [11–13]. This particular porous structure of aerogels allows fast initial water ingress and can also act as a carrier for bioactive compounds with high loading capacity,

enhanced stability upon storage and accelerated drug release [14]. Aerogels are usually obtained from the drying of organic, inorganic or hybrid gels with supercritical $CO_2$ ($scCO_2$), which avoids the pore collapse in the gel network typical of other drying methods and represents a green, safe and innovative technology [15]. The technology is versatile in terms of composition, but aerogels to be applied in biological systems must be made of biocompatible, non-toxic and preferably biodegradable materials [14]. Polysaccharides represent a suitable choice for the preparation of aerogels for wound applications [11,16]. In this regard, chitosan is of particular interest since it can gather together antimicrobial activity against Gram(+) and Gram(-) bacteria, hemostatic activity and stimulation capability of tissue regeneration at the wound site [17,18]. Chitosan forms part of some conventional wound dressings approved by regulatory agencies (e.g., Tegasorb®, HemCon®, ChorioChit®) [19–23] but, to the best of our knowledge, there are no chitosan-based products in the market using chitosan in the form of aerogels.

Chitosan is obtained by deacetylation of chitin in a degree of 50% or higher and its physicochemical properties are characterized by its deacetylation degree and molecular weight. These properties will influence the chitosan solubility in aqueous solutions and their antimicrobial activity [24,25]. Chitosan dissolves in dilute acids through the protonation of its free amino groups, allowing the processing into different gel formulations by sol-gel methods. When the chitosan solution is put in contact with a basic medium, the amino groups of the polysaccharide deprotonate and the polymer precipitates forming the three-dimensional fibrous network of the gel. Chitosan aerogels can then be obtained by supercritical drying of the gels [22,26,27].

Chitosan aerogels are of special interest as drug carriers for those wound applications where a prompt therapeutic level of bioactive agent is needed at high exuding wound environments and shortly after debridement. In contrast to other chitosan-based materials (nanoparticles, xerogels, cryogels, sponges) loaded with drugs, chitosan aerogels encompass the properties of aerogels for exudate management and carrier for bioactive agents, along with those properties of chitosan regarding biological performance and ability of the chemical structure to interact with active molecules [24,28–31]. As bioactive agent to be loaded in the aerogel, vancomycin is a glycopeptide antibiotic widely used parenterally for the treatment of infected wounds in hospitalized patients due to its broad range of efficacy against Gram-positive bacteria, and is specially indicated under suspicion of infection by methicillin-resistant *S. aureus* [32]. Vancomycin may also have a limited antimicrobial effect against Gram-negative bacterial strains [33,34]. The direct local application of vancomycin powder alone instead of intravenous infusion was proposed for surgical wounds with low accessibility during the clinical procedure (e.g., in spine surgery) with relative success, although the risk of microbial wound recolonization and delayed infections was highlighted due to the reduction of the vancomycin concentration over

a postadministration timeframe of 1–3 days [35]. The local administration of vancomycin is thus an alternative therapy and the incorporation of vancomycin in a formulation able to provide a local and controlled delivery of the drug into the wound site is an auspicious solution to reduce the administered dose as well as the risk of appearance of bacterial drug resistance [36–39]. In case of accessible wound sites, the relevance of a local treatment with vancomycin using dressings with specific release characteristics and retained moisture for wound healing has been reinforced with clinical studies proving the bacterial load reduction in the wound [40]. For this case, the change of these dressings is preferred every 1–3 days, the usual exchange frequency used for wound management in nursery [41].

In this work, chitosan aerogels loaded with bioactive agents are herein evaluated for the first time regarding their capacity to treat and prevent infections in chronic wounds. Vancomycin-loaded chitosan aerogel beads were prepared by the sol-gel method followed by gel drying with $scCO_2$. The obtained aerogels were analyzed in terms of morphological, textural and physicochemical properties. The vancomycin content in the chitosan aerogels and its release profile in phosphate buffer solution (PBS pH 7.4) at 37 °C were evaluated. The antimicrobial activity against a *Staphylococcus aureus* bacterial strain, the collagenase activity, the cytocompatibility with fibroblasts and the water sorption capability of the chitosan aerogels were specifically tested to reduce the microbial burden at the wound site after debridement.

## 5.2. Materials and methods

### 5.2.1. Materials

Chitosan (deacetylation degree 90%, viscosity 1000 mPa·s, $M_w$ 200–400 kDa) was supplied by Heppe Medical Chitosan GmbH (Halle, Germany). Vancomycin hydrochloride ($M_w$ 1486 g/mol, 94.3% purity, amorphous) was supplied by Guinama (Valencia, Spain). Collagenase from *Clostridium histolyticum* (Type I, 0.26 FALGPA units/mg solid), N-(3-[2-furyl]acryloyl)-Leu-Gly-Pro-Ala (FALGPA), Fetal Bovine Serum (FBS) and penicillin 10,000 U/mL – streptomycin 10 mg/mL were supplied by Sigma-Aldrich (Saint Louis, MO, USA). BALB/3T3 clone A31 mouse fibroblasts (ATCC CCL-163) and Dulbecco's modified Eagle's medium (DMEM) were from the American Type Culture Collection (ATCC, Manassas, VA, USA). Glacial acetic acid and absolute ethanol (EtOH) were both purchased from VWR (Radnor, PA, USA). NaOH (98.0% purity) and HCl (35%, w/w) were from Panreac (Barcelona, Spain) and Labkem (Barcelona, Spain), respectively. $CO_2$ (99.8% purity) was supplied by Praxair (Madrid, Spain). Water was purified using reverse osmosis (resistivity >18 MΩ·cm, MilliQ, Millipore®, Madrid, Spain).

## 5.2.2. Preparation of chitosan aerogel beads

### 5.2.2.1. Preparation of the chitosan hydrogel

Hydrogel particles were prepared following the sol-gel method. Firstly, chitosan powder was dissolved in Milli-Q water containing 1% (v/v) of acetic acid to a final concentration of 2.5% (w/v). The solution was mechanically stirred for 10 min and then left to settle for 3 h to eliminate gas bubbles formed during the agitation. Thereafter, 8 mL of the chitosan solution were transferred to a plastic syringe (nozzle diameter of 2 mm) and added dropwise to 50 mL of a gelation bath of NaOH 0.1 M at a constant flow rate of 0.65 mL/min using a syringe pump (AL-1000, World Precision Instruments, Sarasota, FL, USA). Droplets gelified just after contact with the NaOH solution and hydrogel beads were formed. These beads were left in the gelation bath for different ageing times (0.5, 1, 2, 4, 10 and 24 h). In the case of vancomycin-loaded aerogels, vancomycin hydrochloride powder was added to the chitosan solution (i.e. the *sol*) in a content of 5, 10 and 20% (w/w of chitosan). Aerogels were denoted as CS*x*-V*y*, where *x* is the ageing time (h) and *y* is the theoretical content of vancomycin (% w/w of chitosan).

### 5.2.2.2. Solvent exchange

The gelation bath was poured out of the beaker containing the gel beads and immediately replaced by 50 mL of absolute EtOH to get *ca.* 60–70 alcogel particles. After 30 min, a second solvent exchange with a similar volume of EtOH was carried out to eliminate any remnant of water in the gel particles.

### 5.2.2.3. Supercritical extraction of the gel solvent

Alcogel particles were introduced into paper cartridges and put into the 100-mL autoclave of the supercritical equipment (Thar Process, Pittsburg, PA, USA). 20 mL of EtOH were previously added to the said pressurized vessel to avoid the premature evaporation of the EtOH contained in the alcogels before reaching the supercritical conditions of the $CO_2$-EtOH mixture. During the 3.5 h-duration drying process, a $scCO_2$ flow of 5 g/min passed through the autoclave where the gels were contained at a processing temperature and pressure of 40 °C and 120 bar, respectively. The extracted liquid ethanol was sampled at selected drying times to monitor the kinetics of the supercritical process.

## 5.2.3. Physicochemical properties of the gel beads

Images of hydrogel, alcogel and aerogel chitosan particles were taken with a digital camera and analyzed with ImageJ v1.49 software (U.S. National Institutes of

Health, Bethesda, MD, USA) to measure the diameter and volume of the beads and thus to calculate the volume shrinkage during each processing step. Values were obtained from the analysis of *ca.* 25 particles.

The envelope density ($\rho_{env}$) of the aerogel beads was calculated as the ratio between the average particle weight obtained with a precision balance (80A-200M, Precisa, Dietikon, Switzerland) and the dimensions obtained by image analysis. Chitosan aerogel beads were compared to xerogels and cryogels obtained from the same alcogel precursors by oven drying (37 °C) and freeze-drying (-85 °C, vacuum), respectively. Skeletal density ($\rho_{skel}$) was measured by helium pycnometry (MPY-2, Quantachrome, Delray Beach, FL, USA) at 25 °C and 1.03 bar from six replicates. The overall porosity ($\varepsilon$) of the dried gels was expressed in percentage and calculated according to Eq. 5.1:

$$\varepsilon = \left(1 - \frac{\rho_{env}}{\rho_{skel}}\right) \cdot 100 \quad (5.1)$$

The textural properties of the aerogel particles were characterized by nitrogen adsorption-desorption analysis (ASAP 2000, Micromeritics, Norcross, GA, USA). The Brunauer-Emmet-Teller (BET) and the Barrett-Joyner-Halenda (BJH) methods were applied to calculate the specific surface area ($a_{BET}$) and the pore size distribution, respectively. The overall specific pore volume ($V_{p,BJH}$) and the mean pore diameter ($d_{p,BJH}$) were also obtained from the BJH method. The specific mesopore volume ($V_{mes}$) was obtained from the cumulative BJH-pore volume profiles of the aerogels in the mesopore range (2–50 nm). The specific volume occupied by the macropores ($V_{MP}$) in the aerogels was calculated as the difference between the total specific pore volumes of the aerogels (i.e. the inverse of the envelope density) and the specific pore volume occupied by mesopores ($V_{mes}$). The surface structure of the aerogel beads was also studied by Scanning Electron Microscopy at 3 kV with a secondary electron detector (SEM, EVO LS15, Zeiss, Oberkochen, Germany). Aerogels were previously sputtered-coated (Q150T S/E/ES, Quorum Technologies, Lewes, UK) with a thin layer (10 nm) of iridium to improve the contrast.

Crystallinity of the raw materials and the aerogels was studied by X-ray diffraction (XRD, PW-1710, Philips, Eindhoven, The Netherlands) in the 2–50° θ2-range using a 0.02° step and Cu $\kappa\alpha_1$ radiation.

Attenuated total reflectance/Fourier-Transform Infrared Spectroscopy (ATR/FT-IR) was performed using a Gladi-ATR accessory equipped with a diamond crystal (Pike, Madison, WI, USA). Solid samples of pure chitosan, pure vancomycin and unloaded and vancomycin-loaded chitosan aerogel beads were characterized in the mid-IR spectrum range (400–4000 $cm^{-1}$) using 32 scans at a resolution of 2 $cm^{-1}$.

### 5.2.4. Water absorption assay

The swelling behavior of chitosan aerogel particles obtained at different ageing times was tested in 50 mL of PBS solutions of pH 6.0, 7.0 and 8.0 under magnetic stirring (250 rpm) and in triplicate. Ten chitosan aerogel beads of known weight (*ca.* 15 mg) were used for each experiment. Particles were introduced into stainless steel baskets to put the whole aerogel surface in contact with the fluid, thus preventing particles from floating. At specific soaking times (0.5, 1, 2, 4, 8 and 24 h), particles were collected and weighed after having their surface water slightly wiped with filter paper. Water uptake at each time was calculated using Eq. 5.2:

$$\text{Water absorption} = \frac{w_t - w_0}{w_0} \cdot 100 \quad (5.2)$$

where $w_t$ is the weight of the wet particles at time $t$, and $w_0$ is the initial weight of the dry particles.

### 5.2.5. Collagenase activity test

Five previously weighed chitosan aerogel beads were placed in Eppendorf tubes with 1 mL of a tricine buffer solution (pH 7.5) containing collagenase at a concentration of 2 units/mL (37 °C, 20 rpm). At selected times (0, 0.5 and 4 h), 33 µL aliquots of the enzyme solution were extracted and mixed with 966 µL of a FALGPA solution at a concentration of 48 mg/mL. The reaction was monitored by measuring the changes in absorbance by UV/Vis spectrophotometry at a wavelength of 345 nm (8453, Agilent, Santa Clara, CA, USA) every 15 s for 5 min. The collagenase activity was calculated following the manufacturer guidelines and expressed as units/mL. One unit of collagenase hydrolyzes 1.0 µmol of FALGPA per minute at 25 °C at pH 7.5 in the presence of calcium ions. A collagenase solution without chitosan aerogel particles was used as the negative control and Milli-Q water was used as blank.

### 5.2.6. Vancomycin encapsulation efficiency assay

Vancomycin encapsulation efficiency was evaluated by immersing eight aerogel beads of known weight and loaded with vancomycin into Falcon tubes containing 5 mL of HCl 0.1 M under magnetic stirring (750 rpm). After 90 min in the acidic medium, the chitosan particles were completely dissolved, the solutions were centrifuged and the vancomycin concentration in the supernatant was measured by UV/Vis spectrophotometry (8453, Agilent, Santa Clara, CA, USA) at a wavelength of 281 nm. The vancomycin loading and entrapment efficiency (in percentage) were calculated using Eq. 5.3 and 5.4, respectively:

$$\text{Loading} = \frac{w_P}{w_{aer}} \cdot 100 \quad (5.3)$$

$$\text{Encapsulation efficiency} = \frac{w_P}{w_T} \cdot 100 \quad (5.4)$$

where $w_P$ is the amount (mg) of vancomycin hydrochloride measured by the UV/Vis analysis, $w_{aer}$ is the total amount of aerogel (mg), and $w_T$ is the initial amount (mg) of vancomycin added for the preparation of the aerogels. The test was carried out in triplicate. Prior to the measurements, a calibration curve of vancomycin in HCl 0.1 M was obtained and validated in the 25–200 mg/mL range ($R^2 > 0.999$). Chitosan aerogel particles without vancomycin (i.e. blank) were also evaluated to eliminate the interference of chitosan in the UV/Vis measurements.

### 5.2.7. Vancomycin release from the aerogel particles

Twenty vancomycin-loaded chitosan aerogel particles were weighed, immersed into recipients containing 10 mL of PBS pH 7.4 medium and put into an oscillating bath (P Selecta Unitronic 320 OR, Barcelona, Spain) at 37 °C and 60 rpm. 2 mL-aliquots of the medium were sampled at selected times (0, 0.25, 0.5, 1, 2, 4, 8, 24, and 48 h) and measured by UV/Vis spectroscopy (8453, Agilent, Santa Clara, CA, USA) at the wavelength of 281 nm. The extracted volume was immediately replaced with equal volumes of fresh PBS medium. Prior to the measurements, a calibration curve of vancomycin in PBS was obtained and validated in the 5–25 µg/mL range (R2 > 0.998). The kinetics of the dissolution process of vancomycin hydrochloride powder in PBS pH 7.4 medium was also studied to compare the dissolution profiles of the free and the entrapped drug.

The vancomycin release profile was fitted to a first-order release model according to Eq. 5.5 and corresponding to a first-order dissolution process reaching a plateau (GraphPad Prism v. 6.04, GraphPad Software, La Jolla, CA, USA):

$$D = (D_0 - D_P) \cdot e^{-k \cdot t} + D_P \quad (5.5)$$

where $D$ denotes the unreleased and/or degraded dosage of vancomycin (in percentage) at time $t$; $D_0$ is the initial vancomycin dosage in the aerogels (in percentage); $D_P$ is the unreleased and/or degraded dosage (in percentage) of vancomycin in the plateau region; and $k$ is the release rate coefficient, in $h^{-1}$.

### 5.2.8. Antimicrobial ability of the gels

A susceptible strain of *Staphylococcus aureus* (ATCC 25923) was suspended in 10 mL of simulated body fluid (SBF pH 7.4) to a final concentration of 8.0 105 CFU/mL. One chitosan aerogel bead of each formulation loaded with vancomycin (CS1-V5, CS1-V10 and CS1-V20) was sterilized by UV radiation during 1 h and put in contact with 200 µL of the bacterial broth. Free bacterial broth was the negative control. Bacterial broth incubated with free vancomycin powder (0.067, 0.101 and 0.214 µg/µL), equivalent to the vancomycin payload of the CS1-V5, CS1-V10 and CS1-V20 aerogels, respectively) was the positive control. At different incubation times (6, 24 and 48 h), turbidity was measured at a wavelength of 600 nm in four replicates to monitor the planktonic

bacteria. For the same time periods, aliquots of the bacterial suspensions were also taken, serially diluted and the planktonic bacteria quantification was measured by spread-plating in plate count agar in four replicates. The colony forming units (CFUs) were quantified and results expressed as decimal logarithm of the number of planktonic bacteria per milliliter of suspension.

### 5.2.9. Cytotoxicity assay

BALB/3T3 fibroblasts (10,000 cells/well) were cultured in 24 well-plates in DMEM supplemented with 10% FBS, penicillin 100 U/mL and streptomycin 100 µg/mL. The plates were incubated for 24 h at 37 °C in a humidified atmosphere with 5% CO2. Then, CS1-V0, CS1-V5, CS1-V10 and CS1-V20 particles were sterilized by UV radiation during 1 h and placed in each well (in triplicate). DMEM medium and medium with unloaded aerogels acted as blanks, and aerogel-free cell culture was the negative control. After 24 and 48 h of culture, 50 µL of WST-1 reagent (Roche, Basel, Switzerland) were added to each well. Plates were incubated for 4 additional hours, shaken thoroughly for 1 min and the absorbance was measured at a wavelength of 440 nm in a plate reader (EnSpire, PerkinElmer, Madrid, Spain).

### 5.2.10. Statistical analysis

Quantitative data were subjected to an analysis of variance (one-way ANOVA, Tuckey's test) using a level of significance (α) of 0.05. An unpaired, non-parametric Mann-Whitney test was used to analyze the data obtained from the enzymatic assay, to compare the activities of the free enzyme and the enzyme incubated with the aerogels using a level of significance (α) of 0.05. Statistical analysis were made with GraphPad Prism v. 6.04 (GraphPad Software, La Jolla, CA, USA).

## 5.3. Results and discussion

### 5.3.1. Morphological and textural properties of the chitosan aerogels

Chitosan hydrogel beads were formed by dripping droplets of a chitosan solution into a basic NaOH 0.1 M solution. In this sol-gel method, the formation of the chitosan gels took place immediately after contact with the gelation bath. The chitosan hydrogels were initially transparent and turned white after *ca.* 1 min in the ageing medium. The gel beads were spherical and the presence of a tail was noticed depending on the distance of the syringe to the gelation bath (Fig. 5.1). After 1 h of ageing, the subsequent solvent exchange to EtOH caused slight volume shrinkage of 11.9 ± 6.3%. The solvent exchange to ethanol is a usual practice for aerogel processing to facilitate the extraction of the solvent by $scCO_2$ during the drying process. The extraction of water is even more crucial for the case of chitosan aerogels, since any remnant of water would form carbonic acid in the presence of $scCO_2$ that would cause

the partial dissolution of the chitosan gel. After the supercritical drying (i.e. alcogel-to-aerogel step, Fig. 5.2), the particles preserved their white and spherical structure, with an overall volume shrinkage of 57.0 ± 4.5% with respect to the original hydrogels, a similar value to that reported in the literature [26,27]. This shrinkage was attributed to the flexibility of the polymeric chains of chitosan that are brought closer after the extraction of the solvent.

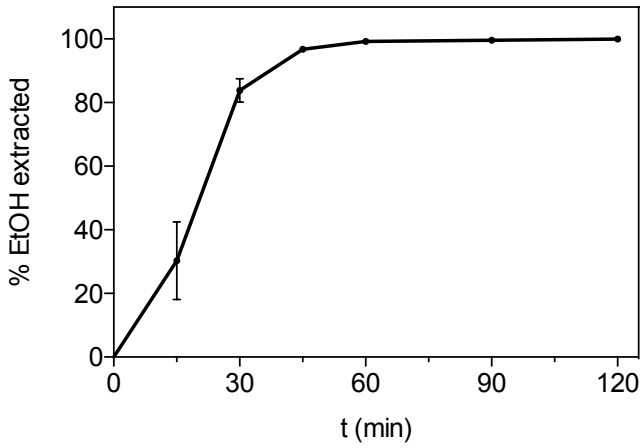


Figure 5.1. Kinetics of extraction of ethanol during the supercritical drying of the chitosan aerogels.

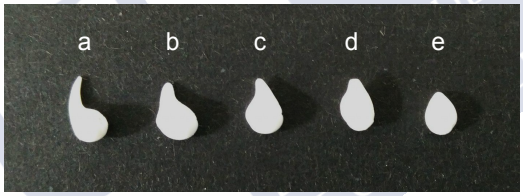


Figure 5.2. CS1-V0 particles prepared with a distance from the syringe to the gelation bath of (a) 13 cm, (b) 30 cm, (c) 50 cm, (d) 70 cm and (e) 90 cm. The shapes are representative of the formation steps – at short distances, the drop did not have time to become spherical and as soon as it reached the gelation bath it started to gelify, so the presence of a tail is perceived. This is due to the high viscosity of the initial chitosan solution.

Shrinkage values were much lower than those obtained by freeze-drying and oven drying of the same chitosan hydrogels (95.9 and 97.7%, respectively). Overall porosity of the chitosan aerogel beads was 96.8 ± 0.4% (CS1-V0 in Table 1), a very high value notably if compared to the traditional evaporative drying and freeze-drying methods (xerogels and cryogels in Table 1, respectively), which are not able to preserve the intrinsic nanoporous structure of the gels.

The highly porous structure of the CS1-V0 chitosan aerogel beads was confirmed by SEM microscopy (Fig. 5.3). Beads were formed by a network of intermingled polysaccharide fiber bundles. Voids within and between the fiber bundles are mesopores (2–50 nm) and macropores (> 50 nm), respectively, according to the IUPAC classification. This dual porous structure of the aerogels was observed in the inner and

outer structure of the particles (Fig. 5.3). Chitosan crystallinity was reduced after the aerogel processing according to the XRD results (Fig. 5.4).

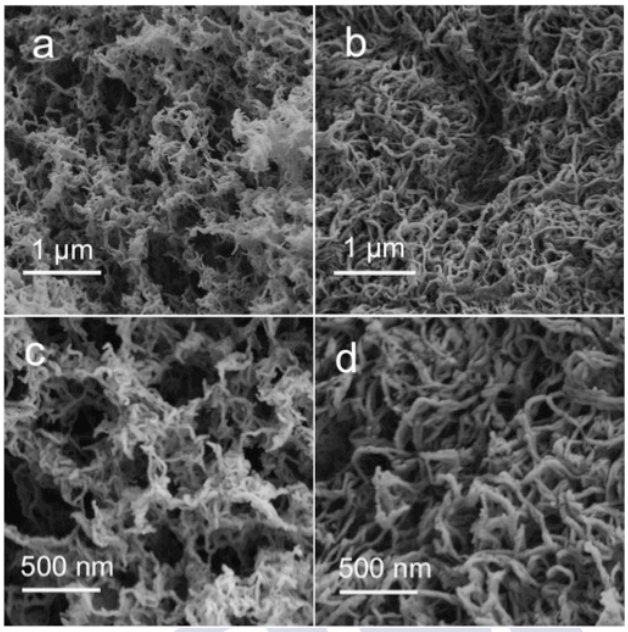


Figure 5.3. Textural appearance of the (a, c) interior and (b,d) surface of the CS1-V0 chitosan aerogel beads by SEM imaging (X50,000 and X100,000). A dual macroporous and mesoporous distribution was observed for the chitosan aerogels.

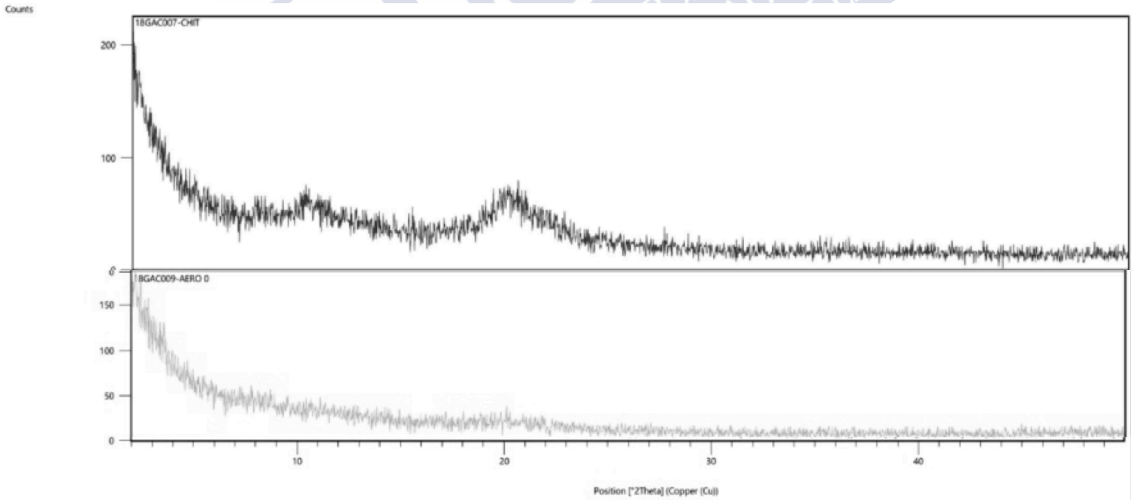


Figure 5.4. X-ray diffraction patterns of the chitosan raw material (top) and the CS1-V0 chitosan aerogels (bottom).

The effect of the ageing time of the chitosan hydrogels in the gelation bath on the particle size and porosity of the resulting chitosan aerogels was studied (Table 5.1). The overall volume shrinkage decreased with ageing time and subsequently larger particles were obtained. Ageing time had a moderate effect on the overall porosity of the aerogels.

Table 5.1. Influence of the ageing time (0.5, 1, 2, 4, 10 and 24 h) of the chitosan gel beads on the physicochemical properties of the resulting chitosan aerogel particles. Results were statistically compared (ANOVA Tuckey's test, $\alpha < 0.05$). Equal letter denotes statistically homogeneous groups. Notation: $\rho_{env}$, envelope density; $\varepsilon$, overall porosity.

| Particles | Diameter (mm) | $\rho_{env}$ (g/cm$^3$) | $\varepsilon^1$ (%) | Overall volume shrinkage (%) |
|---|---|---|---|---|
| CS0.5-V0 | 3.95 (0.12)$^{a}$ | 0.046 (0.004)$^{a}$ | 96.8 (0.4)$^{a}$ | 55.8 (4.0)$^{a}$ |
| CS1-V0 | 4.02 (0.12)$^{a,b}$ | 0.046 (0.004)$^{a}$ | 96.8 (0.4)$^{a}$ | 53.3 (4.1)$^{a}$ |
| CS2-V0 | 4.05 (0.11)$^{b}$ | 0.049 (0.004)$^{a}$ | 96.6 (0.4)$^{a}$ | 52.6 (3.7)$^{a}$ |
| CS4-V0 | 4.35 (0.11)$^{c}$ | 0.041 (0.003)$^{a}$ | 97.2 (0.3)$^{a}$ | 41.3 (4.5)$^{b}$ |
| CS10-V0 | 4.42 (0.11)$^{c,d}$ | 0.041 (0.003)$^{a}$ | 97.2 (0.3)$^{a}$ | 38.3 (4.6)$^{b}$ |
| CS24-V0 | 4.49 (0.21)$^{d}$ | 0.042 (0.006)$^{a}$ | 97.1 (0.5)$^{a}$ | 35.0 (9.4)$^{c}$ |
| cryogels | 1.68 (0.07)$^{e}$ | 0.535 (0.046)$^{b}$ | 63.0 (4.4)$^{b}$ | 95.9 (0.4)$^{d}$ |
| xerogels | 1.48 (0.06)$^{f}$ | 0.900 (0.104)$^{c}$ | 37.8 (8.8)$^{c}$ | 97.7 (0.3)$^{d}$ |

[1] $\rho_{skel}$ of the particles was 1.446 ± 0.116 g/cm$^3$; values obtained applying Eq. 5.1; standard deviation was calculated using measurements of *ca.* 50 aerogel beads.

The textural properties ($a_{BET}$, $V_{P,BJH}$ and $d_{P,BJH}$) of the chitosan aerogel particles gelified at different ageing times were compared by nitrogen adsorption-desorption analysis (Table 5.2). The textural characterization of the chitosan cryogels and xerogels could not be measured since their mesoporosities were below the detection limit of the equipment ($a_{BET}$ < 5 m$^2$/g). All aerogels showed isotherms classified as type IV according to the IUPAC recommendations [42], typical from mesoporous materials and characterized by the presence of a hysteresis loop and a high volume of nitrogen adsorbed (inset in Fig. 5.5).

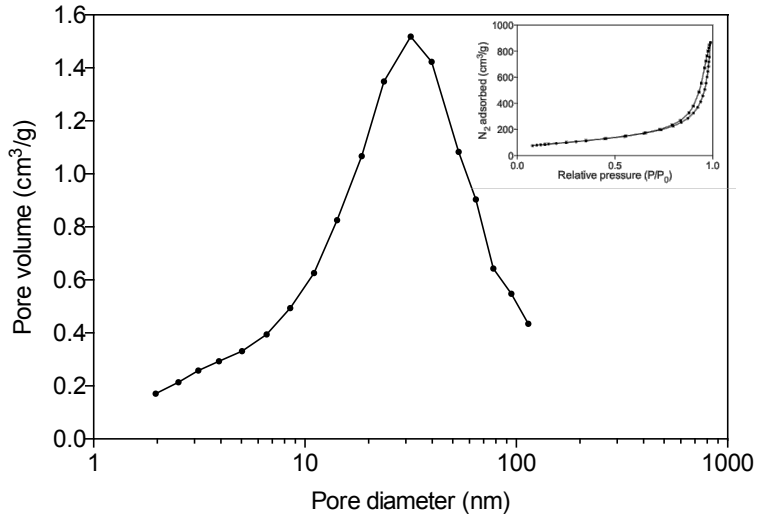


Figure 5.5. BJH-pore size distribution, and nitrogen adsorption-desorption isotherm (inset) obtained from CS1-V0 particles. Similar results were obtained for aerogel particles processed with different ageing times (not shown).

The mesoporous size distribution attributed to the pores within the chitosan fiber bundles had a log-normal, unimodal distribution according to the BJH-method (Fig. 5.5). This mesoporous structure had a mean pore size between 12 to 15 nm depending on the ageing time and was the main responsible of the high specific surface areas obtained for the chitosan aerogels (Table 5.2). A certain improvement in the textural properties was observed when increasing the ageing time up to 4 h, notably regarding the surface area. The contribution of the mesopore and macropore volumes to the total pore volume was also studied ($V_{mes}$ and $V_{MP}$ in Table 5.2, respectively). Results indicate that the macropore volume is highly predominant (above 95% in all cases). This volume is attributed to the widely spaced zones of contact between fibril bundles previously observed by SEM imaging. This dual porosity of chitosan aerogels can be of relevance for their use as carriers of antimicrobial agents for wound treatment just after debridement since mesopores provide large surface areas for high loadings of adsorbed drug, whereas macropores favor the drug diffusion upon contact with the exudate environment resulting in fast release rates and quick antimicrobial responses at the wound site.

Overall, an ageing time of 1 h was chosen as a trade-off solution for ulterior development and testing of chitosan aerogels as vancomycin carriers for wound applications. Although intermediate ageing times (4 h) improved the textural properties of the aerogels (Table 5.2), the high water solubility of the vancomycin hydrochloride (> 100 mg/mL) [43] urged to reduce the ageing time to avoid a dramatic drug loss in the ageing medium.

Table 5.2. Textural properties evaluated by nitrogen adsorption-desorption tests of the chitosan aerogel particles prepared with different ageing times (0.5, 1, 2, 4, 10 and 24 h). Notation: $a_{BET}$, specific surface area by the BET method; $V_{P,BJH}$, overall specific pore volume obtained by the BJH-method; $V_{mes}$, specific mesopore volume; $V_{MP}$, specific macropore volume; $d_{P,BJH}$, mean pore diameter by the BJH-method.

| Particles | $a_{BET}$ ($m^2/g$) | $V_{P,BJH}$ ($cm^3/g$) | $d_{P,BJH}$ (nm) | $V_{mes}$ ($cm^3/g$) | $V_{MP}$ ($cm^3/g$) |
|---|---|---|---|---|---|
| CS0.5-V0 | 360 (18) | 1.42 (0.07) | 14.1 (0.7) | 1.09 (0.05) | 20.14 (2.35) |
| CS1-V0 | 343 (17) | 1.32 (0.07) | 14.0 (0.7) | 1.03 (0.05) | 19.89 (2.21) |
| CS2-V0 | 386 (19) | 1.56 (0.08) | 14.4 (0.7) | 1.19 (0.06) | 18.35 (2.02) |
| CS4-V0 | 479 (24) | 1.70 (0.09) | 12.6 (0.6) | 1.25 (0.06) | 22.30 (2.28) |
| CS10-V0 | 257 (13) | 1.01 (0.05) | 14.2 (0.7) | 0.79 (0.04) | 22.74 (2.03) |
| CS24-V0 | 324 (16) | 1.32 (0.07) | 15.0 (0.8) | 0.99 (0.05) | 22.28 (3.71) |

### 5.3.2. PBS sorption tests

Moisture balance is essential for the adequate healing process of an exudative wound [6]. Wound dressings should be able to maintain an optimum moist

environment needed for the regeneration process while removing the excess of exudate from the wound, which in turn prevents infection. In this work, the aerogels experienced a weight increase between 300 and 400% after 30 min in contact with PBS pH 7 (Fig. 5.6). These water absorption values remained stable at least during the following 24 hours and are comparable or even higher than other bio-based formulations intended for the same application [44].

The pH in the surroundings of the wound varies as a function of the severity (normal or chronic) and the healing stage [45] and influences the associated healing processes. In general, the pH in the wound vicinity moves from basic conditions towards the neutral-to-acidic region as soon as the healing process progresses. Accordingly, the pH values in the chronic wound site are in the 7.2–8.9 range, the epithelialized wound has a pH of 6 and intact skin has a pH of *ca.* 5.5. The water sorption range of the chitosan aerogels was similar in the pH 6–8 range (Fig. 5.6), so no differences would be expected in the wound site regardless of the usual exudate pH range values.

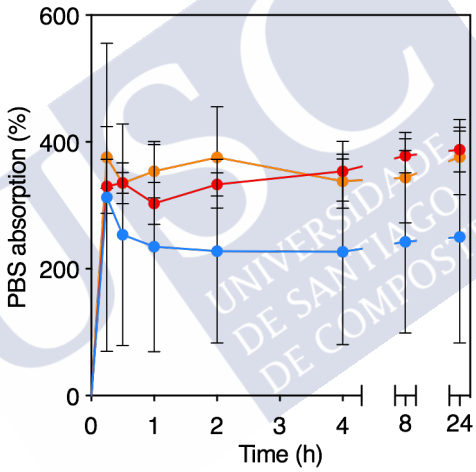


Figure 5.6. Water absorption as a function of time of CS1-V0 aerogels in contact with PBS medium at different pH values: 6 (blue), 7 (red) and 8 (orange).

### 5.3.3. Collagenase activity test

Collagenase is a metalloproteinase that naturally participates in collagen remodeling after an injury, thus favoring the repair of the tissue [46]. However, persistent inflammation in some chronic wounds results in the overexpression of metalloproteinases that degrade collagen, a component playing a key role in the proliferative phase of wound healing, not only in the damaged tissue but also in healthy skin tissue.

Results of the collagenase activity in the presence and absence of CS1-V0 chitosan aerogel particles are shown in Table 5.3. Enzymatic activity results suggested that the presence of chitosan aerogel particles does not inhibit the collagenase activity after 4

hours of contact and for the enzymatic concentration tested (2 units/mL). A slight increase in the collagenase activity seems to take place, although not statistically significant. Therefore, a high enzyme adsorption to the aerogel or a non-specific chitosan degradation are not expected, since no activity loss has been observed during the collagenase tests.

Table 5.3. Collagenase activity expressed in percentage with respect to the initial activity of the enzyme solution alone (Enzyme) and in contact with the chitosan aerogel particles (Enzyme + CS1-V0).

| Solution | 0.5 h (% initial activity) | 4 h (% initial activity) |
|---|---|---|
| Enzyme | 87.6 (15.6) | 70.5 (9.4) |
| Enzyme + CS1-V0 | 111.6 (3.8) | 95.0 (8.0) |

### 5.3.4. Vancomycin-loaded aerogels processing and properties

The loading of vancomycin hydrochloride in the chitosan aerogels was performed during the gelation process itself since vancomycin is highly water-soluble. The direct solvent exchange of the gels from water to pure ethanol prevents further drug losses with respect to the use of water:ethanol sequential dilutions series, since vancomycin is poorly soluble in ethanol. After supercritical drying, the vancomycin loading in the CS1-V5, CS1-V10 and CS1-V20 aerogels were 8.5 ± 4.0, 12.9 ± 1.0 and 27.3 ± 2.8 μg/mg of particle, respectively. The corresponding encapsulation efficiencies were 12.1 ± 1.0, 12.9 ± 1.0 and 13.7 ± 1.4%, respectively.

The vancomycin-loaded chitosan aerogels were characterized by ATR-FTIR spectroscopy (Fig. 5.7). CS1-V20 aerogel had the characteristic stretching bands of the chitosan amino groups at 1588 and 1652 $cm^{-1}$ [47]. The main bands from vancomycin (-OH, C=O, C=C and phenolic C-O stretchings at 3450, 1654, 1504 and 1230 $cm^{-1}$, respectively) [48] cannot be observed in the IR spectrum of the aerogel due to the overlapping with bands from chitosan. Nevertheless, the presence of vancomycin in the aerogel can be ascertained by a shoulder at 703 $cm^{-1}$ and a weak band at *ca.* 1600 $cm^{-1}$, corresponding to the free amino groups and to the amide group from the acetylated amino groups of the drug, respectively [49].

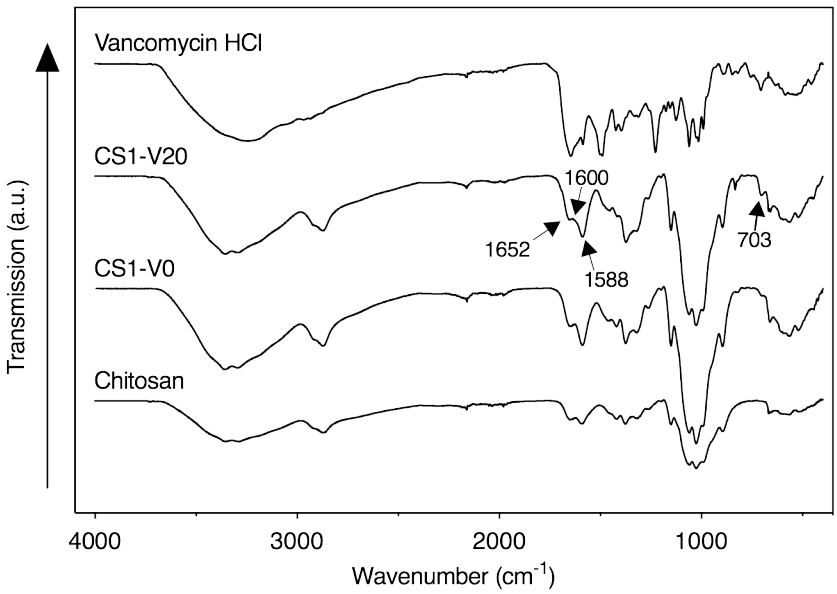


Figure 5.7. ATR-IR spectra of (a) chitosan powder, (b) CS1-V0 particles, (c) CS1-V20 particles and (d) vancomycin powder.

### 5.3.5. Vancomycin release from chitosan aerogels

The vancomycin release from the chitosan aerogel particles followed a first-order release kinetics (Fig. 5.8). A fast release of vancomycin during the first hour was followed by a slower vancomycin release during the next hours when the unreleased vancomycin content was dramatically reduced. The release was prolonged up to 24 h when the release of vancomycin seemed to reach a plateau. Overall, the aerogel carrier allowed a modified vancomycin release since the complete dissolution of pure vancomycin in PBS medium was faster (with 90% dissolved after 5 min).

The release tests showed that 100% vancomycin release was not observed even at prolonged times (7 days). The presence of two different drug fractions 1) drug deposited on the aerogel structure but weakly bound, and 2) drug with a certain drug-chitosan chemical interactions, might explain this release profile. Upon aerogel processing, the step of chitosan gel ageing in the aqueous medium led to significant vancomycin leaching. Anti-solvent precipitation on the gel surface of the vancomycin present in the pore solution can take place during the ulterior solvent exchange to ethanol [50], due to the very low solubility of the drug in ethanol. After supercritical drying, these drug deposits are the source of the vancomycin fraction with fast dissolution in the release medium during the first hours. The second fraction of vancomycin was related to drug molecules with a certain interaction with the chitosan backbone through hydrogen bonding that, after pore water filling and swelling of the gel network, had a very slow release rates limited by the diffusion through the gel as already observed for other vancomycin-polysaccharide gels [51]. This vancomycin fraction, obtained by difference between the vancomycin amount loaded and the

vancomycin amount released after 8 hours, represented *ca.* 4–6 µg drug/mg of particle and was similar for the three vancomycin-loaded aerogel formulations tested.

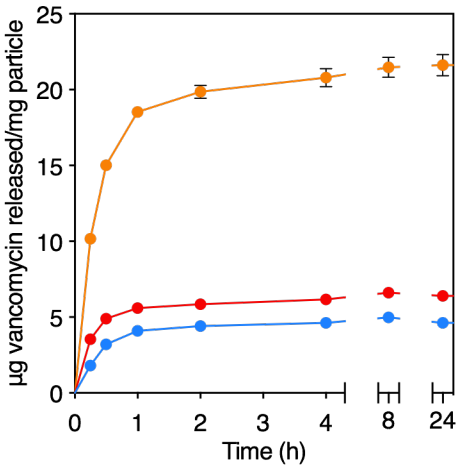


Figure 5.8. Vancomycin release profile from chitosan aerogels in PBS pH 7.4 medium (37°C, 60 rpm) during 2 days. Legend: CS1-V5 (blue), CS1-V10 (red), and CS1-V20 (orange).

The vancomycin release profile fitted to a first-order release model regardless of the initial vancomycin content used in the aerogel processing (Table 5.4). The remaining vancomycin dosage (in percentage) in the plateau stage ($D_p$) was lower for the CS1-V20 aerogels and was related to the processing of this formulation with higher vancomycin contents in the initial hydrogel that favored a higher deposition of weakly bound vancomycin on the gel surface by anti-solvent precipitation.

The release rate coefficients ($k$) were similar for the three aerogel formulations. According to the wellness of the fitting to this model, the vancomycin mass transfer mechanism from the aerogel was mainly governed by a combined dissolution and diffusion process. This vancomycin release behavior is considered as representative for the pH range of skin wounds (5.5–8.9) since sink conditions for the drug release are preserved in this range [52], the slow degradation rate of the aerogel matrix has no influence in the 48-hour timeframe and the matrix swelling is similar for these pH values (Section 5.3.2).

Wound debridement removes or interrupts the formation of biofilms in chronic wounds. 24–48 h after this clinical practice, there is a suitable timeframe to act against bacterial colonization at the wound site [40]. The local administration of vancomycin with the herein presented aerogel formulation can provide a quick therapeutic response, since after 2 h of contact of the aerogels with the release medium the vancomycin concentrations in the PBS medium were above the Minimum Inhibitory Concentration (MIC) for *S. aureus* (1–2 µg/mL) [53], the prevailing virulent bacteria in chronic wound infections. Thereafter, the observed release of the antibiotic during the following hours can be effective in maintaining the vancomycin content above the MIC values to kill the bacterial strains and to prevent the wound site from bacterial recolonization. Thus, the release behavior of vancomycin in aerogels is expected to

maintain local therapeutic levels of vancomycin at the wound site in an *in vivo* environment more effectively than the intrawound application of vancomycin powder [35] by counteracting the local drug losses due to absorption and transport through biological fluids. This release profile is also compatible with the incorporation of these aerogels in wound dressings with exchange frequencies of 24–48 h.

Table 5.4. Kinetic fitting parameters of the vancomycin release profiles from drug-loaded chitosan aerogels in PBS solution (pH 7.4) according to Eq. 5.5. Doses $D_0$ and $D_p$ are expressed as percentage of unreleased and/or degraded vancomycin. Values are denoted as mean ± standard error.

| Aerogel | $D_0$, dose remaining % | $D_p$, dose remaining % | k, $h^{-1}$ | $R^2$ |
|---|---|---|---|---|
| CS1-V5 | 100.2±1.2 | 43.2±0.5 | 2.06±0.10 | 0.988 |
| CS1-V10 | 99.2±1.7 | 49.8±0.7 | 2.78±0.24 | 0.964 |
| CS1-V20 | 98.9±1.8 | 21.3±0.7 | 2.31±0.13 | 0.983 |

### 5.3.6. Antimicrobial test

The antimicrobial performance of the vancomycin-loaded aerogels was tested against a *S. aureus* bacterial strain incubated in SBF medium. Tests were performed so that the release of vancomycin from the chitosan aerogels provided concentrations in the medium above the Minimum Inhibitory Concentration (MIC) for *S. aureus*.

Antimicrobial evaluation test by CFUs counting showed a time-dependent survival rate of *S. aureus* when in contact with the vancomycin-loaded aerogels (Fig. 5.9a). The planktonic bacterial concentration increased during the first 6 hours under all the tested incubation conditions, and then only decreased with time in the case of the presence of vancomycin in the formulation (CS1-V5, CS1-V10 and CS1-V20). Accordingly, there were no cultivable planktonic bacteria in the medium after 48 h of incubation in the presence of vancomycin-loaded aerogels. The results obtained from the turbidity measurements were consistent with the observed inhibition of bacterial growth (Fig. 5.9b). Therefore, the bacterial strain was completely inactivated after 48 h of incubation for the case of the vancomycin-containing chitosan aerogels. As expected, the bacterial growth was inhibited with the free vancomycin powder just after 6 h of incubation, since all the tested drug concentrations (0.0665, 0.101 and 0.214 μg/mL) were above the MIC for *S. aureus* (Fig. 5.9b).

Antimicrobial tests showed no bactericidal effect of chitosan by itself, since the results from the negative control (free bacterial growth) and the chitosan aerogels (CS1-V0) were similar. The antimicrobial mechanism of chitosan is the solubilization of the chitosan in the medium, and the presence of more -$NH^{3+}$ residues in the chitosan molecular structure favors the binding of the polysaccharide to the cell surface causing structural destabilization [25]. In general, the antimicrobial effect of chitosan is promoted at low molecular weights, high deacetylation degrees (DD > 70%) and, mainly, low pHs (pH < 6.5). Null or low bactericidal effect of a similar chitosan to the one used in this work have been previously reported at pHs above 7 because of the high proportion of uncharged amino groups in the macromolecule and the poor solubility of chitosan at this pH [24,25].

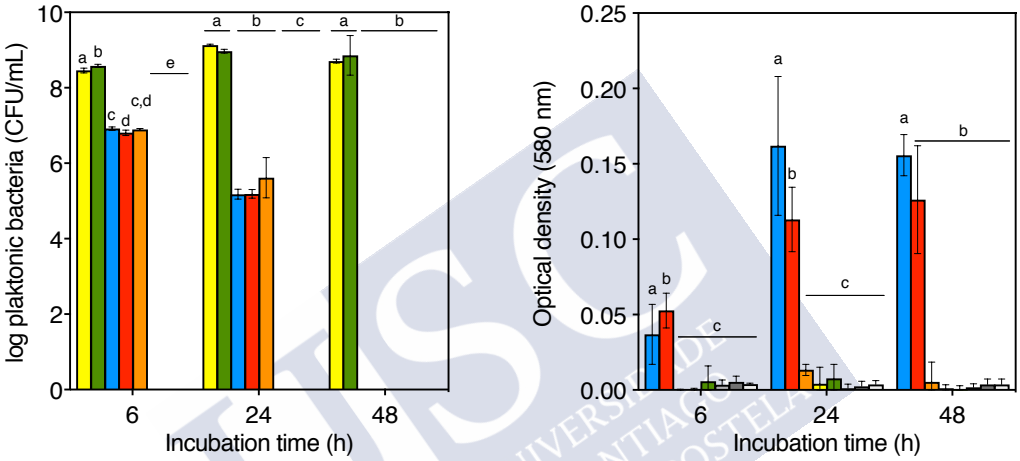


Figure 5.9. Quantification by CFUs counting (left) and turbidity measurements (right) of planktonic *S. aureus* bacteria in contact with vancomycin-loaded chitosan aerogel beads in SBF pH 7.4 during different incubation times. Legend: without aerogel (yellow), CS1-V0 (green), CS1-V5 (blue), CS1-V10 (red) and CS1-V20 (orange). Results were statistically compared (ANOVA Tuckey's test, $\alpha < 0.05$). Equal letter denotes statistically homogeneous groups. After 48 h, no CFUs were quantified for vancomycin-loaded aerogels. The antimicrobial effect after 24 and 48 h was similar for all the vancomycin concentrations.

In the present work, the chitosan was used as a delivery vehicle for antimicrobial drugs to improve wound healing and treatment, due to its inherent characteristics such as biodegradability, biocompatibility and non-toxicity [54,55]. The antimicrobial profiles observed for vancomycin-loaded chitosan aerogels and for the free-form drug emphasize the role of chitosan aerogels as carriers for controlled vancomycin release in an antibacterial treatment. The vancomycin-loaded chitosan aerogel beads showed excellent bactericidal characteristics, killing 98, 99 and 100% of planktonic bacteria population at 6, 24 and 48 h, respectively, independently of the vancomycin concentration used. The results showed that the vancomycin loading in chitosan aerogels did not affect vancomycin bioactivity and therefore these systems could be a good alternative to prevent the wound site from bacterial colonization.

### 5.3.7. Cytotoxicity assay

Cell viability in the presence of chitosan aerogels was tested using a fibroblast cell line. After 24 h of incubation, all of the aerogel formulations presented a good cytocompatibility with values of cell viability above 80%, and there were no significant differences between the cells in contact with the aerogels and the control group (Figure 5.10). After 48 h, the aerogels also presented good cytocompatibility, but the cell viability in the wells cultured with the CS1-V20 aerogels significantly decreased compared to the control group. Several studies have demonstrated that, at high concentrations or after continuous exposure, the vancomycin can present a cytotoxic effect on human cells like fibroblasts [56,57]. Nevertheless, the cell viability was still acceptable (72.6 ± 4.0%) after 48 h of incubation of cells in contact with CS1-V20 particles.

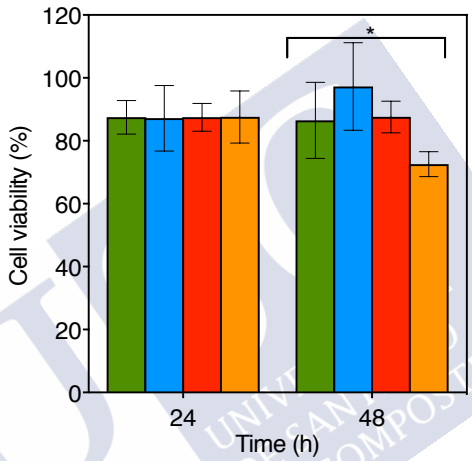


Figure 5.10. Cell viability of fibroblasts after 24 and 48 h of incubation with CS1-V0 (green), CS1-V5 (blue), CS1-V10 (red) and CS1-V20 (orange) particles. Asterisk denotes statistical difference between groups ($\alpha < 0.05$) after Tuckey's analysis of variance. A slight cytotoxic effect was noticed in case of the CS1-V20 particles after 48 h of incubation.

## 5.4. Conclusions

Chitosan aerogels loaded with a bioactive compound (vancomycin) were herein evaluated regarding their potential use in the management of chronic wounds for the first time. The chitosan aerogel beads had a fibrous structure characterized by a high porosity (> 96%) and large surface area (> 200 $m^2/g$). Aerogel particles absorbed large amounts of aqueous fluids in the usual exudate pH range (6–8) upon healing, so they would provide an adequate moisture balance in the wound site. Chitosan aerogels did not have any effect on the collagenase activity and therefore they are not expected to interfere with the normal biological healing process. The loading of vancomycin in the aerogels can provide a fast local administration of the antibiotic at the wound site to prevent infections shortly after wound debridement without compromising cell viability. Overall, vancomycin-loaded chitosan aerogels arise as a promising

formulation to be incorporated in dressings for the management of chronic wounds, particularly when infectious episodes are expected to take place. Future work will be devoted to adapt the aerogel formulation to a powdered form that could be easily applied to the wound or even incorporated into a multi-layered system.

## 5.5. References


1. Harper, D.; Young, A.; McNaught, C.-E. The physiology of wound healing. *Surgery* **2014**, *32*, 445–450.
2. Li, J.; Chen, J.; Kirsner, R. Pathophysiology of acute wound healing. *Clin. Dermatol.* **2007**, *25*, 9–18.
3. Morton, L.M.; Phillips, T.J. Wound healing and treating wounds: Differential diagnosis and evaluation of chronic wounds. *J. Am. Acad. Dermatol.* **2016**, *74*, 589–605.
4. Gosain, A.; DiPietro, L.A. Aging and Wound Healing. *World J. Surg.* **2004**, *28*, 321–326.
5. Guo, S.; DiPietro, L. Factors Affecting Wound Healing. *J. Dent. Res.* **2010**, *89*, 219–229.
6. Bajjada, T. Using a step-up, step-down approach to exudate management. *J. Community Nurs.* **2017**, *31*, 34–38.
7. Hiriart-Ramírez, E.; Contreras-García, A.; Garcia-Fernandez, M.J.; Concheiro, A.; Alvarez-Lorenzo, C.; Bucio, E. Radiation grafting of glycidyl methacrylate onto cotton gauzes for functionalization with cyclodextrins and elution of antimicrobial agents. *Cellulose* **2012**, *19*, 2165–2177.
8. Luna-Straffon, M.A.; Contreras-García, A.; Brackman, G.; Coenye, T.; Concheiro, A.; Alvarez-Lorenzo, C.; Bucio, E. Wound debridement and antibiofilm properties of gamma-ray DMAEMA-grafted onto cotton gauzes. *Cellulose* **2014**, *21*, 3767–3779.
9. Dhivya, S.; Padma, V.V.; Santhini, E. Wound dressings – a review. *BioMedicine* **2015**, *5*, 24–28.
10. Driscoll, P. Global wound care market — double-digit growth from within Available online: http://blog.mediligence.com/2016/01/21/global-wound-care-market-double-digit-growth-from-within/ (accessed on Oct 16, 2017).
11. García-González, C.A.; Alnaief, M.; Smirnova, I. Polysaccharide-based aerogels—Promising biodegradable carriers for drug delivery systems. *Carbohyd. Polym.* **2011**, *86*, 1425–1438.
12. Govindarajan, D.; Duraipandy, N.; Srivatsan, K.V.; Lakra, R.; Korapatti, P.S.; Jayavel, R.; Kiran, M.S. Fabrication of Hybrid Collagen Aerogels Reinforced with Wheat Grass Bioactives as Instructive Scaffolds for Collagen Turnover and Angiogenesis for Wound Healing Applications. *ACS Appl. Mater. Interfaces* **2017**, *9*, 16939–16950.
13. Pierre, A.C.; Pajonk, G.M. Chemistry of Aerogels and Their Applications. *Chem. Rev.* **2002**, *102*, 4243–4266.
14. Maleki, H.; Durães, L.; García-González, C.A.; del Gaudio, P.; Portugal, A.; Mahmoudi, M. Synthesis and biomedical applications of aerogels: Possibilities and challenges. *Adv. Colloid Interface Sci.* **2016**, *236*, 1–27.
15. Şahin, İ.; Özbakır, Y.; İnönü, Z.; Ulker, Z.; Erkey, C. Kinetics of supercritical drying of gels. *Gels* **2018**, *4*, 3–31.
16. García-González, C.A.; Smirnova, I. Use of supercritical fluid technology for the production of tailor-made aerogel particles for delivery systems. *J. Supercrit. Fluid.* **2013**, *79*, 152–158.
17. Jayakumar, R.; Prabaharan, M.; Sudheesh Kumar, P.T.; Nair, S.V.; Tamura, H. Biomaterials based on chitin and chitosan in wound dressing applications. *Biotechnol. Adv.* **2011**, *29*, 322–337.
18. Muzzarelli, R.A.A. Chitosan composites with inorganics, morphogenetic proteins and stem cells, for bone regeneration. *Carbohydr. Polym.* **2011**, *83*, 1433–1445.

19. Ahmed, S.; Ikram, S. Chitosan based scaffolds and their applications in wound healing. *Achiev. Life Sci.* **2016**, *10*, 27–37.
20. Kumar, M.N.V.R.; Muzzarelli, R.A.A.; Muzzarelli, C.; Sashiwa, H.; Domb, A.J. Chitosan Chemistry and Pharmaceutical Perspectives. *Chem. Rev.* **2004**, *104*, 6017–6084.
21. Niekraszewicz, A. Chitosan Medical Dressings. *Fibres Text. East. Eur.* **2005**, *13*, 16–18.
22. Rinki, K.; Dutta, P.K.; Hunt, A.J.; Macquarrie, D.J.; Clark, J.H. Chitosan aerogels exhibiting high surface area for biomedical application: Preparation, characterization, and antibacterial study. *Int. J. Polym. Mater. Po.* **2011**, *60*, 988–999.
23. Wu, T.; Zivanovic, S.; Draughon, F.A.; Conway, W.S.; Sams, C.E. Physicochemical Properties and Bioactivity of Fungal Chitin and Chitosan. *J. Agric. Food Chem.* **2005**, *53*, 3888–3894.
24. Chang, S.-H.; Lin, H.-T.V.; Wu, G.-J.; Tsai, G.J. pH Effects on solubility, zeta potential, and correlation between antibacterial activity and molecular weight of chitosan. *Carbohyd. Polym.* **2015**, *134*, 74–81.
25. Younes, I.; Sellimi, S.; Rinaudo, M.; Jellouli, K.; Nasri, M. Influence of acetylation degree and molecular weight of homogeneous chitosans on antibacterial and antifungal activities. *Int. J. Food Microbiol.* **2014**, *185*, 57–63.
26. Kayser, H.; Müller, C.R.; García-González, C.A.; Smirnova, I.; Leitner, W.; Domínguez de María, P. Dried chitosan-gels as organocatalysts for the production of biomass-derived platform chemicals. *Appl. Catal. A Gen.* **2012**, *445–446*, 180–186.
27. Quignard, F.; Valentin, R.; Di Renzo, F. Aerogel materials from marine polysaccharides. *New J. Chem.* **2008**, *32*, 1300–1310.
28. Ahsan, S.M.; Thomas, M.; Reddy, K.K.; Sooraparaju, S.G.; Asthana, A.; Bhatnagar, I. Chitosan as biomaterial in drug delivery and tissue engineering. *Int. J. Biol. Macromol.* **2017**, *110*, 97–109.
29. Buzia, O.D.; Dima, C.; Dima, Ștefan Preparation and characterization of chitosan microspheres for vancomycin delivery. *Farmacia* **2015**, *63*, 897–902.
30. Cerchiara, T.; Abruzzo, A.; Ñahui Palomino, R.A.; Vitali, B.; De Rose, R.; Chidichimo, G.; Ceseracciu, L.; Athanassiou, A.; Saladini, B.; Dalena, F.; et al. Spanish Broom (Spartium junceum L.) fibers impregnated with vancomycin-loaded chitosan nanoparticles as new antibacterial wound dressing: Preparation, characterization and antibacterial activity. *Eur. J. Pharm. Sci.* **2017**, *99*, 105–112.
31. Pawar, H.V.; Boateng, J.S.; Ayensu, I.; Tetteh, J. Multifunctional Medicated Lyophilised Wafer Dressing for Effective Chronic Wound Healing. *J. Pharm. Sci.* **2014**, *103*, 1720–1733.
32. Kosinski, M.A.; Lipsky, B.A. Current medical management of diabetic foot infections. *Expert Rev. Anti-infect. Ther.* **2010**, *8*, 1293–1305.
33. García-González, C.A.; Barros, J.; Rey-Rico, A.; Redondo, P.; Gómez-Amoza, J.L.; Concheiro, A.; Alvarez-Lorenzo, C.; Monteiro, F.J. Antimicrobial Properties and Osteogenicity of Vancomycin-Loaded Synthetic Scaffolds Obtained by Supercritical Foaming. *ACS Appl. Mater. Interfaces* **2018**, *10*, 3349–3360.
34. Liu, K.-S.; Lee, C.-H.; Wang, Y.-C.; Liu, S.-J. Sustained release of vancomycin from novel biodegradable nanofiber-loaded vascular prosthetic grafts: in vitro and in vivo study. *Int. J. Nanomedicine* **2015**, *10*, 885–891.
35. Zebala, L.P.; Chuntarapas, T.; Kelly, M.P.; Talcott, M.; Greco, S.; Riew, K.D. Intrawound vancomycin powder eradicates surgical wound contamination: An in vivo rabbit study. *J. Bone Joint Surg. Am.* **2014**, *96*, 46–51.
36. Bakhsheshian, J.; Dahdaleh, N.S.; Lam, S.K.; Savage, J.W.; Smith, Z.A. The Use of Vancomycin Powder In Modern Spine Surgery: Systematic Review and Meta-Analysis of the Clinical Evidence. *World Neurosurg.* **2015**, *83*, 816–823.
37. Noel, S.; Courtney, H.; Bumgardner, J.; Haggard, W. Chitosan Sponges to Locally Deliver Amikacin and Vancomycin: A Pilot In Vitro Evaluation. *Clin. Orthop. Relat. Res.* **2010**,

*468*, 2074-2080.
38. O'Neal, P.B.; Itani, K.M.F. Antimicrobial Formulation and Delivery in the Prevention of Surgical Site Infection. *Surg. Infect.* **2016**, *17*, 275–285.
39. Xiong, L.; Pan, Q.; Jin, G.; Xu, Y.; Hirche, C. Topical intrawound application of vancomycin powder in addition to intravenous administration of antibiotics: A meta-analysis on the deep infection after spinal surgeries. *Orthop. Traumatol. Surg. Res.* **2014**, *100*, 785–789.
40. Albaugh, K.W.; Biely, S.A.; Cavorsi, J.P. The Effect of a Cellulose Dressing and Topical Vancomycin on Methicillin-resistant Staphylococcus aureus (MRSA) and Gram-positive Organisms in Chronic Wounds: A Case Series. *Ostomy Wound Manage.* **2013**, *59*, 34–43.
41. Chapter 17 Wound management. *South and West devon formulary* 2018.
42. Sing, K.S.W. Reporting physisorption data for gas/solid systems with special reference to the determination of surface area and porosity (Recommendations 1984). *Pure and Appl. Chem.* **2009**, *57*, 603–619.
43. Varanda, F.; Pratas de Melo, M.J.; Caço, A.I.; Dohrn, R.; Makrydaki, F.A.; Voutsas, E.; Tassios, D.; Marrucho, I.M. Solubility of Antibiotics in Different Solvents. 1. Hydrochloride Forms of Tetracycline, Moxifloxacin, and Ciprofloxacin. *Ind. Eng. Chem. Res.* **2006**, *45*, 6368–6374.
44. Gilotra, S.; Chouhan, D.; Bhardwaj, N.; Nandi, S.K.; Mandal, B.B. Potential of silk sericin based nanofibrous mats for wound dressing applications. *Mater. Sci. Eng. C* **2018**, *90*, 420–432.
45. Gethin, G. The significance of surface pH in chronic wounds. *Wounds UK* **2007**, *3*.
46. Trengove, N.J.; Stacey, M.C.; Macauley, S.; Bennett, N.; Gibson, J.; Burslem, F.; Murphy, G.; Schultz, G. Analysis of the acute and chronic wound environments: the role of proteases and their inhibitors. *Wound Repair and Regen.* **1999**, *7*, 442–452.
47. Chang, X.; Chen, D.; Jiao, X. Chitosan-Based Aerogels with High Adsorption Performance. *J. Phys. Chem. B* **2008**, *112*, 7721–7725.
48. Yao, Q.; Nooeaid, P.; Roether, J.A.; Dong, Y.; Zhang, Q.; Boccaccini, A.R. Bioglass®-based scaffolds incorporating polycaprolactone and chitosan coatings for controlled vancomycin delivery. *Ceram. Int.* **2013**, *39*, 7517–7522.
49. Zarif, M.S.; Afidah, A.; Abdullah, J.M.; Shariza, A. Physicochemical characterization of vancomycin and its complexes with β-cyclodextrin. *Biomed. Res.* **2012**, *23*, 513–520.
50. Gurikov, P.; Smirnova, I. Amorphization of drugs by adsorptive precipitation from supercritical solutions: A review. *J. Supercrit. Fluid.* **2018**, *132*, 105–125.
51. Zhao, Y.; Zhang, X.; Wang, Y.; Wu, Z.; An, J.; Lu, Z.; Mei, L.; Li, C. In situ cross-linked polysaccharide hydrogel as extracellular matrix mimics for antibiotics delivery. *Carbohydr. Polym.* **2014**, *105*, 63–69.
52. Faustino, P.J. *Vancomycin solubility study*; Food and Drug Administration, 2008.
53. Martinez, L.R.; Han, G.; Chacko, M.; Mihu, M.R.; Jacobson, M.; Gialanella, P.; Friedman, A.J.; Nosanchuk, J.D.; Friedman, J.M. Antimicrobial and Healing Efficacy of Sustained Release Nitric Oxide Nanoparticles Against Staphylococcus Aureus Skin Infection. *J. Invest. Dermatol.* **2009**, *129*, 2463–2469.
54. Dai, T.; Tanaka, M.; Huang, Y.-Y.; Hamblin, M.R. Chitosan preparations for wounds and burns: Antimicrobial and wound-healing effects. *Expert Rev. Anti-infect. Ther.* **2011**, *9*, 857–879.
55. Talebian, A.; Mansourian, A. Release of Vancomycin from electrospun gelatin/chitosan nanofibers. *Mat. Today Proc.* **2017**, *4*, 7065–7069.
56. Damour, O.; Zhi Hua, S.; Lasne, F.; Villain, M.; Rousselle, P.; Collombel, C. Cytotoxicity evaluation of antiseptics and antibiotics on cultured human fibroblasts and keratinocytes. *Burns* **1992**, *18*, 479–485.
57. Liu, J.X.; Bravo, D.; Buza, J.; Kirsch, T.; Kennedy, O.; Rokito, A.; Zuckerman, J.D.; Virk,

M.S. Topical vancomycin and its effect on survival and migration of osteoblasts, fibroblasts, and myoblasts: An in vitro study. *J. Orthop.* **2018**, *15*, 53–58.

USC
UNIVERSIDADE
DE SANTIAGO
DE COMPOSTELA

# 6. JET CUTTING TECHNIQUE FOR THE PRODUCTION OF CHITOSAN AEROGEL MICROPARTICLES LOADED WITH VANCOMYCIN

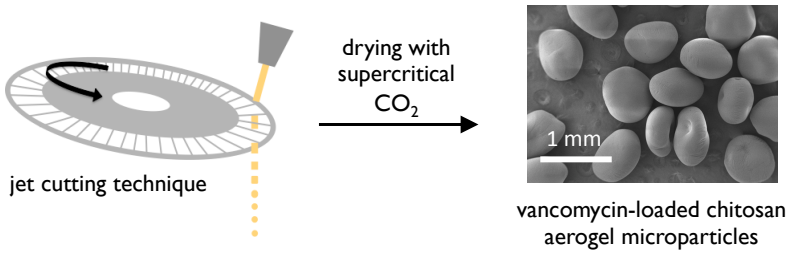


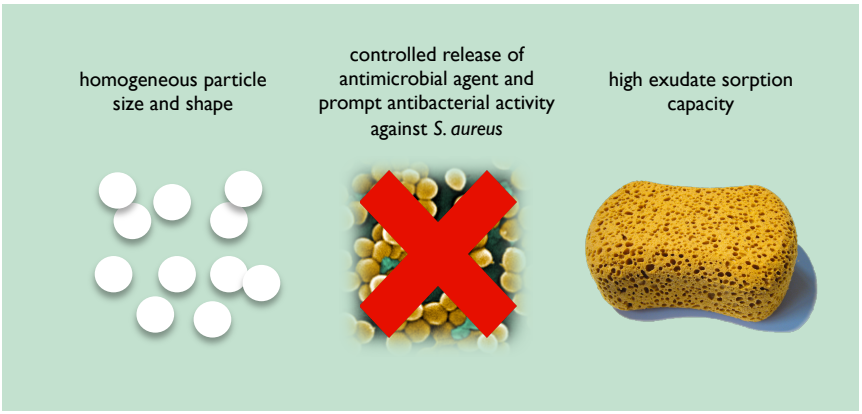


The work described in this chapter was published in López-Iglesias, C. *et al.* Jet cutting technique for the production of chitosan aerogel microparticles loaded with vancomycin. Polymers **2020**, 12, 273–285.

Work carried out in collaboration with the Instituto de Investigação e Inovação em Saúde of the Universidade do Porto, the BioFarma group of the Centro Singular de Investigación en Medicina Molecular y Enfermedades Crónicas of the Universidade de Santiago de Compostela, the Laboratory for Development and Modeling of Novel Nanoporous Materials of the Hamburg University of Technology, and the Institute of Thermal Separation Processes of the Hamburg University of Technology.

USC
UNIVERSIDADE
DE SANTIAGO
DE COMPOSTELA

# 6. JET CUTTING TECHNIQUE FOR THE PRODUCTION OF CHITOSAN AEROGEL MICROPARTICLES LOADED WITH VANCOMYCIN

## 6.1. Introduction

Aerogels are nanostructured, lightweight materials with open, high porosities and large surface areas that currently find applications in many industrial sectors due to their thermal, optical, electrical, or mechanical properties [1,2]. The outstanding textural properties of the aerogels have also attracted the attention from other fields of study such as biomedical and environmental sciences [3–6]. Biomedical applications of aerogels include the encapsulation of bioactive agents with solubility or stability limitations, and their use as synthetic scaffolds for tissue engineering and wound dressing materials for chronic wounds [7–16]. In the latter case, the large surface area of the aerogels confers them the ability to load and release bioactive agents, such as antibiotics or growth factors, which can facilitate the wound healing process [17]. High porosity also provides the aerogels with the ability to absorb exudate fluid in order to maintain a correct moisture balance at the wound site. This in turn alleviates the inflammatory process and prevents the apparition of bacterial infections (one of the main barriers for the wound healing process) [11,18]. Other advantages of using aerogels include high stability upon storage and protection of the drug from the environment [5].

Aerogels are usually processed by supercritical drying of polymeric wet gels with supercritical $CO_2$ ($scCO_2$) [19]. This drying technique can extract the liquid part of the gel under mild conditions of pressure and temperature ($P > 73.8$ bar, $T > 31.1$ °C) whilst preserving the interconnected structure of the polymer network without causing the pore collapse phenomenon. Biopolymer-based materials are preferred for wound care applications, since their biocompatibility and biodegradability may avoid toxicity problems. Natural polysaccharides like alginate, pectin, cellulose, starch, or chitosan are widely used since they are abundant and cost-effective, and have been approved and largely used in the food and pharmaceutical industry [20–22]. The hemostatic, antimicrobial and healing-promoting properties of chitosan are suitable for wound

healing applications [23,24]. Chitosan gels can be processed by physical or chemical crosslinking, resulting in tunable mechanical properties and enhanced biocompatibility [25].

Particulate systems, such as micro- or nanoparticles, are attracting attention in the field of drug delivery as carriers since they present large surface area and can control the release of the drug [26]. Unlike nanoparticles, microparticles are unable to cross most biological barriers and remain in the location of interest [27–29]. This feature entails an advantage for local delivery of drugs, where systemic absorption is not desired and may result in toxicity issues. For the production of aerogel microparticles, several technologies have been described [30]. The emulsion-gelation method is a suitable option to obtain homogeneous particle sizes, but involves the use of emulsifying agents that may modify the surface properties of the particles [31]. Other approaches are often modifications of the conventional dripping method [30], applying different types of forces (electrostatic, vibrational or mechanical) to break the liquid jet into droplets. However, the mechanical forces are the only feasible option to process solutions of high viscosity.

The jet cutting method is a simple technology for the production of gel particles based on the application of mechanical forces to a liquid jet. This technique allows the production of particles with controlled diameters ranging from 100 µm to several millimeters at high production rates [32]. In the jet cutting technique, the fluid is pressed out of a nozzle as a solid jet towards a rotating disc with small wires placed below (Fig.6.1). This disc cuts the liquid jet into cylinders that would eventually form spherical beads due to surface tension forces. The size of the beads can be modulated by the following parameters: fluid jet pressure, nozzle diameter, number and diameter of wires of the cutting disc, and rotation velocity. A small part of the fluid (1–5%) can be lost during the cutting because of its adhesion to the wires and non-zero wire thickness [30]. The adjustment of the parameters to optimize the process along with re-use of the lost solution can lead to production yields close to 100%, making it a very efficient and easily scalable process [33].

Overall, chitosan aerogel microparticles are attractive drug carrier candidates for wound treatment, but their processing difficulties, associated with the high viscosity of the chitosan precursor solution, hamper their potential use. Alternative technologies must be sought to overcome the limitations in the processing of chitosan aerogels as microparticles. In this work, the feasibility of the jet cutting technique to obtain chitosan aerogel microparticles was studied, and their potential application in wound treatment was assessed. Chitosan aerogel microparticles were prepared by the sol-gel method using the jet cutting technique followed by supercritical drying with $scCO_2$ and evaluated for wound healing purposes. The parameters of the jet cutting process were defined regarding the processability of the chitosan solution and the characteristics of the produced particles. Chitosan particles were loaded with vancomycin HCl, a broad-

spectrum antimicrobial drug, and the drug loading and release were evaluated. Specific tests for the application in wound treatment, as the exudate sorption capacity, antimicrobial activity, hemocompatibility, and cytocompatibility, were also carried out.

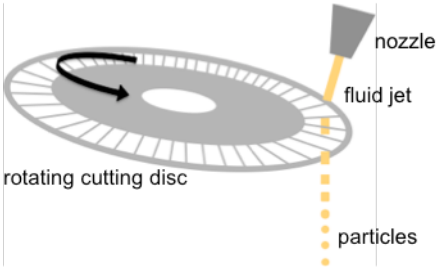


Figure 6.1. Schematic representation of the jet cutting process. The chitosan solution was pressed out of the nozzle as a solid jet and cut into cylinders by the cutting disc. Due to surface tension, the cylinders acquired the spherical shape of droplets before falling into the gelation bath.

## 6.2. Materials and methods

### 6.2.1. Materials

Chitosan (degree of deacetylation 90%, viscosity 500 mPa·s, $M_w$ 200–400 kDa) was purchased from Heppe Medical Chitosan GmbH (Halle, Germany). Glacial acetic acid (100% purity) and ethanol (99.8% purity) were obtained from Carl Roth (Karlsruhe, Germany) and $CO_2$ (purity > 99.5%) was supplied from Praxair (Ratingen, Germany). NaCl and $NH_3$ (25% in $H_2O$) were from PanReac AppliChem (Barcelona, Spain). Triton X-100 was from Merck (Darmstadt, Germany). Vancomycin hydrochloride ($M_w$ 1486 g/mol, 94.3% purity, amorphous) was from Guinama (Valencia, Spain). BALB/3T3 clone A31 mouse fibroblasts (ATCC CCL-163) and Dulbecco's modified Eagle's medium (DMEM) were from the American Type Culture Collection (ATCC, Manassas, VA, USA). Fetal bovine serum (FBS), phosphate buffer saline (PBS) and penicillin 10,000 U/mL-streptomycin 10 mg/mL, NaOH and HCl 37% were supplied by Sigma-Aldrich (Saint Louis, MO, USA). WST-1 reactive was purchased from Roche (Basel, Switzerland).

### 6.2.2. Production of chitosan aerogel microparticles

Chitosan gel particles were produced using a JetCutter Type S equipment (GeniaLab GmbH, Braunschweig, Germany). Table 6.1 summarizes the combinations of parameters used in this study. Briefly, the jetted chitosan solution (250 mL of 2% wt. chitosan in 1% v/v acetic acid aqueous solution) was extruded through a nozzle assisted by compressed air (P = 2 bar). A protective piece of stainless steel was placed around the cutting disc to collect fluid loss. Different nozzle diameters (350, 400 and 500 µm), number of wires (40 and 120) of the cutting disc, and cutting disc rates (1000 to 6000 rpm) were used to test the feasibility of particle production and the

morphology and particle size distribution (PSD) of the resulting particles. The angle of the jet was in all cases perpendicular to the cutting disc. A gelation bath consisting of 2 L of alkaline medium was placed below the jet cutter to form and collect the gel microparticles. Preliminary tests were carried out in aqueous media (0.2 M NaOH) to avoid the use of high volumes of ethanol and thus reducing the amount of organic solvents used in the study. After a preliminary screening of the parameters for the processing of the chitosan solution, the gelation of vancomycin-loaded chitosan particles was performed in 2 L of EtOH containing 26 mL of 25% aqueous $NH_3$. The loading of vancomycin HCl into the particles was performed by addition of the drug to the initial chitosan solution (10 wt.% with respect to chitosan). The microparticles were left in the gelation bath for 1 h for ageing and then the solvent was replaced with absolute EtOH twice. Gel particles were placed in filter paper cartridges and dried for 3.5 h with supercritical $CO_2$ in a 250 mL high pressure autoclave (120 bar, 40 °C, 15 g/min).

Table 6.1. Experimental jet cutting parameters tested for the processing of chitosan gel particles.

| Number of wires in the cutting disc | Gelation bath | Nozzle diameter (µm) | Cutting disc velocity (rpm) |
|---|---|---|---|
| 120 | 0.2 M NaOH (aq.) | 350 | 4500 |
| | | | 1000 |
| 40 | 0.2 M NaOH (aq.) | 400 | 2000 |
| | | | 4000 |
| | | | 6000 |
| | 0.2 M NaOH (aq.) | 500 | 2000 |
| | | | 4000 |
| | | | 6000 |
| | $NH_3$/EtOH | | 6000 |

### 6.2.3. Morphology and textural properties

During the initial screening of the jet cutting process, gel particles processed using nozzle diameters of 400 and 500 µm and gelified for 1 h in aqueous 0.2 M NaOH were examined by optical microscopy (VisiScope TL384H, VWR International GmbH, Darmstadt, Germany) to qualitatively monitor properties such as sphericity and homogeneity. After supercritical drying, the resulting unloaded and vancomycin-loaded aerogels were studied by Scanning Electron Microscopy (SEM) at 3 kV (FESEM ULTRA PLUS, Zeiss, Oberkochen, Germany). Prior to SEM-imaging, aerogels were sputtered-coated (Q150 T/S/E/ES, Quorum Technologies, Lewes, UK) with a 10 nm layer of iridium to improve the contrast. The PSD and sphericity of the aerogels were

determined by dynamic image analysis (CamSizer XT, Retsch, Haan, Germany). All data for the PSD were obtained based on the $x_{area}$, i.e. the particle diameter obtained from the area of particle projection. Sphericity was given as a value between 0 and 1, with 1 being a perfect sphere.

Nitrogen adsorption-desorption measurements (ASAP 2000 Micromeritics Inc, Norcross, GA, USA) were used for the determination of the textural properties of the aerogel particles loaded with vancomycin HCl and gelled in $NH_3$/EtOH medium. Specific surface area ($a_{BET}$) was calculated using the Brunauer-Emmet-Teller (BET) method, whereas the Barrett-Joyner-Halenda (BJH) method was applied for the determination of the pore size distribution, specific pore volume ($V_{p,BJH}$) and mean pore diameter ($d_{p,BJH}$). Overall porosity ($\varepsilon$) was determined using Eq. 6.1:

$$\varepsilon = \left(1 - \frac{\rho_{bulk}}{\rho_{skel}}\right) \cdot 100 \quad (6.1)$$

where $\rho_{bulk}$ is the bulk density determined from the weight of particles of a known volume, and $\rho_{skel}$ is the skeletal density determined by helium pycnometry (MPY-2, Quantachrome, Delray Beach, FL, USA).

### 6.2.4. Fluid sorption capacity test

Approximately 40 mg of aerogel microparticles were placed in 6-well plate inserts of known weight and immersed in Falcon tubes containing 50 mL of PBS (Phosphate Buffered Saline) pH 7.4 solution. At specific times (1, 2, 4, 8 and 24 h) the inserts were removed from the solution and weight gain was determined. The experimental test was carried out in triplicate. The PBS sorption capacity was calculated using Eq. 6.2:

$$\text{PBS sorption} = \frac{w_t - w_0}{w_0} \cdot 100 \quad (6.2)$$

where $w_0$ and $w_t$ are the weights of the particles before the experiment and after the immersion during a certain time $t$, respectively.

### 6.2.5. Vancomycin encapsulation efficiency and release tests

Vancomycin-loaded chitosan aerogel particles (50 mg) were placed in glass vials containing 5 mL of 0.1 M HCl. After 4 h, the particles were dissolved and the concentration of vancomycin in the medium was determined by UV/Vis spectrophotometry at a wavelength of 280 nm (Genesys10uv, Thermo Spectronic, New York, NY, USA). The absorbance of dissolved unloaded chitosan aerogels was also determined to remove the influence of the polymer in the UV-measurements. The concentration of vancomycin HCl was calculated using a calibration curve in 0.1 M HCl validated in the 20–300 µg/mL range ($R^2 > 0.9995$). The encapsulation efficiency of vancomycin into the aerogels was determined using Eq. 6.3:

$$\text{Encapsulation efficiency} = \frac{w_p}{w_t} \cdot 100 \quad (6.3)$$

where $w_p$ is the amount of vancomycin HCl present in the particles and $w_t$ is the total amount of vancomycin added to the initial chitosan solution.

Vancomycin release tests were carried out in Franz cells consisting of a donor chamber and a receptor chamber separated by a 0.45 µm cellulose nitrate membrane filter (Whatman, Maidstone, UK). The receptor chamber was filled with 6 mL of PBS (pH 7.4) and *ca.* 40 mg of particles were added to the donor chamber. Surface available for drug diffusion was 0.8 $cm^2$. The release tests were performed in triplicate in an orbital shaker (VWR® Incubating Mini Shaker, VWR, Chester, PA, USA) at 37 °C and 400 rpm. At preset times, aliquots of 1 mL were taken from the receptor chamber and the withdrawn volume was replaced by fresh PBS. The concentration of vancomycin HCl was determined by UV/Vis spectrophotometry (8453, Agilent, Santa Clara, CA, USA) using a calibration curve in PBS validated in the 25–200 µg/mL range ($R^2$ > 0.9997). Experiments were carried out in triplicate and results were expressed as µg of vancomycin released per mg of loaded aerogel particles.

### 6.2.6. Antimicrobial tests

Antibacterial activity of the aerogel microparticles was tested against *S. aureus* ATCC 25923. Exponential bacterial culture ($10^6$ CFUs/mL) was prepared in simulated body fluid (SBF, pH 7.4). The bacterial suspension (200 mL) and 7 mg of chitosan aerogel particles (with and without vancomycin) were incubated at 37 °C and 150 rpm for 6, 24 and 48 h. After incubation, the planktonic population was quantified by colony-forming units (CFUs) method. A solution of vancomycin HCl (1.85 mg/mL) and free bacterial suspension acted as positive and negative controls, respectively. Three independent experiments were performed in triplicate. Results were expressed as the logarithmic concentration of planktonic bacteria.

### 6.2.7. Biocompatibility tests in vitro

#### 6.2.7.1. Hemolytic activity test

The hemolytic activity of the vancomycin-loaded aerogel microparticles was tested using human blood (Galician Transfusion Center, Spain) obtained in accordance with the rules of the Declaration of Helsinki. A sample of fresh human whole blood was diluted to 33% (v/v) in 0.9% (w/v) NaCl and 1 mL of the diluted blood was poured in Eppendorf tubes containing 5 mg of vancomycin-loaded chitosan aerogel microparticles, 100 µL of 4% (v/v) Triton X-100 (positive control) or 100 µL of 0.9% (w/v) NaCl (negative control). Samples were incubated for 60 min at 37 °C and 100 rpm in an orbital shaker and then centrifuged at 10,000 g for 10 min (Sigma 2-16P, Sigma Laboratory Centrifuges, Germany). Then, 150 µL of the supernatant were transferred to a 96-well plate and the absorbance of the hemoglobin was measured at 540 nm

(FLUOStar Optima, BMG Labtech, Germany). The percentage of hemolysis of the aerogels was determined using Eq. 6.4:

$$\text{Hemolysis} = \frac{Abs_s - Abs_n}{Abs_p - Abs_n} \cdot 100 \quad (6.4)$$

where $Abs_s$ is the absorbance of the samples containing the aerogels, $Abs_n$ is the absorbance of the negative control (0% of hemolysis), and $Abs_p$ is the absorbance of the positive control (Triton X-100, 100% of hemolysis). Tests were carried out in triplicate.

#### 6.2.7.2. Cytotoxicity test

The compatibility of vancomycin-loaded aerogel microparticles was tested against BALB/3T3 mouse fibroblasts. Cells were seeded in 24-well plates (12,350 cells per well) in DMEM supplemented with 10% FBS, penicillin 100 U/mL and streptomycin 100 µg/mL and incubated overnight at 37 °C in a humidified atmosphere with 5% $CO_2$. Then, four replicates of 5 mg of particles were sterilized using UV radiation (30 min, 254 nm), placed in cell culture inserts (Thermo Fisher Scientific, Waltham, MA, USA), and immersed in the wells. Cells cultured without particles were the positive control. After 24 and 48 h of incubation, the inserts with the particles were collected and 50 µL of WST-1 reactive were added to each well. After 4 h of incubation, plates were shaken thoroughly for 1 min and 100 µL from each well were transferred to a 96-well plate in triplicate. The absorbance was measured at 450 nm in a plate reader (EnSpire, PerkinElmer, Madrid, Spain) and cytocompatibility was determined using Eq. 6.5:

$$\text{Cell viability} = \frac{Abs_s}{Abs_c} \cdot 100 \quad (6.5)$$

where $Abs_s$ and $Abs_c$ are the absorbance of the wells cultured with and without (control) the aerogels, respectively.

## 6.3. Results and discussion

### 6.3.1. Jet cutting of chitosan gels and morphology and textural properties of the resulting aerogel particles

The processability of a viscous chitosan solution with the jet was studied producing unloaded gel microparticles under different conditions, using an aqueous basic medium (0.2 M NaOH) as the gelation bath. Chitosan gelation took place immediately after contact of the droplet of chitosan solution with the surface of the gelation bath. The change from an acidic to alkaline medium caused the deprotonation of the amino groups of the chitosan, and thus its gelation by a precipitation mechanism. In general, smaller particle sizes were obtained when using smaller nozzle diameters and a higher number of wires in the cutting disc that cut the fluid jet at a higher frequency. However, the use of the smallest nozzle diameter (350 µm) in this

study led to frequent events of clogging. Nozzle diameters of 400–500 µm showed good processability and particles were produced at different cutting disc rates (2000, 4000 and 6000 rpm). The 120-wired cutting disc resulted in high fluid losses since it was not able to split the fluid jet into cylinders and the solution remained attached to the wires until deviated to the collector of fluid loss instead of to the gelation bath. The chitosan solution successfully reached the gelation bath when the 40-wired cutting disc was used.

Table 6.2. PSD of particles (CamSizer® measurements) processed by nozzle diameters of 400 and 500 µm and using 40-wired cutting disc velocities of 2000, 4000 and 6000 rpm

| | 400 µm | | | 500 µm | | |
|---|---|---|---|---|---|---|
| | 2000 rpm | 4000 rpm | 6000 rpm | 2000 rpm | 4000 rpm | 6000 rpm |
| $x_{area}$[1] ± σ (µm) | 1105 ± 238 | 790 ± 130 | 754 ± 101 | 1358 ± 393 | 820 ± 141 | 877 ± 141 |
| Mean sph[2] | 0.84 | 0.90 | 0.89 | 0.714 | 0.92 | 0.84 |
| % sph > 0.9 | 22 | 63 | 51 | 7 | 84 | 8 |

[1] Mean particle size (µm) obtained from the projected area. [2] Sphericity of the particles.

In accordance to the literature [34], higher nozzle diameters led to larger particle sizes (Table 6.2 and Figs. 6.2a,b) since the mass flow of the chitosan solution was higher, but similar PSDs were observed using nozzle diameters of 400 or 500 µm. Regarding the cutting disc velocity, aerogels processed at 2000 rpm had larger diameters and broader PSD than those processed at 4000 and 6000 rpm. In general, a higher cutting disc velocity results in smaller particle sizes, but this trend was not herein observed at 4000 and 6000 rpm. This could be explained with the values of sphericity (Table 6.2) and SEM images of the particles (Fig. 6.3). When using the projected area as the parameter to estimate particle size, if the particle is not spherical the value may be biased by its orientation. Thus, a flattened particle may have the same projected area as a larger spherical particle. Particles processed at 6000 rpm were flatter, probably because of their lower weight and subsequent deformation upon contact with the surface of the gelation medium [35].

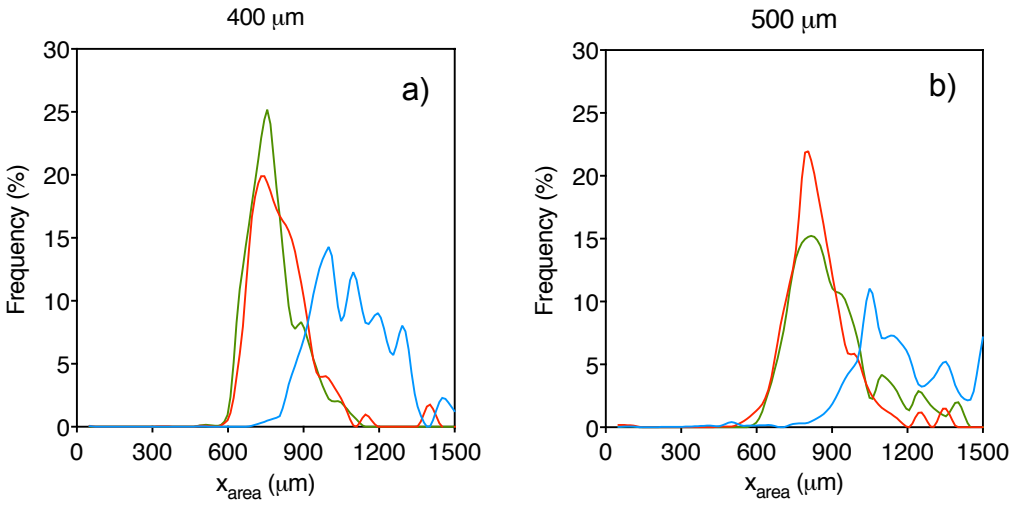


Figure 6.2. Particle size distributions obtained from the dynamic image analysis of chitosan aerogel particles processed using nozzle diameters of (a) 400 μm and (b) 500 μm. Blue, red and green represent cutting disc velocities of 2000, 4000 and 6000 rpm, respectively.

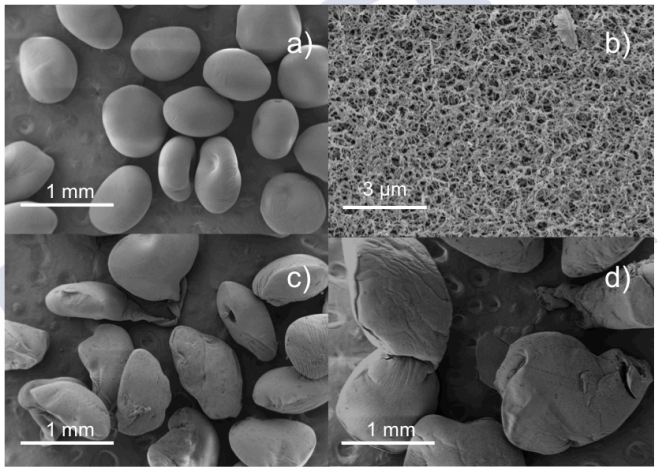


Figure 6.3. SEM images of chitosan aerogel particles processed with the nozzle diameter of 500 μm at (a, b) 4000 rpm; (c) 6000 rpm and (d) 2000 rpm.

The aerogels obtained from chitosan gels processed by jet cutting with a nozzle diameter of 500 μm and cutting disc velocity of 4000 rpm were lightweight ($\rho_{bulk}$ = 0.060 ± 0.002 g/cm$^3$) and highly porous ($\varepsilon$ = 95.6 ± 0.2%), and presented excellent textural properties ($a_{BET}$ = 188.0 ± 9.4 m$^2$/g). Porosity and bulk density values were consistent with previous reports on chitosan aerogels gelified using a similar precipitation method, but the specific surface area was slightly lower [36,37], probably due to a higher degree of shrinkage of the gel during gelation in ethanol medium [38]. Chitosan aerogels with higher specific surface areas have also been described, but involved the use of chemical crosslinkers that could leave toxic residues in the gels, raising regulatory concerns [39].

### 6.3.2. Fluid sorption capacity

A good moisture balance is required at the wound site for adequate wound epithelization and closure. However, wound exudates are environments rich in inflammatory cytokines and chemokines and can also be a suitable broth for bacterial proliferation [40,41]. Thus, it is important that materials used in wound dressings are able to absorb the exudates, maintaining good conditions for the healing process.

The exudate sorption capacity of the aerogel microparticles was determined by a gravimetric method (Fig. 6.4). Due to their high porosity and large surface area, aerogels were able to absorb up to nine times their weight in PBS after 24 h. Unlike chemical crosslinking, where bonds between the polymer fibers are permanent and may lead to rigid structures with limited water sorption capability [42], the physical precipitation of chitosan allowed for a certain degree of swelling in the polymer network, so the microparticles could retain high amounts of water within their structure.

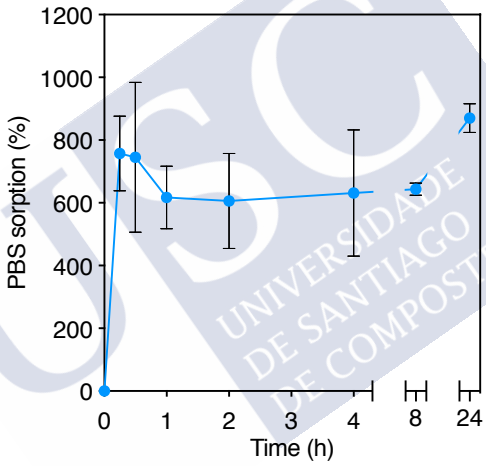


Figure 6.4. Weight gain after immersion in PBS at 25 °C of chitosan aerogel microparticles processed by a nozzle diameter of 500 μm, a cutting disc velocity of 4000 rpm, and gelified in $NH_3$/EtOH solution.

### 6.3.3. Drug encapsulation and release

Vancomycin HCl is a highly hydrosoluble drug (solubility > 100 mg/mL), but it is poorly soluble in ethanol [43]. Accordingly, chitosan gelation was performed in ethanol with $NH_3$ to mitigate drug migration through diffusion to the gelation bath, which would result in low drug loading efficiencies. The encapsulation efficiency for vancomycin contained in the chitosan aerogel microparticles was of 24.6 ± 0.3%, being the final loading in the particles of 22.4 ± 0.3 μg of vancomycin/mg of aerogel particles. The obtained drug loss can be explained by the drainage of the water containing the drug from the chitosan solution when dropped in the ethanol of the gelation bath. In any case, the loading was still high if compared to other drug-loaded aerogel formulations prepared in aqueous medium (≈ 12%) [36].

In the release studies, aerogel microparticles formed a layer on the membrane of the donor compartment of the Franz cells, simulating the application to the wound. Microparticles only released 50% of the drug payload after 4 h (Fig. 6.5) and the complete release was observed after 24 h (the release profile reached a plateau that was kept after 48 h). The microparticles provided concentrations above the MIC (2 µg/mL) for susceptible bacteria already at a short time period, as confirmed in the antimicrobial activity tests (*cf.* Section 6.3.4.).

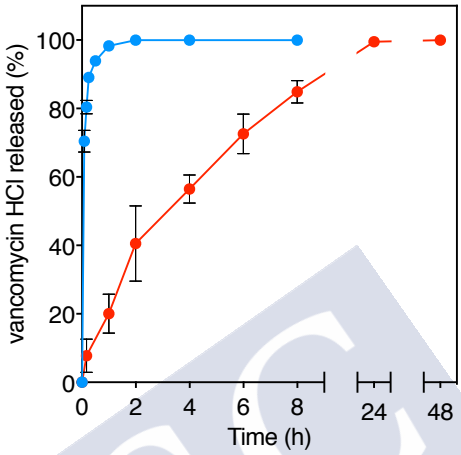


Figure 6.5. Drug release of vancomycin HCl (red line) from the chitosan aerogels (37 °C, 400 rpm, PBS pH 7.4) was sustained over time when compared to the pure drug (blue), and 100% of release was reached after 24 h.

### 6.3.4. Antimicrobial tests

The antimicrobial activity of the vancomycin-loaded aerogel microspheres was tested in SBF medium against *S. aureus* (Fig. 6.6), since it is the most common Gram(+) bacteria in chronic wounds [44]. The aerogel microparticles loaded with vancomycin showed a fast antimicrobial effect, being able to completely inhibit the bacterial growth after 6 h of incubation. Bacterial growth inhibition of the vancomycin-loaded aerogels was maintained during the 48 h of the test. Differently, non-loaded aerogels did not inhibit the bacterial growth.

The antimicrobial effect of the drug-loaded aerogels indicated that the aerogels preserved the active form of vancomycin HCl and released it at an adequate rate. The use of a polymeric matrix that releases the drug instead of the direct use of the drug powder allows more precise adjustment of the dosage, avoiding toxic effects [45]. Although many studies have evaluated the antimicrobial capacity of chitosan [46], it has been reported that chitosan only presents antimicrobial activity when dissolved in acidic media [47], probably due to the protonated free amino groups that interfere with the bacterial membrane.

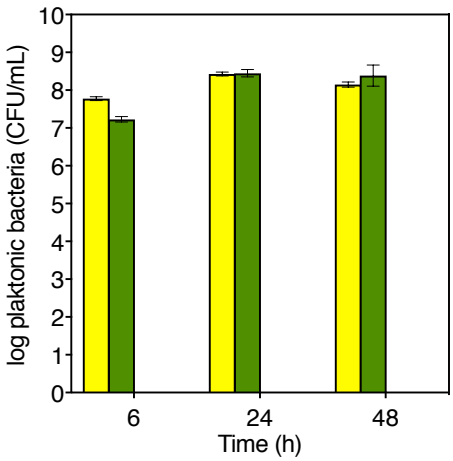


Figure 6.6. Antimicrobial effect against *S. aureus* strains of vancomycin-loaded chitosan aerogels and dissolved vancomycin HCl (positive control) compared with the negative controls: free bacterial culture (yellow) and unloaded chitosan aerogels (green). Vancomycin in the aerogels and the positive control presented a fast antimicrobial effect, with complete bacterial inhibition after 6 h.

## 6.3.5. Biocompatibility and hemocompatibility of vancomycin-loaded aerogel particles

### 6.3.5.1. Hemocompatibility

Biomaterials to be applied directly to the wound need to be compatible to red blood cells, so that they do not interfere with the hemostatic activity. A good hemostatic response of the aerogel formulation is crucial, since the first stage of the wound healing process is intended to reduce blood loss and to start the formation of a provisional wound matrix [48]. In later stages of cell proliferation and repair, a process of formation of new blood vessels (angiogenesis) also takes place. The determination of the hemoglobin released from red blood cells from diluted human blood samples after incubation with the material is a simple method to evaluate hemocompatibility. Results showed that the vancomycin-loaded chitosan aerogel microparticles were completely compatible with the red blood cells compared to the negative control (saline solution), and even the hemolytic activity was lower (-7.7%). According to ISO 10993-4, materials with hemolysis values lower than 5% can be used safely in contact with blood.

### 6.3.5.2. Cytocompatibility

Vancomycin HCl is frequently applied intrawound to prevent post-surgical infection, but it may have a cytotoxic effect at certain concentrations [49]. Therefore, a fibroblast cell line was used to test cell viability after incubation with the vancomycin-loaded chitosan aerogel microparticles. Fibroblasts are the functional cells of the dermis and are responsible for the production of the extracellular matrix, mainly

composed of collagen and elastin [50]. During the proliferative stage of the wound healing process, fibroblasts migrate to the wound site and participate in the granulation process by deposition of collagen fibers that will constitute the scar tissue [51]. Overall, the aerogels presented good biocompatibility, with values higher than 80% (after 24 and 48 h) (Fig. 6.7).

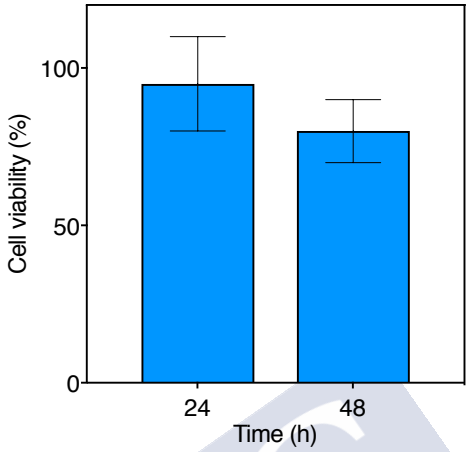


Figure 6.7. Cytocompatibility of the vancomycin-loaded aerogel microparticles with BALB/3T3 mouse fibroblasts.

## 6.4. Conclusions

The use of the jet cutting technology in combination with supercritical fluid-assisted drying technique represents an excellent strategy for the processing of aerogels from highly viscous precursor solutions. Chitosan aerogels were herein successfully produced in the form of spherical microparticles through this combined technology, and presented as suitable drug carriers for wound healing applications. Rotation speed and number of wires of the cutting disc along with nozzle diameter were the key parameters for the jet cutting process to obtain spherical and unimodal aerogel particles in the 700–900 µm range. The processing approach herein presented is compatible with the loading of drugs in the aerogel structure without the involvement of additional steps. The use of ethanol instead of aqueous baths for chitosan gelation turned an attractive strategy for vancomycin loading since the drug encapsulation efficiency in the resulting aerogel particles was significantly. The *in vitro* drug release from the chitosan aerogels provided local concentrations of vancomycin able to inhibit the microbial growth of *S. aureus* bacteria in less than 6 hours after treatment. High fluid sorption capacity, hemocompatibility, and cytocompatibility with fibroblasts of the chitosan aerogel formulation were suitable for the intended biomedical application. This aerogel-based formulation can meet the requirements to prevent infections for those cases of treatment of chronic wounds shortly after debridement. Vancomycin-loaded aerogel particles can be directly applied at the wound site or included as a component of a multi-layered dressing.

## 6.5. REFERENCES


1. García-González, C.A.; Camino-Rey, M.C.; Alnaief, M.; Zetzl, C.; Smirnova, I. Supercritical drying of aerogels using $CO_2$: Effect of extraction time on the end material textural properties. *J. Supercrit. Fluid.* **2012**, *66*, 297–306.
2. Zhao, S.; Malfait, W.J.; Guerrero-Alburquerque, N.; Koebel, M.M.; Nyström, G. Biopolymer aerogels and foams: Chemistry, properties, and applications. *Angew. Chem. Int. Ed.* **2018**, *57*, 7580–7608.
3. García-González, C.A.; Budtova, T.; Durães, L.; Erkey, C.; Del Gaudio, P.; Gurikov, P.; Koebel, M.; Liebner, F.; Neagu, M.; Smirnova, I. An opinion paper on aerogels for biomedical and environmental applications. *Molecules* **2019**, *24*, 1815–1829.
4. Kumar, A.; Rana, A.; Sharma, G.; Sharma, S.; Naushad, Mu.; Mola, G.T.; Dhiman, P.; Stadler, F.J. Aerogels and metal–organic frameworks for environmental remediation and energy production. *Environ. Chem. Lett.* **2018**, *16*, 797–820.
5. Maleki, H.; Durães, L.; García-González, C.A.; del Gaudio, P.; Portugal, A.; Mahmoudi, M. Synthesis and biomedical applications of aerogels: Possibilities and challenges. *Adv. Colloid Interface Sci.* **2016**, *236*, 1–27.
6. Stergar, J.; Maver, U. Review of aerogel-based materials in biomedical applications. *J. Sol-Gel Sci. Technol.* **2016**, *77*, 738–752.
7. *Biobased Aerogels: Polysaccharide and Protein-based Materials*; Thomas, S., Pothan, L.A., Mavelil-Sam, R., Eds.; Green Chemistry Series; Royal Society of Chemistry: Cambridge, UK, 2018.
8. García-González, C.A.; Jin, M.; Gerth, J.; Alvarez-Lorenzo, C.; Smirnova, I. Polysaccharide-based aerogel microspheres for oral drug delivery. *Carbohyd. Polym.* **2015**, *117*, 797–806.
9. Goimil, L.; Santos-Rosales, V.; Delgado, A.; Évora, C.; Reyes, R.; Lozano-Pérez, A.A.; Aznar-Cervantes, S.D.; Cenis, J.L.; Gómez-Amoza, J.L.; Concheiro, A.; et al. scCO2-foamed silk fibroin aerogel/poly(ε-caprolactone) scaffolds containing dexamethasone for bone regeneration. *J. CO2 Util.* **2019**, *31*, 51–64.
10. Raman, S.P.; Keil, C.; Dieringer, P.; Hübner, C.; Bueno, A.; Gurikov, P.; Nissen, J.; Holtkamp, M.; Karst, U.; Haase, H.; et al. Alginate aerogels carrying calcium, zinc and silver cations for wound care: Fabrication and metal detection. *J. Supercrit. Fluid.* **2019**, *153*, 104545–104556.
11. De Cicco, F.; Russo, P.; Reverchon, E.; García-González, C.A.; Aquino, R.P.; Del Gaudio, P. Prilling and supercritical drying: A successful duo to produce core-shell polysaccharide aerogel beads for wound healing. *Carbohyd. Polym.* **2016**, *147*, 482–489.
12. Sabri, F.; Cole, J.A.; Scarbrough, M.C.; Leventis, N. Investigation of polyurea-crosslinked silica aerogels as a neuronal scaffold: A pilot study. *PLoS ONE* **2012**, *7*, e33242–e33248.
13. Hegedűs, V.; Kerényi, F.; Boda, R.; Horváth, D.; Lázár, I.; Tóth-Győri, E.; Dezső, B.; Hegedus, C. β-Tricalcium phosphate silica aerogel as an alternative bioactive ceramic for the potential use in dentistry. *Adv. Appl. Ceram.* **2018**, *117*, 476–484.
14. Ulker, Z.; Erkey, C. An emerging platform for drug delivery: Aerogel based systems. *J. Control. Release* **2014**, *177*, 51–63.
15. Rodriguez Sala, M.; Lynch, K.J.; Chandrasekaran, S.; Skalli, O.; Worsley, M.; Sabri, F. PC-12 cells adhesion and differentiation on carbon aerogel scaffolds. *MRS Commun.* **2018**, *8*, 1426–1432.
16. Lynch, K.; Skalli, O.; Sabri, F. Growing neural PC-12 cell on crosslinked silica aerogels increases neurite extension in the presence of an electric field. *J. Funct. Biomater.* **2018**, *9*, 30–41.
17. García-González, C.A.; Alnaief, M.; Smirnova, I. Polysaccharide-based aerogels—Promising biodegradable carriers for drug delivery systems. *Carbohyd. Polym.* **2011**, *86*,

1425–1438.

18. Anitha, A.; Sowmya, S.; Kumar, P.T.S.; Deepthi, S.; Chennazhi, K.P.; Ehrlich, H.; Tsurkan, M.; Jayakumar, R. Chitin and chitosan in selected biomedical applications. *Progr. Polym. Sci.* **2014**, *39*, 1644–1667.
19. Smirnova, I.; Gurikov, P. Aerogels in Chemical Engineering: Strategies Toward Tailor-Made Aerogels. *Annu. Rev. Chem. Biomol. Eng.* **2017**, *8*, 1-28.
20. Santos-Rosales, V.; Ardao, I.; Alvarez-Lorenzo, C.; Ribeiro, N.; Oliveira, A.; García-González, C. Sterile and dual-porous aerogels scaffolds obtained through a multistep supercritical CO2-based approach. *Molecules* **2019**, *24*, 871–887.
21. Soorbaghi, F.P.; Isanejad, M.; Salatin, S.; Ghorbani, M.; Jafari, S.; Derakhshankhah, H. Bioaerogels: Synthesis approaches, cellular uptake, and the biomedical applications. *Biomed. Pharmacother.* **2019**, *111*, 964–975.
22. García-González, C.A.; López-Iglesias, C.; Concheiro, A.; Alvarez-Lorenzo, C. Chapter 16. Biomedical Applications of Polysaccharide and Protein Based Aerogels. In *Green Chemistry Series*; Thomas, S., Pothan, L.A., Mavelil-Sam, R., Eds.; Royal Society of Chemistry: Cambridge, UK, 2018; pp. 295–323.
23. Dai, T.; Tanaka, M.; Huang, Y.-Y.; Hamblin, M.R. Chitosan preparations for wounds and burns: Antimicrobial and wound-healing effects. *Expert Review of Anti-infective Therapy* **2011**, *9*, 857–879.
24. Ahmed, S.; Ikram, S. Chitosan based scaffolds and their applications in wound healing. *Achiev. Life Sci.* **2016**, *10*, 27–37.
25. Wei, S.; Ching, Y.C.; Chuah, C.H. Synthesis of chitosan aerogels as promising carriers for drug delivery: A review. *Carbohyd. Polym.* **2020**, *231*, 115744–115757.
26. Florence, A.T.; Crommelin, D.J.A. Chapter 5. Nanotechnologies for Drug Delivery and Targeting. Opportunities and Obstacles. In *Drug Delivery: Fundamentals and Applications*; Taylor & Francis Group: Abingdon-on-Thames, UK, 2017; pp. 103–135.
27. Kohane, D.S. Microparticles and nanoparticles for drug delivery. *Biotechnol. Bioeng.* **2007**, *96*, 203–209.
28. Crosera, M.; Bovenzi, M.; Maina, G.; Adami, G.; Zanette, C.; Florio, C.; Filon Larese, F. Nanoparticle dermal absorption and toxicity: A review of the literature. *Int. Arch. Occup. Environ. Health* **2009**, *82*, 1043–1055.
29. Thomas, N.W.; Jenkins, P.G.; Howard, K.A.; Smith, M.W.; Lavelle, E.C.; Holland, J.; Davis, S.S. Particle uptake and translocation across epithelial membranes. *J. Anat.* **1996**, *189*, 487–490.
30. Ganesan, K.; Budtova, T.; Ratke, L.; Gurikov, P.; Baudron, V.; Preibisch, I.; Niemeyer, P.; Smirnova, I.; Milow, B. Review on the production of polysaccharide aerogel particles. *Materials* **2018**, *11*, 2144–2180.
31. García-González, C.A.; Uy, J.J.; Alnaief, M.; Smirnova, I. Preparation of tailor-made starch-based aerogel microspheres by the emulsion-gelation method. *Carbohyd. Polym.* **2012**, *88*, 1378–1386.
32. Prüße, U.; Fox, B.; Kirchhoff, M.; Bruske, F.; Breford, J.; Vorlop, K.-D. New process (jet cutting method) for the production of spherical beads from highly viscous polymer solutions. *Chem. Eng. Technol.* **1998**, *21*, 29–33.
33. Prüße, U.; Dalluhn, J.; Breford, J.; Vorlop, K.-D. Production of spherical beads by JetCutting. *Chem. Eng. Technol.* **2000**, *23*, 1105–1110.
34. Prüße, U.; Ulrich, J.; Wittlich, P.; Breford, J.; Vorlop, K.-D. Practical aspects of encapsulation technologies. *Landbauforsch. Völkenrode* **2002**, *241*, 1–10.
35. Preibisch, I.; Niemeyer, P.; Yusufoglu, Y.; Gurikov, P.; Milow, B.; Smirnova, I. Polysaccharide-based aerogel bead production via jet cutting method. *Materials* **2018**, *11*, 1287–1302.
36. López-Iglesias, C.; Barros, J.; Ardao, I.; Monteiro, F.J.; Alvarez-Lorenzo, C.; Gómez-Amoza, J.L.; García-González, C.A. Vancomycin-loaded chitosan aerogel particles for

chronic wound applications. *Carbohyd. Polym.* **2019**, *204*, 223–231.
37. Quignard, F.; Valentin, R.; Di Renzo, F. Aerogel materials from marine polysaccharides. *New J. Chem.* **2008**, *32*, 1300–1310.
38. Tkalec, G.; Knez, Ž.; Novak, Z. Formation of polysaccharide aerogels in ethanol. *RSC Adv.* **2015**, *5*, 77362–77371.
39. Rinki, K.; Dutta, P.K.; Hunt, A.J.; Macquarrie, D.J.; Clark, J.H. Chitosan aerogels exhibiting high surface area for biomedical application: Preparation, characterization, and antibacterial study. *Int. J. Polym. Mater. Po.* **2011**, *60*, 988–999.
40. Saghazadeh, S.; Rinoldi, C.; Schot, M.; Kashaf, S.S.; Sharifi, F.; Jalilian, E.; Nuutila, K.; Giatsidis, G.; Mostafalu, P.; Derakhshandeh, H.; et al. Drug delivery systems and materials for wound healing applications. *Adv. Drug Deliv. Rev.* **2018**, *127*, 138–166.
41. Cutting, K.F. Wound exudate: Composition and functions. *Br. J. Community Nurs.* **2003**, *8*, S4–S9.
42. Rohindra, D.R.; Nand, A.V.; Khurma, J.R. Swelling properties of chitosan hydrogels. *S. Pac. J. Nat. App. Sci.* **2004**, *22*, 32–35.
43. *Vancomycin (CID=14969)*; PubChem Database; National Center for Biotechnology Information: Bethesda, MD, USA, 2006.
44. Serra, R.; Grande, R.; Butrico, L.; Rossi, A.; Settimio, U.F.; Caroleo, B.; Amato, B.; Gallelli, L.; de Franciscis, S. Chronic wound infections: The role of *Pseudomonas aeruginosa* and *Staphylococcus aureus*. *Expert Rev. Anti-infect. Ther.* **2015**, *13*, 605–613.
45. Guillaume, O.; Garric, X.; Lavigne, J.P.; Berghe, H.; Coudane, J. Multilayer, degradable coating as a carrier for the sustained release of antibiotics: Preparation and antimicrobial efficacy in vitro. *J. Control. Release* **2012**, *162*, 492–591.
46. Chang, S.-H.; Lin, H.-T.V.; Wu, G.-J.; Tsai, G.J. pH Effects on solubility, zeta potential, and correlation between antibacterial activity and molecular weight of chitosan. *Carbohyd. Polym.* **2015**, *134*, 74–81.
47. Hosseinnejad, M.; Jafari, S.M. Evaluation of different factors affecting antimicrobial properties of chitosan. *Int. J. Biol. Macromol.* **2016**, *85*, 467–475.
48. Reinke, J.M.; Sorg, H. Wound repair and regeneration. *Eur. Surg. Res.* **2012**, *49*, 35–43.
49. Liu, J.X.; Bravo, D.; Buza, J.; Kirsch, T.; Kennedy, O.; Rokito, A.; Zuckerman, J.D.; Virk, M.S. Topical vancomycin and its effect on survival and migration of osteoblasts, fibroblasts, and myoblasts: An in vitro study. *Journal of Orthopaedics* **2018**, *15*, 53–58.
50. Iqbal, A.; Jan, A.; Wajid, M.A.; Tariq, S. Management of chronic non-healing wounds by hirudotherapy. *World. J. Plast. Surg.* **2017**, *6*, 9–17.
51. Koehler, J.; Brandl, F.P.; Goepferich, A.M. Hydrogel wound dressings for bioactive treatment of acute and chronic wounds. *Eur. Polym. J.* **2018**, *100*, 1–11.

# SECTION III. ALGINATE AEROGELS FOR PULMONARY DELIVERY

USC
UNIVERSIDADE
DE SANTIAGO
DE COMPOSTELA

# 7. INKJET-PRINTED AEROGEL PARTICLES FOR PULMONARY DELIVERY

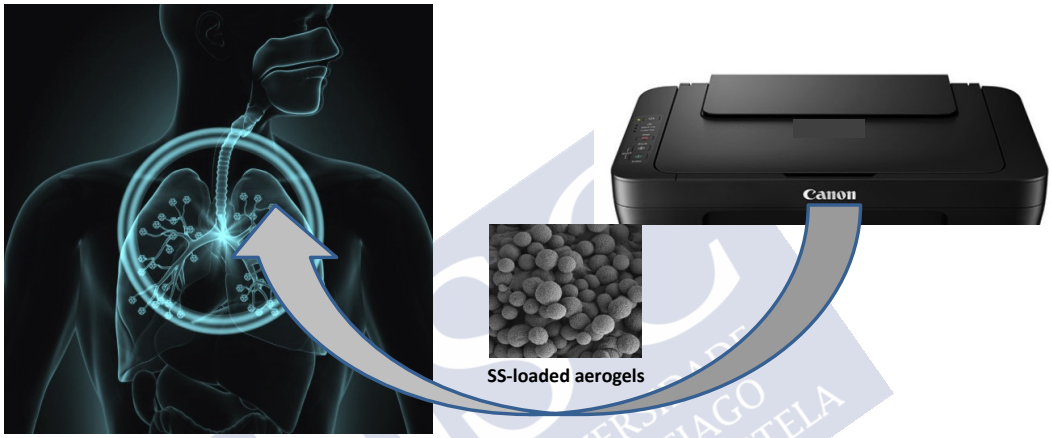




The work described in this chapter was published in López-Iglesias, C. *et al.* From the printer to the lungs: Inkjet-printed aerogel particles for pulmonary delivery. *Chemical Engineering Journal* **2018**, 357, 559–566.

Work carried out in collaboration with the Food and Drug Department of the University of Parma.

USC
UNIVERSIDADE
DE SANTIAGO
DE COMPOSTELA

# 7. INKJET-PRINTED AEROGEL PARTICLES FOR PULMONARY DELIVERY

## 7.1. Introduction

Inkjet printing has emerged as a relevant technique for several applications like electronic devices, photoelectrochemical cells or drug products [1–3]. *Drop on demand* is a particular approach of this technique for the pharmaceutical and biomedical sector to address the current challenges in cost-effective research, scalability, supply chain, flexible production and personalized medicine [3,4]. This technology is also commercially available for 3D-bioprinting with high cell viabilities (above 85%) [5,6]. Thermal inkjet printing in the *drop on demand* mode is a promising technology that allows the versatile and digitally-controlled secondary processing of pharmaceuticals as printed particles for drug delivery systems with repeatability, narrow particle size distribution and high spatial resolution. Using this method, droplet volumes of *ca.* 1–70 pL are ejected from small nozzles due to the expansion of a vapor bubble produced by electrical heating of the liquid itself [4,7]. The resulting ejected droplet has a diameter close to that of the nozzle itself (10–50 µm). Several inkjet-printed pharmaceutical formulations in the form of particles, hydrogels and films were reported for different administration routes (e.g., oral, respiratory or parenteral) [3,4,8–11].

For pulmonary delivery, novel formulations in the form of dry powder are sought for the treatment of respiratory disorders and the systemic delivery of bioactive compounds to maximize their therapeutic effect, resulting in lower doses and reduced public health costs [12]. For these purposes, dry powder formed by particles of aerodynamic diameters targeting 1–5 µm are being developed with optimum aerodynamic particle size distribution (APSD) for penetration to the deep lung. The production of large porous particles with geometric diameters greater than 5 µm preserving the target APSD is desired. The tendency for aggregation of these porous particles is much lower than that of their non-porous counterparts due to their lower densities and larger diameters [12].

Aerogel particles are highly porous, light-weight powders of particular interest as carriers for the pulmonary route [13–15]. Proteins and polysaccharide aerogels are biocompatible, biodegradable mesoporous carriers with high loading capacities for

bioactive compounds [16–19]. The use of these nanostructured materials in the form of microspheres would result in uniform particle dispersion and a subsequent more reliable therapeutic effect. Several approaches are reported for the engineering of the aerogel design in terms of morphology, mechanical strength and composition [13,14,20–22]. In spite of the recent advances in *aerogel engineering*, a current limitation of the aerogel processing for biomedical applications is the simultaneous control of the aerogel particle size and morphology and the release pattern of the loaded bioactive compounds. Current techniques for pulmonary delivery are constrained in terms of particle size (prilling [23], jet cutting [24]), control of particle size distribution (jet milling [25]), or the presence of surfactants (gel-emulsification [26,27]). Overall, no surfactant-free aerogel microspheres with a relevant particle size for pulmonary administration have been reported so far in the literature.

The combination of thermal inkjet printing and aerogel technology is an auspicious engineering solution to obtain nanostructured porous microspheres with narrow particle size distribution for oral inhalation. Excipient-free drug particles of 3–20 µm diameter with pore gradient in the micron-size range were previously obtained by thermal inkjet spray-freeze drying [28,29]. Silica aerogels of 0.1–1.0 µm diameter were prepared using thermal inkjet printing gel-emulsification [30]. To the best of our knowledge, preparation by thermal inkjet printing of aerogel particles with pores in the nano-size range and aerodynamic particle sizes suitable for its use as carriers for oral inhalation has not been reported before.

In this work, a protocol for the preparation of alginate aerogel microspheres by inkjet printing followed by supercritical drying is presented for the first time. Choice of alginate as aerogel source is of relevance since derivatives of this polysaccharide have proven to promote the mucus fluidity and clearance of sputum in Phase 2a clinical trials for the cystic fibrosis treatment [31,32]. Aerogel particles were loaded with salbutamol sulphate, a bronchodilator used for the treatment of asthma and chronic obstructive pulmonary disease. Particles were evaluated regarding their textural, morphological and aerodynamic properties, and the drug release was tested in a relevant medium for the respiratory route.

## 7.2. Materials and methods

### 7.2.1. Materials

Alginic acid sodium salt from brown algae, (guluronic acid/mannuronic acid ratio of 70/30, $M_w$ 403 kDa) was obtained from Sigma Aldrich (Irvine, UK). Salbutamol sulphate (SS, $M_w$ 337.4 g/mol, > 99% purity) and calcium chloride dihydrate ($CaCl_2 \cdot 2H_2O$) were provided by Fagron Ibérica (Terrassa, Spain) and Merck (Darmstadt, Germany), respectively. Carbon dioxide ($CO_2$, > 99.8% purity) was supplied by Praxair, Inc. (Madrid, Spain). Phosphate buffer solution (PBS) pH 7.4 was used in the release

tests and prepared using sodium hydroxide (NaOH, 99% purity) and potassium dihydrogen phosphate (> 99.5% purity) purchased from VWR International (Geldenaaksebaan, Belgium). Absolute-grade ethanol from Merck (Darmstadt, Germany), methanol (VWR International, Milan, Italy) and water purified using reverse osmosis (resistivity > 18 MΩ·cm, MilliQ, Millipore®, Spain) were also used.

### 7.2.2. Preparation of alginate aerogel beads by prilling

Aqueous alginate solutions of varied concentrations (0.25, 0.5, 0.75, 1.0, 1.25 and 1.5% (w/w)) were prepared by mechanical stirring (600 rpm) at room temperature for 15 min. After settling for *ca.* 4 h to remove the air bubbles within the solution, 10 mL of the alginate solutions were added dropwise to 100 mL of 0.5 M $CaCl_2$ aqueous solution and at a flow rate of 5 mL/min by using a syringe pump (AL-1000, World Precision Instruments, Sarasota, FL, USA) with a nozzle diameter of 2.0 mm. Alginate gel beads were immediately formed when in contact with the gelation bath. The gel beads were collected after 5 h of ageing and subjected to either a direct or sequential (ethanol:water volume ratio 0:100, 50:50, 75:25, 100:0 (x2)) solvent exchange to ethanol. The gel beads were placed into paper cartridges and put into the 100-mL extractor vessel of the high pressure equipment used (Waters-Thar Process, Pittsburg, PA, USA). Finally, a flow of 5 g/min of supercritical $CO_2$ (40 °C, 120 bar) passed through the pressurized vessel containing the gel particles and extracted the liquid EtOH contained in the gels whilst preserving their original polymer network [33]. After 3.5 h of drying, alginate aerogel particles were obtained.

### 7.2.3. Preparation of aerogel microspheres prepared by inkjet printing

Aqueous alginate solutions of varied concentrations (0.25, 0.30, 0.35, 0.40% (w/w)) were prepared as above. 10 mL of the alginate solutions were loaded in the cartridges (HP51626A) of a thermal inkjet printer (Hewlett Packard Deskjet 340, Palo Alto, CA, USA). The inkjet printer was previously modified by removing its external cover and mounting it into a support allowing the control of the height of the device (Fig. 7.1). The alginate-based ink was printed over a borosilicate dish (internal diameter: 6.2 cm) containing 25 or 100 mL of $CaCl_2$ 0.5 M solution as gelation bath. This bath was located 4 cm below the printhead and magnetically stirred at 300 rpm. The inkjet printing was carried out at the standard speed, in a 24.7 x 3.6 $cm^2$ rectangular region and using 30 or 120 printing cycles depending on the volume (25 or 100 mL) of the gelation bath. The gel beads were collected in a Falcon tube, left 5 h for ageing, and then subjected to either a direct (twice) or sequential (ethanol:water volume ratio 0:100, 50:50, 75:25, 100:0 (x2)) solvent exchange to ethanol. Finally, alginate alcogel microspheres were filled in paper cartridges and dried under a continuous flow of supercritical $CO_2$ (40 °C, 120 bar, 5 g $CO_2$/min, 3.5 h) to obtain the corresponding aerogels (*cf.* Section 7.2.2).

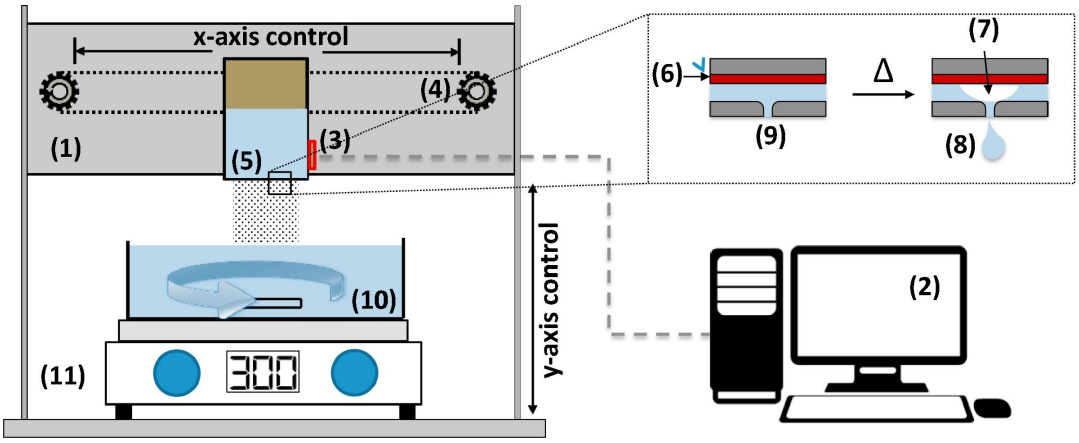


Figure 7.1. Setup used for the preparation of the alginate gel microspheres. The inkjet printer (1) is connected to a computer (2) that allows the control of the printing operation by the heating element (3) of the cartridge and controls the x-axis movement of the printer belt (4). The printer is located in a metallic support with moving parts allowing its y-axis control (i.e. the printhead-to-gelation bath distance). The alginate solution is located in the printhead (5) containing several printing chambers. An electrical signal is applied to a micro-thermal heater (6) located at each printing chamber, and the sudden increase in the temperature generates a vapor bubble (7) that ejects the alginate solution as a picodroplet (8) through the nozzle (9). The droplets are jetted to a gelation bath (10) constantly agitated with a magnetic stirrer (11).

### 7.2.4. Preparation of salbutamol-loaded aerogel microspheres prepared by inkjet printing

For the preparation of salbutamol-loaded aerogels, the same printing procedure as the one reported in Section 7.2.3 was employed but the drug was added at a concentration of 0.35% (w/w) to 25 mL of the gelation bath of $CaCl_2$ solution. A direct solvent exchange of the gel microspheres to ethanol (twice) was used in this case before undergoing the supercritical drying.

### 7.2.5. Structural and physicochemical characterization of the gels and aerogels

Images from the external morphology of the printed aerogels were obtained by scanning electron microscopy (SEM, EVO LS15, Zeiss, Oberkochen, Germany). Samples were iridium-sputtered (10 nm thickness) prior to imaging to minimize charging and to improve the contrast of the images. Focused Ion Beam technique (Dual Beam Helios Nanolab 600, FEI, Hillsboro, OR, USA) coupled with SEM microscopy (FIB-SEM) was used to obtain the images of the internal morphology of the printed aerogels from cross sections of the microspheres. A milling with $Ga^+$ ions (26 pA, 30 kV) was performed for the automated FIB-SEM slice-and-view method used.

Textural properties of the aerogels were characterized using low-temperature $N_2$ adsorption-desorption analysis (ASAP 2000; Micromeritics Inc.; Norcross, GA, USA). Before the measurements, the aerogel powder was dried under vacuum (< 1 mPa) at

room temperature for 24 h. Specific surface area ($a_{BET}$) was calculated applying the BET (Brunauer-Emmett-Teller) method. The BJH (Barrett-Joyner-Halenda) method was used to estimate the specific pore volume ($V_{p,BJH}$) and the mean pore diameter ($d_{p,BJH}$).

Overall porosity ($\varepsilon$) was calculated using equation 7.1, where $\rho_{bulk}$ is the bulk density estimated from the volume occupied by a certain weight of tapped aerogel particles (*ca.* 1.26-fold the tapped density [34]), and $\rho_{skel}$ is the skeletal density of the alginate particles measured from five replicates by helium pycnometry (Quantachrome; Boynton Beach, FL, USA) at 25 °C and 1.03 bar. Tapped density was calculated with the gradual flask method from three replicates of the volume occupied by a certain weight of tapped aerogel particles.

$$\varepsilon = \left(1 - \frac{\rho_{bulk}}{\rho_{skel}}\right) \cdot 100 \quad (7.1)$$

The mass median aerodynamic diameter of the pristine aerogel particles ($d_{aero}$) was obtained from the simplification of Stokes' law for particles with diameters higher than 1 µm (Eq. 7.2) [35], where $d$ is the volume (geometric) diameter of the particles and $\chi$ is the dynamic shape factor (equal to 1.0 for microspheres). $d$ was obtained by visual imaging in SEM from the mean diameter of the particle size distribution of the aerogels expressed in a mass (or volume) basis.

$$d_{aero} = d \cdot \sqrt{\rho_{tapped}/\chi} \quad (7.2)$$

The particle size distribution of the gel precursors was obtained by visual imaging in an inverted optical microscope (IX51, Olympus, Tokyo, Japan). The zeta potential of these gels was measured by laser diffraction (Zetasizer Nano ZSP, Worcestershire, UK) in deionized water medium.

Attenuated total reflectance/Fourier-Transform Infrared Spectroscopy (ATR/FT-IR) was performed with a Gladi-ATR accessory using a diamond crystal (Pike, Madison, WI, USA). Raw salbutamol sulphate, raw sodium alginate, alginate aerogel microspheres and salbutamol sulphate-loaded alginate aerogel microspheres in the powdered from were characterized in the mid-IR spectrum range (400–4000 $cm^{-1}$) using 32 scans at a resolution of 2 $cm^{-1}$.

### 7.2.6. Salbutamol sulphate loading yield and release studies

Salbutamol content in the alcogels was indirectly measured by quantifying the SS content in the gelation medium after the ageing period and determined by difference with respect to the SS amount initially added. The absorbance of the aqueous solution was measured at 276 nm in a UV/Vis spectrophotometer (8453 equipment, Agilent, Santa Clara, CA, USA). Calibration curve of SS in water was obtained from triplicate dilution series, ranging from 0.02 to 0.17 mg/mL ($R^2$ = 0.9997).

Franz diffusion cells with a 6 mL-acceptor chamber were used to determine the release of SS from the alginate aerogel microspheres. Aerogel powder (3 mg) was

evenly distributed on top of a cellulose membrane (0.45 µm pore size, Filter-Lab, Filtros Anoia, Barcelona, Spain) in the donor compartment. The diffusion area was 0.79 $cm^2$ (1 cm diameter). The receptor chamber was filled with PBS medium (pH 7.4 and 5.2) at 37°C and constantly stirred at 100 rpm. Aliquots of 3 mL were sampled at certain time periods for 11 h and the volume was replaced with fresh medium. SS concentrations in the aliquots were measured through UV/Vis spectrophotometry (8453 model, Agilent, USA) at 276 nm. Salbutamol content in the aerogels was measured by quantifying the SS content after 96 hours in the release medium. Calibration curve of SS in PBS was obtained from triplicate dilution series, ranging from 0.02 to 0.17 mg/mL ($R^2 > 0.9999$).

### 7.2.7. Simulated lung deposition tests

*In vitro* aerodynamic assessment of the SS-loaded aerogel particles was performed using a next generation impactor (NGI, Copley, Nottingham, UK) and a medium resistance single-dose dry powder inhaler (Plastiape Spa, Sirone, Italy) as device. The capsules size 3 (Coni-Snap, Capsugel, Colmar, France) were manually filled with 8.0 ± 0.2 mg of powder and the vacuum pump was activated at a flow of 60 L/min for 4.0 s to produce a pressure drop of 4 kPa, following the European Pharmacopeia guidelines. Prior to use, the seven collection stages of the impactor were coated with 1% (w/v) solution of glycerin in methanol and then allowed to dry to prevent rebounding and to stabilize the particles. The terminal stage was a micro-orifice collector (MOC) covered with a glass fiber filter (Type A/E, Pall Corporation, New York, NY, USA). SS was recovered from each stage of the impactor with appropriate volumes of a methanol:water 50:50 (v/v) solution, transferred into vials and drug concentrations measured by HPLC analysis. Stage 2 had a cut-off diameter of 4.46 µm. The aerodynamic performance of the formulation was evaluated from the emitted dose (ED; weight percentage of drug or powder exiting the device and entering the impactor), mass median aerodynamic diameter ($d_{aero}$; the particle diameter at 50% of the cumulative weight undersize), and fine particle fraction (FPF; mass of drug particles that have an aerodynamic diameter less than 5 µm related to the ED).

For the measurements of the SS content at each impactor stage, an HPLC equipment with an UV-detector (Agilent Technologies, Santa Clara, CA, USA) was used. The mobile phase consisted of PBS pH 7 and methanol (40:60 (v/v)) mixture at a rate of 0.6 mL/min, whereas the stationary phase was a Supelcosil™ LC-SCX column (250mmÅ × 4.6 mm, 5 µm) kept at 30 °C. 100 µL of sample were injected and the retention time was 13.3 min.

## 7.3. Results and discussion

### 7.3.1. Gelation mechanism and processing window for alginate gel printing

Alginate is a polysaccharide excipient used in pharmaceutical formulations. Ionic gelation with divalent or trivalent cations, namely with $Ca^{2+}$ cations, is the most common method of manufacture for alginate gels. These cations would form ionic bonds with the guluronic acid residues of the alginate polymeric chains in the so-called *egg-box* mechanism resulting in a gel of varying properties depending on the alginate source and cation-to-alginate content [36,37]. Alginate gelation kinetics can be tuned by means of a prompt or modified release of the cations in the gelation bath. The diffusion method and internal setting method provide a sudden and modified (usually pH-controlled) release of $Ca^{2+}$ cations, respectively. In this work, alginate picodroplets were jetted towards a $CaCl_2$ 0.5 M gelation bath to form the corresponding alginate gel microspheres using the internal setting gelation of alginate which is the only suitable method to preserve the spherical shape of the picodroplets in the gel form.

The processing window of alginate concentrations able to gelify in a bath of $CaCl_2$ 0.5 M aqueous solution was firstly determined by a standard prilling method. The choice of $CaCl_2$ as $Ca^{2+}$ source is of particular interest since it is used as an excipient in dry powder formulations for pulmonary delivery (e.g., present in TOBI® Podhaler commercial product [12]). The minimum alginate concentration leading to stable round gels was determined by prilling droplets of alginate solutions of decreasing concentrations starting at 1.5% (w/w) and with steps of 0.25% (w/w) from a syringe into the gelation bath. Following this method, the minimum alginate concentration was established at 0.25% (w/w). The prilling method and modifications thereof (e.g., vibrating nozzle, jet cutting or spinning disks) can be useful in the preparation of monodisperse gel particles in the diameter range of hundreds of microns and above but fails to reach particle diameters below this threshold [38].

Thermal inkjet printing of alginate solutions is herein tested as a technique to obtain gel particles below 100 µm. However, the translation of the alginate gelation results from the prilling method into the thermal inkjet printing showed that the maximum feasible alginate concentration was limited by the jettability of the solution and directly linked to the viscosity of the propelled solution through the printhead. Higher concentrations of alginate in the aqueous solutions resulted in increased viscosities with the subsequent increase in the Reynolds number and Ohnesorge number of the jetted fluid [39]. Above a certain alginate concentration it will not be possible to print fluid. The maximum possible alginate concentration was set at 0.35% (w/w), since 0.40% (w/w) clogged the nozzles on multiple occasions. Overall, the feasible region for the printing of alginate gels was set at an alginate concentration of 0.25–0.35% (w/w). After supercritical drying, the 0.35% (w/w) provided the best

results in terms of roundness and particle size homogeneity (Fig. 7.2), and was used for further optimization.

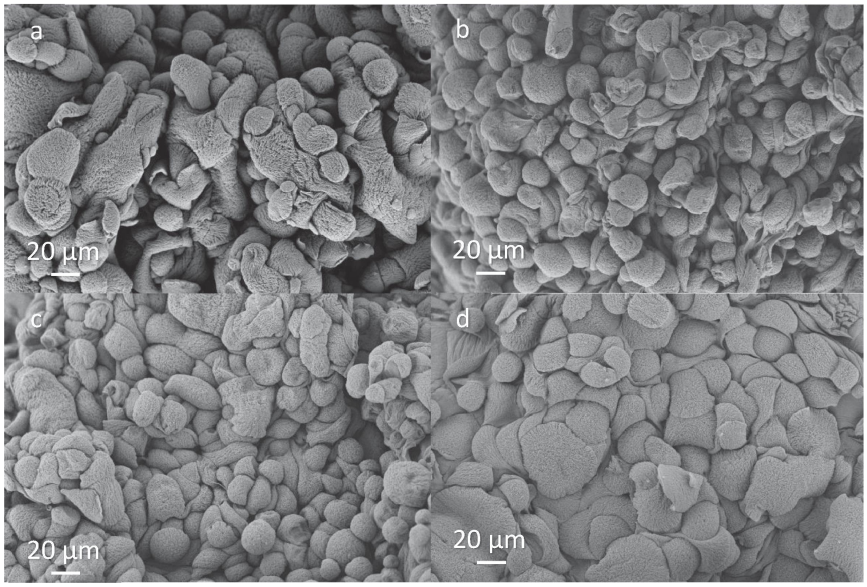


Figure 7.2. SEM images of alginate aerogel microparticles obtained from preliminary inkjet printing trials from alginate aqueous solutions of different concentrations: (a) 0.25, (b) 0.30, (c) 0.35, and (d) 0.40% (w/w). A single gelation bath of 100 mL of $CaCl_2$ 0.5 M and a direct solvent exchange to ethanol was used in all cases. Printhead clogging events occurred when using the 0.40% (w/w) alginate solution.

### 7.3.2. Optimization of the alginate gel printing and solvent exchange process

The optimization of the printing method pursued the homogeneity of the particle sizes and an improvement in the sphericity of the particles. Moreover, the modifications of the process to be attempted should be compatible with the intended application of the aerogel carriers, mainly in terms of the mean particle size for the target administration route (inhalation) and of the drug loading yield (as high as possible).

The sphericity and homogeneity of the alginate microspheres obtained by inkjet printing was dramatically improved by using the same total gelation bath volumes (100 mL, Fig. 7.2c) but splitted into four aliquots of 25 mL each (Fig. 7.3a). The replacement with fresh gelation baths was carried out after 30 printing cycles elapsed since the last bath replacement. The air-water contact surface of the gelation baths (i.e. the vessel internal diameter) and the distance between the printhead and the bath remained constant with respect to the previous attempts. The gel particles stayed at the top fluid layer of the gelation bath for a considerable period of time before settling. Thus, the probability of the jetted droplet of the alginate solution contacting an already formed gel particle on the water surface was lower in the case of the use of multiple gelation baths. As a result, the obtained particles were more spherical and showed less

dimpled particles and less aggregation (Fig. 7.3a) with respect to the use of a single gelation bath (Fig. 7.2c). Gel particles showed a normal distribution with a mean value of 23.6 ± 4.0 µm (in mass basis). Gels had a negative zeta potential (-4.4 ± 0.4 mV) due to the negatively charged molecular chains of alginate that are partially compensated by the $Ca^{2+}$ cations used for the gelation of the alginate [40].

The water contained in the alginate gel pores has low affinity for the extraction medium (i.e. supercritical $CO_2$) used for the supercritical drying. Therefore, water should be replaced by a compatible solvent before undergoing the drying step to prepare the aerogels. In this work, ethanol was used as solvent replacement since it (a) does not dissolve the gel structure, (b) is completely soluble with water, (c) is a poor solvent medium for the intended drug (salbutamol sulphate) to be loaded in the aerogel, and (d) is accepted as solvent for the manufacturing of pharmaceuticals. For alginate aerogel preparation [13,26] as well as for other polysaccharides like chitosan [18] or κ-carrageenan [27], the sequential exchange of the gel solvent with aqueous solutions of increasing ethanol concentrations (*cf.* Section 7.2.3) prior to the supercritical drying may preserve better the structure of the wet gel in the resulting dry form (i.e. aerogel). However, the change of gel printing method to a five-step sequential solvent exchange resulted in a loss of particle sphericity and the appearance of dimples on the surface of the gel particles (Fig. 7.3b), likely due to the softening of the gels during the intermediate solvent exchange steps. Moreover, this solvent exchange procedure would likely reduce the loading yield of the drug, due to the partial solubility of salbutamol sulphate in water-ethanol mixtures.

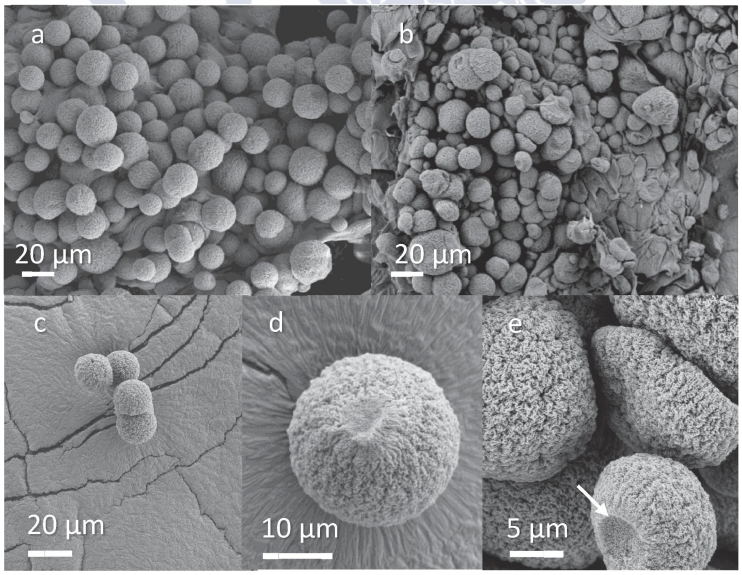


Figure 7.3. SEM images of alginate aerogel microparticles obtained by inkjet printing of 10 mL of 0.35% (w/w) alginate aqueous solutions into multiple gelation baths of 25 mL of $CaCl_2$ 0.5 M with (a) direct or (b) sequential solvent exchange to ethanol. (c,d) Loosely aggregated and spherical particles were obtained using the direct solvent exchange, (e) whereas the sequential solvent exchange resulted in the presence of dimples in the particle surface (white arrow).

Aerogel microspheres obtained through the optimized protocol (Fig. 7.3a) were in the form of free-flowing powder with a bulk density of 0.013 g/cm$^3$. The aerogel microspheres had a normal particle size distribution with a diameter of 23.8 ± 4.5 µm, obtained by direct imaging and expressed as mean value ± standard deviation. The overall porosity of the particles was of 97.7% resulting in aerodynamic diameters of 2.4 µm, i.e. falling in the target size for effective deposition.

The aerogel particles presented a rough surface arising from the presence of surface pores in the nanometric range of mesopores and macropores according to the IUPAC classification (Fig. 7.4a,b). The voids between the intermingled fibrils of highly cross-linked alginate chains were mesoporous, whereas the voids between fibril bundles were macroporous. This mesoporous-to-macroporous contribution ratio was previously reported to be largely influenced by the alginate concentration in the precursor solution [41]. The porous distribution was homogeneous throughout the aerogel particles, since the inner structure of the particles observed by FIB-SEM (Fig. 7.4c,d) had a similar texture as the external one, but with slightly larger macropores (Fig. 7.4a,b).

The excellent textural properties of the optimized alginate aerogel particles were confirmed by nitrogen adsorption-desorption analysis (Table 7.1). Alginate aerogels had high BET-specific surface area (180 m$^2$/g) and BJH-specific pore volume (0.67 cm$^3$/g), whereas the mean pore diameter fell in the mesoporous range (17.8 nm). The values of these microspheres were lower than those obtained using the same printing technology by sequential solvent exchange and this fact was related to volume changes in the gels upon processing [13]. The same influence of the solvent exchange procedure on the textural properties was observed for the alginate aerogel beads (1.7 mm diameter) obtained by prilling techniques. The inkjet-printed particles showed lower BET-specific surface areas than their prilled granular counterparts, likely due to the higher external surface-to-volume ratio of the former ones. Overall, the textural properties of the printed aerogel microspheres seem promising to have enough loading capacity to host bioactive molecules for challenging their use as carriers for the pulmonary route.

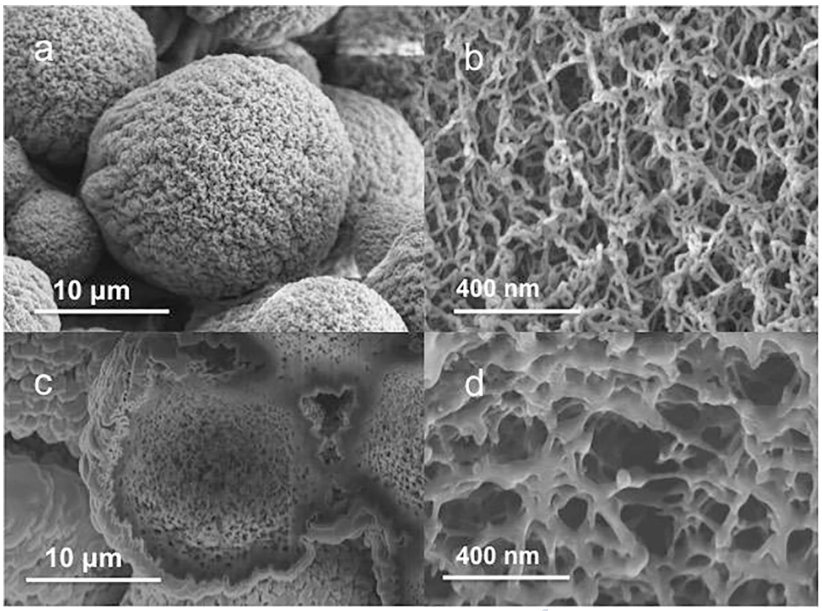


Figure 7.4. Morphological and textural characterization of the alginate aerogel microspheres obtained through the optimized conditions for the printing protocol: External (a) morphology and (b) nanostructure obtained by SEM microscopy; and internal (c) cross section and (d) nanostructure obtained by FIB-SEM microscopy.

Table 7.1. Specific surface area ($a_{BET}$), pore volume ($V_{p,BJH}$) and mean pore diameter ($d_{p,BJH}$) of alginate aerogel microspheres obtained by inkjet printing and followed by a direct or sequential (5 steps) solvent exchange to ethanol. The textural properties of alginate beads obtained by prilling of the same alginate stock solution and followed by the same solvent exchange protocols are also presented for the sake of comparison. Values are expressed as mean values ± standard deviation ($n$=3).

| Gelation method | Solvent exchange | $a_{BET}$ ($m^2/g$) | $V_{p,BJH}$ ($cm^3/g$) | $d_{p,BJH}$ (nm) |
|---|---|---|---|---|
| Inkjet | Direct | 180 ± 9 | 0.67 ± 0.03 | 17.8 ± 0.9 |
| Inkjet | Sequential | 397 ± 20 | 1.48 ± 0.07 | 14.4 ± 0.7 |
| Prilling | Direct | 291 ± 15 | 0.65 ± 0.03 | 9.0 ± 0.5 |
| Prilling | Sequential | 430 ± 22 | 1.10 ± 0.06 | 10.6 ± 0.5 |

### 7.3.3. Salbutamol sulphate-loaded aerogels release study

SS-loaded aerogel microspheres were prepared by dissolving the bioactive agent in the gelation bath before the inkjet printing. This approach was taken to ensure a suitable loading of salbutamol in the gel since the SS is highly soluble in water (i.e. the gel solvent) and has a low solubility in absolute ethanol (i.e. the exchange gel solvent) [42]. After gelation, the content of SS in the printed gel particles was indirectly quantified as 7.8% (w/w dried gel particle). After the subsequent solvent exchange and supercritical drying, a free-flowing powder was obtained with similar morphological and textural properties as the unloaded alginate aerogel microspheres (Fig. 7.5). The presence of SS in the alginate aerogel was confirmed by ATR/FT-IR analysis by the

presence of a band at 1509 $cm^{-1}$, which is characteristic of the aromatic ring stretching mode of the drug molecule (Fig. 7.6). The SS loading in the processed alginate aerogels was 3.0% (w/w), a value compatible with the therapeutic salbutamol doses in commercially available dry powder inhalers (50–100 μg per dose).

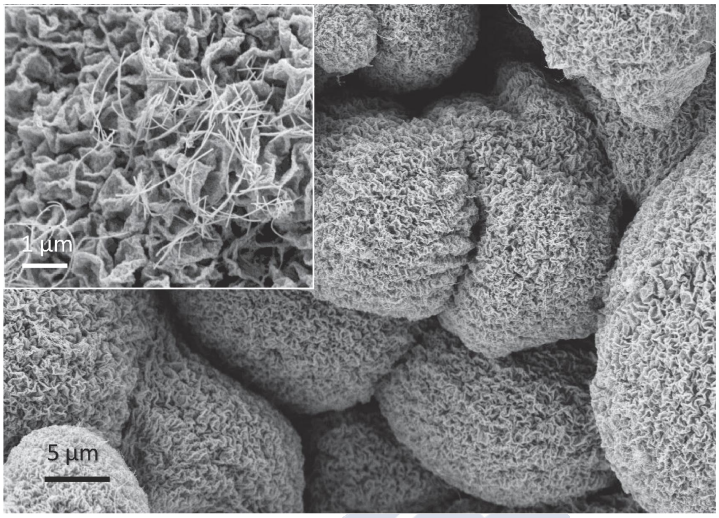


Figure 7.5. SEM image of the porous surface of printed alginate aerogel particles loaded with 3% (w/w) of salbutamol sulphate. Inset: higher magnification of the surface showing a fraction of the drug in the form of needle-like crystals.

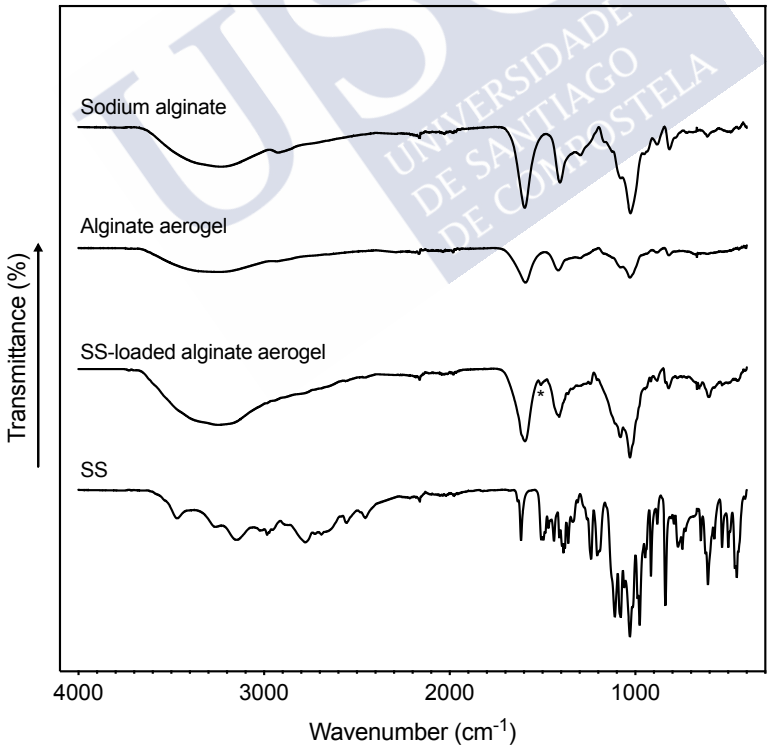


Figure 7.6. ATR/FT-IR spectra of raw salbutamol sulphate (SS), raw sodium alginate, alginate aerogel microspheres and SS-loaded aerogel microspheres. A characteristic band of SS in the aerogel was denoted with an asterisk.

The release of salbutamol sulphate from the aerogel matrix was measured in diffusion Franz cells to mimic the air-liquid interface present in the lung and using a

buffer solution (PBS) at pH 7.4 as simulated lung dissolution medium [43,44]. A modified release profile was obtained for the drug contained in the aerogel microspheres (Fig. 7.7). Two steps can be distinguished in the release pattern: a sudden release during the first 15–30 min followed by a slow and sustained release of the remaining SS payload during a timeframe of 10 hours. The initial burst represents 10% of the total salbutamol contained in the aerogels. The drug fraction released during this step was attributed to the dissolution of weakly bound salbutamol, since the release rate was similar to the dissolution profile of the pure drug. A close observation to the external surface of the aerogels by SEM microscopy unveiled the presence of smooth needle-like salbutamol crystals (inset in Fig. 7.5), which was related to the drug fraction of the initial burst release. The formation of these crystals was attributed to the anti-solvent effect of ethanol during the solvent exchange step, since similar crystal morphologies were obtained by anti-solvent crystallization of SS aqueous solutions with ethanol [45].

The lungs contribute to the physiologic pH regulation through control of the partial pressure of $CO_2$. However, carbon dioxide production may exceed elimination in some acute episodes of asthma due to alveolar hypoventilation leading to respiratory acidosis (pH < 7.4) [46]. Release of the salbutamol sulphate from the alginate matrix was tested at pH 5.2 and 7.4 with similar behavior due to the low variation of the ionic form fractions of the salbutamol sulphate ($pK_a$ 9.3 and 10.3 [47]) and of the alginate ($pK_a$ 1.5–3.5 [48]) in this pH range and the slow degradation of the matrix under these pH conditions [49].

Salbutamol sulphate used in dry powder inhalers as commercial products has a fast onset of action, featured by an action within 3–5 min after administration, with a peak after 15–20 min and duration of action of 4–6 hours. However, sustained release of $ß_2$-adrenergic agonists, particularly salbutamol, is also of therapeutic interest and is a current topic of research [50–52]. The salbutamol release profile obtained from the aerogels seems promising for the sustained release of this bronchodilator agent. The release profile can be of special interest to reduce the dosage administration frequency and side effects as well as to improve the patient compliance for the treatment of chronic obstructive pulmonary disease, or to fit the patient rhythm in nighttime asthma treatments.

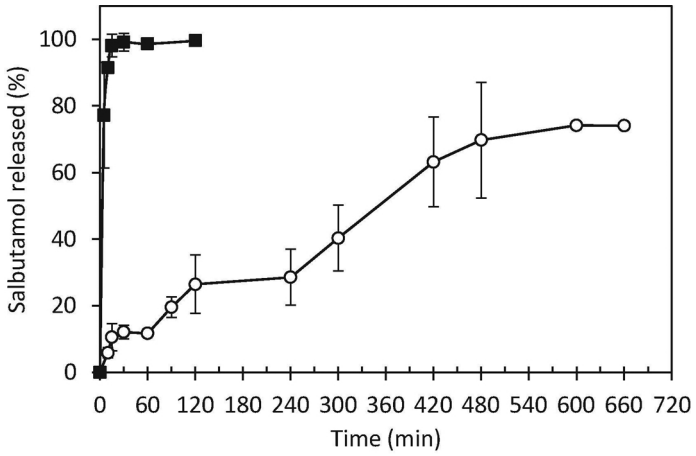


Fig. 7.7. *In vitro* release profile of SS from alginate aerogel micropheres (white circles) in PBS pH 7.4 solution (37°C, 100 rpm). The dissolution profile of SS (black squares) under the same operating conditions is plotted for the sake of comparison.

### 7.3.4. *In vitro* aerodynamic drug deposition of SS-loaded aerogels

The aerosol performance of the SS-loaded aerogels was evaluated from in vitro tests of the powder exiting the DPI device and entering and NGI impactor with 7 stages and a collector (Table 7.2 and Fig. 7.8). Due to the high porosity of the aerogels, the aerodynamic diameter obtained for the particles was *ca.* 6-fold lower than the aerogel particle size and in the respirable range (Table 7.2). The emitted dose as powder was close to 100% indicating the good flowability of the aerogel particles with reduced particle cohesion forces. The FPF values of the aerogels were close to 50%, which means a better performance than other inkjet-printed (5–23%) particles and some SS-commercial formulations (Cyclocaps®) [28,29].

The SS deposition profile from the aerogel particles showed that the drug was mainly present in the first stage of the impactor (36.7%) and the deposited drug contents gradually decreased from stage 1–7 (Fig. 7.8). The low drug contents in the last stages of the NGI impactor indicate that the local drug delivery will mainly take place at the bronchi and bronchioles.

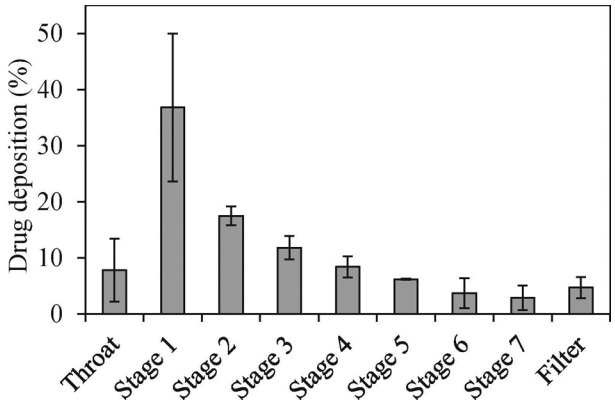


Figure 7.8. Drug deposition profile of salbutamol sulfate loaded in alginate aerogel particles with an NGI impactor ($n$ = 3, mean ± standard deviation).

Table 7.2. Aerodynamic properties of SS-loaded aerogel particles obtained by thermal inkjet printing followed by supercritical drying ($n$ = 3)

| | SS-loaded aerogel |
|---|---|
| ED as powder (%) | 97.5 ± 1.2 |
| ED as drug (%) | 80.3 ± 3.4 |
| $d_{aero}$ (μm) | 4.0 ± 1.5 |
| FPF (%) | 49.7 ± 3.0 |

## 7.4. Conclusions

Particles manufactured by thermal inkjet printing and aerogel technology are endowed with unique nanostructure. Thermal inkjet printing prompted the engineering of reproducible and highly porous alginate-based microspheres. Process development unveiled a feasible printability region restricted by the polysaccharide concentration in the printable aqueous fluid. After supercritical drying of the alginate gels, aerogel microspheres in the form of free-flowing powder were obtained. The optimized formulation of the biopolymer aerogel particles had excellent and homogenous textural properties falling in the nanoporous range. Moreover, the inkjet printing technique allowed for the reproducible gelation of spherical particles with narrow particle size distribution (23.8 ± 4.5 μm). The processing technique was compatible with the incorporation of a bioactive compound (salbutamol sulphate) in the aerogel carrier for ulterior sustained release. The aerodynamic diameter of the drug-loaded printed aerogel particles was in the appropriate size range for lung deposition and local drug delivery. The material obtained by this innovative processing technique can be relevant for the treatment of several pulmonary diseases like asthma, chronic obstructive pulmonary disease, or cystic fibrosis. This unique technology for printed aerogels can be extended to personalized medicine applications demanding nanostructured miniaturized and high-resolution product designs.

## 7.5. References

1. Wang, G.; Wang, Z.; Liu, Z.; Xue, J.; Xin, G.; Yu, Q.; Lian, J.; Chen, M.Y. Annealed graphene sheets decorated with silver nanoparticles for inkjet printing. *Chem. Eng. J.* **2015**, *260*, 582–589.
2. Shin, W.J.; Lee, H.; Sohn, Y.; Shin, W.G. Novel inkjet droplet method generating monodisperse hollow metal oxide micro-spheres. *Chem. Eng. J.* **2016**, *292*, 139–146.
3. Scoutaris, N.; Ross, S.; Douroumis, D. Current trends on medical and pharmaceutical applications of inkjet printing technology. *Pharm. Res.* **2016**, *33*, 1799–1816.
4. Daly, R.; Harrington, T.S.; Martin, G.D.; Hutchings, I.M. Inkjet printing for pharmaceutics – A review of research and manufacturing. *Int. J. Pharm.* **2015**, *494*, 554–567.
5. Garreta, E.; Oria, R.; Tarantino, C.; Pla-Roca, M.; Prado, P.; Fernández-Avilés, F.; Campistol, J.M.; Samitier, J.; Montserrat, N. Tissue engineering by decellularization and 3D bioprinting. *Mat. Today* **2017**, *20*, 166–178.

6. Murphy, S.V.; Atala, A. 3D bioprinting of tissues and organs. *Nat. Biotechnol.* **2014**, *32*, 773–785.
7. de Gans, B.-J.; Duineveld, P.C.; Schubert, U.S. Inkjet printing of polymers: State of the art and future developments. *Adv. Mater.* **2004**, *16*, 203–213.
8. Buanz, A.B.M.; Belaunde, C.C.; Soutari, N.; Tuleu, C.; Gul, M.O.; Gaisford, S. Ink-jet printing versus solvent casting to prepare oral films: Effect on mechanical properties and physical stability. *Int. J. Pharm.* **2015**, *494*, 611–618.
9. Buanz, A.B.M.; Saunders, M.H.; Basit, A.W.; Gaisford, S. Preparation of personalized-dose salbutamol sulphate oral films with thermal ink-jet printing. *Pharm. Res.* **2011**, *28*, 2386–2392.
10. Chung, J.H.Y.; Naficy, S.; Wallace, G.G.; Naficy, S.; O'Leary, S. Inkjet-printed alginate microspheres as additional drug carriers for injectable hydrogels. *Adv. Polym. Technol.* **2016**, *35*, 439–446.
11. Meléndez, P.A.; Kane, K.M.; Ashvar, C.S.; Albrecht, M.; Smith, P.A. Thermal inkjet application in the preparation of oral dosage forms: Dispensing of prednisolone solutions and polymorphic characterization by solid-state spectroscopic techniques. *J. Pharm. Sci.* **2008**, *97*, 2619–2636.
12. Healy, A.M.; Amaro, M.I.; Paluch, K.J.; Tajber, L. Dry powders for oral inhalation free of lactose carrier particles. *Adv. Drug Deliv. Rev.* **2014**, *75*, 32–52.
13. García-González, C.A.; Alnaief, M.; Smirnova, I. Polysaccharide-based aerogels—Promising biodegradable carriers for drug delivery systems. *Carbohyd. Polym.* **2011**, *86*, 1425–1438.
14. Maleki, H.; Durães, L.; García-González, C.A.; del Gaudio, P.; Portugal, A.; Mahmoudi, M. Synthesis and biomedical applications of aerogels: Possibilities and challenges. *Adv. Colloid Interface Sci.* **2016**, *236*, 1–27.
15. Ulker, Z.; Erkey, C. An emerging platform for drug delivery: Aerogel based systems. *J. Control. Release* **2014**, *177*, 51–63.
16. Betz, M.; García-González, C.A.; Subrahmanyam, R.P.; Smirnova, I.; Kulozik, U. Preparation of novel whey protein-based aerogels as drug carriers for life science applications. *J. Supercrit. Fluid.* **2012**, *72*, 111–119.
17. García-González, C.A.; Carenza, E.; Zeng, M.; Smirnova, I.; Roig, A. Design of biocompatible magnetic pectin aerogel monoliths and microspheres. *RSC Adv.* **2012**, *2*, 9816–9823.
18. Kayser, H.; Müller, C.R.; García-González, C.A.; Smirnova, I.; Leitner, W.; Domínguez de María, P. Dried chitosan-gels as organocatalysts for the production of biomass-derived platform chemicals. *Applied Catalysis A: General* **2012**, *445–446*, 180–186.
19. Zhao, S.; Malfait, W.J.; Guerrero-Alburquerque, N.; Koebel, M.M.; Nyström, G. Biopolymer aerogels and foams: Chemistry, properties, and applications. *Angew. Chem. Int. Ed.* **2018**, *57*, 7580–7608.
20. Smirnova, I.; Gurikov, P. Aerogels in chemical engineering: Strategies toward tailor-made aerogels. *Annu. Rev. Chem. Biomol. Eng.* **2017**, *8*, 307–334.
21. Tripathi, A.; Parsons, G.N.; Khan, S.A.; Rojas, O.J. Synthesis of organic aerogels with tailorable morphology and strength by controlled solvent swelling following Hansen solubility. *Sci. Rep.* **2018**, *8*, 1–12.
22. Jung, S.M.; Jung, H.Y.; Dresselhaus, M.S.; Jung, Y.J.; Kong, J. A facile route for 3D aerogels from nanostructured 1D and 2D materials. *Sci. Rep.* **2012**, *2*, 849–843.
23. De Cicco, F.; Russo, P.; Reverchon, E.; García-González, C.A.; Aquino, R.P.; Del Gaudio, P. Prilling and supercritical drying: A successful duo to produce core-shell polysaccharide aerogel beads for wound healing. *Carbohyd. Polym.* **2016**, *147*, 482–489.
24. Pinnow, M.; Fink, H.-P.; Fanter, C.; Kunze, J. Characterization of highly porous materials from cellulose carbamate. *Macromol. Symp.* **2008**, *262*, 129–139.

25. Lee, K.P.; Gould, G.L. Aerogel powder therapeutic agents. *U. S. Pat.* 6994842 B2, 2006.
26. Alnaief, M.; Alzaitoun, M.A.; García-González, C.A.; Smirnova, I. Preparation of biodegradable nanoporous microspherical aerogel based on alginate. *Carbohydr. Polym.* **2011**, *84*, 1011–1018.
27. Alnaief, M.; Obaidat, R.; Mashaqbeh, H. Effect of processing parameters on preparation of carrageenan aerogel microparticles. *Carbohydr. Polym.* **2018**, *180*, 264–275.
28. Mueannoom, W.; Srisongphan, A.; Taylor, K.M.G.; Hauschild, S.; Gaisford, S. Thermal ink-jet spray freeze-drying for preparation of excipient-free salbutamol sulphate for inhalation. *Eur. J. Pharm. Biopharm.* **2012**, *80*, 149–155.
29. Sharma, G.; Mueannoom, W.; Buanz, A.B.M.; Taylor, K.M.G.; Gaisford, S. In vitro characterisation of terbutaline sulphate particles prepared by thermal ink-jet spray freeze drying. *Int. J. Pharm.* **2013**, *447*, 165–170.
30. García-Torres, B.A.; Aguilar-Elguezabal, A.; Román-Aguirre, M.; Álvarez-Contreras, L. Synthesis of silica aerogels microspheres prepared by ink jet printing and dried at ambient pressure without surface hydrophobization. *Materials Chemistry and Physics* **2016**, *172*, 32–38.
31. Walshaw, M.; McElvaney, G.; Williams, R.; Morice, A.; Carroll, M.; Haworth, C.; Herzig, M.; Ketchell, I.; Myrvold, R.; Meland, N.; et al. 45 A first-in-patient clinical trial demonstrates that inhaled alginate oligosaccharide (OligoG) is well tolerated in cystic fibrosis (CF) patients. *J. Cyst. Fibros.* **2014**, *13*, S58.
32. Pritchard, M.F.; Powell, L.C.; Jack, A.A.; Powell, K.; Beck, K.; Florance, H.; Forton, J.; Rye, P.D.; Dessen, A.; Hill, K.E. A low-molecular-weight alginate oligosaccharide disrupts pseudomonal microcolony formation and enhances antibiotic effectiveness. *Antimicrob. Agents Chemother.* **2017**, *61*, e00762-17.
33. Goimil, L.; Braga, M.E.M.; Dias, A.M.A.; Gómez-Amoza, J.L.; Concheiro, A.; Alvarez-Lorenzo, C.; de Sousa, H.C.; García-González, C.A. Supercritical processing of starch aerogels and aerogel-loaded poly(ε-caprolactone) scaffolds for sustained release of ketoprofen for bone regeneration. *J. CO2 Util.* **2017**, *18*, 237–249.
34. Wu, D.; Wang, C.; Yang, J.; Wang, H.; Han, H.; Zhang, A.; Yang, Y.; Li, Q. Improving the intracellular drug concentration in lung cancer treatment through the codelivery of doxorubicin and miR-519c mediated by porous PLGA microparticles. *Mol. Pharmaceutics* **2016**, *13*, 3925–3933.
35. Hickey, A.J.; Edwards, D.A. Density and shape factor terms in Stokes' equation for aerodynamic behavior of aerosols. *J. Pharm. Sci.* **2018**, *107*, 794–796.
36. Gurikov, P.; Smirnova, I. Non-Conventional methods for gelation of alginate. *Gels* **2018**, *4*, 14–27.
37. Lee, K.Y.; Mooney, D.J. Alginate: Properties and biomedical applications. *Progress in Polymer Science* **2012**, *37*, 106–126.
38. Mishra, M. *Handbook of Encapsulation and Controlled Release*; CRC press: Boca Raton, FL, USA, 2015.
39. McKinley, G.H.; Renardy, M. Wolfgang von Ohnesorge. *Phys. Fluids* **2011**, *23*, 127101–127106.
40. Kaneko, D.; Thi le, N.Q.; Shimoda, T.; Kaneko, T. Preparation methods of alginate micro-hydrogel particles and evaluation of their electrophoresis behavior for possible electronic paper ink application. *Polym. J.* **2010**, *42*, 829–833.
41. Veronovski, A.; Knez, Ž.; Novak, Z. Preparation of multi-membrane alginate aerogels used for drug delivery. *J. Supercrit. Fluid.* **2013**, *79*, 209–215.
42. Ali, H.S.M.; York, P.; Blagden, N.; Khoubnasabjafari, M.; Acree, W.E.; Jouyban, A. Solubility of salbutamol and salbutamol sulphate in ethanol+water mixtures at 25°C. *J. Mol. Liq.* **2012**, *173*, 62–65.
43. May, S.; Jensen, B.; Wolkenhauer, M.; Schneider, M.; Lehr, C.M. Dissolution techniques

for in vitro testing of dry powders for inhalation. *Pharm. Res.* **2012**, *29*, 2157–2166.

44. Shah, K.; Chan, L.W.; Wong, T.W. Critical physicochemical and biological attributes of nanoemulsions for pulmonary delivery of rifampicin by nebulization technique in tuberculosis treatment. *Drug Deliv.* **2017**, *24*, 1631–1647.
45. Davies, M.J.; Kerry, T.D.; Seton, L.; Murphy, M.F.; Gibbons, P.; Khoo, J.; Naderi, M. The crystal engineering of salbutamol sulphate via simulated pulmonary surfactant monolayers. *Int. J. Pharm.* **2013**, *446*, 34–45.
46. Johnson, R.A. A Quick Reference on Respiratory Acidosis. *Veterinary Clinics of North America: Small Animal Practice* **2017**, *47*, 185–189.
47. Sutariya, V.; Mashru, R.; Sankalia, M.; Sankalia, J. Transbuccal delivery of salbutamol sulphate: In vitro determination of routes of buccal transport. *Ars. Pharm.* **2005**, *46*, 337–352.
48. García-González, C.A.; Jin, M.; Gerth, J.; Alvarez-Lorenzo, C.; Smirnova, I. Polysaccharide-based aerogel microspheres for oral drug delivery. *Carbohydr. Polym.* **2015**, *117*, 797–806.
49. Guarino, V.; Caputo, T.; Altobelli, R.; Ambrosio, L. Degradation properties and metabolic activity of alginate and chitosan polyelectrolytes for drug delivery and tissue engineering applications. *AIMS Mat. Sci.* **2015**, *2*, 497–502.
50. Kumaresan, C.; Sathishkumar, K. Development of an inhaled sustained release dry powder formulation of salbutamol sulphate, an antiasthmatic drug. *Indian J. Pharm. Sci.* **2016**, *78*, 136–142.
51. Ducharme, F.M.; Ni Chroinin, M.; Greenstone, I.; Lasserson, T.J. Addition of long-acting beta2-agonists to inhaled corticosteroids versus same dose inhaled corticosteroids for chronic asthma in adults and children. *Cochrane Database Syst. Rev.* **2010**, CD005535.
52. Li, Q.; Zhan, S.; Liu, Q.; Su, H.; Dai, X.; Wang, H.; Beng, H.; Tan, W. Preparation of a sustained-release nebulized aerosol of R-terbutaline hydrochloride liposome and evaluation of its anti-asthmatic effects via pulmonary delivery in Guinea pigs. *AAPS PharmSciTech* **2018**, *19*, 232–241.

# 8. CONCLUSIONS

In this PhD Thesis, the development of drug carriers for two applications (wound treatment and pulmonary delivery) using supercritical fluid technology was carried out. Namely, supercritical $CO_2$ was advantageously applied for the micronization of particles for wound management purposes, as well as for the production of aerogels both for wound and pulmonary applications. The research was carried out in three steps, and the following conclusions can be drawn.

1. In the first section of the PhD Thesis, solid lipid microparticles (SLMPs) were produced at low temperatures and avoiding the use of solvents in the Particles from Gas-Saturated Solutions (PGSS®) technique assisted by the use of supercritical $CO_2$. In the first part of this section, the modelling of the processing of lipid glycerylmonostearate (GMS) particles with the PGSS® technique was carried out using artificial intelligence tools (artificial neural networks and fuzzy logic). First, a depletion in the melting point of GMS from 61 °C down to 52 °C with increasing pressure was measured in the presence of compressed $CO_2$, which served to determine the feasible region for PGSS® processing. Then, the GMS particle size distribution and yield of the PGSS® process were modeled using pressure, temperature and nozzle diameter as control variables. The mean particle diameter was highly influenced by the operating conditions, obtaining smaller particles at high temperatures and pressures, and small nozzle diameters. In the second part of this section, GMS particles loaded with the anesthetic drug lidocaine hydrochloride were prepared using the PGSS® technique for specific wound applications. The obtained particles presented a mean diameter of 114 ± 39 µm. Particles were loaded with different lidocaine contents showing high encapsulation efficiencies (70–79%) and lidocaine contents between 0.7 and 7.5 wt.%. Lidocaine was released from the SLMPs following a first-order kinetic model with lag time, with 50% of the drug payload released after 4 h. Antimicrobial tests against *Escherichia coli*, *Staphylococcus aureus* and *Pseudomonas aeruginosa* bacterial strains were carried out to evaluate the potential use of the particles in the prevention of wound infection, showing a complete inhibition of bacteria growth after 24 h of incubation. The diffusion of lidocaine through intact and damaged skin was evaluated using 3D-bioprinted skin equivalents, achieving faster diffusion through dermal tissue than through the intact skin and a delayed diffusion from the lipid microparticles with respect to pure lidocaine. The obtained drug-loaded particles can be regarded as an attractive option for local treatment that combines anesthetic and antimicrobial effects at the wound site.

2. In the second section of this PhD Thesis, chitosan aerogels loaded with vancomycin were produced and evaluated for chronic wound applications. The aerogel beads produced by the dripping method presented outstanding textural properties such as high porosity (> 96%) and large surface area (> 200 $m^2/g$). This high porosity was reflected in a high PBS sorption capacity of up to 400 wt.%. The aerogels did not interfere with the collagenase activity, responsible for the remodeling phase of the healing process. Vancomycin hydrochloride was loaded into the aerogels with encapsulation efficiencies close to 12%, and was released following a first-order kinetic model, providing a fast antimicrobial activity against *S. aureus* bacterial strain as confirmed in the antimicrobial tests. The vancomycin-loaded aerogels were tested for biocompatibility with mouse fibroblasts, presenting good cell viability at all the vancomycin concentrations tested. In the following chapter of this section, the jet cutting method was applied to a chitosan aqueous solution to produce vancomycin-loaded chitosan aerogels with small particle sizes that are easier to apply to wounds. A preliminary screening was carried out to optimize the parameters of the jet cutting process. The particles obtained using a nozzle diameter of 500 µm and a cutting disk velocity of 4000 rpm presented the narrower size distribution, with a mean diameter of *ca.* 820 µm. The reduction of the particle size resulted in enhanced PBS sorption capacity (up to 800 wt.%). The use of an ethanolic solution as gelation bath resulted in a one-fold increment of the encapsulation efficiency of vancomycin with respect to aqueous baths, and the drug release was sustained for 24 h. Particles presented good antimicrobial activity, completely inhibiting the growth of *S. aureus* after 6 h of incubation, and excellent biocompatibility as confirmed in the cytocompatibility and hemocompatibility assays. The obtained drug-loaded aerogels seem especially relevant for the local treatment of infected and highly exudative wounds.

3. In the last section of the Thesis, a processing method for the preparation of alginate aerogel microparticles for pulmonary delivery of salbutamol sulphate coined as *aerogel printing* was developed. The choice of the aerogel formulation was based on its high porosity that allows for the preparation of microparticles of larger diameters with similar aerodynamic behavior than smaller, non-porous particles. After an optimization of the polymer concentration, thermal inkjet printing was used to produce alginate gel microparticles. The obtained particles were dried with supercritical $CO_2$ to obtain the aerogels, which consisted in spherical particles with good textural properties and narrow particle size distribution (23.8 ± 4.5 µm). The drug salbutamol sulphate was incorporated in the aerogel and was released in a sustained manner, which can be advantageous with respect to conventional formulations. Particles presented suitable aerodynamic diameters for local pulmonary delivery, as confirmed by the simulated lung deposition tests. The developed technology is promising for the production of drug-loaded porous particles for pulmonary delivery in local and systemic treatments, and has a straight-forward production scalability.

# Appendix

## Conflicts of interest

The doctoral student declares that there is no conflict of interest regarding this Doctoral Thesis.

## List of publications

1. García-González, C.A.; López-Iglesias, C.; Concheiro, A.; Alvarez-Lorenzo, C. Chapter 16. Biomedical Applications of Polysaccharide and Protein Based Aerogels. In *Biobased Aerogels: Polysaccharide and Protein-based Materials. Green Chemistry Series*; Thomas, S., Pothan, L.A., Mavelil-Sam, R; Royal Society of Chemistry: Cambridge, UK, 2018; pp. 295–323.
2. López-Iglesias, C., Barros, J.; Ardao, I.; Monteiro, F.J.; Alvarez-Lorenzo, C.; Gómez-Amoza, J.L., García-González, C.A. Vancomycin-loaded chitosan aerogel particles for chronic wound applications. *Carbohydrate Polymers* **2018**, *204*, 223–231.
3. López-Iglesias, C.; Casielles, A.M.; Altay, A.; Bettini, R.; Alvarez-Lorenzo, C.; García-González, C.A. From the printer to the lungs: Inkjet-printed aerogel particles for pulmonary delivery. *Chemical Engineering Journal* **2019**, *357*, 559–566.
4. Rodríguez-Dorado, R.; López-Iglesias, C.; García-González, C.A.; Auriemma, J.; Aquino, R.P.; del Gaudio, P. Design of aerogels, cryogels and xerogels of alginate: Effect of molecular weight, gelation conditions and drying method on particles' micromeritis. *Molecules* **2019**, *24*, 1049–1060.
5. López-Iglesias, C.; Barros, J.; Ardao, I.; Gurikov, P.; Monteiro, F.J.; Smirnova, I.; Alvarez-Lorenzo, C.; García-González, C.A. Jet cutting technique for the production of chitosan aerogel microparticles loaded with vancomycin. *Polymers* **2020**, *12*, 273–285.
6. Martínez-Borrajo, R.; Diaz-Rodriguez, P.; Santos-Rosales, V.; López-Iglesias, C.; Iglesias-Mejuto, A.; Gómez-Amoza, J.L.; García-González, C.A.; Landin, M. Capítulo 2. Biomateriales en medicina regenerativa: Del diseño a la aplicación. In *Avances de la Bioingeniería para el envejecimiento saludable*; González, P.; Iberos: España-Portugal, 2020; pp: 10–20.
7. López-Iglesias, C.; Quílez, C.; Barros, J.; Velasco, D.; Alvarez-Lorenzo, C.; Jorcano, J.L.; Monteiro, F.J.; García-González, C.A. Lidocaine-loaded solid lipid microparticles (SLMPs) produced from gas-saturated solutions for wound applications. *Pharmaceutics* **2020**, *12*, 870–885.
8. López Iglesias, C.; López, E.R.; Fernández, J.; Landin, M.; García-González, C.A. Modelling of the production of lipid microparticles using PGSS® technique. *Molecules* **2020**, *25*, 927–940.

## Conference contributions

1. C. López-Iglesias, A. Concheiro, C. Álvarez-Lorenzo, C.A. García-González; *Vancomycin-loaded chitosan aerogel particles prepared by supercritical $CO_2$ extraction for biomedical applications* (poster). ExTech2017 - 19th International Symposium on Advances in Extraction Technologies. Santiago de Compostela (Spain), June 2017.

2. C.A. García-González, L. Goimil, C. López-Iglesias, A. Concheiro, C. Alvarez-Lorenzo; *Supercritical $CO_2$ technology: A green solution for the processing of advanced pharmaceutical and biomedical products* (poster). I Jornada Científica IBEROS. Porto (Portugal), July 2017.

3. C. López-Iglesias, A. Concheiro, C. Alvarez-Lorenzo, C.A. García-González; *Chitosan aerogel particles as advanced vancomycin carriers for wound healing applications* (poster). 11th World Meeting on Pharmaceutics, Biopharmaceutics and Pharmaceutical Technology. Granada (Spain), March 2018.

4. C. López-Iglesias, C. Álvarez-Lorenzo, C.A. García González; *Solid lipid microparticles using the PGSS technique for the prevention and treatment of chronic wound infections* (poster). Skin Forum 2018 Annual Meeting. Tallinn (Estonia), June 2018.

5. C. López-Iglesias, A. Concheiro, C. Álvarez-Lorenzo, C.A. García-González. *Drug-loaded chitosan aerogels for chronic wound applications* (poster). 4th International Seminar on Aerogels Hamburg. Hamburg (Germany), September 2018.

6. C. López Iglesias, C. Álvarez-Lorenzo, C.A. García-González. *Inkjet printing of aerogels: Promising technology for the processing of nanostructured microparticles for life sciences purposes* (poster). 4th International Seminar on Aerogels Hamburg. Hamburg (Germany), September 2018.

7. C. López-Iglesias, A. Concheiro, A. Altay, R. Bettini, C. Álvarez-Lorenzo, C.A. García-González. *From the printer to the lungs: Inkjet-printed aerogel microspheres for pulmonary delivery of salbutamol sulphate* (oral). XIV Meeting of the Spanish Society of Pharmaceutics and Pharmaceutical Technology. Santiago de Compostela (Spain), January 2019.

8. C. López-Iglesias, M. Landín, C. Álvarez-Lorenzo, C.A. García-González. *Preparación de micropartículas sólidas lipídicas mediante tecnología supercrítica para aplicación en heridas crónicas* (poster). XIV Meeting of the Spanish Society of Pharmaceutics and Pharmaceutical Technology. Santiago de Compostela (Spain), January 2019.

9. C. López-Iglesias, I. Ardao, A. Concheiro, C. Alvarez-Lorenzo, C.A. García-González. *Drug-loaded chitosan aerogels prepared by supercritical $CO_2$-assisted drying for biomedical applications* (poster). 17th European Meeting on Supercritical Fluids and 7th European Meeting in High Pressure Technology. Ciudad Real (Spain), April 2019.

10. C. López-Iglesias, A. Concheiro, C. Alvarez-Lorenzo, C.A. García-González. *Aerogel printing technology assisted by supercritical $CO_2$ technology for biomedical applications* (oral). 17th European Meeting on Supercritical Fluids and 7th European Meeting in High Pressure Technology. Ciudad Real (Spain), April 2019.

11. C. López-Iglesias, P. Gurikov, C. Alvarez-Lorenzo, I. Smirnova, C.A. García-González. *Antibiotic-loaded chitosan aerogel particles produced by jet cutting for chronic wound applications* (poster). 30th Annual Conference of the European Society for Biomaterials (ESB) and 26th Conference of the German Society for Biomaterials (DGBM). Dresden (Germany), September 2019.

12. C.A. García-González, V. Santos-Rosales, C. López-Iglesias, C. Alvarez-Lorenzo, A. Concheiro, J.L. Gómez-Amoza. *Supercritical fluid technology: a green alternative for the processing of cyclodextrin-based materials* (poster). 6th European Conference on Cyclodextrins - EURO CD 2019. Santiago de Compostela (Spain), October 2019.

13. C. López-Iglesias, I. Ardao, J. Barros, P. Gurikov, I. Smirnova, C.A. García-González. *Highly porous polysaccharide-based formulations for wound treatment* (poster). 6th EPNOE International Polysaccharide Conference. Aveiro (Portugal), October 2019.

14. C.A. García-González, C. López-Iglesias, V. Santos-Rosales, C. Álvarez-Lorenzo, A. Concheiro, M. Landín, J.L. Gómez-Amoza. *Desarrollo de aerogeles como materiales nanoestructurados para medicina regenerativa* (oral). XLII Congreso de la Sociedad Ibérica de Biomecánica y Biomateriales. Madrid (Spain), November 2019.

15. C. López-Iglesias, C. Quílez, J. Barros, E.R. López, D. Velasco, J.L. Jorcano, F.J. Monteiro, C. Alvarez-Lorenzo, J. Fernandez, C.A. García-González. *Solid lipid microparticles (SLMPs) for the local delivery of an anaesthetic agent* (poster). 1º Encuentro Ibérico de Fluidos Supercríticos. Santiago de Compostela (Spain), February 2020.

16. C. López-Iglesias, J. Barros, I. Ardao, F.J. Monteiro, C. Alvarez-Lorenzo, C.A. García-González. *Bio-based aerogels for drug delivery in selected biomedical applications* (oral). International Conference on Aerogels for Biomedical and Environmental Applications. Santiago de Compostela (Spain), February 2020.

17. C. López-Iglesias, J. Rey-Varela, L. Diego-González, P.K. Szewczyk, U. Stachewicz, J.L. Gómez-Amoza, R. Simón-Vazquez, C.A. García-González. *Alginate aerogel microparticles for pulmonary drug delivery* (poster). International Conference on Aerogels for Biomedical and Environmental Applications. Santiago de Compostela (Spain), February 2020.

18. C. López-Iglesias, J. Barros, P. Gurikov, I. Ardao, I. Smirnova, F.J. Monteiro, C. Alvarez-Lorenzo, C.A. García-González. *Aerogel microparticles processed by jet cutting for wound treatment* (poster). International Conference on Aerogels for Biomedical and Environmental Applications. Santiago de Compostela (Spain), February 2020.

19. C. López-Iglesias, C.A. García-González, P. Mikes. *Electrospun mats embedded with starch aerogel and xerogel microparticles for wound applications* (poster). International Conference on Aerogels for Biomedical and Environmental Applications. Santiago de Compostela (Spain), February 2020.

20. Carlos A. García-González, Clara López-Iglesias, Víctor Santos-Rosales, Mariana Landín, José L. Gómez-Amoza. *Engineering of aerogels for biomedical applications linked to ageing of population* (oral). Online Aerogel Seminar 2020. Hamburg (Germany), online. September 2020.

# Awards

Science Xpression 2017 (Universidade da Coruña & Instituto de Investigación Biomédica de A Coruña) – Best Oral Presentation Award, A Coruña (Spain), 2017.

IACOBUS Programme – Scientific Publications Prize, *Vancomycin-loaded chitosan aerogel particles for chronic wound applications*, 2019.

1st Prize for the Best Collaborative Work, Highly porous polysaccharide-based formulations for wound treatment, 6th EPNOE International Polysaccharide Conference, Aveiro (Portugal), 2019.